THIOPHENOPHANES AND THEIR COORDINATION CHEMISTRY

SHUANG LIU, B.Sc., M.Sc.

THIOPHENOPHANES AND THEIR COORDINATION CHEMISTRY

by

© Shuang Liu, B.Sc., M.Sc.

A thesis submitted to the School of Graduate Studies in partial fulfillment of the requirements for the degree of Doctor of Philosophy

Department of Chemistry
Memorial University of Newfoundland
St. John's, Newfoundland
Canada A1B 3X7

August 1990

ISBN 0-315-61798-5

SUBJECT CATEGORIES

Dissertation Abstracts International is arranged by broad, general subject categories. Choose the ***one*** listed below (capital letters) which most nearly describes the general content of your dissertation. If the major subject category has sub-fields under it, and ***only*** if it does, please choose ***one*** (small letters). (Ex.: ECONOMICS, Theory). Enter subject category on Item 7 of Agreement Form.

HUMANITIES

IA COMMUNICATIONS AND THE ARTS
- ARCHITECTURE
- CINEMA
- FINE ARTS
- INFORMATION SCIENCE
- JOURNALISM
- LIBRARY SCIENCE
- MASS COMMUNICATIONS
- MUSIC
- SPEECH
- THEATER

IIA EDUCATION
- EDUCATION
  - General
  - Administration
  - Adult
  - Agricultural
  - Art
  - Audiovisual
  - Business
  - Community and Social
  - Community Colleges
  - Curriculum and Instruction
  - Early Childhood
  - Elementary
  - Finance
  - Guidance and Counseling
  - Health
  - Higher
  - History
  - Home Economics
  - Industrial
  - Language and Languages
  - Mathematics
  - Middle School
  - Minorities
  - Music
  - Personality Development and Mental Hygiene
  - Philosophy
  - Physical
  - Preschool
  - Programmed Instruction
  - Psychology
  - Religion
  - Sciences
  - Secondary
  - Social Sciences
  - Special
  - Teacher Training
  - Teaching Machines
  - Tests and Measurements
  - Theory and Practice
  - Vocational

IIIA LANGUAGE, LITERATURE AND LINGUISTICS
- LANGUAGE
  - General
  - Ancient
  - Linguistics
  - Modern
- LITERATURE
  - General
  - Classical
  - Comparative
  - Medieval
  - Modern
  - American
  - Asian
  - Dutch and Scandinavian
  - English
  - Germanic
  - Latin American
  - Romance
  - Russian and East European
  - Slavic and Finno-Ugrian

IVA PHILOSOPHY, RELIGION AND THEOLOGY
- PHILOSOPHY
- RELIGION
  - General
  - Clergy
  - History
  - Music
  - Philosophy
- THEOLOGY

VA SOCIAL SCIENCES
- ACCOUNTING
- AMERICAN STUDIES
- ANTHROPOLOGY
  - Archaeology
  - Cultural
  - Physical
- BANKING
- BUSINESS ADMINISTRATION
- ECONOMICS
  - General
  - Agricultural
  - Commerce-Business
  - Finance (includes Public Finance)
  - History
  - Theory
- FOLKLORE
- HISTORY
  - General
  - Ancient
  - Medieval
  - Modern
  - Black
  - Church
  - Africa
  - Asia
  - Australia and Oceania
  - Canada
  - Europe
  - Latin America
  - United States
- HISTORY OF SCIENCE
- LAW
- MANAGEMENT
- MARKETING
- POLITICAL SCIENCE
  - General
  - International Law and Relations
  - Public Administration
- PUBLIC RELATIONS
- RECREATION
- SOCIAL GEOGRAPHY
- SOCIAL STRUCTURE
- SOCIAL WORK
- SOCIOLOGY
  - General
  - Community Organization
  - Criminology
  - Demography
  - Educational
  - Individual and Family Studies
  - Industrial
  - Labor Relations
  - Public Welfare
  - Race Relations
  - Social Problems
  - Statistics—Research Methods
  - Theory
- TRANSPORTATION
- URBAN AND REGIONAL PLANNING
- WOMEN'S STUDIES

SCIENCES

IB BIOLOGICAL SCIENCES
- AGRICULTURE
  - General
  - Animal Culture
  - Animal Pathology
  - Forestry & Wildlife
  - Plant Culture
  - Plant Pathology
  - Plant Physiology
  - Range Management
  - Wood Technology
- AGRONOMY
- ANATOMY
- BIOLOGICAL OCEANOGRAPHY
- BIOLOGY
- BIOPHYSICS
  - General
  - Medical
- BIOSTATISTICS
- BOTANY
- ECOLOGY
- ENTOMOLOGY
- GENETICS
- LIMNOLOGY
- MICROBIOLOGY
- PHYSIOLOGY
- RADIATION BIOLOGY
- VETERINARY SCIENCE
- ZOOLOGY

IIB EARTH SCIENCES
- GEOCHEMISTRY
- GEODESY
- GEOLOGY
- GEOPHYSICS
- HYDROLOGY
- MINERALOGY
- PALEOBOTANY
- PALEONTOLOGY
- PALEOZOOLOGY
- PHYSICAL GEOGRAPHY
- PHYSICAL OCEANOGRAPHY

IIIB HEALTH AND ENVIRONMENTAL SCIENCES
- ENVIRONMENTAL SCIENCES
- FOOD TECHNOLOGY
- HEALTH SCIENCES
  - General
  - Audiology
  - Chemotherapy
  - Dentistry
  - Education
  - Hospital Management
  - Human Development
  - Hygiene
  - Immunology
  - Medicine & Surgery
  - Mental Health
  - Nursing
  - Nutrition
  - Pathology
  - Pharmacy
  - Public Health
  - Radiology
  - Recreation
  - Speech Pathology
- HOME ECONOMICS
- PHARMACOLOGY

IVB PHYSICAL SCIENCES
- PURE SCIENCES
  - CHEMISTRY
    - General
    - Analytical
    - Biological
    - Inorganic
    - Nuclear
    - Organic
    - Pharmaceutical
    - Physical
    - Polymer
    - Radiation
    - Water
  - MATHEMATICS
  - PHYSICS
    - General
    - Acoustics
    - Astronomy & Astrophysics
    - Atmospheric Science
    - Atomic
    - Electronics and Electricity
    - Elementary Particles and High Energy
    - Fluid and Plasma
    - Molecular
    - Nuclear
    - Optics
    - Radiation
    - Solid State
  - STATISTICS
- APPLIED SCIENCES
  - APPLIED MECHANICS
  - ASTRONAUTICS
  - COMPUTER SCIENCE
  - ENGINEERING
    - General
    - Aerospace
    - Agricultural
    - Automotive
    - Biomedical
    - Chemical (includes ceramics and fuel)
    - Civil
    - Electronics and Electrical
    - Heat and Thermodynamics
    - Hydraulic
    - Industrial
    - Marine
    - Materials Science
    - Mechanical
    - Metallurgy
    - Mining
    - Nuclear
    - Petroleum
    - Sanitary and Municipal
    - System Science
  - OPERATIONS RESEARCH
  - PLASTICS TECHNOLOGY
  - TEXTILE TECHNOLOGY

VB PSYCHOLOGY
- PSYCHOLOGY
  - General
  - Clinical
  - Experimental
  - Industrial
  - Physiological
  - Psychobiology
  - Social

ABSTRACT

This thesis describes studies of thiophenophane ligands and their coordination chemistry. In Chapter 1, aspects of macrocyclic thioether chemistry have been briefly reviewed. In Chapter 2, synthesis and characterization of eight thiophenophane ligands are described. The molecular structures of 2,5,8-trithia[9](2,5)thiophenophane, 2,5,8,11-tetrathia[12](2,5)thiophenophane and 2,5,9,13-tetrathia[13](2,5)thiophenophane have been determined by X-ray methods. The effect of the rigid thiophene subunit with its two attached methylenes on the solid state conformations of the three macrocycles is discussed. In chapter 3, synthesis and properties of 15 copper(I) and (II) complexes of thiophenophane ligands and the open-chain ligand, 2,5-bis(2-hydroxyethylthiomethyl)thiophene, are described. The molecular structures of seven of these compounds are presented and spectral details are interpreted in the light of these structures. The redox properties of the complexes have been examined by cyclic voltammetry and the effect of solvent on their electrochemistry is discussed. In the first part of Chapter 4, synthesis and properties of palladium(II) and platinum(II) complexes of open-chain and macrocyclic thioether ligands are presented. The molecular structure of $[PdBr_2 \cdot L1]$ (L1=2,5,8-trithia[9](2,5)thiophenophane) has been determined. Variable temperature ^1H nmr spectra show that the open-chain dithioether complexes undergo rapid conformational exchange at room temperature but are configurationally rigid while the macrocyclic thioether complexes, $[MX_2 \cdot L1]$ (M=Pt, X=Cl; M=Pd, X=Cl, Br, I, SCN), undergo very limited conformational and no configurational exchange up to their decomposition temperatures. Chemical exchange of acidic ligand hydrogens and a metal-ligand dissociative equilibrium were detected when M=Pd and X=SCN. In the second part of Chapter 4, preparations of seven π-allylpalladium complexes of open-chain dithioether and macrocyclic thiophenophane

ligands are described. The molecular structure of $[Pd(C_3H_5)\cdot L1]^+$ reveals an asymmetric π-allyl group and a rare, unusually short apical Pd-S(thiophene) bond (2.786(4) Å). Variable temperature ^1H nmr spectra of these complexes show that open-chain dithioether complexes undergo rapid inversion at coordinated sulfurs while the complex, $[Pd(C_3H_5)\cdot L1]CF_3SO_3$, undergoes a 1.4-metallotropic shift on the heteroatoms of the macrocycle at room temperature and a dissociative inversion at thioether sulfurs at elevated temperatures. In Chapter 5, synthesis and properties of thirteen silver(I) complexes are presented. The molecular structure of $[Ag_2(L2)_2](ClO_4)_2$, which contains a centrosymmetric dinuclear cation with a slightly distorted trigonal bypyramidal coordination geometry about each silver atom has been determined. The chemical and photochemical stabilities of these complexes are discussed with respect to the structure of $[Ag_2(L2)_2](ClO_4)_2^{2+}$.

ACKNOWLEDGEMENTS

I would like to express my sincere gratitude to my supervisor, Dr. C.R. Lucas, for his constant encouragement, and stimulating discussion throughout the course of this work, and for his patience on those occasions when the work was not proceeding rapidly. I am also grateful to Dr. L.K. Thompson for his kind advice with my work and for his help with variable temperature magnetic studies of my copper(II) complexes; to Dr. M.J. Newlands for X-ray crystallography and to Dr. S.K. Mandal, Dr. P. Pickup and Mr. Huanyu Mao for their great help with electrochemical studies. My thanks are due as well to Dr. B. Gregory and Miss M. Baggs for their help with mass spectrometry, to Dr. C.R. Jablonski and his group for their help with nmr spectrometry; to Dr. J.N. Bridson for his recommendation to Graduate Studies for my Hatcher Scholarship and fellowships, to Dr. C.E. Loader and Miss T. Barker for their help with word processing and to all the people who have helped me with my research and course studies. I am particularly grateful to my colleagues and friends for their kind tolerance of the smell of some of my sulfur compounds. Financial support in the form of a Hatcher Scholarship, teaching assistantships and fellowships from Memorial University of Newfoundland and from the Natural Sciences and Engineering Research Council of Canada in the form of an operating grant to my supervisor, Dr. C.R. Lucas, is also acknowledged. Finally I am most grateful to my wife who has cheerfully borne the vicissitudes of the last three years and without whose help and encouragement this thesis would never have been completed.

Table of Contents

List of Tables

List of Figures

List of Abreviations

DMF: N,N-dimethylformamide

DMSO: dimethylsulfoxide

NHE: normal hydrogen electrode

SCE: aqueous saturated calomel electrode

Λ_M: molar conductance in $ohm^{-1} \cdot cm^2 \cdot mol^{-1}$

$E_{1/2}$: half potential, $E_{1/2} = (Ecp + Eap)/2$

E^f: formal redox potential

C: throughout the thesis, a capital C represents the concentration of a compound.

[n]aneS_m: n, the number of atoms in the macrocycle; m, the number of sulfur atoms in the macrocycle

[9]aneS3(O): mono-oxadized [9]aneS3

Me_2-2,3,2-S_4: 2,5,9,12-tetrathiatridecane

Et_2-2,3,2-S_4: 3,6,10,13-tetrathiapentadecane

2,3,2-S_4(TTU): 1,4,8,11-tetrathiaundecane

Py_2-2,2,2-S_2: 1,6-bis(2-pyridyl)-2,5-dithiahexane

Py_2-2,3,2-S_2: 1,7-bis(2-pyridyl)-2,6-dithiaheptane

Py_2-3,2,3-S_2: 1,8-bis(2-pyridyl)-3,6-dithiaoctane

Py_2-3,3,3-S_2: 1,9-bis(2-pyridyl)-3,7-dithianonane

2,2,2-NSSN: 1,8-diamino-3,6-dithiaoctane

2,3,2-NSSN: 1,9-diamino-3,7-dithianonane

2,2,2-N_4(trien): triethyleneamine

CHAPTER 1

MACROCYCLIC THIOETHER CHEMISTRY

Abstract:

The synthesis and coordination chemistry of macrocyclic thioethers have been briefly reviewed. The structural aspects of these macrocyclic thioether ligands are discussed in relation to many unusual properties of their transition metal complexes.

1.1. Introduction

Compounds composed of sequential -(YCH_2CH_2)- groups have been known for many years. It was not until 1967, however, that crown ether chemistry was really born when Pederson (1) first reported the synthesis and unique cation complexing properties of a number of macrocyclic compounds similar to I. Due to his pioneering discovery and contribution to this area of study he shared the Nobel Prize in chemistry in 1987 with Cram and Lehn. Since that time, a number of macrocyclic compounds with a variety of donor atoms have been prepared and investigated for their cation complexing properties (2-5). A number of excellent review articles have been published which deal with their synthesis (6-7), thermodynamics and kinetics (8), and their applications in organic synthesis, analytical chemistry and biomimetic modelling of metal ions in living systems (9-10).

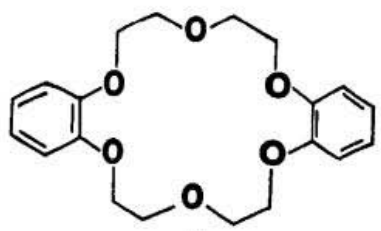

I

Examples of macrocyclic compounds containing one or more thioether linkages (11), including crown thioethers, cryptates (12-13) and cyclophanes (14) have been studied because of their selectivity for heavy metal cations in agreement with the theory of hard and soft acids and bases. They have also been studied because of the occurrence of sulfide linkages in some natural macrocyclic compounds (15). In 1978, the coordination of copper to thioether in methionyl residues in plastocyanin (16) and azurin (17) was discovered, which has spurred the development of thioether

coordination chemistry.

The synthesis of macrocyclic thioethers (11a, 18-19), including those with pyridine, furan and thiophene heterocyclic subunits (11c, 19) and their coordination chemistry (11c, 18-19) have been reported. However, the design of these macrocycles remains an essentially empirical exercise. In this chapter, synthetic and structural aspects of macrocyclic thioether compounds will be presented and discussed in the light of the X-ray crystal structures of some macrocycles. Also, the coordination chemistry of these macrocyclic thioether ligands will be discussed to provide some background for detailed study in the area of thioether chemistry.

1.2. General Synthetic Methods for Macrocyclic Thioether Ligands

1.2.1. High Dilution Method

Macrocyclic compounds contain 12 or more atoms in their ring (11a). Macrocyclic chemistry began in 1926 when the perfume component muscone was isolated and shown to have a large ring structure (20). One of the most prevalent synthetic methods for macrocyclic thioethers is the reaction of α,ω-dichlorides with α,ω-dimercaptans under high dilution conditions in basic media (Scheme 1-1). The ring closure is based on S_N2 α-mercaptide displacement of an ω-halide function. The α-mercapto-ω-halo-polythiomethylene intermediates are available by in situ generation from the treatment of α,ω-dihaloalkanes with active metal sulfides (21), or precondensed α,ω-polythiopolymethylene dimercaptides (22).

Unlike the strong template effect and corresponding high yields of macrocyclic polyoxaethers offered by oxygen coordination of alkali metal ions during cyclization of polyoxa units (1, 23), poor coordination by sulfur to active metal ions renders analogous template effects for macrocyclic polythioethers less successful. Thus, the com-

competition between cyclization and linear polymerization is more statistically defined by entropy, especially under conditions of high reagent concentrations. Under high dilution conditions, however, cyclization is favored kinetically.

Scheme 1-1

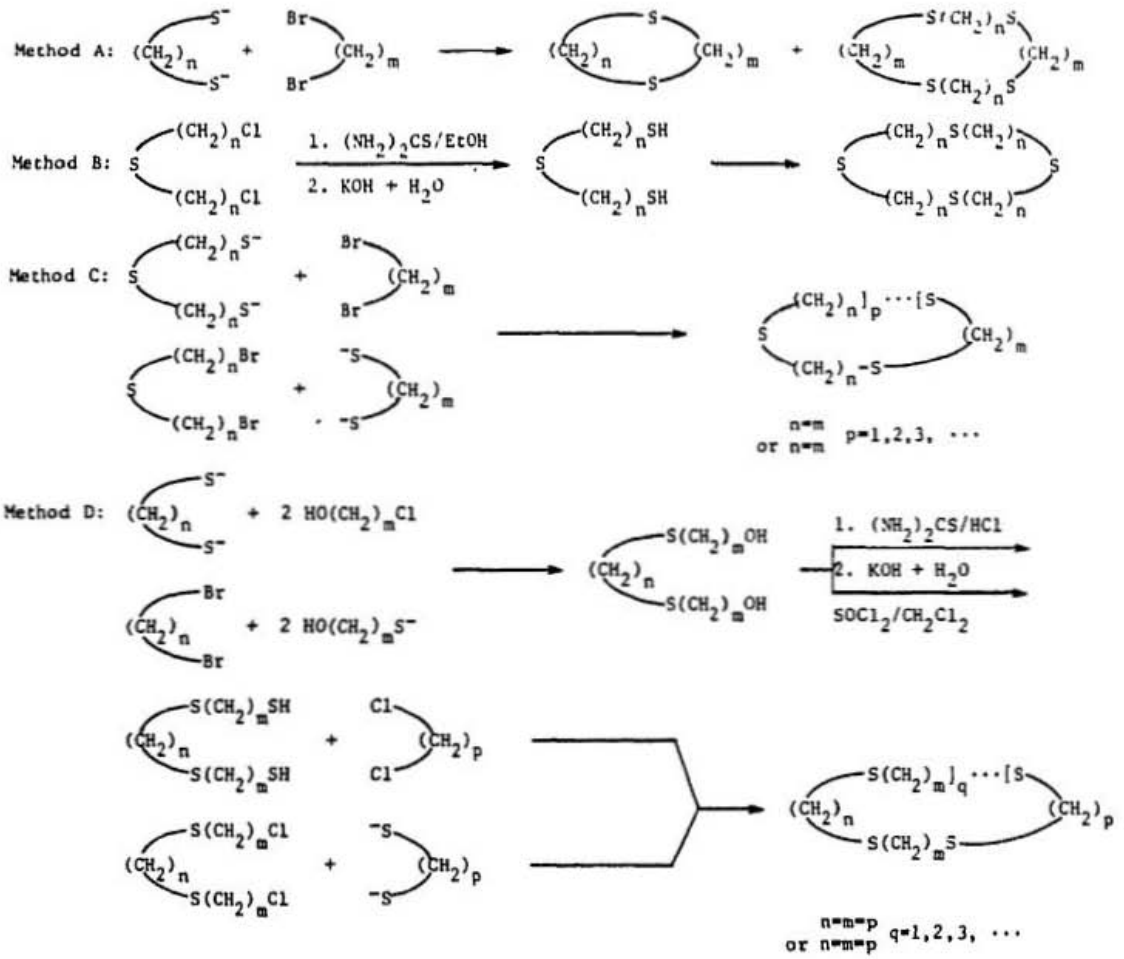

Method A is suitable for the preparation of tetra- and pentamethylene-bridged macrocyclic tetrathia and hexathia ethers but not for the large ethylene or trimethylene-bridged rings (24) since the internal strain is at a minimum for 6-, 14- and greater than 17-membered polymethylene rings (25). With inclusion of two to four sulfur atoms, internal crowding would minimize ring strain in the 9- through 13-membered ring systems (26). The entropy constraints to cyclization appear to converge with the kinetics of linear polymerization at macrocyclic polythioethers of greater than 24 ring atoms (24).

Conformationally flexible molecules containing a number of sulfide linkages are generally formed only in low yields since entropy constraints to cyclization favor linear polymerization. However, when a "rigid aromatic group" such as ortho-disubstituted phenyl (27) is made part of the macrocycle, cyclization proceeds in excellent yields under high dilution conditions. This is caused probably by the combination of high dilution techniques, which favor cyclization kinetically, and rigidity of the aromatic group, which disfavors the linear polymerization.

1.2.2. Template Method

One of the interesting methods for preparation of organic ring compounds is metal template synthesis. This method has been reviewed by both Busch (28) and Black (29). Metal template reactions have been defined as those ligand reactions which are dependent on or can be enhanced in yield by particular geometrical orientations imposed by metal coordination. An early example of template synthesis involved preparation of compound II from the corresponding square planar Ni(II) complex and α,α'-dibromo-o-xylene (30) as shown in Scheme 1-2.

Scheme 1-2

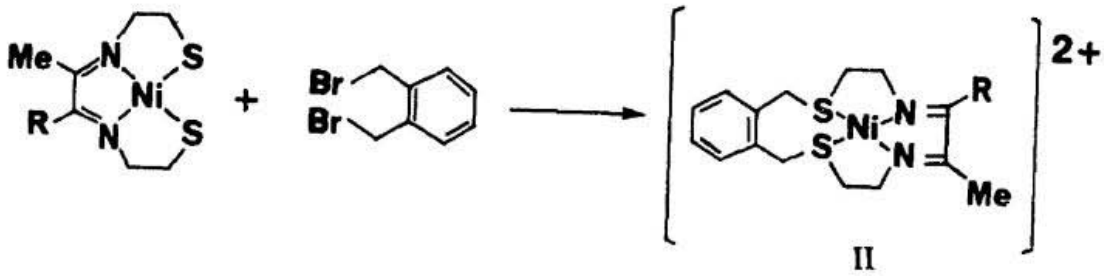

II

Likewise, Schrauzer and coworkers (31) have prepared a 14-membered macrocyclic thioether compound IV by refluxing the complex III with α,α'-dibromo-o-xylene as shown in Scheme 1-3. The crystalline nickel(II) complex decomposes on dissolution in methanol to release compound IV.

Scheme 1-3

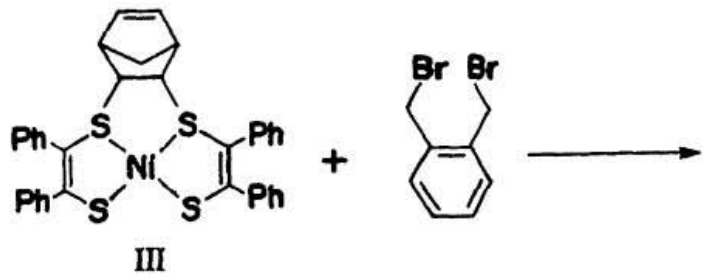

III

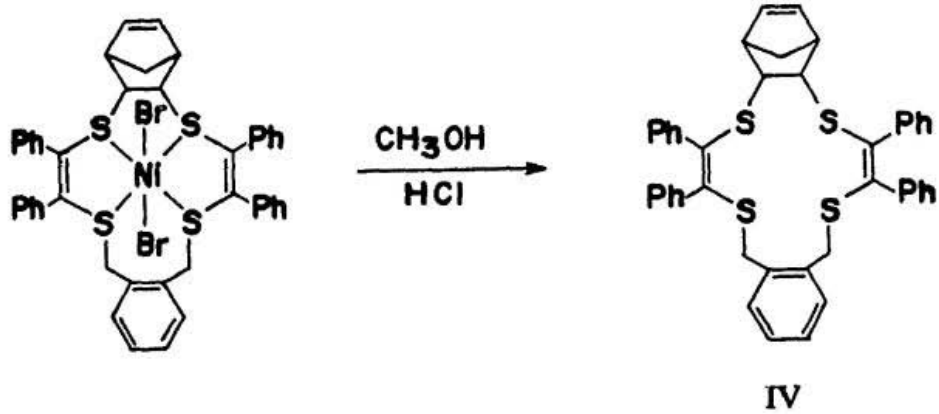

IV

Butter and Kellogg (32) have prepared a series of macrocyclic thioethers in very high yield using cesium as a template. They found that macrocycle formation often proceeds in remarkably good yield when cesium carbonate is present in DMF. Thiols were found to be deprotonated readily by Cs_2CO_3 and $CsHCO_3$ in DMF to form cesium thiolates , which are reasonably soluble in DMF. In most cases conditions of moderate dilution were also achieved by adding the thiol and bromide reactants simultaneously to the DMF solution.

In recent years, organometallic centers such as $[Mo(CO)_3]$ (33) have been used as the template for the preparation of macrocyclic thioether ligands. The ligand [9]aneS3 (1,4,7-trithiacyclononane) was prepared using $[Mo(CO)_3]$ as the template in yields of 60%, which is much higher than that achieved under high dilution conditions (34). Since one of the complexes (V) formed early in the process is regenerated in the third step (Scheme 1-4), the synthesis can, in principle, be performed catalytically.

Scheme 1-4

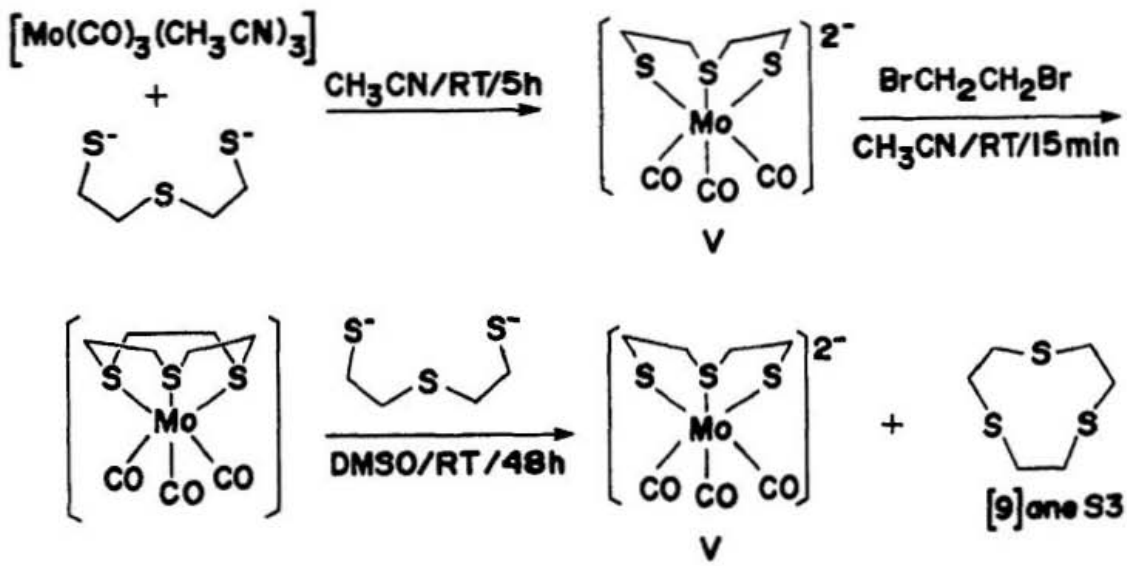

These catalytic reactions are sensitively influenced by the properties of the metal template centers. For example, Sellmann and Frank (35a) have found that [FeCO] centers are exceptionally suitable for the preparation of dibenzo[18]aneS6, as shown in Scheme 1-5, while complex [Ru(Bzo-[9]aneS3)(CO)Br_2] was isolated when the [Ru(CO)] fragment was used for alkylation of dpttd (dpttd=2,2´-[thiobis(ethylenethio)]bis(thiophenolate) (35b) as shown in Scheme 1-6. This may be explained by the fact that the [Ru(CO)] fragment is more electron-rich than the [Fe(CO)] fragment and its CO ligand is kinetically inert in contrast to that of [Fe(dpttd)(CO)]. However, it remains unclear whether the reaction occurs by an electrophilic mechanism or by a radical one.

Scheme 1-5

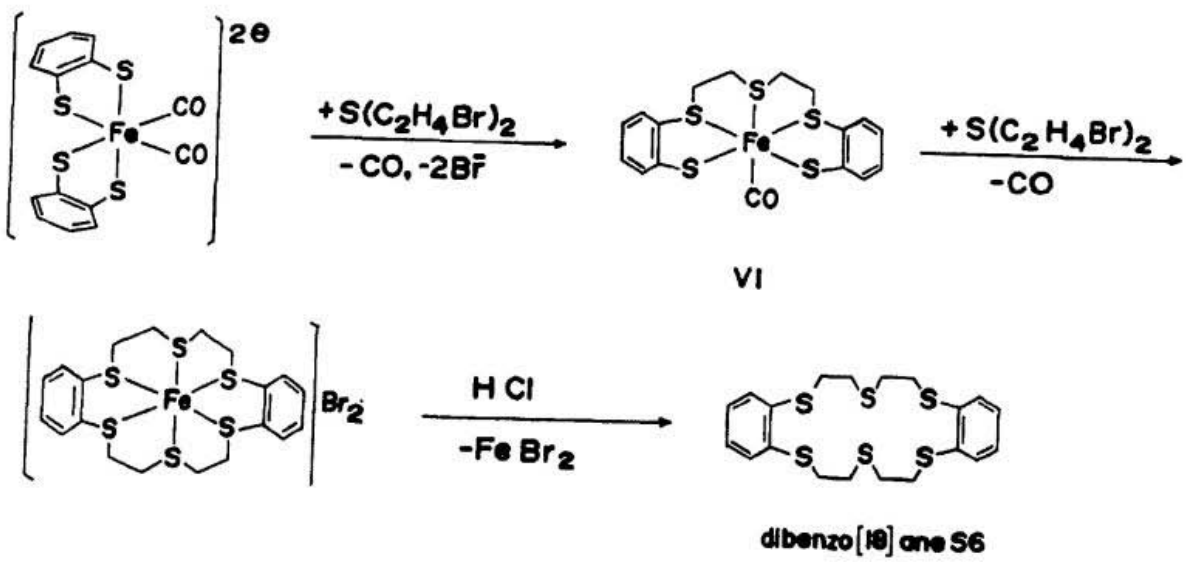

Scheme 1-6

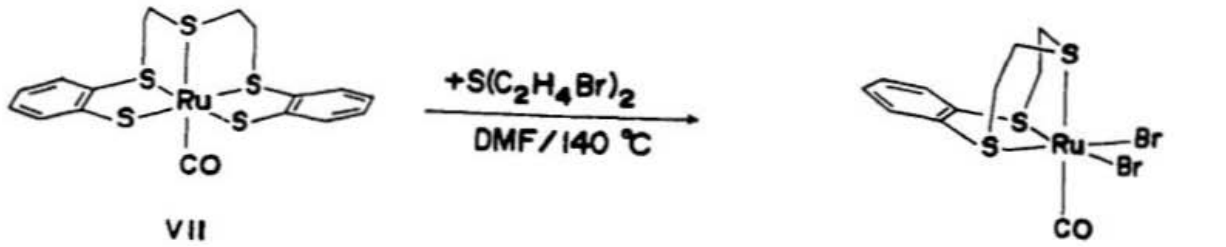

VII

[Ru(Bzo-[9]aneS3)(CO)Br$_2$]

In conclusion, thioether chemistry has received much recent interest. Although some new synthetic methods have been developed, the yield of thioether compounds, especially homoleptic macrocyclic thioether compounds, remains a major obstacle. It seems likely that the introduction of rigid aromatic group(s) into the macrocyclic ring will increase the yield of the macrocycle but at the same time the metal cation complexing properties are expected to be changed also as the flexibility of the macrocycle changes.

1.3. Structural Properties of Macrocyclic Thioether Ligands

Although recent examinations of macrocyclic thioether ligands and their metal complexes have extended the scope of macrocyclic chemistry, the design of these ligands remains largely an empirical exercise and the significance of ligand conformation for coordinating behaviour has not been widely recognized. For example, it has been shown that reaction of [14]aneS4 with Cu^{2+} and Ni^{2+} gives mononuclear complex cations $[Cu([14]aneS4)]^{2+}$ (36) and $[Ni([14]aneS4)]^{2+}$ (37) while reaction with $NbCl_5$ and $HgCl_2$ gives $[(NbCl_5)_2 \cdot [14]aneS4]$ (38) and $[(HgCl_2)_2 \cdot [14]aneS4]$ (39), respectively. Earlier structural work (40-41) has also shown that macrocyclic thioether ligands, including mixed oxygen-sulfur crown ethers, adopt "exodentate conformations" in which the sulfur donor atoms always point out of the ring. On the basis of

these results, it is reasonable to ask why these macrocyclic thioethers adopt "exodentate conformations" in contrast to the "endodentate conformations" of other crowns with oxygen or nitrogen donor atoms and how the conformation of a macrocycle affects its coordinating properties. To answer these questions, structural and conformational studies have been carried out on [14]aneS4 by Glick (42), [9]aneS3 by Glass (43), and [12]aneS3, [12]aneS4, [15]aneS5 and [18]aneS6 by Cooper (44-45). Studies on mixed oxygen- sulfur crown ethers have also been reported (40-41).

Scheme 1-7

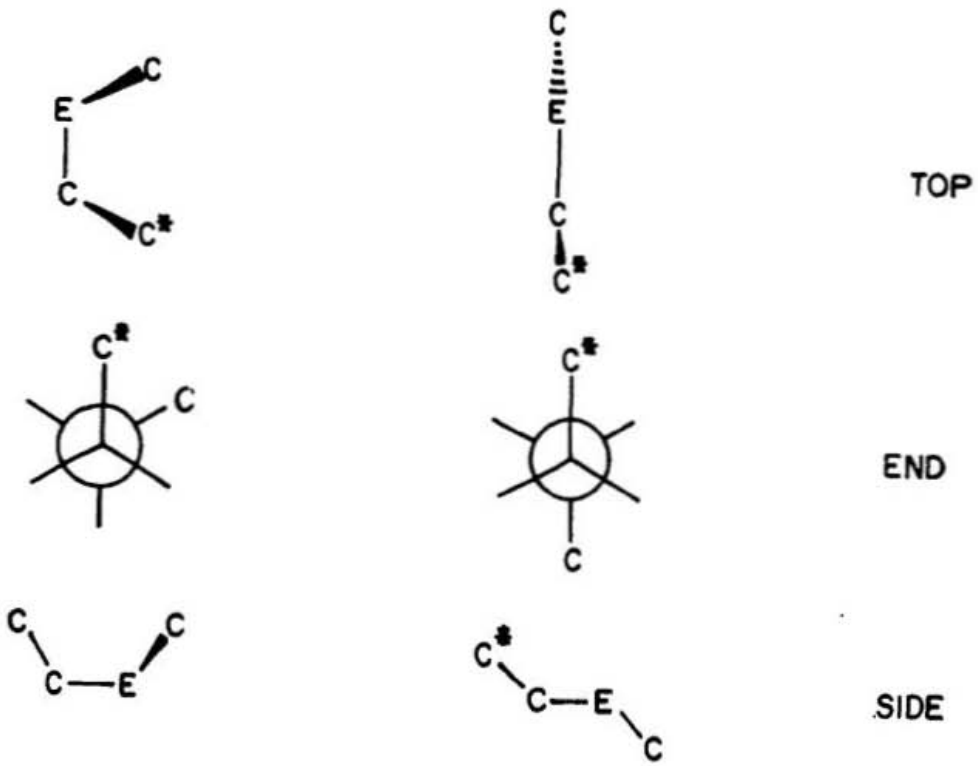

Gauche and anti placement in C-C-E-C Units (E = O, S)

The most important conformational parameters for crown type ligands are torsion angles at C-S and C-C bonds. In a molecular fragment C-C-E-C, the torsion angles of ± 60° at E-C bonds are classified as gauche and those of ± 180° as anti (Scheme 1-7). The torsion angles of macrocyclic thioethers display a clear pattern: all C-S bonds in even-membered rings are surrounded by gauche placements in [12]aneS3, [12]aneS4, [14]aneS4, [18]aneS6 (45) and other mixed oxygen-sulfur crown ethers (40-41). Although odd-membered rings often show anomalous torsion angles because of ring strain (46), [9]aneS3 shows six gauche placements (six of the six C-S bonds) (43) and [15]aneS5 shows seven gauche placements (seven of the ten C-S bonds) (45). Thus, macrocyclic thioethers display a strong preference for gauche placements at the C-S bonds. There is also a clear preference for anti placements about the C-C portion of each C-C-E-C unit. This behaviour contrasts with that of crown ethers (47-48). Exceptions occur when ring strain becomes significant as in the cases of [15]aneS5 (odd-membered ring) and thiophenophanes, which will be discussed in detail in the next chapter.

The marked difference between crown ethers and macrocyclic thioethers has been explained in terms of intramolecular interactions in gauche C-C-E-C and E-C-C-E (E=O,S) fragments (45) as shown in Scheme 1-8.

Mark and Flory (49) pointed out that gauche placement at a CH_2-CH_2-O-CH_2 fragment results in repulsion between the terminal hydrogen atoms since the separation (1.8 Å) of both H atoms is shorter than the sum of their van der Waals' radii (2.4 Å) (50). In the CH_2-CH_2-S-CH_2 fragment, however, the greater length of C-S bonds places the terminal H atoms relatively far apart and gauche placement at C-S bonds suffers little or no repulsion (45). From this point of view, intramolecular interactions in CH_2-CH_2-E-CH_2 fragments disfavor gauche placement at C-O but not C-S bonds

Scheme 1-8

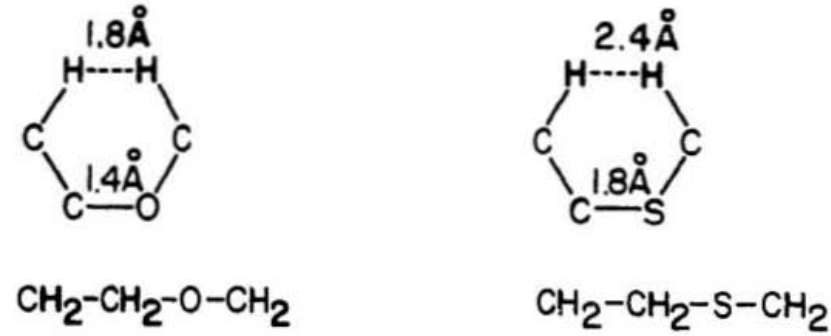

$CH_2-CH_2-O-CH_2$ $CH_2-CH_2-S-CH_2$

Intramolecular interactions in gauche
$CH_2-CH_2-E-CH_2$ (E = O, S) Units

stabilizing destabilizing

Intramolecular interactions in gauche
$E-CH_2-CH_2-E$ (E=O,S) Units

For the interactions between heteroatoms in a $E-CH_2-CH_2-E$ fragment, studies (51-52) have shown that dipersion forces between E atoms (E=N, O, F) stabilize gauche placement at $E-CH_2-CH_2-E$ bonds (attractive gauche effect) while the greater electron-electron repulsion (due to the larger size) between sulfur atoms destabilizes gauche placement at $S-CH_2-CH_2-S$ bonds (repulsive gauche effect). Therefore, intramolecular interactions at $O-CH_2-CH_2-O$ bonds favor gauche placements but those at $S-CH_2-CH_2-S$ bonds do not.

To achieve a cyclic structure some bonds must assume gauche placement at C-E or C-C linkages (45). Since intramolecular interactions in crown ethers favor gauche placement at $O-CH_2-CH_2-O$ bonds but disfavor them at $CH_2-CH_2-O-CH_2$ bonds

and in macrocyclic thioethers the opposite is true, the tendency for gauche placement should follow the order C-S> C-C> C-O (45). This order has been established experimentally.

On the basis of Dale´s observation that even-membered rings with 10-18 members generally adopt quadrangular conformations (square or rectangular) with sides composed of all-anti runs and each corner formed from two successive gauche bonds of the same sign (e.g. $g^{\pm}g^{\pm}$) (46), Cooper (45) has been able to predict the conformation of a macrocycle and to decide whether the heteroatoms will be in the sides (E=O) or the corners (E=S) of the quadrangle. Cooper´s model emphasizes the consequences of torsion strain and non-bonded interactions but neglects dipolar contribution as well as bond length and bond angle deformations. His simplification applies only to ethylene-bridged systems and to molecules of high symmetry. For propylene-bridged and small ring systems, exceptions do occur. For example, in [12]aneS3, four of the six C-S bonds and four of the six C-C bonds assume gauche placements. The conformation of [12]aneS3 resembles that of cyclododecane and [12]aneS4 but with only one sulfur donor atom in the corner and the other two sulfur atoms in the sides of the square (44). In [9]aneS3, all six C-S bonds and three C-C bonds are in gauche placements probably due to the small ring size (43).

As noted by Cooper (45), the two types of intramolecular interactions at C-E and C-C bonds reinforce each other to influence conformation. As a result, macrocyclic thioethers display a strong affinity for "exodentate conformation" and crown ethers for "endodentate conformation". With this in mind, one may ask how these conformations can influence the coordinating properties to transition metals and the structures of their metal complexes.

Unlike other macrocyclic thioether ligands, [9]aneS3 adopts an "endodentate conformation" because of torsional strain in the small ring. It is this special geometric placement of three sulfur donor atoms that makes it especially suitable to form sandwich type complexes and to stabilize some uncommon oxidation states of transition metals with octahedral or elongated octahedral geometries. Examples of this type of complex are $[M([9]aneS3)_2]^{n+}$ (M= Fe(III)/Fe(II) (54-55), Co(III)/Co(II) (54, 56-58) , Ni(II) (57), Cu(II) (57), Zn(II) (59), Cd(II) (59), Ru(II) (60-62), Rh(II) (63-64), Pd(III)/Pd(II) (65-66), Ag(I) (67), Pt(II) (68), Au(III) (69)and Hg(II) (59), $[Mn(CO)_3 \cdot [9]aneS3]_3(PF_6)_2Br \cdot 2H_2O$ (70), $[Mo(CO)_3 \cdot [9]aneS3]$ (71), and $[Fe(C_5H_5) \cdot [9]aneS3]^+$ (72). When ligands such as Cl^- attached to a metal center are not readily replaced by [9]aneS3 it acts as a monodentate ligand with "exo-coordination" as in the case of [Au([9]aneS3)Cl] (73). Also, special geometric requirements may force [9]aneS3 to be an exodentate ligand as in $[Au([9]aneS3)_2]^+$ (69).

The ligand [12]aneS3 is also an exception. Although the conformation of [12]aneS3 is similar to that of [12]aneS4, only one sulfur donor atom is placed in a corner and the other two are in the sides of a square. Reaction of [12]aneS3 with copper(II) chloride affords $[Cu([12]aneS3)_2Cl_2]$, in which only one sulfur donor atom coordinates strongly to the copper atom (44). It is interesting that the conformation of the ligand remains unchanged upon coordination. The conformational preference suggests that the conformation of the free ligand may largely reflect an intrinsic energy minimum rather than crystal-packing forces (44). In $[Ru([12]aneS3)_2](BF_4)_2$, however, both ligands assume an endodentate conformation with three sulfur donor atoms occupying trigonal faces of the octahedral coordination sphere of Ru(II) (61-62) in the absence of coordinating anions. Upon coordination, part of the [12]aneS3 ring retains its conformation and the remainder of the ring suffers considerable conformational

change. Since conformational change requires energy, the stability of a [12]aneS3 complex is expected to be lower than that of a [9]aneS3 complex. This is supported by observations that $[Fe([12]aneS3)_2]^{2+}$ decomposes instantly on contact with water, but $[Fe([9]aneS3)_2]^{2+}$ resists attack by this solvent (62).

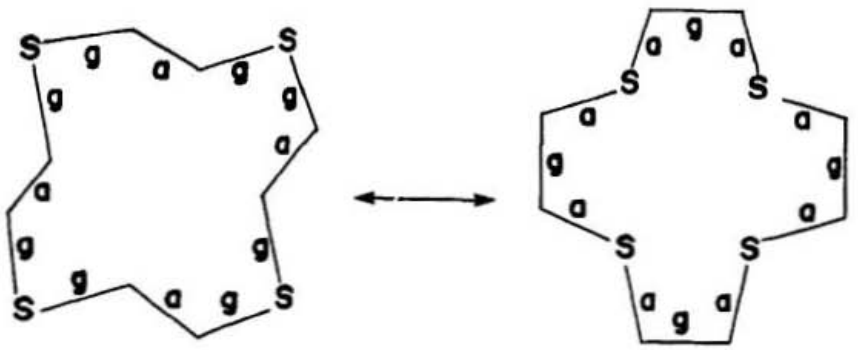

VIII IX

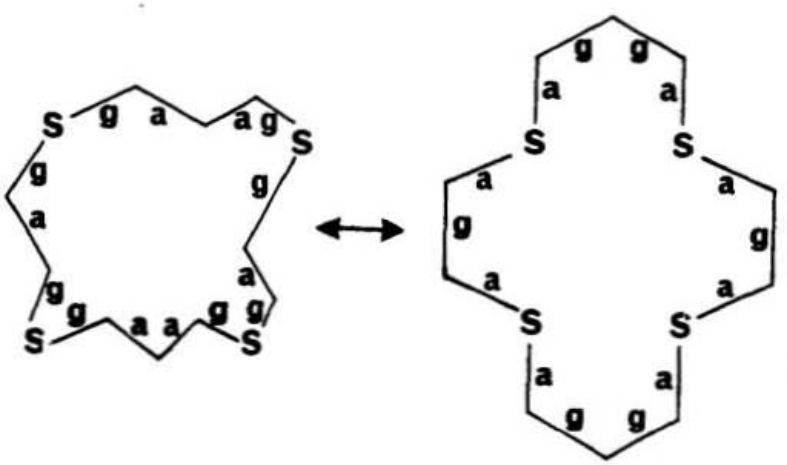

X XI

In [12]aneS4 and [14]aneS4, all four of the sulfur donor atoms point out of the ring (exodentate). By comparing the conformations of the free ligands (VIII and X) and those found in their metal complexes (IX and XI), it can be seen that both conformations (exo/endo) are related by a "pseudo-rotation" process (42), in which each anti is rotated into a gauche interaction and each gauche interaction is rotated into an anti interaction. The process is kinetically controlled but the energy differences between two conformations are relatively small. Coordination to a metal ion requires changes from exo to endo conformations. From a kinetic standpoint, steric hindrance arising from conformational effects in the exo conformers should be minimal with respect to first-bond formation. Second-bond formation, however, requires a major conformational reorganization. This step is expected to be a rate-determining one for chelate formation. Kinetic studies (74-75) on copper(II) complexes of macrocyclic thioethers support second-bond formation as the rate-determining step.

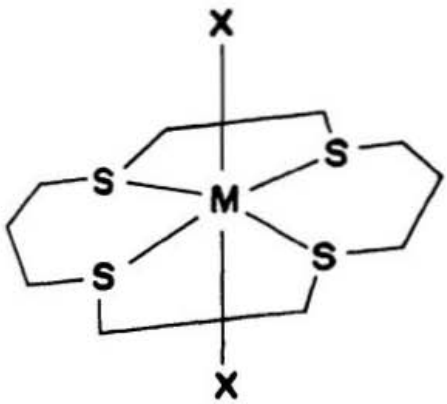

XII

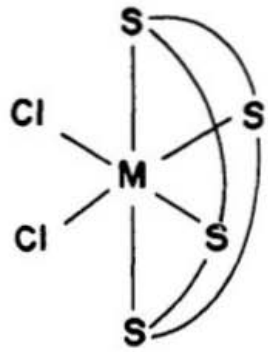

XIII

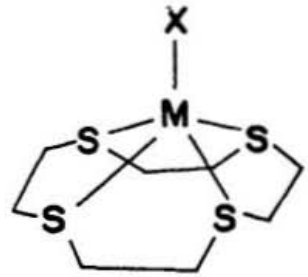

XIV

When the size of a metal ion is such that it fits into the cavity of the macrocycle, the metal ion occupies the cavity of the macrocyclic ring (XII), and the endodentate conformation is stabilized by donation of lone-pair electron density of the sulfur atoms. This conformation has been found in $[Ni([14]aneS4)]^{2+}$ (37), $[Cu([14]aneS4)]^{2+}$, $[Pd([14]aneS4)]^{2+}$ (76) and trans-$[RhCl_2([16]aneS4)]PF_6$ (77). When a metal ion is simply too large to fit into the cavity, either folding to an endodentate cis-configuration (XIII) or exodentate coordination may occur. Examples of this kind are $[Rh([14]aneS4)Cl_2]\cdot 2H_2O$ (78) and $[Ir([14]aneS4)Cl_2](BPh_4)$ (79). A third possibility (XIV) is for the metal to coordinate to a planar endodentate ligand, but for it to reside out of the plane of the ring as in $[Hg([14]aneS4)Cl]^+$ (39), $[Cu([12]aneS4)(H_2O)]^{2+}$ and $[Cu([13]aneS4)(H_2O)]^{2+}$ (80). When the ligands coordinated to the metal are not readily replaced by the macrocycle, exodentate coordination is expected to occur as in $[(HgCl_2)_2\cdot[14]aneS4]$ (39), $[(NbCl_5)_2\cdot[14]aneS4]$ (38), $[Rh_2Cl_2(C_5H_5)_2\cdot[14]aneS4]$ (76) and $[Al(CH_3)_3\cdot[12]aneS4]$ (81-82).

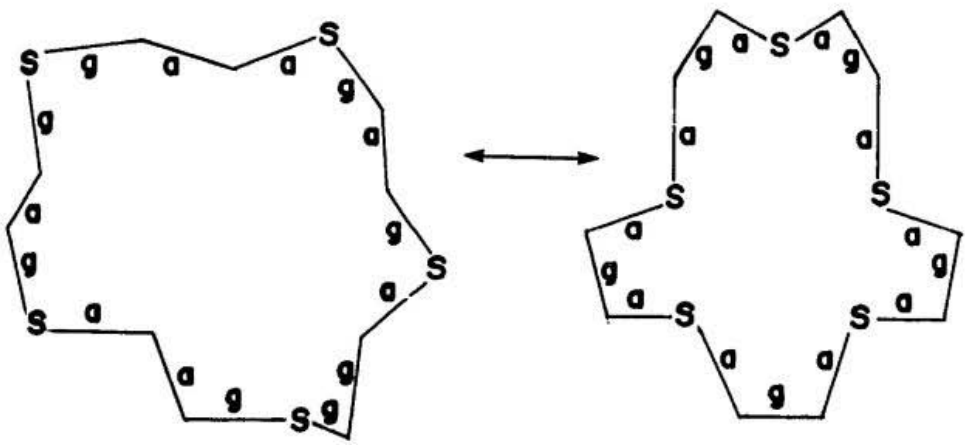

XV XVI

Ligand [15]aneS5 (XV) adopts an irregular shape with all sulfur atoms exodentate (45). Unlike even-membered macrocyclic thioethers, only seven of the ten C-S bonds assume gauche placements and four of five C-C bonds assume anti placements. Upon coordination to Cu(II) as in $[Cu([15]aneS5)]^{2+}$ (83), part of the conformation of [15]aneS5 is retained and the remainder of the molecule suffers a major conformational change with all gauche placements at C-C bonds and anti placements at C-S bonds (XVI).

In [18]aneS6, four of its six sulfur atoms are exodentate and the other two are endodentate. The four exodentate atoms occupy the corners of a rectangle while the other two reside in the sides. These sides buckle to yield gauche placements at the C-S bonds (45). In spite of the endodentate orientation of the two sulfur atoms, all 12 C-S bonds are gauche. When coordinated to metal ions, [18]aneS6 is found to be centrosymmetric and each triad of adjacent sulfur atoms coordinates to a trigonal face of the coordination octahedron or tetragonally distorted octahedron (84). This conformation maximizes the number of gauche placements at C-S bonds and minimizes the energy for conformational changes upon coordination. The fact that all 12 C-S bonds remain gauche suggests that it requires little energy for conformational changes to occur. In this conformation, the metal center is wrapped by [18]aneS6 and the positive charge of the metal ion is dipped into a negatively charged sphere of sulfur donor atoms. In this regard, [18]aneS6 may stabilize unusual oxidation states of some transition metals as does [9]aneS3.

In conclusion, exodentate conformations are characteristic of macrocyclic thioethers and have profound impact on the coordinating behaviour of the ligands and on the structures of their metal complexes. The exodentate conformation of a macrocyclic thioether ligand arises from the reinforcement of intramolecular interactions at

C-C-S-C and S-C-C-S bonds and is largely dependent on the number of atoms in the ring, the flexibility of the hydrocarbon chain as well as ring strain. Coordination to metal ions as a chelating ligand requires conformational changes. Macrocyclic thioether ligands, forming the most stable metal complexes are expected to be those which require least conformational change. This is supported by the fact that [9]aneS3 and [18]aneS6 form very stable complexes with many transition metals.

1.4. Coordination Chemistry of Thioether Ligands

Development of the coordination chemistry of thioethers has been stimulated at least in part by the discovery of thioether coordination to copper in the blue copper proteins (16, 17). Metal ligation through thioethers has been considered to contribute not only to anomalously high redox potentials of these proteins but also to their exceptionally rapid electron transfer reactions. As a result, the recent literature on copper complexes has focussed on thioether ligands, including homoleptic macrocyclic thioethers (80, 83-86), open-chain polythioethers (87) and chelating ligands with built-in thioether and imidazole or pyridine functions (88-91). In addition to reactions involving copper, those with other metals suggest that thioether coordination chemistry is potentially similar to that of phosphines (92, 93) and in some respects is now in a stage of development comparable to that of phosphines thirty years ago. The intent of the present discussion is to provide an overview of the coordination chemistry of thioether ligands under the following headings:

1. Structural, Spectral and Electrochemical Properties of Copper Complexes of Thioether Ligands

2. Stabilization of Low Oxidation States of Metal Ions

3. Stabilization of Unusual Oxidation States of Metal Ions

4. Non-rigidity of Coordinated Thioether Ligands

5. Conclusions

1.4.1. Structural, Spectral and Electrochemical Properties of Copper Complexes of Thioether Ligands

1.4.1.1. Structural Properties of Some Copper Complexes

Some structural data for selected "type 1" copper model compounds are given in Table 1-1. In order to decide whether a Cu-S bond is "normal" in length, it should be compared with 2.34 Å, which is the sum of Pauling's covalent radii (94) for Cu(II) and thioether sulfur.

The structures of copper(II) complexes of a series of macrocyclic tetrathioether ligands show regularities in their coordination geometries as a function of the ring size (80, 85, 86, 88). For a macrocyclic tetrathioether ligand to accommodate Cu(II) coplanar with four sulfur donor atoms, it must have a cavity of 4.61 x 4.61 Å. When the ring contains 14 or more atoms as in [14]aneS4 and [16]aneS4, the sulfur donor atoms form a square planar arrangement around a copper center with perchlorate oxygens at axial positions to complete the overall tetragonally distorted geometry. For those with less than 14 atoms such as [12]aneS4 and [13]aneS4, the cavity of the macrocycle is too small to accommodate the Cu(II) cation. Thus, the copper atom is forced to sit above the plane defined by the four sulfur atoms with water oxygen coordinated axially to produce a five-coordinated square pyramidal complex. The stronger Cu-O interaction in the five-coordinated complexes is suggested to account for the preference for the more basic water oxygen over perchlorate oxygen in these complexes (80).

It is worth noting that despite the slight change in geometry and substitution of a coordinated water for perchlorate anion, the sum of the four Cu-S and one Cu-O bond lengths in these complexes is virtually constant. This observation is in agreement with conclusions drawn by Gazo, Bersuker and coworkers (95) that the sum of all coordinate bond lengths was constant for any series of Cu(II) complexes having the same set of donor atoms regardless of the ligand in which the donor atoms were incorporated e.g. oxygen in H_2O, OH^-, NO_3^-, ClO_4^-, etc.).

Table 1-1: Selected structural data for "type 1" copper models.

complex	Bond	Distance (Å)	Cu-S-C angle (deg.)	Σ Cu-X (Å)	reference
$[Cu([9]aneS3)_2]^{2+}$	Cu-S(1)	2.419(3)	102.9	14.608	(57)
	Cu-S(2)	2.426(3)			
	Cu-S(3)	2.459(3)			
$[Cu([12]aneS4)(H_2O)]^{2+}$	Cu-S(1)	2.34(1)	98.63	11.44	(80)
	Cu-S(2)	2.30(1)			
	Cu-S(3)	2.37(1)			
	Cu-S(4)	2.32(2)			
	Cu-O	2.11(2)			
$[Cu([13]aneS4)(H_2O)]^{2+}$	Cu-S(1)	2.334(4)	101.25	11.447	(80,89)
	Cu-S(2)	2.333(4)			
	Cu-S(3)	2.310(5)			
	Cu-S(4)	2.330(5)			
	Cu-O	2.14(1)			
$[Cu([14]aneS4)(ClO_4)_2]$	Cu-S(1)	2.308(1)	102.20	14.514	(36,89)
	Cu-S(2)	2.297(1)			
	Cu-O	2.652(4)			
$[Cu([15]aneS4)(ClO_4)_2]$	Cu-S(1)	2.3314(13)	107.1	14.402	(89)
	Cu-S(2)	2.3874(17)			
	Cu-O	2.4824(50)			
$[Cu([15]aneS5)]^{2+}$	Cu-S(1)	2.318(2)	100.7	11.67	(86)
	Cu-S(2)	2.398(2)			
$[Cu([18]aneS6)]^{2+}$	Cu-S(1)	2.323(1)	102.25	14.720	(87)
	Cu-S(2)	2.402(1)			

$[Cu(Et_2\text{-}2,2,2\text{-}S4)(H_2O)(ClO_4)]^+$	Cu-S(3)	2.635(1)			
	Cu-S(1)	2.327(4)	104.34	14.418	(80)
	Cu-S(2)	2.329(3)			
	Cu-S(3)	2.316(4)			
	Cu-S(4)	2.338(3)			
	Cu-O(1)	2.296(7)			
	Cu-O(2)	2.812(8)			
$[Cu([9]aneS3)_2]_n^{n+}$	Cu-S(1)	2.342(3)	104.84	9.267	(85)
	Cu-S(2)	2.338(4)			
	Cu-S(3)	2.327(4)			
	Cu-S(4)	2.260(4)			
$[Cu([14]aneS4)]_n^{n+}$	Cu-S(1)	2.260(4)		9.267	(80,89)
	Cu-S(2)	2.338(4)			
	Cu-S(3)	2.327(4)			
	Cu-S(4)	2.342(3)			
$[Cu([15]aneS5)]^+$	Cu-S(1)	2.338(5)	99.3	9.143	(86)
	Cu-S(2)	2.317(5)			
	Cu-S(3)	2.245(5)			
	Cu-S(4)	2.243(5)			
$[Cu([18]aneS6)]^+$	Cu-S(1)	2.245(2)	101.35	9.216	(87)
	Cu-S(2)	2.358(2)			
	Cu-S(3)	2.360(2)			
	Cu-S(4)	2.253(2)			
$[Cu(Py_2\text{-}3,2,3\text{-}S2)(ClO_4)]^+$	Cu-S	2.314(2)	101.20	10.912	(104)
	Cu-N	2.010(5)			
	Cu-O	2.264(5)			
$[Cu(Py_2\text{-}3,2,3\text{-}S2)]^+$	Cu-S	2.345(1)	101.25	8.774	(104)
	Cu-N	2.042(5)			

Furthermore, the bond angles about sulfur in these complexes are approximately tetrahedral, consistent with the presence of a lone pair of electrons in an orbital that can be roughly described as sp^3. Most Cu-S-C angles lie below rather than above the tetrahedral angle. This can be attributed either to the larger steric effect of a lone pair or to a less than complete involvement of the s orbital in any orbital hybridization (94).

In contrast with that of Cu(II) complexes, the overall geometry of Cu(I) complexes of macrocyclic thioether ligands is distorted tetrahedral. In the Cu(II) complexes of [9]aneS3, two [9]aneS3´s coordinate to a copper atom in a slightly distorted octahedral geometry (57). In the Cu(I) complex (85), however, two of the original

Cu-S bonds of one of the two [9]aneS3 ligands in the Cu(II) complex are broken while the ligand re-orientates to give a distorted tetrahedral coordination. In the complex of [14]aneS4, one of the original Cu-S bonds and two Cu-O bonds are broken and the fourth coordination site is then occupied by the free thioether sulfur atom of an adjacent Cu(I)-L complex. The result is a continuous coordination polymer in which each copper atom is bonded to three sulfur atoms of one ligand and one sulfur of a second ligand. The sulfur atom from the second ligand is exodentate. This arrangement maximizes the gauche placements at C-S bonds and accounts for the fact that [14]aneS4 forms a polymeric $[Cu([14]aneS4)]_n^{n+}$ instead of a monomeric $[Cu([14]aneS4)]^+$ (80, 89). In the case of $[Cu(Et_2\text{-}2,3,2\text{-}S4)]^+$, the structural study reveals a polymeric chain in which each copper atom is coordinated to two sulfurs each from two different ligands. The polymeric structure is believed to be fortuitous and it is expected that the complex exists as a tetrahedrally coordinated monomer in aqueous solution (89).

The structure of $[Cu([15]aneS5)]^+$ (86) was found to be monomeric in the solid state with only four Cu-S bonds. Due to the restrictions imposed by the ethylene bridges, the tetrahedral coordination sphere is considerably distorted with three smaller than "normal" S-Cu-S angles formed by the pairs of sulfur atoms which are separated by only one ethylene bridge and a large S-Cu-S angle formed by the two sulfurs on either side of the uncoordinated sulfur atom. This is also observed in $[Cu([18]aneS6)]^+$ (87).

Examination of the copper-sulfur bond distances in Table 1-1 shows that Cu(I)-S bonds are typically shorter than the sum of the covalent radii (2.39 Å) (94), suggesting some π-character in Cu(I)-S bonds. A molecular orbital study suggests a higher affinity of thioether sulfur for softer Cu(I) than Cu(II) (97).

1.4.1.2. Electronic Spectra

One of the most striking features of blue copper proteins is their intense absorption at about 600 nm (ε= 3000 to 5000 $cm^{-1} \cdot M^{-1}$). Solutions of the Cu(II)-polythioethers are intensely colored as a result of strong absorption bands at about 600 and 400 nm (98), the former of which is considerably more intense. Ancillary crystallographic structural studies (36) and single crystal spectra indicate that the characteristic absorption at about 600 nm results from a thioether sulfur to copper charge transfer band which is not dependent on the coordination geometry. From analysis of Raman spectra (99), these two bands have been attributed to S(π)→Cu(II) and S(σ)→Cu(II) charge transfers, respectively. These bands are of great interest since the intense visible absorption exhibited by the blue copper proteins is attributed to a similar S→Cu charge transfer band.

1.4.1.3. Electrochemical Properties

Another characteristic feature of the blue copper proteins is the markedly positive potentials (+0.2 to +0.8 V vs NHE at pH=7) for the Cu(II)/Cu(I) couple. Ligands which sterically and electronically destabilize tetragonal Cu(II) and/or enhance the stabilization of Cu(I) can produce more positive values of the formal Cu(II)/Cu(I) redox potential. Since these proteins have a distorted tetrahedral coordination sphere, some workers have proposed that potentials of these systems are directly related to the copper coordination geometry distortion (100, 101).

Investigation of the redox properties (Table 1-2) (96, 102) of a series of Cu(II) polythioether and polyaminothioether complexes has shown that (i) the large positive Cu(II)/Cu(I) redox potentials do not appear to depend primarily on the coordination sphere's distortion; (ii) coordination to either mercaptide sulfur or thioether sulfur

produces a similar influence on Cu(II)/Cu(I) redox potentials and (iii) decreasing the number of available sulfur donor atoms is accompanied by a dramatic decrease in potential. Based on these observations, it has been suggested that the presence of π-acceptor atoms is more essential to the high redox potentials of blue copper proteins than is the tetrahedral geometry imposed by the protein superstructure (85). This conclusion appears to be corroborated by the study on Cu(II) complexes of tetradentate bis-(pyridyl)-dithioether ligands (103). Structures of Cu(II) and Cu(I) complexes of 1,8-di-2-pyridyl-3,6-dithiooctane (pdto) show that favorable geometries are found for both oxidation states of copper and the Cu(II)/Cu(I) potential of this system exceeds that found for most of the blue copper proteins even though the coordination donor set is nearly identical with that found at "type 1" copper centers (104).

Studies (105) on structural, spectral and electrochemical properties of copper complexes of a series of tripodal ligands have shown that chelate ring size has little influence on the coordination geometry of Cu(I), but has profound consequences for the structure of Cu(II) analogs, with smaller rings favoring trigonal bipyramidal geometry and larger ones favoring square pyramidal geometry. It has been concluded that electron transfer is slower for square pyramidal species where basal ligand displacement is involved than for the trigonal bipyramidal species where a more labile axial site is involved (105).

Table 1-2: Electrochemical properties of copper(II) complexes of polythioether ligands.

Ligand	$E_{1/2}$(mV)[a]	$E_{1/2}$ (mV)	ΔEp (mV)[b]	reference
polythioethers				
[12]aneS3	733(H_2O)	789(80% methanol)	60(H_2O)	(96)
[12]aneS4	641(H_2O)	723(80% methanol)	76(H_2O)	(96)
[13]aneS4	595(H_2O)	674(80% methanol)	63(H_2O)	(96)
[14]aneS4	600(H_2O)[c]	689(80% methanol)	85(H_2O)	(96)
[15]aneS4	727(H_2O)	785(80% methanol)	65(H_2O)	(96)
[16]aneS4	771(H_2O)	798(80% methanol)	70(H_2O)	(96)
[15]aneS5	752(H_2O)	855(80% methanol)	72(H_2O)	(96)
[18]aneS6		720(CH_3NO_2)	60(CH_3NO_2)	(87)
[20]aneS6	718(H_2O)[c]	805(80% methanol)	70(H_2O)	(96)
Me_2-2,3,2-S4	818(H_2O)[c]	892(80% methanol)	74(H_2O)	(96)
Et_2-2,3,2-S4		892(80% methanol)		(96)
polythiolatothioether				
2,3,2-S4(TTU)		842(80% methanol)		(96)
bispyridyldithioethers				
Py_2-2,2,2-S2	596(H_2O)	709(CH_3CN)	99(CH_3CN)	(96,103)
Py_2-2,3,2-S2	643(H_2O)	749(CH_3CN)	110(CH_3CN)	(96,103)
Py_2-3,2,3-S2	577(H_2O)	844(CH_3CN)	120(CH_3CN)	(103,104)
Py_2-3,3,3-S2		894(CH_3CN)	120(CH_3CN)	(103)
polyaminothioethers				
[14]aneS3N	399(H_2O)[c]		83(H_2O, pH=7.8)	(96)
[14]aneS2N2	76(H_2O)		181(H_2O, pH=7.5)	(96)
[14]aneSNNS	155(H_2O)		153(H_2O, pH=7.8)	(96)
[14]aneSN3	255(H_2O)		98(H_2O, pH=8.0)	(96)
2,2,2-NSSN	291(H_2O)		96(H_2O, pH=8.0)	(96)
2,3,2-NSSN		312(80% methanol)		(96)
2,2,2-N4(trien)		-280(80% methanol)		(96)

[a] The $E_{1/2}$ values are based on the lower potential oxidation peak for all systems where two peaks were observed.

[b] ΔEp represents the potential difference of the cathodic and anodic peaks (theoretical value is ΔEp = 57 mV for one-electron reversible systems).

[c] Second oxidation peak appeared at higher potential at very fast sweep rates.

Kinetic studies have revealed an apparent K_{11} value (self-exchange rate constant) of 3×10^4 $M^{-1} \cdot s^{-1}$ for the copper(II)-[15]aneS5 system. This represents the largest self-exchange rate constant reported for any low molecular weight copper system (83). Since the copper center is encased by the hydrophobic ligand in both oxidation states, it is likely that the rapid electron transfer exhibited by this system is a consequence of the hydrophobic environment surrounding the copper center while the donor set in the inner-coordination sphere contributes primarily to the high redox potential. This model accounts for the behaviour of the blue copper proteins because the copper center is encased by a hydrophobic environment in these proteins. In this regard, efficient inorganic copper redox catalysts may be developed by encapsulating a copper ion in a large hydrophobic macrocyclic or acyclic multidentate ligand with substituents blocking the approach of solvent to any unoccupied sites on the metal center.

1.4.2. Stabilization of Low Oxidation States of Metal Ions

As discussed above, high redox potentials are characteristic of copper complexes of macrocyclic thioether ligands. These highly positive potentials are suggested to arise from stabilization of Cu(I) by thioethers, which, like phosphines (85, 86), exhibit π-acidity. Stabilization of low oxidation states of other transition metals by macrocyclic thioethers has also been reported and will be the focus of the following discussion.

As noted before, [9]aneS3 adopts a conformation with all three sulfur atoms endodentate (43). In this conformation, it can be a tridentate ligand without any conformational change. Owing to this geometric placement of the three sulfur atoms many of its metal complexes are found to be of a sandwich type with six donor atoms in a octahedral arrangement.

Reaction of $FeCl_2 \cdot 4H_2O$ with two equivalents of [9]aneS3 in the presence of

$NaClO_4$ produces $[Fe([9]aneS3)_2](ClO_4)_2$. The $[Fe([9]aneS3)_2]^{2+}$ species was found to be diamagnetic in d_6-DMSO solution (54). The electronic spectrum of this complex displays two d-d absorption maxima typical of low spin Fe(II) in an octahedral coordination sphere. Compared with $[Fe([9]aneN3)_2]^{2+}$ (106), [9]aneS3 produces a much stronger ligand field than does [9]aneN3. A structural study has revealed a nearly perfect octahedral environment with two tridentate ligands facially coordinating to the metal center. The S-Fe-S angles average 90° and the average Fe-S bond distance is 2.250 Å. A cyclic voltammogram of $[Fe([9]aneS3)_2]^{2+}$ in acetonitrile shows a reversible one-electron transfer process at $E_{1/2} = +0.982$ V vs Fc^+/Fc(Fc=ferrocene). The ratio i_a/i_c of unity and ΔEp of 90 mV are nearly independent of the scan rate. Since [9]aneS3 also displays a quasi-reversible one electron transfer process at a formal potential of 0.97 V vs Fc^+/Fc, it is difficult to tell whether this is due to oxidation of the metal center or the free ligand in the absence of further detailed evidence.

In 1 M sulfuric acid, $[Fe([9]aneS3)_2]^{2+}$ can be oxidized by PbO_2 at ambient temperature (55). Addition of $NaPF_6$ to the green solution affords $[Fe([9]aneS3)_2](PF_6)_3$. This species was found to be unstable even under a dry argon atmosphere and it is a very strong one-electron oxidant, capable of oxidizing chloride to chlorine and H_2O_2 to oxygen in aqueous solution (55). A cyclic voltammogram of this complex in acetonitrile at a Pt-button working electrode (0.1 M n-Bu_4NPF_6) was found to be identical with that of the corresponding Fe(II) complex under the same conditions (54). Thus, the oxidation at $E_{1/2}$=0.982V vs Fc^+/Fc is due to a one-electron transfer from Fe(II) to Fe(III). The highly positive potential of this Fe(III)/Fe(II) couple indicates a pronounced stabilization of the Fe(II) species by two [9]aneS3 ligands.

It is of interest to note that $[Fe([9]aneS3)_2](PF_6)_3$ displays an effective magnetic moment of 2.09 BM at 110K and 2.46 BM at 293K. These values are very similar to those of $K_3[Fe(CN)_6]$ (107) and indicate a genuine low spin Fe(III) center in a pseudo-octahedral ligand field of six thioether sulfur atoms. This shows that macrocyclic thioether ligands may form complexes with transition metals in high oxidation states, although the low oxidation states are clearly stabilized by thioether π-acidity (55).

In aqueous solution, oxidation of $[Fe([9]aneS3)_2]^{2+}$ by $Na_2S_2O_8$ produces an orange diamagnetic material that contains $[Fe([9]aneS3)_2]^{2+}$ and $[Fe([9]aneS3)([9]aneS3(O))]^{2+}$ in equimolar amounts. From the mother liquor, $[Fe([9]aneS3)([9]aneS3(O))](ClO_4)_2 \cdot 2NaClO_4 \cdot H_2O$ was isolated (55). A structural study reveals a sandwich type coordination of [9]aneS3 and [9]aneS3(O), which occupy the two faces of the octahedron (55).

Reaction of $[Fe(C_5H_5)I(CO)_2]$ with one molar equivalent of [9]aneS3 in refluxing CH_3CN under N_2 affords the complex cation $[Fe(C_5H_5)([9]aneS3)]^+$. It has been fully characterized by nmr and fast atom bombardment mass spectroscopic methods (72). The single crystal X-ray structure confirms the facial coordination of [9]aneS3 and cyclopentadienyl ligands to Fe(II). The average Fe-S bond length is 2.2077(19) Å, which is comparable to those found in $[Fe([9]aneS3)_2]^{2+}$ and in $[Fe([9]aneS3)([9]aneS3(O))]^{2+}$. Cyclic voltammetry of $[Fe(C_5H_5)([9]aneS3)]PF_6$ shows a reversible one-electron Fe(III)/Fe(II) couple at $E_{1/2} = +0.44$ V vs Fc^+/Fc with ΔEp of 63 mV in CH_3CN at a platinum electrode. The redox potential for this process is intermediate between that of $[Fe([9]aneS3)_2]^{2+}$ (54, 55) and ferrocene itself, indicating the destabilization of the Fe(III) by [9]aneS3 relative to a cyclopentadienyl ligand (72).

Cobalt complexes of thioethers have also been reported (54, 56-58). It is of interest to note that attempts to prepare low spin Co(II) complexes of acyclic tetrathioethers have been marginally successful (108, 109) while hexakis(thioether) coordination to Co(II) results in formation of rare low-spin octahedral cobalt(II) complexes (54, 56-58), indicating a stronger ligand field effect from [9]aneS3 than that from its nitrogen-containing analog [9]aneN3 and open chain tetrathioethers. The low-spin character of $[Co([9]aneS3)_2]^{2+}$ is consistent with a d-d transition at 478 nm (ϵ=90 $M^{-1}\cdot cm^{-1}$) and with esr data (56, 110). The solution esr spectrum consists of the expected eight lines for cobalt (I=7/2). The line width is 20.2 G and g_{av}=2.067, suggesting a tetragonal compression of the coordination sphere due to the Jahn-Teller effect. The tetragonal compression has been established by X-ray methods (57).

Cyclic voltammetry of $[Co([9]aneS3)_2](BF_4)_2$ in CH_3CN at a platinum-flag working electrode yields three diffusion-controlled one-electron steps with waves at +0.573, -0.292 and -0.998 V vs NHE (56). It has been proposed that the three waves correspond to Co(III)/Co(II), Co(II)/Co(I) and Co(I)/Co(0). The Co(I)/Co(0) reduction step is irreversible and release of the free ligand has been detected as a result (56). In aqueous 0.1 M NaCl, however, cyclic voltammograms of $[Co([9]aneS3)_2]^{3+}$ display only two quasi-reversible one-electron transfer steps at formal potentials of +0.42 and -0.48 V vs NHE at a gold working electrode. The former is assigned to Co(III)/Co(II) whereas the latter corresponds to the couple Co(II)/Co(I) (58). By comparing the redox potentials of the couples $[Co([9]aneS3)_2]^{3+/2+}$ and $[Co([9]aneN3)_2]^{3+/2+}$ (58), it is clear that the thioether ligand [9]aneS3 strongly stabilizes low oxidation state Co(II), whereas its saturated nitrogen-containing analog [9]aneN3 stabilizes the high oxidation state Co(III).

Oxidation of $[Co([9]aneS3)_2]^{2+}$ by the strong oxidant $Na_2S_2O_8$ affords $[Co([9]aneS3)_2]^{3+}$ in aqueous solution (58), from which $[Co([9]aneS3)_2](ClO_4)_3$ was isolated upon addition of $NaClO_4$. In contrast with $[Co([9]aneN3)_2]^{3+}$, $[Co([9]aneS3)_2]^{3+}$ was shown to be diamagnetic, indicating an increased ligand field strength of [9]aneS3 relative to [9]aneN3. An X-ray structural study (58) has revealed that Co(III) is in a nearly regular octahedral environment of six sulfur atoms. The average Co-S bond distance is 2.253 Å, which is comparable to that found in low spin $[Fe([9]aneS3)_2]^{2+}$ (average Fe-S distance 2.246(1) Å) (58).

The first Ni(II) complex of [18]aneS6 with a 1:1 ligand:metal ratio (as indicated by elemental analysis) was reported by Black and McLean (22a, 111). Examination of $[Ni([18]aneS6)](picrate)_2$ by diffraction methods (112, 113) shows a unique octahedral geometry with the macrocyclic thioether wrapped around the metal center. The Ni-S bond lengths (ranging from 2.376(1) to 2.397(1) Å) are much shorter than the typical values of 2.44(5) Å found for other Ni(II)-thioether complexes of open chain ligands (94, 114). This suggests that [18]aneS6 compresses the Ni coordination sphere by constraining the donor atoms to be close to the metal center.

A very similar structure was reported for $[Co([18]aneS6)](picrate)_2$ (115). However, the Co(II)-S6 coordination sphere suffers a remarkable tetragonal distortion from octahedral microsymmetry due to its d^7 configuration. Magnetic and esr data of the complex demonstrate that it is low spin and d_z^2 is the ground state for the metal ion in agreement with the axial elongation as found in the crystal structure.

Cyclic voltammetry of $[Co([18]aneS6)]^{2+}$ in nitromethane shows a one-electron oxidation wave at +0.844 V vs NHE with ΔEp=77 mV (115). Controlled potential coulometry establishes this to be a one-electron process from Co(II) to Co(III). In

addition, the complex also exhibits an irreversible reduction at -0.16 V vs NHE corresponding to the Co(II)/Co(I) couple. Compared with $[Co([9]aneS3)_2]^{2+}$, it is apparent that a change in ligand from [18]aneS6 to [9]aneS3 decreases the stabilization of Co(II) over Co(III) (decreased $E_{1/2}$) and at the same time permits facile formation of the corresponding Co(I) complex. It has been suggested that the small cavity of [18]aneS6 for Co(I) is responsible for the irreversibility of the second reduction process, whereas in $[Co([9]aneS3)_2]^{2+}$ two tridentate ligands can be further apart. Very similar electrochemical behavior has also been reported for a low spin Co(II) complex of 1,1,1-tris(2-methylthioethylthiomethyl)ethane (116).

In contrast with [18]aneS6 in $[Ni[18]aneS6)]^{2+}$, [24]aneS6 was found to have a cavity large enough to accommodate Ni(II) without any significant compression of its Ni-S bond (113, 117). These results suggest that the cavity size of [24]aneS6 is just suitable for a first row transition metal ion (117). Larger metal ions, in particular those in low oxidation states and those from the second and third row, will require macrocyclic thioether ligands with a larger cavity size to accomplish octahedral coordination.

Recently coordination chemistry of thioether ligands has been extended to second- and third-row transition metals. The macrocyclic thioether coordination chemistry of molybdenum is dominated by the zero oxidation state. Complexes with monodentate ligands are either fairly unstable, $[Mo(CO)_3L_3]$ (L=SMe_2, tetrahydrothiophene, SEt_2) (118-119), or very unstable, $[Mo(CO)_5L]$ (L=SBu_2, tetrahydrothiophene) (120-121). However, $[Mo(CO)_3$·[9]aneS3] was reported to be fairly stable and it showed nc sign of decomposition when exposed to the air for several days (71). The complex $[Mo(CO)_3$·[9]aneS3] is readily prepared in high yield either from the template reaction (Scheme 1-4) (33) or from the reaction of $[Mo(CO)_3(CH_3CN)_3]$ with an equivalent of [9]aneS3 in acetonitrile (71). An X-ray

crystal structure of $[Mo(CO)_3 \cdot [9]aneS3]$ has revealed a pseudo-octahedral symmetry at the metal center with Mo-C≡O fragments that are linear and with angles between carbonyl groups of 90°. It is interesting to note that the Mo-C distances are approximately 0.1 Å shorter than those found in $[Mo(CO)_6]$ (122), and the CO stretching frequencies are reduced by ~ 200 cm^{-1}. These results suggest that [9]aneS3 is an ineffective π-acid in comparison with carbonyl groups (33).

Yoshida and coworkers (123) reported the first example of a Mo(0) dicarbonyl complex, trans-$[Mo(CO)_2(Me_8[16]aneS4)]$, which is stable at room temperature. A structural study revealed an octahedral geometry with all four thioether sulfur atoms coplanar and two carbonyl groups in the axial positions. The Mo-S distances (average 2.436(2) Å) are considerably shorter than those found in $[Mo(CO)_3 \cdot [9]aneS3]$ (average 2.520(6) Å), presumably due to the absence of the stronger trans effect of carbonyl groups at trans positions.

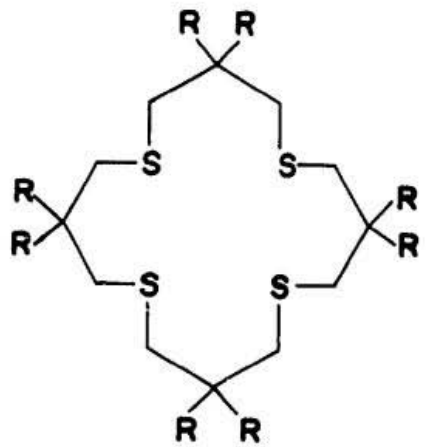

XVII R=H
XVIII R=Me

Mo(II) forms a variety of complexes with thioether ligands (93). A dimeric complex $[Mo(SH)([16]aneS4)]_2^{2+}$ has been reported (124). Two Mo(II) centers are shown to be bridged by [16]aneS4 (XVII) and each Mo(II) center contains an unusual terminal SH group. In ethanol the dimeric complex converts to the monomeric $[MoO(SH)([16]aneS4)]^+$ (125).

A paramagnetic Mo(II) dibromo complex trans-$[Mo(Me_8[16]aneS4)Br_2]$ has also been prepared by Yoshida and coworkers (123). It was obtained from the reaction of $[MoBr_2(CO)_4]_2$ with two molar equivalents of Me_8[16]aneS4 (XVIII) in toluene under reflux. A similar reaction of $[MoCl_2(CO)_4]_2$ with Me_8[16]aneS4 did not yield the corresponding Mo(II) dichloro complex; instead fac-$[MoCl_3(Me_8[16]aneS4)]$ was isolated as paramagnetic orange crystals. Alternatively, fac-$[MoCl_3(Me_8[16]aneS4)]$ was obtained in high yield (71%) by treating $[MoCl_4(CH_3CN)_2]$ with Me_8[16]aneS4 in CH_2Cl_2 at room temperature. Reduction of fac-$[MoCl_3(Me_8[16]aneS4)]$ with Zn powder in CH_2Cl_2 gives trans-$[MoCl_2(Me_8[16]aneS4)]$ as paramagnetic yellow crystals. Cyclic voltammetry of trans-$[MoBr_2(Me_8[16]aneS4)]$ and trans-$[MoCl_2(Me_8[16]aneS4)]$ in CH_3CN (0.1 M n-Bu_4NBF_4) at a scan rate of 100 mV/s shows two essentially reversible redox couples due to Mo(III)/Mo(II) ($E_{1/2}$ = +1.21 V vs SCE, ΔEp = 120 mV, i_a/i_c = 1.00 for trans-$[MoBr_2(Me_8[16]aneS4)]$; $E_{1/2}$ = +1.19 V vs SCE, ΔEp = 80 mV, i_a/i_c = 1.22 for trans-$[MoCl_2(Me_8[16]aneS4)]$) and Mo(II)/Mo(I) ($E_{1/2}$ = -0.15 V vs SCE, ΔEp = 100 mV, i_a/i_c = 0.92 for trans-$[MoBr_2(Me_8[16]aneS4)]$; $E_{1/2}$ = -0.28 V vs SCE, ΔEp = 75 mV, i_a/i_c = 1.08 for trans-$[MoCl_2(Me_8[16]aneS4)]$). The high redox potential for Mo(III)/Mo(II) results probably from stabilization of Mo(II) relative to Mo(III) by π-acidity of thioether sulfur atoms.

Reaction of rhodium(III) triflate with 2 molar equivalents of [9]aneS3 in methanol affords a homoleptic thioether complex $[Rh([9]aneS3)_2]^{3+}$ with slightly distorted octahedral geometry (63-64). Cyclic voltammetry in nitromethane on a glassy carbon electrode shows two quasi-reversible one-electron processes at -0.309 and -0.720 V vs SCE (ΔEp=71 and 98 mV, respectively, at a scan rate of 50 mV/s). Preparative electrolysis at -0.5 V vs SCE gives the corresponding Rh(II) complex. Esr studies (64) show that the Rh(II) complex may have an octahedral geometry with axial elongation due to Jahn-Teller distortion of a d^7 system.

The exceptional stability of $[Rh([9]aneS3)_2]^{2+}$ with respect to disproportionation ($K_{disp} = 10^{-7}$) demonstrates again that thioether ligands tend to stabilize low oxidation states of transition metals by virtue of their π-acidity while the six-coordinate environment imposed by the rigid conformation of [9]aneS3 destabilizes Rh(I), which usually adopts square planar coordination geometry.

The complex $[Ru([9]aneS3)_2](CF_3SO_3)_2$ has also been obtained from the reaction of $Ru(CF_3SO_3)_2$ with two equivalents of [9]aneS3 in methanol. X-ray diffraction methods (60-62) reveal an almost perfect octahedral geometry. Cyclic voltammetry in nitromethane on a glassy carbon electrode shows an oxidation wave at $E_{1/2} = +1.8$ V vs NHE. The high redox potential indicates that [9]aneS3 interacts much more strongly with Ru(II) than with Ru(III). In comparison with amines and H_2O, [9]aneS3 imposes a much stronger ligand field and nephelauxetic effect (62). Ligand [12]aneS3 is also shown to coordinate to Ru(II) in a very similar way to that of [9]aneS3 (62). The resulting trigonal flattening in $[Ru([12]aneS3)_2]^{2+}$ reflects the large effective size of [12]aneS3 relative to that of [9]aneS3.

1.4.3. Stabilization of Unusual Oxidation States of Metal Ions

As noted previously, [9]aneS3 is especially suitable for occupying one or two faces in an octahedral complex. In this regard, metal ions with a strong preference for octahedral coordination are expected to be stabilized by [9]aneS3 and other related macrocyclic thioether ligands such as [12]aneS3, [18]aneS6, [20]aneS6 and [24]aneS6.

Reaction of [9]aneS3 with $PdBr_2$ gives a monomeric complex [$PdBr_2$·[9]aneS3] (65), in which the Pd atom is surrounded by a distorted square pyramidal array of two Br and three sulfur atoms. The apical Pd-S distance is significantly longer than those at equatorial positions. In the absence of strongly coordinating anion ligands, however, $[Pd([9]aneS3)_2](PF_6)_2 \cdot H_2O$ was isolated (65). An X-ray structural study reveals that the Pd atom is located in a distorted octahedral environment with four short equatorial Pd-S bonds and two weak Pd-S interactions in the two axial positions. Since Pd(II) prefers a square planar coordination, the above observation suggests that the weak Pd-S interactions may be derived from constraints imposed by [9]aneS3 ligands and these interactions may facilitate formation of higher oxidation state Pd(III), which prefers octahedral coordination.

Cyclic voltammetry of $[Pd([9]aneS3)_2]^{2+}$ in CH_3CN at 20℃ (0.1 M n-Bu_4NPF_6) shows a reversible redox wave at $E_{1/2}$ = +0.65 V vs Fc^+/Fc with ΔEp of 84 mV (66). The complex $[Pd([9]aneS3)_2]^{2+}$ can be oxidized chemically (70% $HClO_4$) and electrochemically. Controlled potential oxidation of $[Pd([9]aneS3)_2]^{2+}$ at +0.70 V at a platinum gauze in CH_3CN affords an orange solution (λ_{max} =476 nm, ϵ =5350 $M^{-1} \cdot cm^{-1}$), the esr spectrum of which as a frozen glass at 77K shows an anisotropic signal with $g_{||}$ =2.008, $g_{\perp}$ =2.048, g_{av} =2.032. Electronic and esr spectral data are consistent with the formation of an oxidized paramagnetic Pd(III) complex. The

single crystal X-ray diffraction study of $[Pd([9]aneS3)_2](ClO_4)_3 \cdot HClO_4 \cdot 4H_2O$ shows that the Pd atom is bonded to six sulfur atoms in a tetragonally elongated octahedral geometry as expected for a d^7 Pd(III) (66). In contrast with the corresponding Pd(II) complex, the axial thioether sulfur atoms are brought in towards the metal center. Therefore, the Pd(III) oxidation state is stabilized by an octaheral coordination sphere of sulfur donor atoms.

Reaction of $PtCl_2$ with two equivalents of [9]aneS3 affords $[Pt([9]aneS3)_2](PF_6)_2$ in the presence of NH_4PF_6 (68, 76). A structural study shows that the central Pt atom is coordinated by four sulfur donor atoms from two [9]aneS3 molecules in a square plane. An elongated square pyramidal coordination sphere is achieved using the third sulfur atom from one of the two ligand molecules giving a Pt-S (apical) distance of 2.90 Å. Unlike its Pd(II) analog, $[Pd([9]aneS3)_2]^{2+}$, the final ligand sulfur atom does not interact with Pt (Pt-S=4.11 Å). Cyclic voltammetry of $[Pt([9]aneS3)_2](PF_6)_2$ in CH_3CN shows a quasi-reversible one-electron redox wave with $E_{1/2} = +0.39$ V vs Fc^+/Fc and $\Delta Ep = 145$ mV. Controlled potential electrolysis of $[Pt([9]aneS3)_2]^{2+}$ ($\lambda_{max} = 432$ nm, $\varepsilon = 95\ M^{-1} \cdot cm^{-1}$) at +0.5 V under N_2 in CH_3CN affords a stable oxidized product $[Pt([9]aneS3)_2]^{3+}$ ($\lambda_{max} = 401$ nm, $\varepsilon = 3500\ M^{-1} \cdot cm^{-1}$). The esr spectrum (77K, CH_3CN) shows an anisotropic signal with $g_\perp = 2.044$, $g_{||} = 1.978$ with coupling to 195 Pt (33.8%), $A_\perp = 30$ G, $A_{||} = 85$ G ($1G = 10^{-4}$ T). These results suggest that it may have a similar coordination geometry to that of $[Pd([9]aneS3)_2]^{3+}$. It has been proposed that the ability of [9]aneS3 to adjust its mode of coordination is responsible for the high stability of Pt(III) (68, 76).

Reaction of $PdCl_2$ or $PtCl_2$ with [18]aneS6 gives a 1:1 product $[M([18]aneS6)]^{2+}$ (M=Pd and Pt) (76, 126). Structural studies of these complexes confirm the square planar coordination of four thioether sulfur donors to the metal ions (Pd-S=2.309 Å

and Pt-S=2.296 Å) with two remaining sulfur atoms of [18]aneS6 essentially nonbonded (Pd-S=3.273 Å, Pt-S=3.380 Å). In contrast with $[M([9]aneS3)_2]^{2+}$ (M=Pd and Pt), complexes $[M([18]aneS6]^{2+}$ show no oxidative processes by electrochemical methods (76). It has been suggested that the inability of [18]aneS6 to complete octahedral coordination to Pd(II) and Pt(II) centers may contribute to the electrochemical inactivity of these complexes (76). From the crystal structure of $[M([18]aneS6)]^{2+}$, it appears that the cavity of [18]aneS6 is too small to fully encapsulate the large Pd(II) and Pt(II) ions octahedrally. From this point of view, Pt(III) and Pd(III) may be stabilized by more flexible macrocyclic thioethers with larger ring cavities or by replacement of two nonbonded thioether sulfurs with smaller nitrogen donors. This has been shown to be true by Blake and coworkers (127) from studies of N_2S_4 macrocycles (XIX and XX).

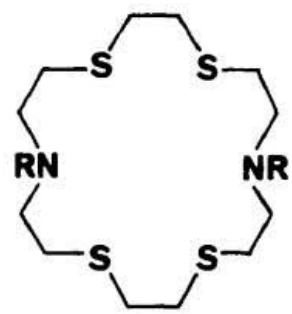

XX **R=H**
XIX **R=Me**

Structural studies (127) have shown that $[Pd(Me_2[18]aneN2S4)]^{2+}$ has a square planar coordination sphere of four thioether sulfur donor atoms (average Pd-S=2.3308 Å). Two nitrogen atoms are oriented away and do not interact with Pd(II) (Pd-N=3.744(7) and 3.760(6) Å). In $[Pd([18]aneN2S4)]^{2+}$, however, the Pd atom is

coordinated to an N_2S_2 donor set in a square planar configuration (average Pd-S=2.334(3) Å; average Pd-N=2.095(7) Å). The two remaining thioether sulfur atoms interact weakly in axial positions of Pd(II) (average Pd-S=2.977(4) Å). The overall geometry is distorted octahedral with one of four thioether sulfur atoms and two nitrogen atoms binding meridionally to the Pd atom in $[Pd([18]aneN2S4)]^{2+}$ while the coordination geometry at Pd in $[Pd([18]aneS6]^{2+}$ is square planar with two non-bonded sulfur atoms. By comparison with $[Pd(Me_2[18]aneN2S4)]^{2+}$, it is clear that the steric effect of two methyl groups on the N-donors prevents coordination of Me_2[18]aneN2S4. The stereochemical differences are expected to be reflected by electrochemical properties of these compounds.

Cyclic voltammetry of $[Pd(Me_2[18]aneN2S4)]^{2+}$ in CH_3CN at Pt electrodes shows a reversible one-electron reduction at -0.74 V vs Fc^+/Fc with $\Delta Ep=72$ mV at a scan rate of 100 mV/s. The esr spectrum (77K, CH_3CN glass) is shown to be anisotropic ($g_{||}$ 2.115, $g_{\perp}$ 2.049) with coupling to ^{105}Pd (I=5/2, 22%) and $A_{||}$ 48 G and $A_{\perp}$ 34 G, which is consistent with the presence of a mononuclear d^9 Pd(I) species (127). However, the related homoleptic thioether complexes $[Pd([18]aneS6)]^{2+}$ and $[Pd([9]aneS3)_2]^{2+}$ show irreversible reductions at Ep=-0.75 V and -0.875 V vs Fc^+/Fc, respectively, in CH_3CN at 293K. These differences are suggested to be caused by the larger ring cavity and flexibility of Me_2[18]aneN2S4 than that of [18]aneS6 (27). Furthermore, $[Pd([18]aneN2S4)]^{2+}$ shows a chemically reversible oxidation wave at $E_{1/2}=+0.57$ V vs Fc^+/Fc with $\Delta Ep=195$ mV at a scan rate of 150 mV/s. A totally irreversible reduction is also observed at Ep=-1.03 V at 293K. The esr spectrum of the oxidized product suggests the formation of a monomeric d^7 Pd(III) species. Based on these results, it appears that the high oxidation state of Pd(III) can be stabilized by 4+2 coordination of a macrocyclic thioether ligand in a distorted

octahedral geometry while stabilization of low oxidation state Pd(I) can be achieved by tetrahedrally coordinating macrocyclic ligands with π-acidity and a larger ring cavity.

In general, silver(I) shows a preference for linear two-coordination and, occasionally, tetrahedral four-coordination. Higher coordination numbers may be achieved by constraints imposed by macrocyclic ligands (128, 129). These complexes usually exhibit irregular geometries and ambiguous coordination numbers due to poor "fit" between the ligand and the metal center. However, reaction of silver triflate with two equivalents of [9]aneS3 gives $[Ag([9]aneS3)_2]CF_3SO_3$, in which the Ag atom is sandwiched by six sulfur donor atoms with Ag-S distances ranging from 2.696(2) to 2.753(3) Å (130). The coordination sphere around Ag deviates from octahedral geometry by virtue of a severe trigonal elongation. The distorted octahedral geometry of $[Ag([9]aneS3)_2]^+$ suggests that the corresponding Ag(II) complex may be stabilized by six-coordinate geometry imposed by rigid [9]aneS3. Cyclic voltammetry of $[Ag([9]aneS3)_2]^+$ in nitromethane (0.1 M Et_4NBF_4) at a platinum wire working electrode shows a quasi-reversible oxidation wave at $E_{1/2} = +1.30$ V vs NHE with $\Delta Ep = 106$ mV at a scan rate of 500 mV/s (130). On electrolysis at +1.5 V vs NHE, the colorless solution becomes deep blue. Esr spectral data are consistent with the presence of paramagnetic $[Ag([9]aneS3)_2]^{2+}$. The low oxidation potential (1.30 V vs NHE, cf $E° = 1.98$ V vs NHE (130, 131) for the Ag(II)/Ag(I) couple) has been suggested to be a consequence of the enhancement of the "electron richness" of the metal ion by virtue of the high coordination number (130).

Reaction of $AgNO_3$ with one molar equivalent of [18]aneS6 affords a colorless product $[Ag([18]aneS6)]PF_6$, which is shown by X-ray methods (132) to have a distorted octahedral geometry around Ag(I) with four equatorial Ag-S bonds (average

Ag-S=2.7813(10) Å) and two short apical Ag-S bonds (average Ag-S=2.6665(12) Å). Usually $[M([18]aneS6)]^{2+}$ complexes show a tetragonally elongated octahedral coordination sphere, but $[Ag([18]aneS6)]^{+}$ has a tetragonally compressed octahedral stereochemistry. The ability of [18]aneS6 to encapsulate Ag^{+}, which is much larger than first row transition metal ions, suggests that the cavity of macrocyclic thioether ligands can be flexible depending upon the size of the metal ion and the strength of the interaction between the metal center and donor atoms. Cyclic voltammetry of $[Ag([18]aneS6)]^{+}$ in CH_3CN (0.1 M n-Bu_4PF_6) at a platinum working electrode shows an essentially irreversible oxidation wave. Addition of concentrated H_2SO_4 (98%) solution to $[Ag([18]aneS6)]^{+}$ at 298K affords a blue solution (λ_{max}=564 nm, ϵ=5000 $M^{-1}\cdot cm^{-1}$). The esr spectrum of the frozen glass at 77K shows a paramagnetic Ag(II) species. In comparison with $[Ag([9]aneS3)_2]^{2+}$, $[Ag([18]aneS6)]^{+}$ is less stable and the blue solution decays to colorless quickly (130) while $[Ag([9]aneS3)_2]^{2+}$ is stable at room temperature for several days.

Like Ag(I), d^{10} Au(I) has a particularly strong preference for linear two-coordination. However, studies (69) show that $[Au([9]aneS3)_2]PF_6$ has a structure that is a combination of linear and tetrahedral coordination at Au(I) with two short Au-S bonds (Au-S=2.302(6) and 2.350(7) Å) and two long Au-S bonds (Au-S=2.733(8) and 2.825(8) Å). This contrasts with that of $[Ag([9]aneS3)_2]^{+}$, in which Ag(I) is bonded by six sulfur atoms in a slightly distorted octahedral geometry. The complex $[Au([9]aneS3)_2]^{+}$ can be readily oxidized chemically or aerially to give a Au(II) species as evidenced by the esr spectrum of the oxidized product (69). Further oxidation of the Au(II) species affords a Au(III) analog $[Au([9]aneS3)_2]^{3+}$ (λ_{max}=460, 340, 254 nm), in which the Au atom is coordinated by six sulfur donor atoms in a distorted octahedral geometry with four equatorial Au-S bonds (average

Au-S=2.351(4) Å) and two weak apical interactions (average Au-S=2.926(4) Å). It is proposed that the facile interconversion of $Au^{3+/2+/+}$ species in the presence of [9]aneS3 is caused by the ability of [9]aneS3 to adjust its coordination modes as a formal 2-, 4-, or 6-electron donor (69).

The coordinating properties of [9]aneS3 and related macrocyclic thioethers with d^{10} metal ions such as Zn(II), Cd(II) and Hg(II) have also been investigated (59). It is very interesting that cyclic voltammetry of $[Hg([9]aneS3)_2]^{2+}$ in CH_3CN (0.1 M n-Bu_4NP_6) at Pt electrodes shows a chemically reversible reduction at $E_{1/2}$=-0.15 V vs Fc^+/Fc with ΔEp=80 mV at a scan rate of 90 mV/s (59). The low redox potential for the Hg(II)/Hg(I) couple (in aqueous solution E°=0.911 V vs NHE for Hg(II)/Hg(I)) suggests that Hg(II) is strongly stabilized by hexathia coordination by virtue of stereochemical constraints imposed by [9]aneS3 rather than by π-acidity. On the other hand, the strong preference of Hg(I) for the formation of Hg_2^{2+} species may also contribute to the instability of Hg(I) in CH_3CN.

1.4.4. Non-rigidity of Coordinated Dithioether Ligands

The pyramidal environment at coordinated sulfur atoms has been conclusively established by X-ray methods (93). Rapid inversion at coordinated thioether sulfur is very common and the stereodynamics of metal complexes of sulfur containing ligands have been reviewed extensively by Abel and coworkers (133). The intent of the following discussion is to examine the dynamic non-rigidity of open-chain dithioether and macrocyclic thioether ligands in palladium(II) and platinum(II)/(IV) complexes.

1.4.4.1. Inversion at Coordinated Thioether Sulfur

The majority of inversion studies of transition metal complexes have involved palladium(II) and platinum(II)/(IV) complexes of thioether ligands. The ability of nmr methods to differentiate between the syn and anti isomers of Pd(II) and Pt(II) chelate complexes and their interconversions at high temperatures has generated numerous studies (133, 134-138) of inversion at coordinated thioether sulfur atoms.

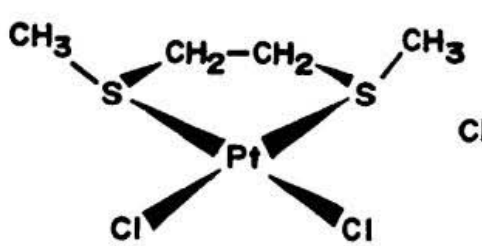

syn
(or meso)

XXI

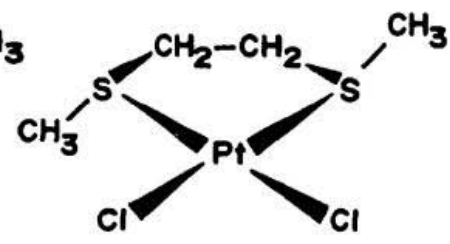

anti
(or d,l)

XXII

The temperature-dependent ^{1}H nmr spectra of $[PtCl_2(MeSCH_2CH_2SMe)]$ (139) show that at low temperature there are two isomers (XXI and XXII) in the solution, which interconvert at high temperatures as evidenced by the coalescence of two sets of resonance signals originating from the methyl groups. The palladium(II) complex resembles the platinum(II) analog, but coalescence occurs at a much lower temperature. The coalescence of methyl hydrogen signals is suggested to be caused by inversion at coordinated sulfur atoms (140). Since the calculated activation energy for

the rapid inversion at sulfur atoms is 5 Kcal/mol for $[PtCl_2(MeSCH_2CH_2SMe)]$ (139) and 18 Kcal/mol for $[PtCl_2\{(PhCH_2)_2S\}_2]$ (140), it was proposed that the mechanism for the inversion process may involve a simultaneous bond-making by the S lone-pair as the original coordinate bond breaks (139-140) (Scheme 1-9). Thus inversion proceeds through a planar transition state stabilized presumably by back-bonding from the metal to sulfur. However, this hardly explains the fact that inversion occurs in complexes of dimethyl sulfide with BH_3 (141) and BCl_3 (142).

Scheme 1-9

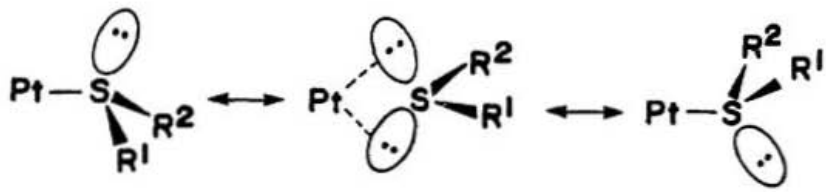

For bidentate dithioether complexes (139), a skew conformation is expected for the ethylene bridge. The relative positioning of the alkyl groups outside the bridge may be either both up with respect to the plane of the chelate ring or one may be up and one down (XXI and XXII). This will produce a meso- and d,l-enantiomeric pair of isomers, respectively. By analysis of the temperature-dependent ^1H nmr spectra of $[PdX_2(BzSCH_2CH_2SBz)]$ (X=Cl and Br) (143) using computer simulation of the spectra for complex spin systems under exchange conditions, it has been demonstrated that inversion at coordinated sulfur atoms is responsible for the coalescence of the ethylene hydrogen signals as well as for other spectral changes that occur as the sample's temperature is raised.

1.4.4.2. Fluxionality of Cyclic Thioether Ligands

In a metal complex of mono- and/or bidentate thioether ligands, pyramidal inversion of coordinated sulfur atoms occurs at high temperatures as indicated by the coalescence of hydrogen resonances of the ligand. Such intramolecular movements in many cases are the prelude to additional stereochemical non-rigidity in metal complexes (133). In a metal complex of a macrocyclic thioether ligand, inversion of coordinated sulfur atoms is largely restricted due to the relative rigidity of the coordinated macrocycle and ligand pivoting may occur instead. This involves considerable reorganization of M-S bonding and leads to metallotropic shifts.

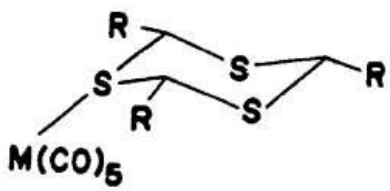

XXIII (R=H, M=Cr and W)

XXIV (R=Me, M=Cr and W)

An early example of this kind of fluxional behavior was reported by Schenck and Schmidt (144) in Group VI metal pentacarbonyl complexes of β-2,4,6,-trimethyl-1,3,5-trithian, $[M(CO)_5(\overline{SCHMeSCHMeSCHMe})]$ (M=Cr and W). The bandshape changes of the ^1H nmr spectra of XXIV (R=Me, M=Cr and W), between -10 and 30°C implied an equilibration of the three methyl groups. The coalescence of methyl resonances was suggested to be a consequence of an intramolecular commutation of the $M(CO)_5$ moiety over all three sulfur donor atoms via 1,3-metallotropic shifts (144). Analogous motion was, however, not observed in the unsubstituted ring complexes (XXIII) (R=H, M=Cr and W), the spectra at 30°C being consistent with coordination of the heterocyclic ligand via a single sulfur atom.

Complexes of Pt(IV) with other cyclic polythioether ligands such as 1,3,5-trithian (145) and 1,3,5,7-tetrathian (146) have also been investigated by ^{1}H nmr methods and 1,3- and 1,5-metallotropic shifts were observed. Although 1,3- and 1,5-shifts are well documented (133), only one example of a 1,4-shift has been reported (147-148), which involves a platinum(IV) complex of [12]aneS4.

Complexes $[PtMe_3 \cdot L]^+$ (L=[9]aneS3, [12]aneS4 and [12]aneOS3) were obtained from the reaction of $[PtClMe_3]_4$ with an excess of appropriate macrocyclic thioether ligands and recrystallization from dichloromethane-hexane (147-148). The ^{1}H and ^{13}C nmr spectra of [12]aneS4 and [12]aneOS3 complexes show that both complexes adopt similar structures in which, however, one of the sulfur atoms in [12]aneS4 and the oxygen atom in [12]aneOS3 remain uncoordinated. At low temperature (243K), the ^{1}H spectrum of $[PtMe_3 \cdot$[12]aneS4] exhibits two platinum-methyl resonances, which collapse at higher temperatures (>333K) to give a single platinum methyl signal (δ 1.12 ppm, ^{3}J (Pt-H) 66.9 Hz) while the methylene resonance simplifies to an AA'BB' multiplet. The coalescence of platinum methyl signals is suggested to be caused by an intramolecular ligand rotation fluxion proceeding via a series of correlated 1,4-metallotropic shifts. These studies also show that the presence of at least one uncoordinated sulfur atom is necessary for the proposed 1,4-shift.

1.5. Conclusions

In conclusion, the conformations of macrocyclic thioether ligands have profound influence on their coordinating properties and structures of their metal complexes. The ability of macrocyclic thioether ligands to adjust their coordination modes is responsible for their controversial stabilization of both low oxidation states and some unusual high oxidation states of transition metals. Like the corresponding phosphines,

thioethers can stabilize the low oxidation states of transition metals by virtue of their π-acidity. On the other hand, some unusual higher oxidation states of transition metals may also be stabilized by a coordination sphere of thioether sulfurs and by steric constraints imposed by macrocyclic thioether ligands. Application of these properties of macrocyclic thioethers to organometallics should produce a very rich chemistry in this area of study and will stimulate further fruitful studies of the organometallic chemistry of these macrocyclic thioether complexes.

1.6. References

1. C.J. Pederson. J. Am. Chem. Soc. *89*, 7017 (1967).
2. R.M. Izatt and J.J. Christensen. *Progress in macrocyclic chemistry*. Vol. 1, John Wiley and Son, New York. 1979.
3. G.A. Melson. *Coordination chemistry of macrocyclic compounds*. Plenum Press, New York. 1979.
4. B. Dieltrich. J. Chem. Educ. *62*, 954 (1985).
5. D.J. Cram. Angew. Chem. Int. Ed. Engl. *25*, 1039 (1986).
6. a: D.J. Cram. Angew. Chem. Int. Ed. Engl.*27*, 1009 (1988); b: J.M. Lehn. Angew. Chem. Int. Ed. Engl. *27*, 89 (1988).
7. a: P.G. Potvin and J.M. Lehn. In *Synthesis of macrocycles: the design of selective complexing agents* (*Progress in macrocyclic Chemistry* (Vol. 3)). Edited by R.M. Izatt and J.J. Christensen, Wiley, New York. 1987. p. 167; b: G. van Binst. *Design and synthesis of organic molecules based on molecular recognition*. Springer, Berlin. 1986.

8. R.M. Izatt, J.S. Bradshaw, S.A. Nielson, J.D. Lamb, J.J. Christensen and D. Sen. Chem. Rev. *85*, 271 (1985).

9. G.W. Gokel and H.D. Durst. Synthesis 168 (1976).

10. a: J.M. Lehn. In *Physical chemistry of transmembrane ion motions*. Edited by G. Spach. Elsevier, Amsterdam. 1983. p.181; b: J.M. Lehn. In *Biomimetic chemistry*. Edited by Z.I. Yoshida and N. Ise. Konasha, Tokyo/Elsevier, Amsterdam. 1983. p. 163.

11. a: J.S. Bradshaw and J.Y. Hui. J. Heterocycl. Chem. *11*, 649 (1974); b: J.S. Bradshaw and P.E. Scott. Tetrahedron *36*, 461 (1980); c: G.G. Newkome, J.D. Sauer, J.M. Roper and D.C. Hager. Chem. Rev. *77*, 513 (1977).

12. a: J.S. Bradshaw, J.Y. Hui, B.L. Haymore, J.J. Christensen and R.M. Izatt. J. Heterocycl. Chem. *10*, 1 (1973); b: J.S. Bradshaw, J.Y. Hui, B.L. Haymore, R.M. Izatt and J.J.Christensen. J. Heterocycl. Chem. *11*, 45 (1974).

13. a: B. Dieltrich, J.M. Lehn and J.P. Sauvage. J. Chem. Soc., Chem. Commun. 1005 (1970); b: A.H. Albert, R. Annunziata and J.M. Lehn. J. Am. Chem. Soc. *99*, 8502 (1977); c: O. Kohn, I. Morgenstern-Badarau, J.P. Audiers, J.M. Lehn and S.A. Sullivan. J. Am. Chem. Soc. *102*, 5935 (1980).

14. F. Vögtle and P. Neumam. Synthesis 85 (1978).

15. E. Munekata, H. Faulstich and T. Wieland. J. Am. Chem. Soc. *99*, 6151 (1977).

16. P.M. Colman, H.C. Freeman, J.M. Guss, M. Murata, V.A. Norris, J.A.M. Ramshaw and M. P. Venkatappa. Nature (London) *272*, 319 (1978).

17. E.T. Adman, R.E. Stenkamp, L.L. Sieker and J.H. Jensen. J. Mol. Biol. *13*, 35 (1978).

18. W. Wieder, P. Natsher and F. Vögtle. Justus Liebigs Ann. Chem. 924 (1976).

19. E. Weber and F. Vögtle. Justus Liebigs Ann. Chem. 891 (1976).

20. L. Ruzicka. Helv. Chim. Acta *9*, 1008 (1926).

21. N.B. Tucker and E.E. Reid. J. Am. Chem. Soc. *55*,775 (1933).

21. a: D.St. C. Black and I.A. McLean. Tetrahedron Lett. 3961 (1969). b: W. Rosen and D.H. Busch. J. Am. Chem. Soc. *91*, 4694 (1969). c: W. Rosen and D.H. Busch. Inorg. Chem. *9*, 262 (1970).

23. J.L. Down, J. Lewis, B. Moore and G. Wilkinson. J. Chem. Soc. 3767 (1959).

24. L.A. Ochrymowycz, C.P. Mak and J.D. Machna. J. Org. Chem. *39*, 2079 (1974).

25. E.L. Eliel. *Stereochemistry of carbon compounds*. McGraw-Hill, New York, N.Y. 1962. p. 188.

26. E.L. Eliel, N.L. Albinger, S.J. Angyal and G.A. Morrison. *Conformational analysis*. Wiley, New York, N.Y. 1965.

27. a: W. Baker, J.F.W. McOmie and W.D. Ollis. J. Chem. Soc. 200 (1950); b: W. Baker, R. Banks, D.R. Lyons and F.G. Mann. J. Chem. Soc. 27 (1945).

28. D.H. Busch. Record. Chem. Progr. *25*, 107 (1964).

29. D.St.C. Black. Rev. Pure & Appl. Chem. *25*, 109 (1965).

30. a: M.C. Thompson and D.H. Busch. J. Am. Chem. Soc. *84*, 1726 (1962). b: M.C. Thompson and D.H. Busch. J. Am. Chem. Soc. *86*, 213 (1964).

31. a: G.N. Schrauzer, R.K.Y. Ho and R.P. Murillo. J. Am. Chem. Soc. *92*, 3508 (1970). b: G.N. Schrauzer. In *Sulfur research trends*. Adv. chemistry series, 110. Edited by D.J. Miller and T.K. Wiewiorowski. American Chemical Society, 1972.

32. J. Butter and R.M. Kellogg. J. Org. Chem. *46*, 4481 (1984).

33. D. Sellmann and I. Zapf. Angew. Chem. Int. Ed. Engl. *23*, 807 (1984).

34. W.N. Setzer. C.A. Ogle, G.S. Wilson and R.S. Glass. Inorg. Chem. *22*, 266 (1983).

35. a: D. Sellmann and P. Frank. Angew. Chem. Int. Ed. Engl. *25*, 1107 (1986). b: D. Sellmann, F. Knoch and C. Wronna. Angew. Chem. Int. Ed. Engl. *27*, 691 (1988).

36. M.D. Glick, D.P. Gravel, L.L. Diaddario and D.B. Rorabacher. Inorg. Chem. *15*, 1190 (1976).

37. P.H. Davis, L.K. White and R.L. Belford. Inorg. Chem. *14*, 1753 (1975).

38. R.E. DeSimone and M.D. Glick. J. Am. Chem. Soc. *97*, 942 (1975).

39. N.W. Alcock, N. Herron and P. More. J. Chem. Soc., Dalton Trans. 394 (1978).

40. N.K. Dalley, J.S. Smith, S.B. Larson, K.L. Matheson, J.J. Christensen and R.M. Izatt. J. Chem. Soc., Chem. Commun. 84 (1975).

41. N.K. Dalley, S.B. Larson, J.S. Smith, K.L. Matheson, R.M. Izatt and J.J. Christensen. J. Heterocycl. Chem. *18*, 463 (1981).

42. R.E. DeSimone and M.D. Glick. J. Am. Chem. Soc. *98*, 762 (1976).

43. R.S. Glass, G.S. Wilson and W.N. Setzer. J. Am. Chem. Soc. *102*, 5068 (1980).

44. S.C. Rawle, G.A. Admans and S.R. Cooper. J. Chem. Soc., Dalton Trans. 93 (1988).

45. R.E. Wolf, J.R. Hartman, J.M.E. Storey, B.M. Foxman and S.R. Cooper. J. Am. Chem. Soc. *109*, 4328 (1987).

46. J. Dale. Acta Chem. Scand. *27*, 1115 (1973).

47. N.K. Dalley. In *Synthetic multidentate macrocyclic compounds*. Edited by R.M. Izatt and J.J. Christensen. Academic Press, New York. 1978. p. 207.

48. I. Goldberg. In *Chemistry of ethers, crown ethers, hydroxyl groups and their sulfur analogs*. Edited by S. Patai. Wiley , New York. Part I, Suppl. E. 1980. p. 175.

49. J.E. Mark and P.J. Flory. J. Am. Chem. Soc. *87*, 1415 (1965).

50. A. Bondi. J. Phys. Chem. *68*, 441 (1964).

51. N.S. Zefirov. Tetrahedron *33*, 3193 (1977).

52. E. Juaristi. J. Chem. Educ. *56*, 438 (1979).

53. S. Wolfe. Acc. Chem. Res. *5*, 102 (1972).

54. K. Wieghardt, H.J. Küppers and J. Weiss. Inorg. Chem. *24*, 3067 (1985).

55. H.J. Küppers, K. Wieghardt, B. Nuber, J. Weiss, E. Bill and A.X. Trautwein. Inorg. Chem. *26*, 3762 (1987).

56. G.S. Wilson, D.D. Swanson and R.S. Glass. Inorg. Chem. *25*, 3827 (1986).

57. W.N. Setzer, C.A. Ogle, G.S. Wilson and R.S. Glass. Inorg. Chem. *22*, 266 (1983).

58. H.J. Küppers, A. Neves, C. Pomp, D. Ventur, K. Wieghardt, B. Nuber and J. Weiss. Inors g. Chem. *25*, 2400 (1986).

59. A.J. Blake, A.J. Holder, T.I. Hyde, G. Reid and M. Schröder. Polyhedron *8*, 204 (1989).

60. M.N. Bell, A.J. Blake, M. Schröder, H.J. Küppers and K. Wieghardt. Angew. Chem. Int. Ed. Engl. *26*, 250 (1987).

61. S.C. Rawle and S.R. Cooper. J. Chem. Soc., Chem. Commun. 308 (1987).

62. S.C. Rawle, T.J. Sewell and S.R. Cooper. Inorg. Chem. *26*, 3769 (1987).

63. S.C. Rawle, R. Yagbasan, K. Prout and S.R. Cooper. J. Am. Chem. Soc. *109*, 6181 (1987).

64. A.J. Blake, R.O. Gould, A.J. Holder, T.I. Hyde and M. Schröder. J. Chem. Soc., Dalton Trans. 1861 (1988).

65. K. Wieghardt, H.J. Küppers, E. Raabe and C. Krüger. Angew. Chem. Int. Ed. Engl. *25*, 1101 (1986).

66. A.J. Blake, A.J. Holder, T.I. Hyde, A.J. Lavery and M. Schröder. J. Chem. Soc., Chem. Commun. 987 (1987).

67. J. Clarkson, R. Yagbasan, P.J. Blower, S.C. Rawle and S.R. Cooper. J. Chem. Soc., Chem. Commun. 950 (1987).

68. A.J. Blake, R.O. Gould, A.J. Holder, T.I. Hyde, A.J. Lavery, M.O. Odulate and M. Schröder. J. Chem. Soc., Chem. Commun. 118 (1987).

69. A.J. Blake, R.O. Gould, J.A. Greig, A.J. Holder, T.I. Hyde and M. Schröder. J. Chem. Soc., Chem. Commun. 876 (1989).

70. H. Elias, G. Schmidt, H.J. Küppers, M. Saher, K. Wieghardt, B. Nuber and J. Weiss. Inorg. Chem. *28*, 3021 (1989).

71. M.T. Ashby and D.L. Lichtenberger. Inorg. Chem. *24*, 636 (1985).

72. A.J. Blake, R.D. Crofts, G. Reid and M. Schröder. J. Organomet. Chem. *359*, 371 (1989).

73. D. Parker and P.S. Roy, G. Ferguson and M.M. Hunt. Inorg. Chim. Acta *155*, 227 (1989).

74. L.L. Diaddario, L.L. Zimmer, T.E. Jones, L.S.W.L. Sokol, R.B. Cruz, E.L. Yee, L.A. Ochrymowycz and D.B. Rorabacher. J. Am. Chem. Soc. *101*, 3511 (1979).

75. D.B. Rorabacher, M.M. Bernardo, A.M.Q. Vande Linde, G.H. Leggett, B.C. Westerby, M.J. Martin and L.A. Ochrymowycz. Pure & Appl. Chem. *60*, 501

(1988).

76. M. Schröder. Pure & Appl. Chem. *60*, 517 (1988).

77. A.J.Blake, G. Reid and M. Schröder. J. Chem. Soc., Dalton Trans. 1675 (1989).

78. T.F. Lai and C.K. Poon. J. Chem. Soc., Dalton Trans. 1465 (1982).

79. A.J.Blake, R.O. Gould, G. Reid and M. Schröder. J. Organomet. Chem. *356*, 389 (1988).

80. V.B. Pett, L.L. Diaddario, E.R. Dockal, P.W.R. Corfield, C. Ceccarelli, M.D. Glick, L.A. Ochrymowycz and D.B. Rorabacher. Inorg. Chem. *22*, 3661 (1983).

81. G.H. Robinson, H. Zhang and J.L. Atwood. Organometallics *6*, 887 (1987).

82. G.H. Robinson and S.A. Sangokoya. J. Am. Chem. Soc. *110*, 1494 (1988).

83. a: J.A. Clarkson, R. Yagbasan, P.J. Blower and S.R. Cooper. J. Chem. Soc., Chem. Commun. 1244 (1989); b: H.J. Küpers, K. Wieghardt, Y.H. Tsay, C. Krüger, B. Nuber and J. Weiss. Angew. Chem. Int. Ed. Engl. *26*, 575 (1987).

84. P.W.R. Corfield, C. Ceccarelli, M.D. Glick, I.W.Y. Moy, L.A. Ochrymowycz and D.B. Rorabacher. J. Am. Chem. Soc. *107*, 2399 (1985).

85. J.R. Hartman and S.R. Cooper. J. Am. Chem. Soc. *108*, 1202 (1986).

86. V.B. Pett, G.H. Leggett, T.H. Cooper, P.R. Reed, D. Situmeanh, L.A. Ochrymowycz and D.B. Rorabacher. Inorg. Chem. *27*, 2164 (1988).

87. L.L. Diaddario, E.R. Dockal, M.D. Glick, L.A. Ochrymowycz and D.B. Rorabacher. Inorg. Chem. *24*, 356 (1985).

88. J.V. Dagdigian, V. McKee and C.A. Reed. Inorg. Chem. *21*, 1332 (1982).

89. F.J. Rietmeijer, P.J.M.W.L. Birker, S. Gorter and J. Reedijk. J. Chem. Soc., Dalton Trans. 1191 (1982).

90. E. Bouwmann, A. Burik, J.C. Ten Hove, W.J. Drissen and J. Reedijk. Inorg. Chim. Acta *150*, 125 (1988).

91. A.R. Amundsen, J. Whelm and B. Bosnich. J. Am. Chem. Soc. *99*, 6730 (1977).

92. C.R. Lucas. Can. J. Chem. *61*, 1096 (1983).

93. C.R. Lucas. Can. J. Chem. *64*, 1758 (1986).

94. S.G. Murray and F.R. Hartley. Chem. Rev. *81*, 365 (1981).

95. J. Gazo, I.B. Bersuker, J. Garaj, M. Kabseova, H. Langfelderova, M. Melnik, M. Serator and F. Velach. Coord. Chem. Rev. *19*, 253 (1976).

96. K.D. Karlin and J. Zubieta. *Copper coordination chemistry: biochemical and inorganic perspectives*. Adenine Press; Guilderland, New York. 1983.

97. D.E. Nikles, A.B. Anderson and F.L. Urbach. In *Copper coordination chemistry: biochemical and inorganic perspectives*. Adenine Press; Guilderland, New York. 1983. p. 203.

98. T.E. Jones, D.B. Rorabacher and L.A. Ochrymowycz. J. Am. Chem. Soc. *97*, 7485 (1975).

99. N.S. Ferris, W.H. Woodroff, D.B. Rorabacher and L.A. Ochrymowycz. J. Am. Chem. Soc. *100*, 5939 (1978).

100. H.C. Freeman. Coord. Chem. *21*, 29 (1980).

101. M.J. Lunden. J. Coord. Chem. *12*, 1 (1982); Inorg. Chim. Acta, *56*, 149 (1981).

102. E.R. Dockal, T.E. Jones, W.F. Sokol, R.E. Engerer, D.B. Rorabacher and L.A. Ochrymowycz. J. Am. Chem. Soc. *98*, 4322 (1976).

103. D.E. Nikles, M.J. Powers and F.L. Urbach. Inorg. Chim. Acta *37*, L499 (1979).

104. G.R. Brubaker, J.N. Brown, M.K. Yoo, R.A. Kinsey, T.M. Kutchan and E.A. Mottel. Inorg. Chem. *18*, 299 (1979).

105. J. Zubieta, K.D. Karlin and J.C. Hayes. In *Copper coordination chemistry: biochemical and inorganic perspectives*. Adenine Press; Guilderland, New York. 1983. p. 97.

106. K. Wieghardt, W. Schmidt, W. Herrman, and H.J. Küppers. Inorg. Chem. *22*, 2953 (1983).

107. B.N. Figgis. Trans. Faraday Soc. *57*, 204 (1961).

108. W. Levason, C.A. McAuliffe, S.G. Murray. J. Chem. Soc., Dalton Trans. 1566 (1975).

109. W. Levason, C.A. McAuliffe and S.G. Murray. Inorg. Chim. Acta *17*, 247 (1976).

110. D. Reinen, A. Ozarowski, B. Jackob, J. Pebler, H. Stratemeier, K. Wieghardt and I. Tolksdrof. Inorg. Chem. *26*, 4010 (1987).

111. D. St. C. Black and I.A. McLean. Aust. J. Chem. *24*, 1401 (1971).

112. E.J. Hintsa, J.R. Hartman and S.R Cooper. J. Am. Chem. Soc. *105*, 3738 (1983).

113. S.R. Cooper, S.C. Rawle, J.R. Hartman, E.J. Hintsa and G.A. Adams. Inorg. Chem. *27*, 1209 (1988).

114. L.A. Drammond, K. Henrick, M.J.L. Kanagasundaram, L.F. Kindoy, M. McPartlin and P.A. Tasker. Inorg. Chem. *21*, 3923 (1982).

115. J.R. Hartman, E.J. Hintsa and S.R. Cooper. J. Am. Chem. Soc. *108*, 1208 (1986).

116. C.M. Thorne, S.C. Rawle, G.A. Adams, and S.R. Cooper. J. Chem. Soc., Chem. Commun. 306 (1987).

117. a: S.C. Rawle, J.R. Hartman, D.J. Watkin and S.R. Cooper. J. Chem. Soc., Chem. Commun. 1083 (1986); b: S.R. Cooper, S.C. Rawle, J.R. Hartman, E.J. Hintsa and G.A. Adams. Inorg. Chem. *27*, 1209 (1988).

118. F.A. Cotton and F. Zingales. Chem. Ind. (London) 1219 (1960).

119. F.A. Cotton and F. Zingales. Inorg. Chem. *1*, 145 (1962).

120. W. Ströhmeier, J.F. Guttenberger and G. Popp. Chem. Ber. *98*, 2248 (1965).

121. H. Schumamn, O. Stelzer, R. Weiss, R. Mohtachemi and R. Fischer. Chem. Ber. *106*, 48 (1973).

122. N.A. Beach and H.B. Gray. J. Am. Chem. Soc. *90*, 5713 (1968).

123. T. Yoshida, T. Adachi, T. Ueda, M. Watanabe, M. Kaminaka and T. Higuchi. Angew. Chem. Int. Ed. Engl. *26*, 1171 (1987).

124. J. Cragel, V.B. Pett, M.D. Glick and R.E. DeSimone. Inorg. Chem. *17*, 2885 (1978).

125. R.E. DeSimone and M.D. Glick. Inorg. Chem. *17*, 3574 (1978).

126. A.J. Blake, R.O. Gould, A.J. Holder and M. Schröder. Angew. Chem. Int. Ed. Engl. *26*, 274 (1987).

127. G. Reid, A.J. Blake, T.I. Hyde and M. Schröder. J. Chem. Soc., Chem. Commun. 1397(1988).

128. R. Louis, D. Pelissard and R. Weiss. Acta Crystallogr., Sect. B 32, 1480 (1976).

129. M.G.B. Drew, D.A. Rice and S.B. Silong. Acta Crystallogr., Sect. C 40, 2014 (1984).

130. a: J. Clarkson, R. Yagbasan, D.J. Blower, S.C. Rawle and S.R. Cooper. J. Chem. Soc., Chem. Commun. 950 (1987); and b: P.J. Blower, J.A. Clarkson, S.C. Rawle,

J.R. Hartman, R.E. Wolf, R. Yagbasan, S.G. Bott and S.R. Cooper. Inorg. Chem. *28*, 4040 (1989).

131. D. Dobos. *Electrochemistry data*. Elsevier, Amsterdam. 1985.

132. A.J. Blake, R.O. Gould, A.J. Holder, T.I. Hyde and M. Schröder. Polyhedron *8*, 513 (1989).

133. E.W. Abel, S.K. Bharghava and K.G. Orrell. Prog. Inorg. Chem. *32*, 1 (1984).

134. R.J. Cross, I.G. Dalgleish, G.J. Smith and R. Wardle. J. Chem. Soc., Dalton Trans. 992 (1972).

135. R.J. Cross, T.H. Green, R. Keat and J.F Paterson. J. Chem. Soc., Dalton Trans. 1486 (1976).

136. E.W. Abel, I. Moss, K.G. Orrell, V. Šik and D. Stephenson. J. Chem. Soc., Dalton Trans. 2695 (1987).

137. E.W. Abel, K. Kite and P.S. Perkins. Polyhedron *6*, 549 (1987).

138. E.W. Abel, K.G. Orrell, K.B. Qureshi and V. Šik. Polyhedron *7*, 1321, 1329 (1988).

139. E.W. Abel, R.P. Busch, F.J. Hopton and C.R. Jenkins. J. Chem. Soc., Chem. Commun. 58 (1966).

140. P. Haake and P.C. Turley. J. Am. Chem. Soc. *89*, 4611 (1967).

141. S. Brownstein. J. Am. Chem. Soc., *98*, 2663 (1976).

142. N.G. Connelly, G.A. Johson, B.A. Kelly and P. Woodward. J. Chem. Soc., Chem. Commun. 436 (1977).

143. G. Binsch. J. Am. Chem. Soc. *91*, 1304 (1969).

144. W.A. Schenck and M. Schmidt. Z. Anorg. Allg. Chem. *416*, 311 (1975).

145. a: E.W. Abel, S.K. Bharghava, K.G. Orrell and V. Šik. J. Chem. Soc., Dalton Trans. 2073 (1981). b: E.W. Abel, M. Booth, K.G. Orrell, G.M. Pring and T.S. Cameron. J. Chem. Soc., Chem. Commun. 29 (1981).

146. E.W. Abel, G.D. King, K.G. Orrell, V. Šik, T.S. Cameron and K. Jochem. J. Chem. Soc., Dalton Trans. 2047 (1984).

147. E.W. Abel, S.K. Bharghava, I. Moss, K.G. Orrell, V. Šik, P.A. Bates M.B. Hursthouse. J. Chem. Soc., Chem. Commun. 978 (1987).

148. E.W. Abel, P.D. Beer, I. Moss, K.G. Orrell, V. Šik, P.A. Bates and M.B. Hursthouse. J. Organomet. Chem. *341*, 559 (1988).

CHAPTER 2

SYNTHESIS AND CHARACTERIZATION OF THIOPHENOPHANE LIGANDS

Abstract:

Thiophenophane ligands have been prepared from condensation of 2,5-bis(chloromethyl)thiophene and appropriate dimercaptans under high dilution conditions in basic media. The ^{1}H and ^{13}C nmr spectra of these ligands are described. The molecular structures of macrocycles, 2,5,8-trithia[9](2,5)thiophenophane (L1), 2,5,8,11-tetrathia[12](2,5)thiophenophane (L2) and 2,5,9,12-tetrathia[13](2,5)thiophenophane (L3), have been determined by single crystal X-ray diffraction methods. The solid state conformations of these macrocycles show a strong preference for gauche placements in the C-S-C-C units and anti placements in the S-C-C-S units. The unusual behavior of C-C-S-C and S-C-C-S units in the SCH_2-thiophene-CH_2S portion of these three macrocycles compared to crown thioethers will be discussed in terms of rigidity of the thiophene subunit and its two attached methylenes and steric effects of hydrogens on the hydrocarbon chain.

2.1. Introduction

As discussed in the previous chapter, exodentate conformations are characteristic of macrocyclic thioethers in contrast with endodentate conformations of crown ethers. The exodentate conformation of a macrocyclic thioether ligand arises from the steric and electronic effects of non-bonded atoms and is also largely dependent on the number of atoms in the ring and presumably the flexibility of the macrocycle.

Thiophenophane ligands prepared in our study contain one or two thiophene subunits in the macrocycle as shown in Scheme 2-1.

Scheme 2-1

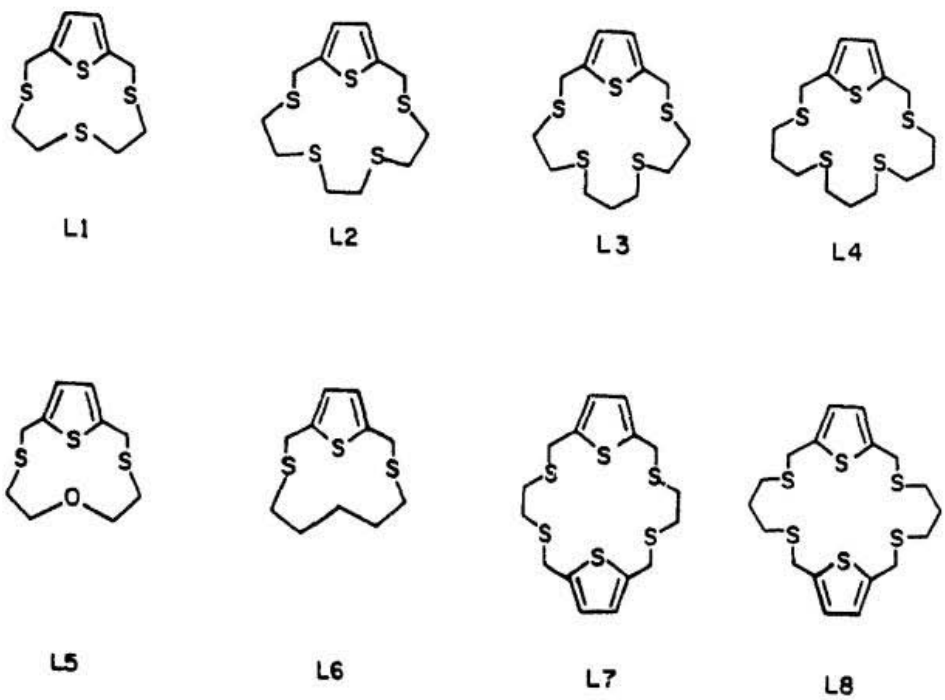

It is of interest to study the influence of the thiophene subunit on conformations and coordinating properties of these macrocycles. Since a thiophene subunit is incorporated in the macrocycle, it is also of interest to examine the coordination of thiophene sulfur to transition metals, which is of great importance in the study of catalytic hydrodesulfurization processes. With this in mind, we have prepared a series of macrocyclic thiophenophane ligands and examined structures of some of these macrocycles to provide detailed structural data for the study of their coordination chemistry

2.2. Experimental

Reagents were obtained from the Aldrich Chemical Co. Inc. and were used without further purification. Spectroscopic data were obtained using the following instruments: ir, Perkin-Elmer Model 283; nmr, General Electric 300-NB; mass spectra, VG-micromass 7070HS. Melting points were obtained on a Fisher-John's melting point apparatus and are uncorrected.

Preparation of 2,5-bis(chloromethyl)thiophene was by the reported method (1). Purification of the crude product can be achieved by washing the brown liquid with saturated sodium carbonate solution and then water until the washings are neutral, drying over anhydrous $MgSO_4$ and recrystallizing from petroleum ether (60-80°C) or by vacuum distillation. Literature methods (2-3) for 1,4,7,10-tetrathiadecane, 1,4,8,11-tetrathiaundecane and 1,5,9,13-tetrathiatridecane were used and the products were purified by vacuum distillation.

General Methods for The Preparation of Macrocyclic Thiophenophanes

Sodium metal (1.15g, 50 mmol) was dissolved in commercial absolute ethanol (500 ml) under an atmosphere of dry nitrogen and 25.0 mmol of dimercaptan was added cautiously. The resulting mixture was refluxed for about 15 minutes. Over 6-8

hours, a solution of purified 2,5-bis(chloromethyl)thiophene (4.25g, 25 mmol) in dry benzene was added dropwise with stirring to the refluxing mixture. Refluxing and stirring were continued for a further 2h. Volatiles were removed on a rotary evaporator and the residue was taken up with chloroform, washed with water several times, dried over anhydrous $CaCl_2$ and taken to dryness. The crude product was recrystallized twice from benzene to give the desired product. The yields range from 20% to 75%. All thiophenophane ligands are solids and easily purified by recrystallization.

2.3. Results and Discussion

2.3.1. Preparative

Thiophenophane ligands were prepared from the condensation of 2,5-bis(chloromethyl)thiophene with appropriate dimercaptans under high dilution conditions in basic media. The general preparation for these macrocycles is shown in Scheme 2-2.

It is interesting to note that chain length of the dimercaptan plays a very important role in the formation of a macrocycle. When R is ethylene or propylene, only 18- or 20-membered macrocycles were isolated with no trace of the corresponding monomer. When R contains five carbon atoms, monomeric L6 was isolated as the only product and the yield is moderately high (57%).

Scheme 2-2

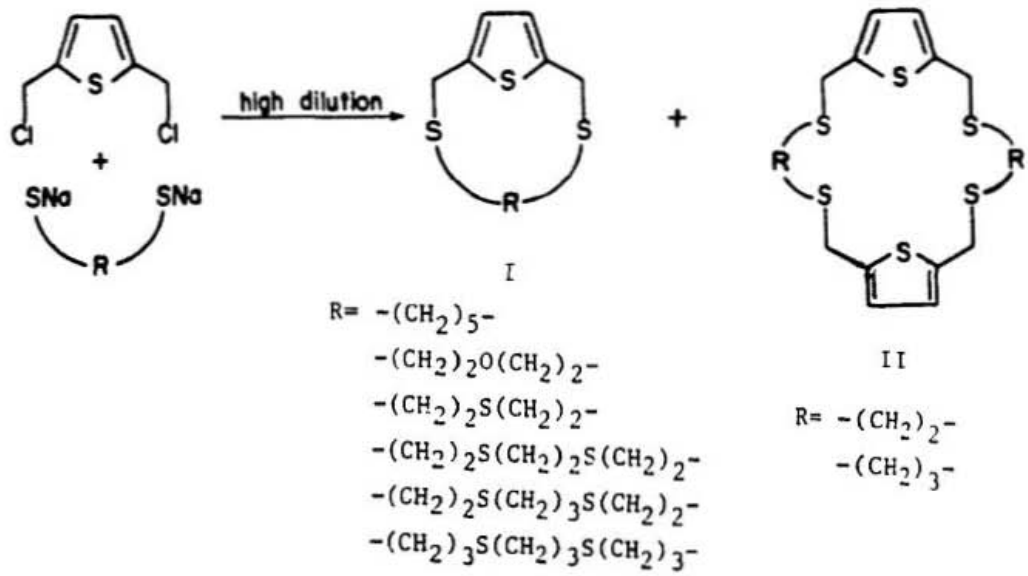

During attempts to prepare a 24-membered macrocycle (II, R=-$(CH_2)_2S(CH_2)_2$-), L1 (I, R=-$(CH_2)_2S(CH_2)_2$-) was isolated from the reaction of 2,5-bis(chloromethyl)thiophene and 2-mercaptoethyl sulfide in basic media under high dilution conditions. However, the reaction of 2,5-bis(chloromethyl)thiophene with 2-mercaptoethyl ether produces L5 (I, R=-$(CH_2)_2O(CH_2)_2$-) in moderately high yield (54%) with a small amount of a 24-membered macrocycle (II, R=-$(CH_2)_2O(CH_2)_2$-) as evidenced by mass spectrometry. Therefore, ring closure to a 12-membered macrocycle is the preferred process under high dilution conditions but closure to a 9- or 10-membered macrocycle is severely limited presumably due to ring strain in small ring compounds. On the other hand, it seems that the flexibility of the hydrocarbon chain is an important factor in the ring closure. For more flexible 2-mercaptoethyl ether, both dimer and monomer have been detected by mass spectroscopy. For relatively rigid 2-mercaptoethyl sulfide, monomeric L1 (I, R=-$(CH_2)_2S(CH_2)_2$-) is the only product,

the structure of which has been confirmed by nmr and mass spectrometries (both low resolution and high resolution) and by X-ray crystallography.

For conformationally flexible macrocycles with a longer hydrocarbon chain, yields are generally low even when the reaction is carried out under high dilution conditions since entropy constraints to cyclization favor linear polymerization (4-5). When a thiophene subunit is introduced into the macrocycle, cyclization proceeds in relatively high yields. This is analogous to the case where ortho-substituted phenyl derivatives are in the ring (4-5). Therefore, introduction of rigid aromatic groups increases the yield of a macrocycle and at the same time will change the complexing properties of it to transition metals.

The isolated compounds and their physical properties are given in Table 2-1. All these thiophenophane ligands are soluble in halocarbons and benzene, but not in ethanol. Their proposed structures are consistent with ir, nmr and mass spectroscopic data (Table 2-2) and some have been confirmed by X-ray methods (Figures 2-1, 2-2 and 2-3).

Nmr spectra (Table 2-2) show aromatic hydrogen signals at 6.8 ± 0.15 ppm; CH_2 α to the thiophene ring at 3.91 ± 0.06 ppm and ethylene hydrogen signals at 2.53 ± 0.15 ppm. The signals of the central methylene hydrogens of a propylene bridge appear at 1.86 ± 0.06 ppm. All assignments are consistent with the ^{1}H-^{1}H and ^{1}H-^{13}C COSY nmr spectra of these ligands.

Table 2-1: Thiophenophane ligands and their physical properties.

Ligand	Formula	Yield (%)	m.p. (°C)	High Resolution (m^+/e)	Low Resolution (m^+/e)
L1	$C_{10}H_{14}S_4$	73.2	151-152	261.9979(261.99776)	262(262)
L2	$C_{12}H_{18}S_5$	56.4	86-87	322.0096(322.00111)	322(322)
L3	$C_{13}H_{20}S_5$	46.9	128-129	336.0179(336.01675)	336(336)
L4	$C_{15}H_{24}S_5$	3.5	81-82	364.0487(364.04803)	364(364)
L5	$C_{10}H_{14}OS_3$	54.0	101-103	246.0201(246.02060)	246(246)
L6	$C_{11}H_{16}S_3$	57.0	93-94		244(244)
L7	$C_{16}H_{20}S_6$	42.6	126-127	403.9813(403.98882)	404(404)
L8	$C_{18}H_{24}S_6$	49.6	122-123		432(432)

Table 2-2: The nmr data for macrocyclic thiophenophane ligands in $CDCl_3$ (chemical shift in ppm vs.TMS).

Ligand	δ (^{1}H, ppm)	$^3J_{HH}$(Hz)	group	δ (^{13}C, ppm)
L1	6.92 s(2H)	---	aromatic	140.21(2C); 128.14(2C)
	3.95 s(4H)	---	methylene	31.60(2C)
	2.58 t(4H)	8.67	SCH_2CH_2S	30.24(2C)
	2.22 t(4H)	8.46	SCH_2CH_2S	31.45(2C)
L2	6.85 s(2H)	---	aromatic	141.95(2C); 126.19(2C)
	3.93 s(4H)	---	methylene	31.05(2C)
	2.61 m(4H)	---	SCH_2CH_2S	30.94(2C)
	2.59 m(4H)	---	SCH_2CH_2S	31.84(2C)
	2.53 s(4H)	---	SCH_2CH_2S	32.54(2C)

L3	6.78 s(2H)	---	aromatic	142.59(2C); 125.74(2C)
	3.90 s(4H)	---	methylene	31.27(2C)
	2.64 m(4H)	---	SCH_2CH_2S	31.34(2C)
	2.60 m(4H)	---	SCH_2CH_2S	31.55(2C)
	2.46 t(4H)	7.63	$SC^*H_2CH_2$	31.63(2C)
	1.69 m(2H)	---	$CH_2C^*H_2CH_2$	32.01(1C)
L4	6.75 s(2H)	---	aromatic	142.22(2C); 125.60(2C)
	3.97 s(4H)	---	methylene	31.20(2C)
	2.58 m(12H)	---	$SC^*H_2CH_2$	31.12(2C); 30.46(2C)
	1.79 m(6H)	---	$CH_2C^*H_2CH_2$	29.45(2C); 29.41
L5	6.80 s(2H)	---	aromatic	142.58(2C); 126.83(2C)
	3.95 s(4H)	---	methylene	32.01(2C)
	3.01 s(4H)	---	$OC^*H_2CH_2S$	68.56(2C)
	2.66 s(4H)	---	$SC^*H_2CH_2O$	28.58(2C)
L6	6.79 s(2H)	---	aromatic	142.85(2C); 126.75(2C)
	3.85 s(4H)	---	methylene	32.05(2C)
	2.45 s(4H)	---	$SC^*H_2CH_2$	29.29(2C)
	1.32 s(2H)	---	$SCH_2C^*H_2$	24.99(2C)
	0.94 s(4H)	---	$CH_2C^*H_2CH_2$	28.38(2C)
L7	6.71 s(4H)	---	aromatic	142.94(4C); 125.23(4C)
	4.09 s(8H)	---	methylene	31.66(4C)
	2.67 s(8H)	---	SCH_2CH_2S	32.31(4C)
L8	6.75 s(4H)	---	aromatic	141.92(4C); 125.68(4C)
	3.86 s(8H)	---	methylene	30.86(4C)
	2.49 t(8H)	7.23	$SC^*H_2CH_2$	30.08(4C)
	1.72 q(4H)	---	$CH_2C^*H_2CH_2$	29.33(2C)

Table 2-3: Selected bond lengths and angles in L1 ($C_{10}H_{14}S_4$).

Bond	Distance (Å)	Bonds	Angle(deg.)
S(1)-C(1)	1.737(5)	C(1)-S(1)-C(4)	91.7(3)
S(1)-C(4)	1.721(5)	C(5)-S(2)-C(6)	101.7(3)
S(2)-C(5)	1.805(8)	C(7)-S(3)-C(8)	101.2(3)
S(2)-C(6)	1.816(7)	C(9)-S(4)-C(10)	101.2(3)
S(3)-C(7)	1.814(6)	C(9)-S(4)-C(10)	102.4(3)
S(3)-C(8)	1.800(7)	S(1)-C(1)-C(2)	109.8(4)
S(4)-C(9)	1.800(8)	S(1)-C(1)-C(5)	120.6(5)
S(4)-C(10)	1.840(8)	C(2)-C(1)-C(5)	129.5(5)
C(1)-C(2)	1.344(9)	C(2)-C(3)-C(4)	111.6(5)
C(1)-C(5)	1.485(8)	S(1)-C(4)-C(3)	111.6(5)
C(2)-C(3)	1.406(9)	S(1)-C(4)-C(10)	119.2(4)
C(3)-C(4)	1.363(8)	C(3)-C(4)-C(10)	128.8(5)
C(4)-C(10)	1.505(8)	S(2)-C(5)-C(1)	115.3(5)
C(6)-C(7)	1.529(9)	S(2)-C(6)-C(7)	112.2(4)
C(8)-C(9)	1.53(1)	S(3)-C(6)-C(7)	111.8(4)
S(1)-S(2)	3.972(8)	S(3)-C(8)-C(9)	114.2(5)
S(1)-S(3)	4.579(3)	S(4)-C(8)-C(9)	114.7(5)
S(1)-S(4)	3.479(5)	S(4)-C(10)-C(4)	112.8(4)
S(2)-S(4)	6.662(5)		

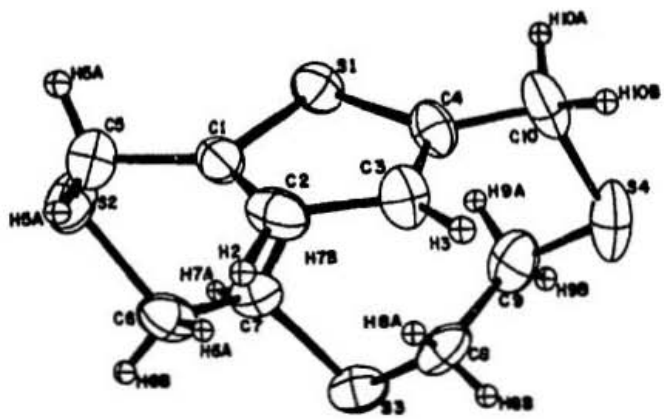

Table 2-4: Selected bond lengths and angles in L2 ($C_{12}H_{18}S_5$).

Bond	Distance (Å)	Bonds	Angle(deg.)
S(1)-C(1)	1.720(5)	C(1)-S(1)-C(4)	92.03(22)
S(1)-C(4)	1.737(4)	C(5)-S(2)-C(8)	103.4(3)
S(2)-C(5)	1.820(5)	C(7)-S(3)-C(8)	107.4(3)
S(2)-C(6)	1.833(6)	C(9)-S(4)-C(10)	105.1(3)
S(3)-C(7)	1.836(5)	C(11)-S(5)-C(12)	98.4(3)
S(3)-C(8)	1.783(6)	S(1)-C(1)-C(2)	110.2(3)
S(4)-C(9)	1.859(6)	S(1)-C(1)-C(12)	122.9(4)
S(4)-C(10)	1.762(8)	C(2)-C(1)-C(12)	126.9(5)
S(5)-C(11)	1.815(5)	C(1)-C(2)-C(3)	113.6(5)
S(5)-C(12)	1.822(5)	C(2)-C(3)-C(4)	114.0(5)
C(1)-C(2)	1.345(7)	S(1)-C(4)-C(3)	110.2(3)
C(1)-C(12)	1.487(6)	S(1)-C(4)-C(5)	119.9(4)
C(2)-C(3)	1.409(6)	C(3)-C(4)-C(5)	129.9(4)
C(3)-C(4)	1.327(7)	S(2)-C(5)-C(4)	113.1(3)
C(4)-C(5)	1.495(6)	S(2)-C(6)-C(7)	112.7(4)
C(6)-C(7)	1.450(9)	S(3)-C(7)-C(6)	113.7(4)
C(8)-C(9)	1.504(8)	S(3)-C(8)-C(9)	113.9(4)
C(10)-C(11)	1.531(8)	S(4)-C(9)-C(8)	113.2(4)
		S(4)-C(10)-C(11)	118.2(5)
		S(5)-C(11)-C(10)	111.2(4)
		S(5)-C(12)-C(1)	113.5(3)

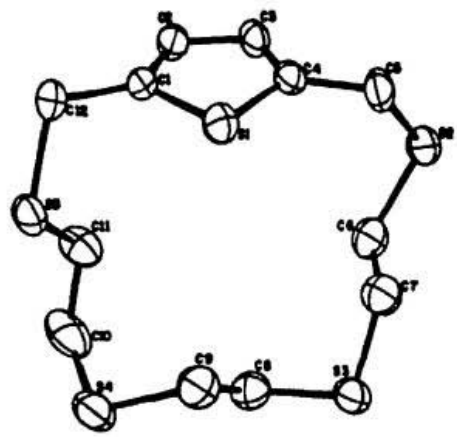

Table 2-5: Selected bond lengths and angles in L3 ($C_{13}H_{20}S_5$).

Bond	Distance (Å)	Bonds	Angle(deg.)
S(1)-C(1)	1.721(4)	C(1)-S(1)-C(4)	92.53(19)
S(1)-C(4)	1.721(4)	C(5)-S(2)-C(6)	101.54(23)
S(2)-C(5)	1.819(5)	C(7)-S(3)-C(8)	102.30(20)
S(2)-C(6)	1.808(5)	C(10)-S(4)-C(11)	103.18(21)
S(3)-C(7)	1.821(5)	C(12)-S(5)-C(13)	101.48(22)
S(3)-C(8)	1.804(4)	S(1)-C(1)-C(2)	110.6(3)
S(4)-C(10)	1.807(4)	S(1)-C(1)-C(13)	121.7(3)
S(4)-C(11)	1.808(5)	C(2)-C(1)-C(13)	127.6(4)
S(5)-C(12)	1.809(5)	C(1)-C(2)-C(3)	113.0(4)
S(5)-C(13)	1.827(5)	C(2)-C(3)-C(4)	113.6(4)
C(1)-C(2)	1.343(6)	S(1)-C(4)-C(3)	110.2(3)
C(1)-C(13)	1.493(5)	S(1)-C(4)-C(5)	121.7(3)
C(2)-C(3)	1.424(5)	C(3)-C(4)-C(5)	128.1(4)
C(3)-C(4)	1.344(6)	S(2)-C(5)-C(4)	115.1(3)
C(4)-C(5)	1.495(6)	S(2)-C(6)-C(7)	114.2(3)
C(6)-C(7)	1.495(7)	S(3)-C(7)-C(6)	113.5(3)
C(8)-C(9)	1.508(6)	C(8)-C(9)-C(10)	110.6(4)
C(9)-C(10)	1.504(6)	S(4)-C(10)-C(9)	117.0(3)
C(11)-C(12)	1.504(7)	S(4)-C(11)-C(12)	113.5(3)
		S(5)-C(12)-C(11)	114.8(3)
		S(5)-C(13)-C(1)	114.9(3)

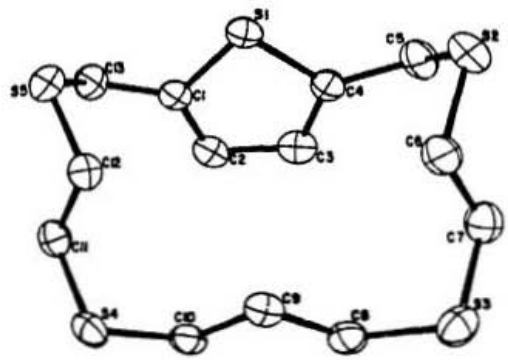

Table 2-6: Selected torsion angles in L1, L2 and L3.

L1		L2		L3	
Bonds	Angle (deg.)	Bonds	Angle (deg.)	Bonds	Angle (deg.)
C1-S1-C4-C10	171.56	C1-S1-C4-C5	179.38(6)	C1-S1-C4-C3	-1.66
C4-S1-C1-C5	1.93	C4-S1-C1-C12	179.03(2)	C4-S1-C1-C2	1.75
C5-S2-C6-C7	-114.46	C5-S2-C6-C7	65.83(3)	C5-S2-C6-C7	63.11
C6-S2-C5-C1	43.24	C6-S2-C5-C4	55.92(6)	C6-S2-C5-C4	51.62
C7-S3-C8-C9	-80.60	C7-S3-C8-C9	73.58(3)	C7-S3-C8-C9	-87.14
C8-S3-C7-C6	-82.42	C8-S3-C7-C6	65.36(5)	C8-S3-C7-C6	83.13
C9-S4-C10-C4	53.61	C9-S4-C10-C11	50.62(4)	C10-S4-C11-C12	-81.66
C10-S4-C9-C8	-94.05	C10-S4-C9-C8	63.07(4)	C11-S4-C10-C9	88.56
S1-C1-C5-S2	56.90	C11-S5-C12-C1	56.42(3)	C12-S5-C13-C1	-49.65
S2-C6-C7-S3	167.65	C12-S5-C11-C10	175.56(5)	C13-S5-C12-C11	-67.46
S3-C8-C9-S4	-176.82	S1-C4-C5-S2	117.63(6)	S1-C4-C5-S2	64.41
S4-C10-C4-S1	-104.77	S2-C6-C7-S3	164.23(7)	S2-C6-C7-S3	177.02
		S3-C8-C9-S4	164.20(3)	S3-C8-C9-C10	-166.87
		S4-C10-C11-S5	52.20(3)	S4-C10-C9-C8	167.41
		S5-C12-C1-S1	50.85(5)	S4-C11-C12-S5	-177.31
				S5-C13-C1-S1	-65.92

2.3.2. Structures of Thiophenophane Ligands (L1, L2 and L3)

In the last decade, a large number of macrocyclic thioether ligands have been prepared and studied for their metal complexing properties (6-10). However, the design and synthesis of these macrocycles remain essentially empirical exercises and the significance of conformations of macrocyclic thioethers to their coordinating behavior has not been widely recognized. Although many metal complexes of thioether ligands have been studied by X-ray crystallography, only a few examples of structural studies of the free ligands have been reported (11-15). As part of our research project, our interest was focused on the solid state conformations of thiophenophane ligands and how these conformations influence their coordinating behavior. With this in mind, the structures of L1, L2 and L3 have been examined by X-ray methods to provide some structural data for the detailed study of the structural and chemical properties of their transition metal complexes.

Selected bond lengths and angles in L1, L2 and L3 are given in Tables 2-3, 2-4 and 2-5. Their ORTEP drawings are shown in Figures 2-1, 2-2 and 2-3.

Bond lengths in L1, L2 and L3 compare well to those in crown thioethers (11-15). Carbon-sulfur bond lengths at thioether sulfurs range from 1.762(8) to 1.859(6) Å and agree with those in [12]aneS4 (14), [14]aneS4 (11), [15]aneS5 (14) and [18]aneS6 (14). The carbon-sulfur bond distances at thiophene-sulfur (Tables 2-3, 2-4 and 2-5), however, are significantly shorter than those at thioether sulfurs, indicating certain π-bonding in the aromatic thiophene ring. Carbon-carbon bond distances in ethylene bridges range from 1.450(9) to 1.53(1) Å, which is shorter than those expected for C-C single bonds (1.54 Å). Similar results have been reported for crown thioethers (11-15). In the thiophene ring, the C(1)-C(2) and C(3)-C(4) distances (ranging from 1.327(7)

to 1.363(8) Å) are characteristic of C=C double bonds while C(2)-C(3) bond lengths (ranging from 1.406(9) to 1.424(5) Å) are between C-C single bonds and C=C double bonds, consistent with the typical diene structure.

Structures of macrocyclic thioethers have been described in terms of exodentate and endodentate orientations of the lone pairs of sulfur atoms (11-15). The sulfur atoms pointing out of the ring are exodentate while those pointing into the ring are endodentate. Our studies of three thiophenophane ligands show that in their solid state conformations all thioether sulfur atoms are exodentate but the thiophene-sulfur atoms in L1 and L2 point into the great ring.

The most important structural parameters in describing the conformation of a macrocyclic thioether ligand are torsion angles in the C-C-S-C and S-C-C-S units, where torsion angles of ±60° are classified as gauche and those of ±180° as anti. The torsion angles of the three thiophenophane ligands (Table 2-6) display a clear pattern: In L1 and L3, both of which contain even numbers of ring atoms, every C-C-S-C unit at thioether sulfurs adopts gauche placement and the remaining two C-C-S-C units at thiophene-sulfur assume an anti placement; in L2, which contains an odd number of ring atoms, a strong preference for gauche placement at thioether sulfurs (seven out of eight torsion angles) is observed again with the two remaining C-C-S-C units in the thiophene ring being similar to those in L1 and L3, even though odd-membered rings often show anomalous torsion angles due to ring strain (16). Most S-C-C-S units in the polythioether chain of all three thiophenophane ligands, however, show a strong affinity for anti placements. These affinities for gauche placement in the C-C-S-C unit and anti placement in the S-C-C-S unit have also been reported recently in crown thioethers (11-15) and contrast with those for anti placement in C-C-O-C and gauche placement in O-C-C-O units (17, 18).

The marked difference between macrocyclic thioethers and crown ethers has been explained in terms of different intramolecular interactions between non-bonded atoms in C-C-E-C and E-C-C-E (E=O or S) units as discussed in the previous chapter. It should be noted that the gauche placement at C-S bonds in a C-C-S-C unit is strongly dependent on ring strain and flexibility of a macrocycle. In our thiophenophane ligands, exceptions to the rules above occur due to the rigidity of the thiophene subunit and its two attached methylenes in the 2 and 5 positions.

In L1 (Figure 2-1), all three thioether sulfur atoms are exocyclic , but the thiophene-sulfur points into the macrocyclic ring. This is unusual since in a closely related crown thioether [12]aneS4 (14) all four thioether sulfurs are exocyclic. Examination of conformations of both macrocycles indicates that the endo-orientation of thiophene-sulfur is caused by the rigidity of the macrocycle and steric hindrance from hydrogens on the hydrocarbon chain. In [12]aneS4, S2 and S4 are bridged by a flexible CH_2-CH_2-S-CH_2-CH_2 fragment and it is possible to turn the S1 atom to be exocyclic by simply rotating about C-S1 and C-C single bonds. In L1, however, S2 and S4 are bridged by a rigid thiophene ring and its two attached methylenes in the 2 and 5 positions. Rotation around C-S1 and C-C bonds is severely limited by the rigidity of the thiophene subunit and by steric hindrance from hydrogens on C6, C7, C8 and C9. Therefore, the C5-C1-S1-C4 and C10-C4-S1-C1 units have to assume anti placements instead of gauche ones while S1-C1-C5-S2 and S1-C4-C10-S4 units assume gauche placements instead of anti ones. The special endo-arrangement of the lone pairs of thiophene-sulfur suggests that it should be possible for thiophene-sulfur to form a bond to a transition metal without major conformational changes in that part of the ligand molecule. Thiophene-sulfur coordination has been established in L1 complexes of copper(II) (p96) and palladium(II) (p156, p186) by X-ray methods.

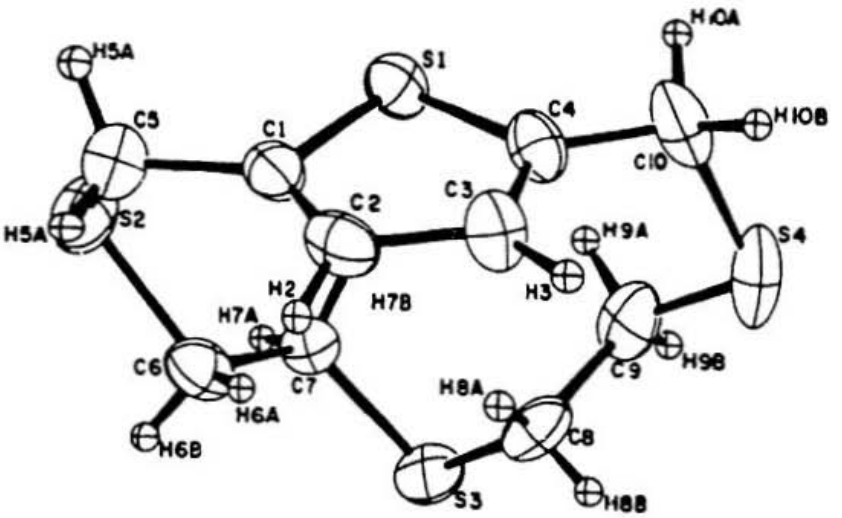

Figure 2-1. ORTEP drawing of L1 ($C_{10}H_{14}S_4$).

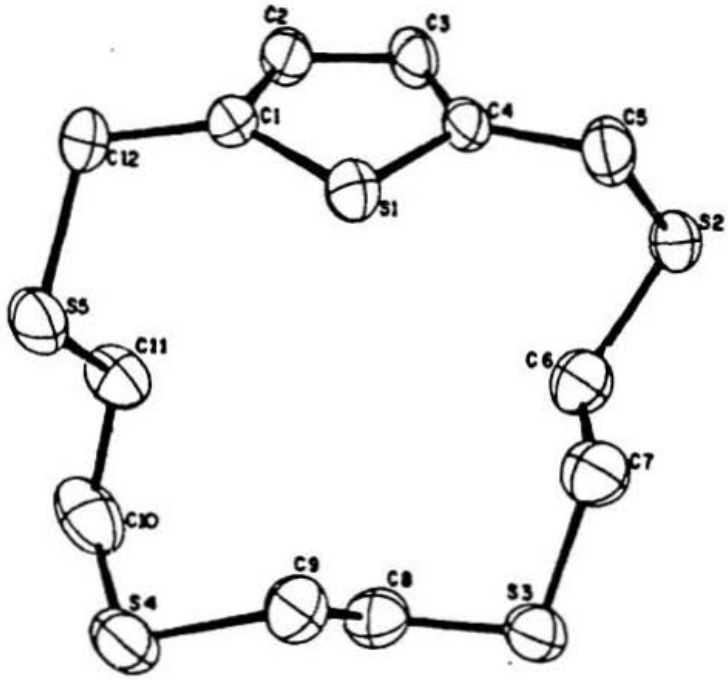

Figure 2-2. ORTEP drawing of L2 ($C_{12}H_{18}S_5$).

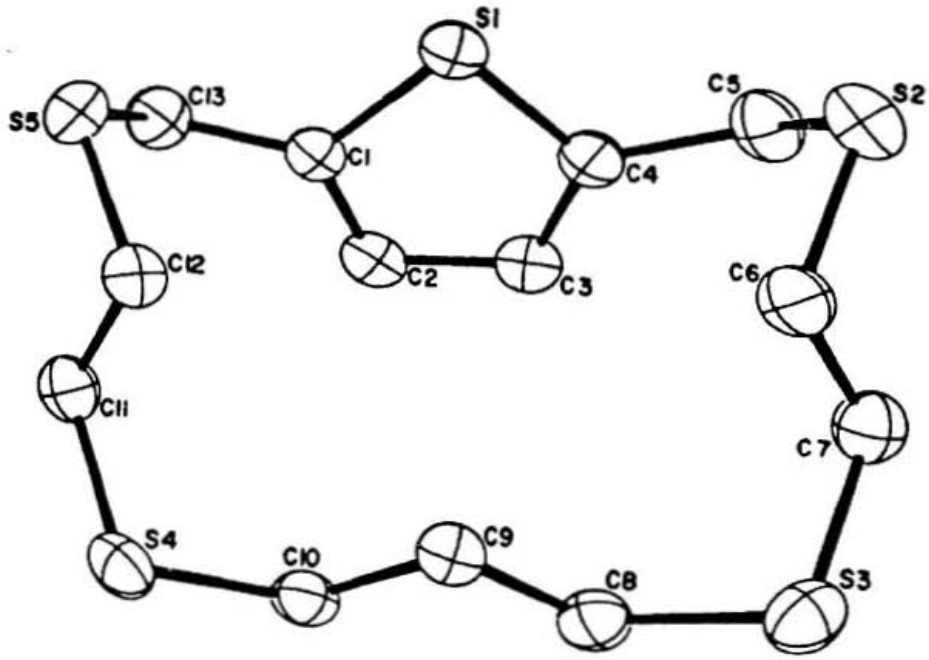

Figure 2-3. ORTEP drawing of L3 ($C_{13}H_{20}S_5$).

L2 (Figure 2-2) is a 15-membered macrocycle. Like L1, its thiophene-sulfur is endocyclic due to the rigidity of the aromatic ring and steric hindrance from hydrogens on the polythioether chain. In addition, the C12-C5 bond assumes anti placement instead of gauche. This unusual behavior has been observed in [15]aneS5 (14) and is caused probably by ring strain in odd-membered macrocycles.

L3 (Figure 2-3) is a 16-membered macrocycle, in which all sulfur atoms are exocyclic. Compared with L2, a more flexible polythioether chain makes it possible for the thiophene ring to rotate more freely around the C4-C5 and C1-C13 bonds. Therefore, the thiophene-sulfur atom points out of the macrocyclic ring. However, rotation of a thiophene ring can only change the torsion angles of C1-C13-S5-C12 and C4-C5-S2-C6, and the anti placements at C-S1 bonds in the C-C-S-C units are still retained. The conformation of L3 resembles that of [14]aneS4 as a rectangle with four thioether sulfurs in the four corners (11), but the S2-S5 distance is slightly longer than that of S3-S4.

2.4. Conclusions

On the basis of these results, it is concluded that exocyclic orientation of the lone pairs of thioether sulfur is characteristic of macrocyclic thioether ligands although exceptions do occur as a result of special conditions such as ring strain in odd-membered rings and rigidity of the macrocycle. Such structural deviations are expected to be reflected by the different coordinating behavior of these ligands and properties of their transition metal complexes. These will be discussed in detail in later chapters.

2.5. References

1. J.M. Griffing and L.F. Salisbury. J. Am. Chem. Soc. *70*, 3146 (1948).
2. W. Rosen and D.H. Busch. Inorg. Chem. *9*, 262 (1970).
3. W. Rosen and D.H. Busch. J. Am. Chem. Soc. *91*, 4694 (1969).
4. W. Baker, R. Banks, D.R. Lyons and F.G. Mann. J. Chem. Soc. 27 (1945).
5. W. Baker, J.F.W. McOmie, W.D. Ollis. J. Chem. Soc. 200 (1950).
6. J.R. Hartman and S.R. Cooper. J. Am. Chem. Soc. *108*, 1202 (1986).
7. H.J. Küppers, H. Neves, C. Pomp, D. Ventur, K. Wieghardt, B. Nuber and J. Weiss. Inorg. Chem. *25*, 2400 (1986).
8. P.W.R. Corfield. C. Ceccarelli, M.D. Glick, I.W.Y. Moy, L.A. Ochrymowycz and D.B. Rorabacher. J. Am. Chem. Soc. *107*, 2399 (1985).
9. M. Schröder. Pure & Appl. Chem. *60*, 517 (1988).
10. V.B. Pett, G.H. Leggett, T.H. Cooper, P.R. Reed, D. Situmeanh, L.A. Ochrymowycz and D.B. Rorabacher. Inorg. Chem. *27*, 2164 (1988).
11. R.E. DeSimone and M.D. Glick. J. Am. Chem.Soc. *98*, 762 (1976).
12. R.S. Glass, G.S. Wilson and W.N. Setzer. J. Am. Chem. Soc. *102*, 5068, (1980).
13. S.C. Rawle, G.A. Adams and S.R. Cooper. J. Chem. Soc. Dalton Trans. 93 (1988).
14. R.E.W. Wolf, J.R. Hartman, J.M.E. Storey, M.B. Foxman and S.R. Cooper. J. Am. Chem. Soc. *109*, 4238 (1987).
15. B. de Groot and S.J. Loeb. Inorg. Chem. *28*, 3573 (1989).

16. J. Dale. Acta Chem. Scand. *27*, 1115 (1973).

17. N.K. Dalley. In *Synthetic multidentate macrocyclic compounds. Edited by R.M. Izatt and J.J. Christensen. Academic Press, New York. 1978. p207.*

18. I. Goldberg. In Chemistry of ethers, crown ethers, hydroxyl groups and their sulfur analogs. *Edited by S. Patai. Wiley, New York, Part I, Suppl. E. 1980. p175.*

CHAPTER 3

COPPER(II) AND COPPER(I) COMPLEXES OF THIOPHENOPHANE LIGANDS AND 2,5-BIS(2-HYDROXYETHYLTHIOMETHYL)THIPHENE

Abstract:

Synthesis and properties of 15 copper(II) and copper(I) complexes of thiophenophane ligands and of one open-chain ligand, 2,5-bis(2-hydroxyethylthiomethyl)-thiophene, are described. The molecular structures of seven of the compounds are presented and spectral details (ir, electronic, esr) are interpreted in the light of these structures. The redox properties of the complexes have been examined by cyclic voltammetry and the effect of solvent on the electrochemistry of some of these complexes is discussed and related to their structural and spectroscopic details.

3.1. Introduction

As discussed previously, thiophenophane ligands show a strong affinity for gauche placement at C-S bonds in the C-C-S-C unit and anti placement at C-C bonds in the S-C-C-S unit although exceptions do occur at thiophene-sulfur. This is in contrast to crown thioethers (1-3), in which all thioether-sulfurs are exocyclic. The differences between thiophenophane and crown thioethers are expected to be reflected in their coordinating properties with transition metals. The endocyclic orientation of the thiophene-sulfur may render an opportunity to investigate coordination of thiophene-sulfur to transition metals, which is of great importance in the study of catalytic hydro-desulfurization processes (4).

In chapter 2, synthesis and characterization of thiophenophane ligands have been described. We now present the preparation, structure and properties of copper(II) and copper(I) complexes of these ligands and of 2,5-bis(2-hydroxyethylthiomethyl) thiophene. Electrochemical properties of these complexes are of particular interest and will be discussed in conjunction with their X-ray crystal structures.

The ligands described in this chapter are given in Scheme 3-1.

Scheme 3-1

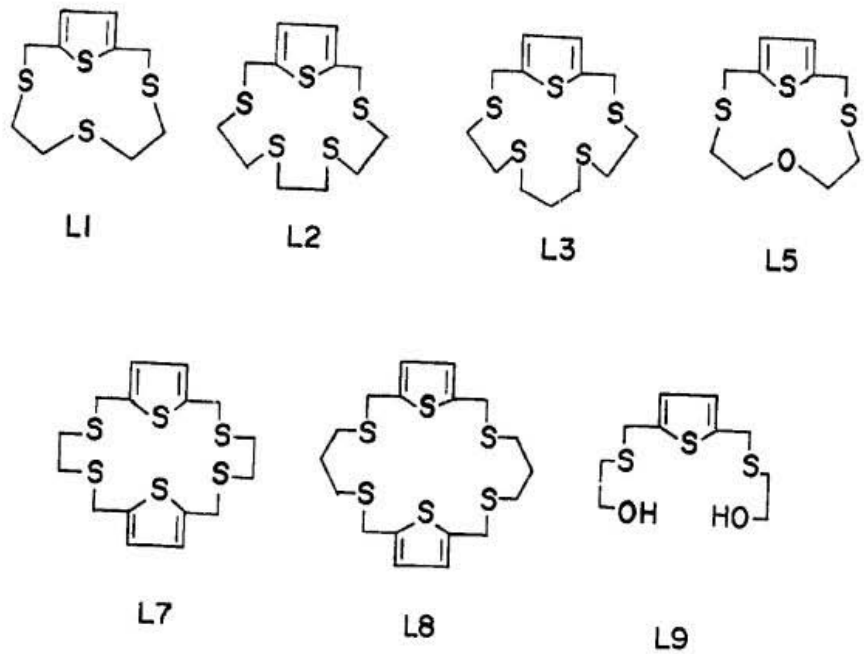

3.2. Experimental

Reagents were obtained from the Aldrich Chemical Co. or from Morton Thiokol Alfa Products Inc. and were used without further purification except those for conductivity measurements. Infrared spectra were recorded as nujol mulls on a Perkin-Elmer 283 spectrophotometer and electronic spectra both in solution and in the solid state were obtained using a Cary 17 UV/visible spectrophotometer. Conductivities were measured at 25℃ using a cell calibrated with standard potassium chloride solution (0.1 M KCl). Magnetic data were obtained at room temperature by the Faraday method using $Hg[Co(NCS)_4]$ as calibrant. The susceptibility data were corrected for diamagnetism using Pascal's constants. A value of 60 x 10^{-6} cgs units per mole of copper atoms was used as a correction for temperature independent paramagnetism (TIP) where such a term appears in the calculations (5). Esr spectra of polycrystalline

samples and of dichloromethane solutions were recorded at room temperature and 77K on a Bruker ESP-300 X-band spectrometer at ~9.5 GHz. Electrochemical measurements were carried out under a dry nitrogen atmosphere at room temperature. Solution concentrations were $\sim 10^{-3}$ M in complex and 0.1 M in supporting electrolyte (tetraethylammonium perchlorate, TEAP). Cyclic voltammograms were recorded on a BAS CV27 Voltammograph and a Houston 2000-Omnigraph X-Y recorder using a glassy carbon working electrode, a platinum counter electrode and an aqueous saturated calomel reference electrode. Junction potential corrections were not used. X-ray diffraction data were collected using an Enraf Nonius CAD4 or Picker diffractometer. Analyses were performed by Canadian Microanalytical Service Ltd. Melting points were measured on a Fisher-John's melting point apparatus and are uncorrected.

Synthesis of thiophenophane ligands (Scheme 3-1) has been described in Chapter 2. The ligands have been characterized by spectroscopic techniques and some by X-ray methods. The acyclic analog, 2,5-bis(2-hydroxyethylthiomethyl)thiophene, was prepared by the procedure described below.

3.2.1. 2,5-Bis(2-hydroxyethylthiomethyl)thiophene

Sodium metal (2.3 g, 0.1 mol) was dissolved in 300 ml of commercial absolute ethanol under a dry nitrogen atmosphere. To the solution, 2-mercaptoethanol (7.8 g, 0.1 mol) was added cautiously and the mixture was heated to reflux for about 10 minutes. A solution of 2,5-bis(chloromethyl)thiophene (9.1 g, 0.05 mol) in 150 ml of absolute ethanol was added dropwise to the refluxing solution over 2-3 hours. After addition the reaction mixture was refluxed for another 2 hours. Volatiles were removed on a rotary evaporator and the residue was taken up with chloroform,

washed with water several times and dried over anhydrous $CaCl_2$. Upon filtration, chloroform was removed to give a thick liquid, which was kept at -20℃ overnight to give white crystals. The solid was collected by filtration, washed with a small portion of cold ethanol and then diethyl ether and dried in air. Yield 10g (76.3%). M.p.=34-36℃. Ir: 3360 cm^{-1}, a strong band due to OH stretching vibration. Mass spectrum: parent ion 264 for $[C_{10}H_{16}O_2S_3]^+$. Nmr ($CDCl_3$, ppm from TMS int. std., assignments from ^{13}C-^1H heteronuclear correlation and attached proton test, position identification from the following structure):

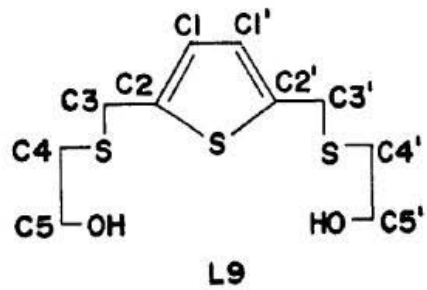

L9

^1C: 141.6, C1-C1′; 125.9, C2-C2′; 60.5, C5-C5′; 34.3, C4-C4′; 30.7, C3-C3′. ^1H: 6.73 (s, 2H), C2-C2′; 3.87 (s, 4H), C3-C3′; 3.66 (quartet, $^3J_{H-H}$=6.12 Hz, $^3J_{H-OH}$=6.07 Hz, 4H), C5-C5′; 2.85 (t, $^3J_{H-H}$=5.95 Hz, 2H), OH; 2.69 (t, $^3J_{H-H}$=6.19 Hz, 4H), C4-C4′.

3.2.2. $[Cu(L1)_2]ClO_4$ and $[Cu(L1)_2]BF_4$

Method A. Solutions of L1 (300 mg, 1.14 mmol) in 5 ml of CH_2Cl_2 and of $Cu(ClO_4)_2 \cdot 6H_2O$ (185 mg, 0.50 mmol) in acetonitrile/absolute ethanol (1:1, 15 ml) were mixed. The resulting deep green solution was filtered and left to stand in a loosely covered 100 ml beaker for a week. Pale yellow crystals that formed were collected by filtration, washed with CH_2Cl_2 and diethyl ether, and dried in air. Yield 175 mg (51%). Caution must be taken when handling perchlorate salt since those of thioether metal complexes are potentially explosive.

Method B. Cuprous chloride (25 mg, 0.25 mmol) was dissolved in 10 ml of acetonitrile and a solution of $AgClO_4$ (52 mg, 0.25 mmol) in 5 ml of the same solvent was added. The mixture was stirred for about 15 minutes and then filtered. To the filtrate was added a solution of L1 (131 mg, 0.50 mmol) in 5 ml of CH_2Cl_2. The mixed solutions were left to evaporate slowly until pale yellow crystals deposited. The isolated product was identical to that obtained by Method A as shown by ir, m.p. and chemical analysis. Yield 125 mg (73%).

Preparations of $[Cu(L1)_2]BF_4$ are analogous to those for the perchlorate salt, but the yield by Method A is low. By Method B, the yield is 68%.

3.2.3. $[CuCl_2 \cdot L1]_2$ and $[CuCl_2 \cdot L3]_2$

Solutions of $CuCl_2 \cdot 2H_2O$ (42.6mg, 0.25 mmol) in 10 ml of acetonitrile and of L1 (80 mg, 0.30 mmol) in 5 ml of CH_2Cl_2 were mixed and the deep green solution was filtered quickly. The filtrate was left to evaporate slowly until dark green crystals deposited. The crystals were collected by filtration, washed with acetonitrile and CH_2Cl_2 and dried in air. Yield 70 mg (76%).

A similar procedure to that above was followed using $CuCl_2 \cdot 2H_2O$ (42.6 mg, 0.025 mmol) in THF (10 ml) and L3 (84 mg, 0.25 mmol) in the same solvent (5 ml) to give greenish brown crystals. Yield 95 mg (82%). Replacement of THF by acetonitrile, ethanol and their 1:1 mixture (v:v) afforded badly twinned greenish brown crystals that were unsuitable for X-ray studies.

3.2.4. $[Cu_2Cl_3 \cdot (L5)_2]_n$

Solutions of L5 (123 mg, 0.5mmol) in 10 ml of THF and $CuCl_2 \cdot 2H_2O$ (85 mg, 0.5 mmol) in 10 ml of the same solvent were mixed. The resulting reddish brown solution was filtered and the filtrate were left to evaporate until reddish brown crystals were deposited. The crystals were separated, washed with diethyl ether and dried in air. Yield 127 mg (70%).

3.2.5. $[(CuCl_2)_2 \cdot L]$ (L=L2, L7 and L8)

Preparations of these three compounds are analogous to that for $[CuCl_2 \cdot L3]_2$ in THF. Yields for the three compounds are 88%, 74% and 82%, respectively. Attempts to obtain crystals for these three compounds suitable for X-ray structural studies failed due to the formation of badly twinned crystals.

3.2.6. $[CuCl_2 \cdot L9]_n$

Solutions of $CuCl_2 \cdot 2H_2O$ (85 mg, 0.5 mmol) in 10 ml of acetone and of L9 (160 mg, 0.6 mmol) in the same solvent (10 ml) were mixed. The resulting deep green solution was left to evaporate slowly until greenish brown crystals were deposited. The crystals were collected by filtration, washed with acetone and dried in vacuum to afford 145 mg (73%) of polymeric complex. The compound decomposes upon prolonged storage at room temperature.

3.2.7. $[(CuCl)_2 \cdot L]_n$ (L=L2, L3, L7 and L8)

Cuprous chloride (25 mg, 0.25 mmol) was dissolved in 15 ml of acetonitrile and the appropriate number of moles of ligand in 5 ml of CH_2Cl_2 was added. The solution was left to evaporate until off-white crystals were deposited. The product was collected by filtration, washed with acetone and dried in vacuum. Yield 70-88%.

3.2.8. $[(CuBr)_2 \cdot L]_n$ (L=L2 and L7)

A procedure similar to that above was followed using the appropriate ligand (0.3 mmol) and $CuBr \cdot S(CH_3)_2$ (103 mg, 0.5 mmol) instead of cuprous chloride. Two copper(I) complexes, $[(CuBr)_2 \cdot L2]_n$ and $[(CuBr)_2 \cdot L7]_n$, were isolated as white crystals in 79% and 87% yields, respectively.

3.3. Results and discussion

All isolated copper complexes and their analytical data are given in Table 3-1. In view of their structural differences, they will be discussed separately.

Table 3-1: Analytical and physical data for Cu(II)/Cu(I) complexes of thiophenophane ligands and 2,5-bis(2-hydoxyethylthiomethyl)thiophene.

Complex	Color	C(%)*	H(%)	M(%)	Cl(%)	M.P. (°C)
$[CuCl_2 \cdot L1]_2$	dark green	30.40(30.24)	3.56(3.56)	16.1(16.0)	18.04(17.88)	132-135d**
$[Cu(L1)_2]ClO_4$	pale yellow	34.89(34.90)	4.10(4.10)	9.05(9.24)	---	170-175d
$[Cu(L1)_2]BF_4$	pale yellow	34.70(35.56)	4.25(4.18)	---	---	167-170d
$[(CuCl_2)_2 \cdot L2]$	dark green	24.56(24.35)	3.13(3.07)	20.8(21.5)	23.55(23.98)	130-135d
$[(CuCl)_2 \cdot L2]_n$	off-white	27.99(27.67)	3.57(3.48)	---	---	180-185d
$[(CuBr)_2 \cdot L2]_n$	white	24.37(23.63)	3.09(3.00)	---	---	187-191d
$[CuCl_2 \cdot L3]_2$	dark green	33.05(33.12)	4.26(4.28)	---	---	123-125d
$[(CuCl)_2 \cdot L3]_n$	white	29.38(29.19)	3.79(3.77)	24.0(23.8)	13.17(13.27)	225-228d
$\{[Cu_2Cl_3 \cdot (L5)_2]^+ (C_4H_8O)_{0.5}\}_n$	brown	34.31(34.64)	4.12(4.23)	15.8(16.7)	13.56(13.95)	139-142d
$[(CuCl_2)_2 \cdot L7]$	dark green	29.38(28.51)	3.16(2.99)	18.4(18.9)	21.29(21.06)	140-143d
$[(CuCl)_2 \cdot L7]_n$	white	32.18(31.87)	3.44(3.35)	19.8(21.1)	12.3(11.8)	197-202d
$[(CuBr)_2 \cdot L7]_n$	white	28.16(27.77)	2.92(2.92)	17.8(18.4)	23.89(23.11)	179-184d
$[(CuCl_2)_2 \cdot L8]_n$	dark green	31.62(30.79)	3.45(3.51)	17.6(18.1)	19.46(20.22)	140-145d
$[(CuCl)_2 \cdot L8]$	white	33.97(34.27)	3.81(3.84)	19.6(20.2)	10.93(11.24)	203-207d
$[CuCl_2 \cdot L9]_n$	brownish green	30.27(30.09)	4.09(4.04)	15.7(15.9)	17.83(17.78)	113-115d

* Found (calculated)

** decomposition

3.3.1. Bis-Ligand Complexes

3.3.1.1. Preparation

The bis-ligand copper(I) complexes $[Cu(L1)_2]ClO_4$ and $[Cu(L1)_2]BF_4$, in which L1 acts as a bidentate ligand, were isolated when attempts were made to prepare the corresponding copper(II) complexes. Both complexes can be also obtained by reaction of copper(I) perchlorate or tetrafluoroborate in acetonitrile. Products obtained by the two different methods are shown to be identical by ir, melting point and analytical data.

It is interesting to note that copper(II) undergoes reduction in the presence of L1 in CH_3CN and its mixtures with CH_2Cl_2, CH_3OH, or C_2H_5OH. As a result, $[Cu(L1)_2]^+$ was isolated instead of the corresponding copper(II) complex. The complex $[Cu(L1)_2]^+$ is stable under aerobic and anaerobic conditions, which confirms the stability of $[Cu(L1)_2]^+$ towards oxidation by atmospheric oxygen. Similar results have been reported for Cu(II)-[n]aneS4 (n = 12,13 and 14) systems (6-7). It seems that the copper(I) state is sufficiently stabilized by L1 so that no copper(II) compound is isolated in the absence of strongly coordinating anionic ligands such as Cl^-. The formation of a bis-ligand complex suggests that the cavity of L1 is not suitable to accommodate copper(II) coplanar with all four thioether sulfur atoms.

Other macrocyclic thiophenophane ligands have also been investigated for their complexing properties with Cu(II) in the absence of coordinating anions. In a mixture of acetonitrile and chloroform, Cu(II) undergoes reduction in the presence of these ligands as can be seen by the disappearance of the dark green color of Cu(II) from the solution. However, from the solution, no pure compounds were isolated.

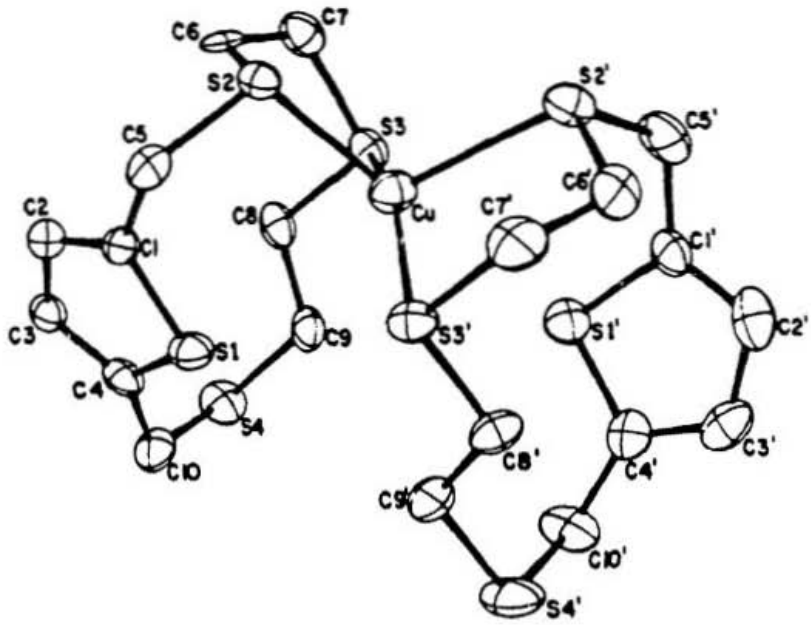

Cu-S(2)	2.359(3)	S(2)-Cu-S(3)	92.84(9)
Cu-S(3)	2.307(3)	S(2)-Cu-S(2')	109.49(9)
Cu-S(2')	2.392(3)	S(2)-Cu-S(3')	105.22(9)
Cu-S(3')	2.301(3)	S(3)-Cu-S(2')	103.76(9)
		S(3)-Cu-S(3')	150.3(1)
		S(2')-Cu-S(3')	92.36(9)

Figure 3-1. ORTEP drawing of $[Cu(L1)_2]^+$ and selected bond lengths (Å) and angles (degrees). The primes only represent the positions of atoms in the macrocycle.

3.3.1.2. Structure of $[Cu(L1)_2]^+$

To explain the observations above and to study the conformational change of L1 upon coordination, the molecular structure of $[Cu(L1)_2]ClO_4$ has been determined by X-ray crystallography. The ORTEP drawing and selected bond lengths and angles are given in Figure 3-1.

As discussed before, the free ligand (Figure 2-1) consists of a puckered polythioether chain extending in space at about 60° to the plane defined by the thiophene ring. The shape of the cavity of L1 is roughly triangular with an S2-S4 distance of 6.662 Å representing the base and an S1-S3 distance of 4.579 Å representing the height of the triangle. If we count thiophene-sulfur as a potential donor atom, the shape of the cavity of L1 is irregular. It has been shown by Rorabacher and coworkers (8) that macrocyclic tetrathioethers should have a cavity of 4.61 x 4.61 Å, which is the minimum that will accommodate Cu(II) coplanar with the four sulfur atoms. L1 fails to perform as a macrocyclic ligand not because of the size of its cavity but because the cavity is blocked by hydrogens on C6, C7, C8 and C9. The rigidity of the thiophene ring and its substituents in the 2 and 5 positions is also responsible for the ligand's inability to use all four sulfur atoms in one complex molecule. In the solid state of L1, all three thioether sulfur atoms are exocyclic, but the thiophene-sulfur is endocyclic. Therefore, it is impossible for L1 to be a polydentate ligand unless some conformational changes occur.

In $[Cu(L1)_2]^+$ (Figure 3-1), conformational change has occurred that mainly involves inversion of S3 and C8 of the free ligand (Figure 2-1, p74). The copper atom is coordinated by two pairs of thioether sulfurs, each pair lying in a separate ligand molecule, so that coordination geometry about copper is distorted tetrahedral. When

two coordinated sulfurs are in the same ligand molecule, the S-Cu-S angle is compressed to ~92° as is often found in 5-membered chelate complexes (9-10). When the sulfur atoms are in different ligand molecules, the S-Cu-S angles are close to the tetrahedral values except for one (S3-Cu-S3´) which has opened to ~150° due to the crowding of hydrogens on C8, C8´, C9 and C9´. The Cu-S bond lengths vary between 2.301 and 2.392 Å with an average length of 2.340 Å. These fall in the range found for $[Cu([15]aneS5)]^+$ (from 2.243 to 2.338 Å with an average 2.286 Å) (8) and for $[Cu(3,6\text{-dithiooctane})]^+$ (from 2.280 to 2.338 Å with an average of 2.286 Å) (9). Upon coordination to copper, there are no major changes in bond lengths in L1 and the greatest changes in bond angles are those associated with conformational change as mentioned earlier. The failure of L1 to use all of its coordination sites can be compared with that of [14]aneS4 in $[Cu([14]aneS4)]_n^{n+}$ (11), in which only three sulfur atoms are used because of the strain that would be introduced if all sulfur atoms coordinated to one copper atom or in $[(HgCl_2)_2 \cdot [14]aneS4]$ (12), in which only two sulfur atoms are coordinated to mercury due to the presence of the coordinating anion Cl^-. The simultaneous use of all three thioether sulfur atoms of L1 is precluded by the exocyclic orientation of their non-bonding electron pairs and by the rigidity of the C10-thiophene-C5 portion of the ligand molecule, which locks the third thioether sulfur into a position that is inappropriate for bond formation to the metal.

Examination of the conformation of coordinated L1 indicates that the endocyclic orientation of the thiophene-sulfur remains although conformational changes have occurred in other parts of the molecule. The Cu-S(thiophene) distance is 3.315 Å, which is significantly longer than the sum of the van der Waals' radii (3.20 Å) (13). By comparison with [9]aneS3 in $[Cu([9]aneS3)_2]^+$ (11) and [14]aneS4 in $[Cu([14]aneS4)]_n^{n+}$ (11), it is likely that the rigidity of the thiophene subunit and its

substituents in the 2 and 5 positions prevents L1 from occupying three basal sites of Cu(I). Therefore, L1 coordinates to Cu(I) as a bidentate ligand instead of a tridentate one.

3.3.1.3. Ir Spectra

The ir spectrum of $[Cu(L1)_2]ClO_4$ shows a very strong band at 1075 cm^{-1} and a strong band at 617 cm^{-1}, indicating an ionic perchlorate anion. In the spectrum of the tetrafluoroborate salt, those two bands have vanished and are replaced by the characteristic absorption bands of uncoordinated BF_4^- anion at 1050 cm^{-1} and 521 cm^{-1}. Attempts to characterize the complexes by nmr methods failed due to the fact that both complexes are insoluble in many organic solvents and are easily oxidized in DMF and DMSO.

3.3.1.4. Electrochemistry

Cyclic voltammetry of $[Cu(L1)_2]ClO_4$ in DMF shows a single quasi-reversible redox wave (Figure 3-2) associated with a Cu(I)/Cu(II) process with $E_{1/2}$ = 150 mV vs. SCE and ΔEp = 170 mV at a scan rate of 50 mV/s. The potential of the ferrocenium/ferrocene couple relative to the SCE was checked periodically under the same conditions and was observed to be constant at 400 mV. No redox activity has been detected for the free ligand in the range of -1.50 V to +0.80 V vs. SCE. In comparison with other copper complexes with open-chain and macrocyclic tetrathioether ligands (14), the low value of $E_{1/2}$ suggests that stabilization of Cu(I) relative to Cu(II) by L1 is less effective than that achieved by either open-chain or macrocyclic tetrathioether ligands, in which all four thioether sulfur atoms bonded to the metal center are in the same ligand molecule. It also seems that solvent plays a very important role in the electrochemical behavior of the complex. This kind of electrochemical

solvent effect is not well recognized and will be discussed in more detail later in this chapter.

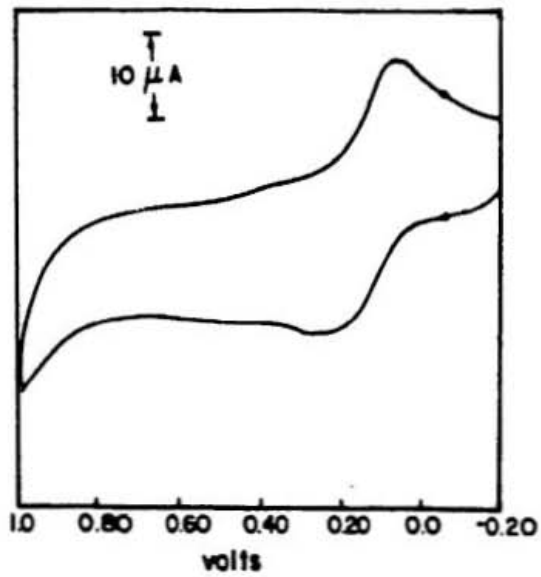

Figure 3-2. Cyclic voltammogram of $[Cu(L1)_2]ClO_4$ in DMF ($\sim 10^{-3}$ M, 0.1 M TEAP, glassy carbon working electrode, platinum wire counter electrode, SCE reference electrode) at a scan rate of 50 mV/s.

3.3.2. Binuclear Copper(II) Complexes of L1 and L3

As noted in the discussion above, copper(I) is stabilized sufficiently by L1 that the corresponding copper(II) complex can not be isolated in the absence of coordinating anions such as Cl^- nor can it be isolated in alcoholic or other easily oxidized solvents. It is of interest therefore to examine the coordinating behavior of L1 to copper(II) in the presence of the coordinating anion Cl^-. In addition, the cavity of the macrocycle in L3 can be increased by lengthening the aliphatic chain and the number of sulfur donor atoms. The increased flexibility that results may lead to some changes in the structural and physical properties of the copper(II) complexes. With this in mind, $[CuCl_2 \cdot L1]_2$ and $[CuCl_2 \cdot L3]_2$ have been prepared and studied by spectroscopic, electrochemical and X-ray methods.

3.3.2.1. Preparation

Complex $[CuCl_2 \cdot L1]_2$ was prepared from the reaction of L1 with copper(II) dichloride in an acetonitrile/dichloromethane mixture while $[CuCl_2 \cdot L3]_2$ was isolated from THF. Changing the solvent often produces badly twinned crystals and prolonged storage of either complex in solution with alcoholic or other easily oxidized components leads to the reduction of Cu(II) to Cu(I). This demonstrates again the stabilization of Cu(I) relative to Cu(II) by macrocyclic soft donor ligands and the high affinity of thioether sulfur for Cu(I).

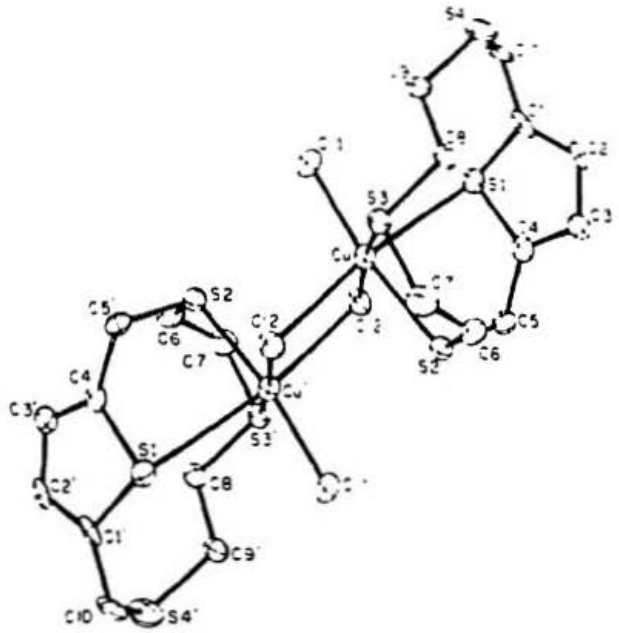

Cu-Cl(1)	2.234(3)	Cl(1)-Cu-Cl(2)	96.29(12)
Cu-Cl(2)	2.321(3)	Cl(1)-Cu-Cl(2')	100.89(11)
Cu-Cl(2')	2.702(3)	Cl(1)-Cu-S(2)	170.04(12)
Cu-S(1)	3.014(4)	Cl(1)-Cu-S(3)	91.25(12)
Cu-S(2)	2.349(3)	Cl(2)-Cu-Cl(2')	93.13(10)
Cu-S(3)	2.358(3)	Cl(2)-Cu-S(2)	84.29(12)
		Cl(2)-Cu-S(3)	172.46(12)
		Cl(2')-Cu-S(2)	88.99(11)
		Cl(2')-Cu-S(3)	85.45(10)
		S(2)-Cu-S(3)	88.28(12)
		Cu-Cl(2)-Cu'	86.87(10)

Figure 3-3. ORTEP drawing of $[CuCl_2 \cdot L1]_2$ and selected bond lengths (Å) and angles (degrees). The primed and unprimed atoms are related by a symmetry center.

3.3.2.2. Structures

The ORTEP drawing of $[CuCl_2 \cdot L1]_2$ is shown in Figure 3-3. It is clear that the conformation of L1 in $[CuCl_2 \cdot L1]_2$ resembles that in $[Cu(L1)_2]^+$ (Figure 3-1). The conformational change upon coordination to copper(II) mainly involves inversion at S3 and C8 of the free ligand and the endodentate orientation of thiophene-sulfur is retained.

The complex $[CuCl_2 \cdot L1]_2$ has two identical copper centers, each of which is surrounded by two chlorine-bridges to the other copper atom. One of these bridge-chlorines occupies a position on the tetragonal axis of a copper atom while the other one is in an equatorial site. The remaining three equatorial sites are taken by a terminal chlorine and two adjacent thioether sulfur atoms from L1. The molecule is centrosymmetric and thus the two terminal Cu-Cl bonds project on opposite sides of the Cu_2Cl_2 plane and the same is true for the macrocyclic ligands. All but one of the bond angles at Cu deviate less than 10° from ideal values with the largest deviation being 10.89° at Cl(1)-Cu-Cl(2′). Each copper atom lies 0.09 Å above the least-squares plane of the four nearest neighbours. The axial bridging Cu-Cl distance is 2.702(3) Å and equatorial bridging Cu-Cl distance is 2.321(3) Å while the terminal Cu-Cl bond length is only 2.234(3) Å. Angles at the chlorine bridgeheads are 86.87(10)° and the Cu-Cu distance is 3.464(7) Å. Corresponding distances and angles in the open chain chelate $[CuCl_2(BBTE)]_2$ (BBTE = $BuSCH_2CH_2SBu$) (15) are 2.825(2) (axial), 2.266(2) (equatorial) and 2.242 Å (terminal) while the chlorine bridgehead angle is 94.22(5)° and the Cu-Cu distance is 3.749(2) Å.

The structure of $[CuCl_2 \cdot L1]_2$ can be compared with that of a fragment of anhydrous cupric chloride consisting of two copper centers and four chlorines from two

adjacent bands in the band structure of anhydrous cupric chloride (16). In that structure, each copper atom is coordinated by four chlorines at 2.30 Å in a two-dimentional $[CuCl_2]_n$ band and by two more chlorines from adjacent bands at a distance of 2.95 Å to give a tetragonally distorted octahedral coordination sphere. In $[CuCl_2 \cdot L1]_2$, the bridge angles at Cl are close to 90° as at the inter-band bridgehead in cupric chloride and the bridging equatorial Cu-Cl distance is within 0.02 Å of the corresponding length in cupric chloride. The terminal Cu-Cl bond length of 2.23 Å is shorter than the 2.30 Å found in cupric chloride due to the fact that the bond is terminal in $[CuCl_2 \cdot L1]_2$ while it is bridging in cupric chloride. The axial Cu-Cl bond length of 2.70 Å in $[CuCl_2 \cdot L1]_2$ is shorter than the 2.95 Å found in cupric chloride because of the absence of the trans-influence of a second Cl on the tetragonal axis of $[CuCl_2 \cdot L1]_2$.

The Cu-S distances in $[CuCl_2 \cdot L1]_2$ are 2.349(3) and 2.358(3) Å, which fall in the range of 2.289-2.398 Å found in $[Cu([15]aneS5)]^{2+}$ (10). In comparison with the corresponding copper(I) complex $[Cu(L1)_2]^+$ (Cu-S bond lengths in the range of 2.301-2.392 Å), the similar bond lengths demonstrate the higher affinity of thioether sulfur for low oxidation state copper. Interestingly, the thiophene-sulfur of L1 is found to coordinate to copper(II) on the tetragonal axis of $[CuCl_2 \cdot L1]_2$ with a bond length of 3.014(4) Å which is reasonably close to that expected (2.98 Å) and significantly shorter than 3.20 Å, which is the sum of the van der Waals' radii (13). Thiophene-sulfur coordination is rather rare although examples with iron (17), ruthenium (18), silver (19) and copper(I) (20) are known. To our knowledge, the present example is the first involving copper(II). The observed Cu-S(thiophene) distance of 3.014(4) Å in $[CuCl_2 \cdot L1]_2$ falls in the range 2.96-3.16 Å as expected from recent studies of iron (17), silver (19) and copper(I) (20) thiophene complexes. It should be noted that the angles Cu-S(1)-C(1) and Cu-S(1)-C(4) are 136.8(4)° and 90.87(8)°, respectively, which

reveals that the bonding between copper(II) and thiophene-sulfur is asymmetric and strained. Spectroscopic evidence (vide infra) supports the conclusion that the thiophene-sulfur in $[CuCl_2 \cdot L1]_2$ is coordinated to copper(II). Thus, the coordination geometry about copper centers in $[CuCl_2 \cdot L1]_2$ is best regarded as distorted octahedral.

By comparing with $[Cu(L1)_2]^+$, it seems that the cavity of L1 is large enough for it to occupy one face of a distorted octahedron and it coordinates to copper(II) as a tridentate ligand instead of a bidentate one. Since the thiophene subunit is incorporated into the macrocycle, thiophene-sulfur coordination to copper(II) may be caused more by constraints imposed by the rigidity of the macrocyclic ring than by its intrinsic capacity to bind copper(II). When S2 and S3 coordinate to copper(II) at two equatorial positions, the endodentate orientation of thiophene-sulfur makes it possible to interact with the copper atom at its axial site without significant conformational change in the ligand molecule. From this point of view, it can be expected that L1 will also coordinate to other transition metals in a similar way.

In comparison with L1, the cavity of L3 is larger (4.8 x 8.0 Å) with all sulfur atoms exocyclic. Although the shape of the cavity of L3 is similar to that of [14]aneS4 (1), the rigidity of the thiophene subunit and its two substituents keeps S2 and S5 well separated. Therefore, unlike [14]aneS4 the cavity of L3 is not suitable for chelate formation at least in the solid state conformation. Furthermore, in the solid state conformation, the cavity of L3 is shielded by hydrogen atoms in the aliphatic chain, which prevents the approach of the metal ion.

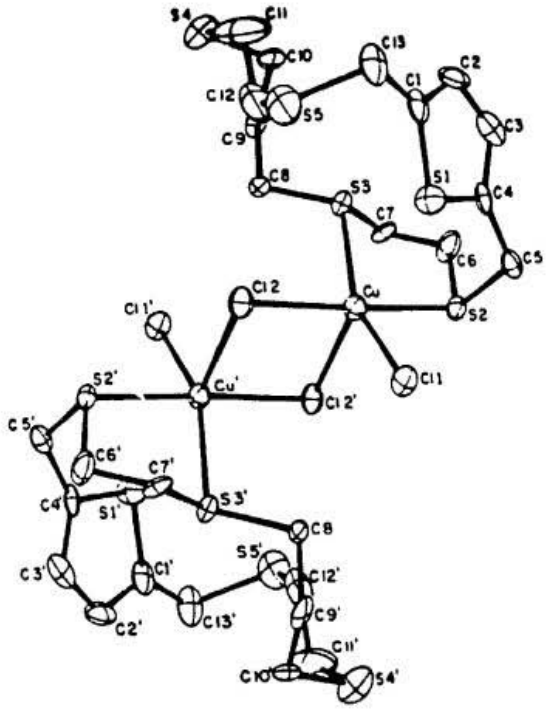

Cu-Cl(1)	2.265(4)	Cl(1)-Cu-Cl(2)	98.17(16)
Cu-Cl(2)	2.277(4)	Cl(1)-Cu-Cl(2')	101.69(15)
Cu-Cl(2')	2.661(4)	Cl(1)-Cu-S(2)	84.50(16)
Cu-S(2)	2.355(5)	Cl(1)-Cu-S(3)	153.12(17)
Cu-S(3)	2.358(4)	Cl(2)-Cu-Cl(2')	89.06(14)
		Cl(2)-Cu-S(2)	177.29(17)
		Cl(2)-Cu-S(3)	94.71(16)
		Cl(2')-Cu-S(2)	90.80(14)
		Cl(2')-Cu-S(3)	102.01(15)
		S(2)-Cu-S(3)	82.67(15)
		Cu-Cl(2)-Cu'	90.94(14)

Figure 3-4. ORTEP drawing of $[CuCl_2 \cdot L3]_2$ and selected bond lengths (Å) and angles (degrees). The primed and unprimed atoms are related by a symmetry center.

The ORTEP drawing of $[CuCl_2 \cdot L3]_2$ and selected bond lengths and angles are shown in Figure 3-4. The molecule is dimeric and its coordination geometry is somewhat different from that of $[CuCl_2 \cdot L1]_2$. Additional atoms in the macrocycle make it possible for the thiophene-sulfur to be further away from the copper in $[CuCl_2 \cdot L3]_2$ (3.307(9) Å) than in $[CuCl_2 \cdot L1]_2$ (3.014(4) Å). In fact, the Cu-S (thiophene) distance of 3.307(9) Å is too large for the two atoms to be considered bonded. The Cu-Cl bond distance trans to thiophene-sulfur is shorter in $[CuCl_2 \cdot L3]_2$ than in $[CuCl_2 \cdot L1]_2$. The geometry about each copper atom in $[CuCl_2 \cdot L3]_2$ is approximately square pyramidal. The dimeric molecule is also centrosymmetric and each copper lies 0.42 Å out of the least squares plane defined by Cl1, Cl2′, S2 and S3. The reduced crowding near copper that results from the retreat of the thiophene-sulfur makes it possible for both S3 and Cl1 to swing down about 12° below the basal plane of an idealized square pyramid. If viewed as a trigonal bipyramid, the angles at copper between axial and equatorial positions deviate less than 10° from the ideal 90° but the angles within the equatorial plane are the sites of distortion. They have values of 101.69(15)°, 102.01(15)° and 153.12(17)° and it is readily apparent that the first two arise from ~ 12° distortion from the ideal value for a square pyramid. Apparently, the preferred geometry about copper for this S_2Cl_3 donor set is trigonal bipyramidal because in the presence of thiophene-sulfur coordination and steric crowding in $[CuCl_2 \cdot L1]_2$, the corresponding S_2Cl_3 donor set adopts a square pyramidal geometry. As crowding decreases in $[CuCl_2 \cdot L3]_2$ the square pyramidal structure distorts towards t igonal bipyramidal. Thus the structure of $[CuCl_2 \cdot L3]_2$ is probably better regarded as a slightly distorted square pyramid than as a grossly distorted trigonal bipyramid.

The Cu-S(thioether) distances in $[CuCl_2 \cdot L3]_2$ are 2.355(5) and 2.358(4) Å and the Cu-Cl distances are 2.661(4) (bridging), 2.277(4) (bridging) and 2.265(4)

(terminal). These are very similar to those found in $[CuCl_2 \cdot L1]_2$. Angles at the chlorine bridgeheads are 90.94(14)° compared to 86.87(10)° in $[CuCl_2 \cdot L1]_2$ and the Cu-Cu distance is 3.530(4) Å compared to 3.464(7) Å.

Despite the slight change in geometry, the sum of the two Cu-S(thioether) and three Cu-Cl bond lengths for the three complexes listed in Table 3-2 is virtually constant (the difference is less than 0.1 Å) if the geometry around copper in $[CuCl_2 \cdot L1]_2$ is regarded as a five coordinated square pyramid. This observation is in accordance with the conclusion drawn by Gazo and coworkers (21) that the sum of all coordinate bond lengths is a constant for any series of Cu(II) complexes having the same donor set regardless of the nature of the ligand in which the donor atoms are incorporated (e.g. oxygen in H_2O, OH^-, NO_3^-, ClO_4^-, etc.). For $[CuCl_2 \cdot L1]_2$ and $[CuCl_2 \cdot L3]_2$, the average of the sums of Cu-S(thioether) and Cu-Cl bond distances is 11.940 Å. According to the general correlation above, the sum of Cu-S(thiophene) (van der Waals' radii, 3.20 Å), Cu-S(thioether) and Cu-Cl bond lengths is expected to be 15.14 Å for both complexes. For $[CuCl_2 \cdot L1]_2$, the observed value 14.978 Å is within the range of that expected. For $[CuCl_2 \cdot L3]_2$, the observed value 15.223 Å is larger than 15.14 Å and it is better to consider $[CuCl_2 \cdot L3]_2$ as a five- rather than six-coordinated complex.

Table 3-2: Comparison of structural parameters for binuclear Cu(II) complexes of thioether ligands.

Complex	Bond	Distance(Å)	Σ Cu-X(Å)***	Further remarks	Reference
$[CuCl_2 \cdot (BTTE)]_2$	Cu-Cl(1) Cu-Cl(2) Cu-Cl(2´) Cu-s(1) Cu-S(2)	2.242(2) 2.266(2) 2.825(2) 2.369(2) 2.308(2)	12.010	Cu is either square pyramidal with a bridging Cl as apical ligand or trigonal bipyramidal apical Cl and S	(15)
$[CuCl_2 \cdot L1]_2$	Cu-Cl(1) Cu-Cl(2) Cu-Cl(2´) Cu-S(1) Cu-S(2) Cu-S(3)	2.234(3) 2.321(3) 2.702(3) 3.014(4)* 2.349(3) 2.358(3)	11.964 (14.978)	Cu is either square pyramidal with a weak Cu-S (thiophene) interaction or octahedral with a weak Cu-S (thiophene) bond	this work
$[CuCl_2 \cdot L3]_2$	Cu-Cl(1) Cu-Cl(2) Cu-Cl(2´) Cu-S(1) Cu-S(2) Cu-S(3)	2.265(4) 2.277(4) 2.661(4) 3.307(9)** 2.355(4) 2.358(4)	11.916 (15.223)	Cu-S (thiophene) distance is too long to be considered a bond, Cu is either distorted square pyramidal or grossly distorted trigonal bipyramidal	this work

* The sum of the van der Waals radii is 3.20Å

** Cu-S (thiophene) distance is too long to be considered as a coordinate bond.

*** Σ Cu-X (Å): the sum of Cu-Cl and Cu-S bond lengths.

3.3.2.3. Ir Spectra

The ir spectra of both complexes exhibited strong bands at ~ 300 and 250 cm^{-1}, which are absent from the spectra of the free ligands and the analogous copper(I) complexes. In comparison with $[CuCl_3]_2^{2-}$, which has ir active Cu-Cl stretching modes at 236 and 193 cm^{-1} due to the double chlorine bridge and 300 and 278 cm^{-1} due to the terminal Cu-Cl stretching vibrations (22), the higher energy, more intense bands near 300 cm^{-1} in the spectra of both complexes are tentatively assigned to terminal Cu-Cl stretching vibrations and those near 250 cm^{-1} are also assigned to Cu-Cl stretching modes but specific assignment to a terminal or bridging Cu-Cl vibration is more problematical and has not been attempted.

3.3.2.4. Electronic Spectra and Conductivities

The electronic spectral data are listed in Table 3-3. Detailed assignments of those absorption bands are mainly based on the literature data for $[CuCl_2.BTTE]_2$ (23), in which each copper has a distorted square pyramidal CuS_2Cl_3 unit and two copper(II) centers are connected by two bridging chlorines as in $[CuCl_2.L1]_2$ and $[CuCl_2.L3]_2$. The lowest energy band in the spectra of both complexes is basically an envelope of unresolved d-d transitions even though $\pi(S) \rightarrow d_{x^2-y^2}$ charge transfer may enhance the intensity of this absorption. No further absorption bands have been detected up to 2000 nm. By comparison, changing from a distorted octahedral CuS_3Cl_3 chromophore in $[CuCl_2.L1]_2$ towards a distorted square pyramidal one in $[CuCl_2.L3]_2$ or $[CuCl_2.BTTE]_2$ has little effect on the charge transfer bands. It does, however, shift the maximum of the ligand field envelope to longer wavelength. The shift is probably due to a change in the relative intensity of the unresolved d-d transition bands. The spectrum of $[CuCl_2.L1]_2$ is largely unaffected by variation of solvent in contrast to the

noticeable effect of solvent on the ligand field band of $[CuCl_2.L3]_2$. These observations support the conclusions concerning coordination of thiophene-sulfur from the X-ray study. Thus, in $[CuCl_2.L1]_2$, thiophene-sulfur occupies the axial position of the copper atoms in both the solid state and in solution. The coordination of thiophene-sulfur to the metal center prevents the approach of a solvent molecule in the axial position. In $[CuCl_2.L3]_2$, however, thiophene-sulfur is too far away to interact with the copper atoms in either the solid state or in solution. It is not surprising therefore that the spectra of $[CuCl_2.L3]_2$ are affected by changes in solvent through coordination of a solvent molecule at the vacant octahedral site. In this regard, it may be noted that the shift in wavelength of the ligand field band of $[CuCl_2.L3]_2$ parallels the change in ligand field strength of the solvent. A strong absorption band at 260 nm due to the thiophene portion of the organic ligand (thioether bands are expected at 194 and 215 nm) (24) obscures the highest energy $Cl \rightarrow d_{x^2-y^2}$ LMCT band which should appear in the same region.

When the solvent is DMSO, remarkable changes occur in the ligand field transition bands for both complexes. Since DMSO is a strong σ-donor, replacement of one or more bridging chlorine ligands is possible. In support of this argument, conductivities of both complexes have been measured in different solvents and are given in Table 3-4. In nitromethane and acetonitrile, $[CuCl_2.L1]_2$ and $[CuCl_2.L3]_2$ are non-electrolytes and the binuclear structures appear to remain intact in solution. In DMSO, however, they are shown to be 1:2 electrolytes by both molar conductivities at 10^{-3} M and by Onsager plots (plots of Λ_o-Λ_M vs. $\sqrt{C}$) (Figure 3-5) (25).

Table 3-3: Electronic spectral data and assignments for Cu(II) complexes.

Complex	λ_{max} in nanometers (ϵ)						Assignment
	Solids	CH_2Cl_2	CH_3NO_2	CH_3CN	DMF	DMSO	
$[CuCl_2 \cdot BBTE]_2$ [a]	800	750(460)					d-d transition
	570(sh)						$\pi(S) \rightarrow d_{x^2-y^2}$
	448	449(2740)					$\sigma(S) \rightarrow d_{x^2-y^2}$
	387	363(6380)					$Cl \rightarrow d_{x^2-y^2}$
	240	272(3830)					$Cl \rightarrow d_{x^2-y^2}$
	215						Thioether
$[CuCl_2 \cdot L1]_2$	650	750(100)	725(170)	735(120)	875(100)	900(100)	d-d transition
	440	452(900)	430(sh)	450(840)	430(300)	420(sh)	$\sigma(S) \rightarrow d_{x^2-y^2}$
	355	325(2700)		360(sh)	350(sh)	310(1300)	$Cl \rightarrow d_{x^2-y^2}$
	290	275(sh)		280(sh)			$Cl \rightarrow d_{x^2-y^2}$
		250(6700)		250(7000)			b
$[(CuCl_2)_2 \cdot L2]$	650	725(200)		850(90)	925(120)	940(100)	d-d transition
	425	400(640)		456(1200)	430(400)		$\sigma(s) \rightarrow d_{x^2-y^2}$
	355				330(sh)	360(650)	$Cl \rightarrow d_{x^2-y^2}$
	265	250(23,800)		260(5000)			b
$[CuCl_2 \cdot L3]_2$	700	730(100)	750(130)	850(100)	880(90)		d-d transition
	450	450(1200)	425(sh)	460(900)	425(600)		$\sigma(s) \rightarrow d_{x^2-y^2}$
	360	350(2000)	365(1400)	360(sh)	345(sh)		$Cl \rightarrow d_{x^2-y^2}$
	310			300(3200)			$Cl \rightarrow d_{x^2-y^2}$
		250(6900)		250(7200)			b
$[(CuCl_2)_2 \cdot L7]$	770			900(120)	920(180)		d-d transition
	470			425(1000)	425(600)		$\sigma(s) \rightarrow d_{x^2-y^2}$
	340			350(sh)	360(sh)		$cl \rightarrow d_{x^2-y^2}$
				265(4700)			b
$[(CuCl_2)_2 \cdot L8]$	650				925(170)	950(200)	d-d transition
	460				425(600)	345(sh)	$\sigma(s) \rightarrow d_{x^2-y^2}$
	350				350(sh)	295(sh)	$Cl \rightarrow d_{x^2-y^2}$
					260(3500)		b
$[CuCl_2 \cdot L9]_n$	650				875(80)	900(80)	d-d transition
	450				420(600)	420(100)	$\sigma(s) \rightarrow d_{x^2-y^2}$
	350				340(sh)	330(sh)	$Cl \rightarrow d_{x^2-y^2}$
	315						$Cl \rightarrow d_{x^2-y^2}$

a. BBTE = $BuSCH_2CH_2SBu$ (reference 23); b. $Cl \rightarrow d_{x^2-y^2}$ + thiophene.

Table 3-4: Ir and conductivity data for Cu(II) complexes.

Complex	ν(Cu-Cl)[a]	Solvent	Λ_M[b]	Slope[c]
$[CuCl_2 \cdot L1]_2$	310(s),290(sh)	$MeNO_2$	18.8	-
	263(s)	MeCN	45.0	-
		DMSO	37.3	350
$[(CuCl_2)_2 \cdot L2]$	306(s),275(s)	$MeNO_2$	15.0	-
	248(m)	DMSO	45.5	725
$[CuCl_2 \cdot L3]_2$	278(vs),251(sh)	$MeNO_2$	23.0	-
	248(s)	DMSO	37.0	-
$[(CuCl_2)_2 \cdot L7]$	335(m),362(s)	$MeNO_2$	27.6	-
	287(s),275(sh)	DMSO	52.0	850
$[(CuCl_2)_2 \cdot L8]$	330(s),260(w)	$MeNO_2$	24.2	-
		DMSO	48.5	770
$[CuCl_2 \cdot L9]_n$	302(m),292(m)	$MeNO_2$	< 10	-
	232(m)	DMSO	27.5	320

a: in cm^{-1}; b: in $ohm^{-1} \cdot cm^2 \cdot mol^{-1}$ at a concentration of 5×10^{-4} M; c: $(\Lambda_o - \Lambda_M)/\sqrt{C}$.

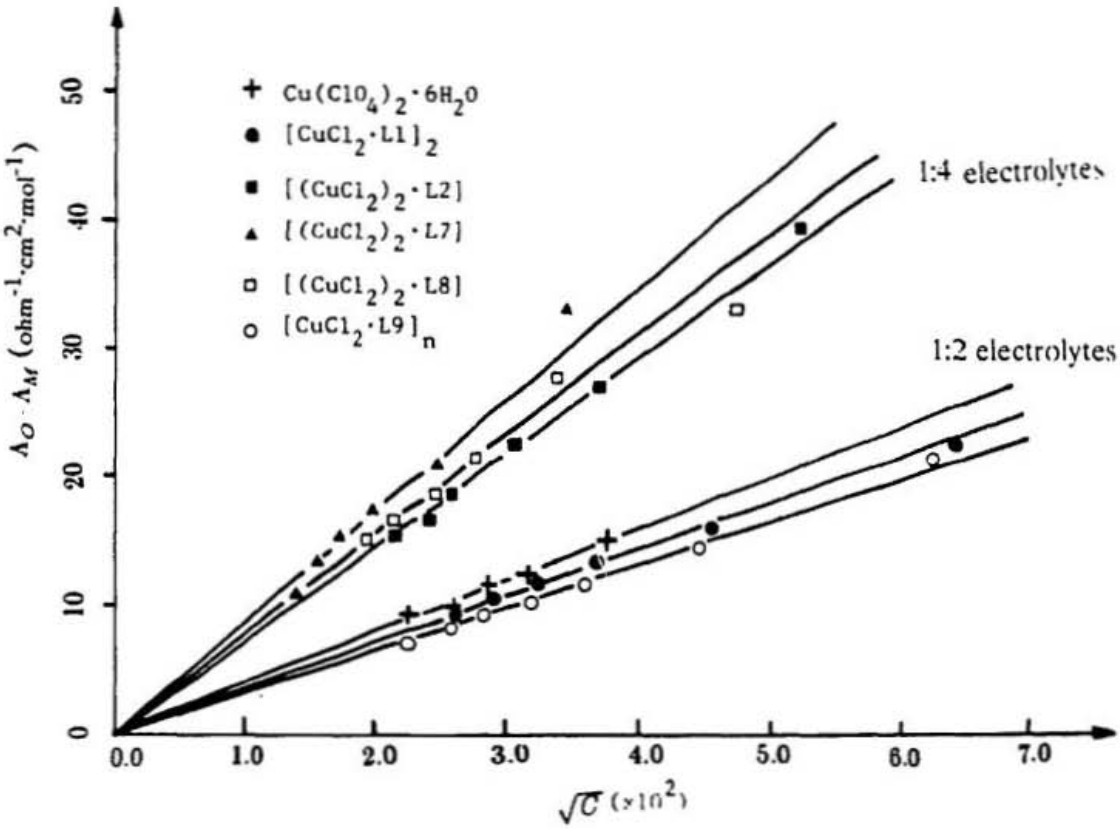

Figure 3-5. Onsager plots for copper(II) complexes of thiophenophane ligands and 2,5-bis(2-hydroxyethylthiomethyl)thiophene.

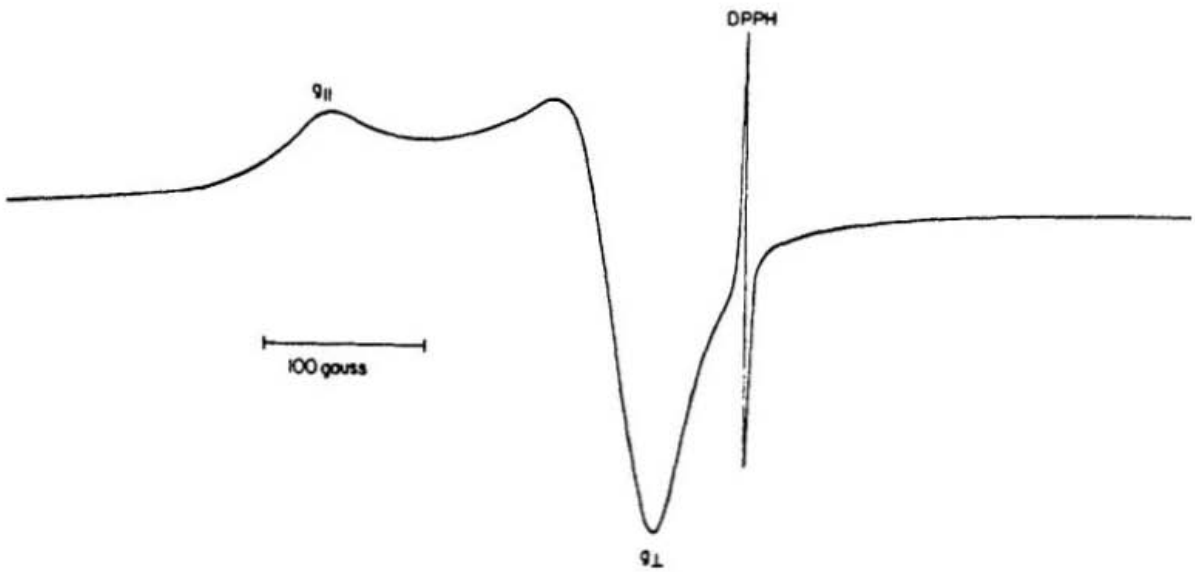

Figure 3-6. X-band esr spectrum of $[CuCl_2 \cdot L1]_2$ (polycrystalline sample) at room temperature.

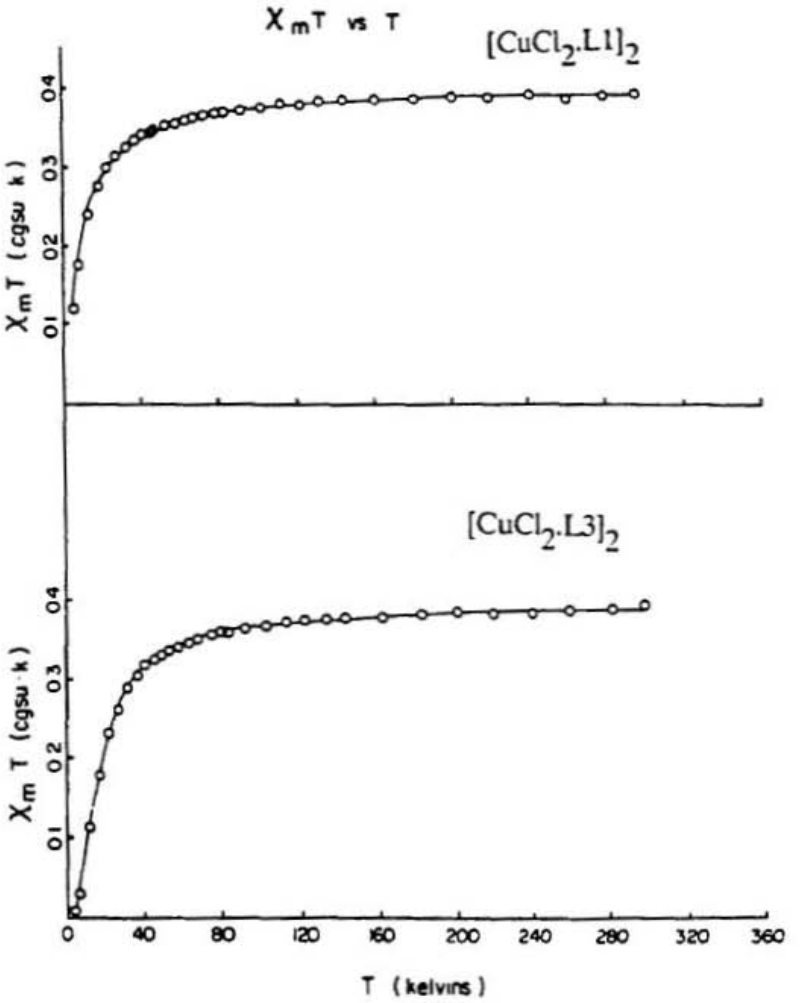

Figure 3-7. Plots of $\chi_M T$ versus T for $[CuCl_2 \cdot L1]_2$ and $[CuCl_2 \cdot L3]_2$.

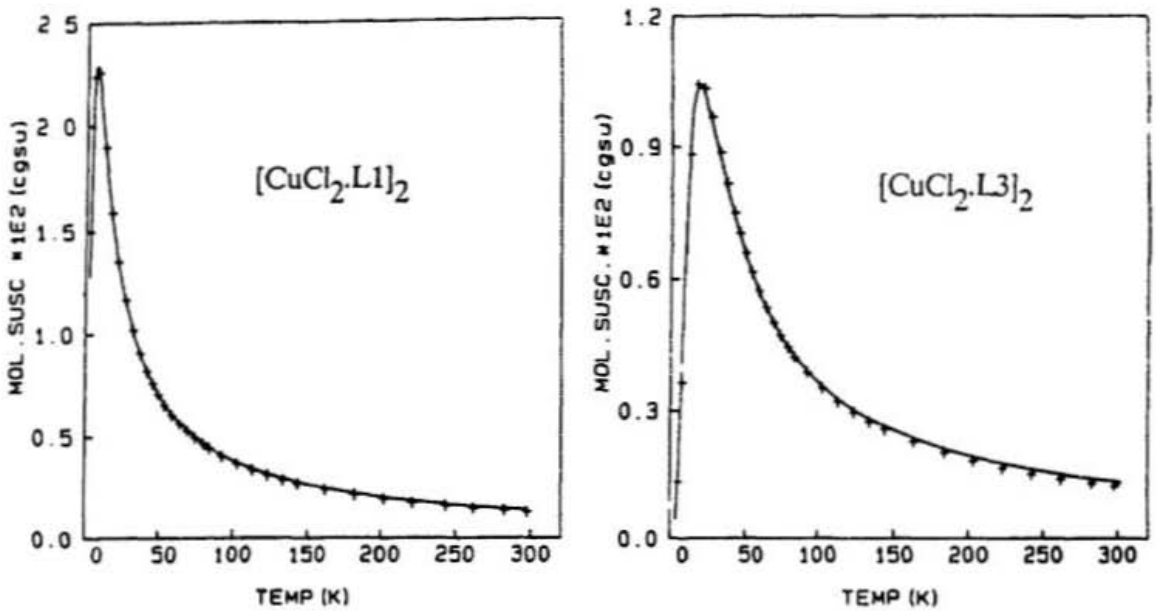

Figure 3-8. Plots of χ_M versus T for $[CuCl_2 \cdot L1]_2$ and $[CuCl_2 \cdot L3]_2$.

Table 3-5: Magnetic and esr data for Cu(II) complexes.

Complex	μ_{eff} (B.M.)	$g_{\|\|}$	$g_{\perp}$	g_{av}
$[CuCl_2 \cdot L1]_2$	1.74	2.151(2.145[a])	2.047(2.042)	2.082(2.077)
		2.176[b]	2.032	2.081
$[(CuCl_2)_2 \cdot L2]$	1.73			g_i = 2.085(2.086)
$[CuCl_2 \cdot L3]_2$	1.86	2.176(2.176[a])	2.037(2.032)	2.084(2 081)
$\{[Cu_2Cl_3(L5)_2](C_4H_8O)_{0.5}\}_n$	1.39			
$[(CuCl_2)_2 \cdot L7]$	2.10			
$[(CuCl_2)_2 \cdot L8]$	1.71	2.176(2.174)[a]	2.026(2.026)	2.077(2.076)
$[CuCl_2 \cdot L9]_n$	1.77			

a: at 77 K; b: in CH_2Cl_2 at 77 K.

3.3.2.5. Magnetic and Esr Properties

Magnetic moments (Table 3-5) were obtained at room temperature (298K). The values of μ_{eff} are 1.74 and 1.86 BM for $[CuCl_2.L1]_2$ and $[CuCl_2.L3]_2$, respectively. Esr spectra of polycrystalline samples of both complexes were obtained at 298K and 77K. The spectra, an example of which is shown in Figure 3-6, are all similar both in the solid state and in solution. Both complexes show simple axial spectra ($g_{||} > g_{|}$) with no resolvable metal hyperfine coupling and no detectable half-field absorption associated with a $\Delta M_s = \pm 2$ transition. These observations suggest that $d_{x^2-y^2}$ is the singly occupied orbital of Cu(II) and are consistent with the structural conclusions that the coordination geometry about each copper atom in $[CuCl_2 \cdot L3]_2$ is slightly distorted square pyramidal rather than severely distorted trigonal bipyramidal since a trigonal bipyramidal complex should display a "reverse axial" spectrum ($g_{\perp} > g_{||}$) (26-28). The absence of metal hyperfine splitting is probably related to the distorted coordination geometry about copper (29, 30) and to the formation of a dimeric structure (31).

Magnetic susceptibility data on powdered samples of the dinuclear complexes $[CuCl_2 \cdot L1]_2$ and $[CuCl_2 \cdot L3]_2$ were collected in the range 5-297K. The data were fitted to the Friedberg magnetization expression containing a molecular field correction (32, 33). Plots of either $\chi_M T$ versus T (Figure 3-7) or χ_M versus T (Figure 3-8) clearly indicate the presence of antiferromagnetic interactions that become apparent only at very low temperatures. From curve fitting, intradimer exchange, -2J (7.4(3) cm^{-1}, $[CuCl_2 \cdot L1]_2$; 20.8(1) cm^{-1}, $[CuCl_2 \cdot L3]_2$), and interdimer exchange, J´ (-0.9(1) cm^{-1}, $[CuCl_2 \cdot L1]_2$; -0.3(3) cm^{-1}, $[CuCl_2 \cdot L3]_2$) were obtained. Likewise, the g values were calculated to be 2.066(9) and 2.08(1) for $[CuCl_2 \cdot L1]_2$ and $[CuCl_2 \cdot L3]_2$, respectively. These values compare well with the average esr g values of 2.077 for $[CuCl_2 \cdot L1]_2$ and

2.084 for $[CuCl_2 \cdot L3]_2$. Since the dimers are formed from two square pyramidal monomers linked apex-to-base and apex-to-base (Figures 3-3 and 3-4) and since the partially occupied orbital in each monomer lies in its basal plane, the two magnetically active orbitals are remote from each other. Therefore, the small intramolecular coupling that is observed is not unexpected.

3.3.2.6. Electrochemistry

All electrochemical results (Table 3-6) were obtained in nitromethane, acetonitrile and DMSO solutions which were 0.1 M in supporting electrolyte (TEAP) and ~ 10^{-3} M in metal complex. Cyclic voltammogr.. of $[CuCl_2 \cdot L1]_2$ and $[CuCl_2 \cdot L3]_2$ are given in Figures 3-9 and 3-10. In acetonitrile, no redox activity has been detected for the two free ligands in the range -1.5 V to +1.0 V vs. SCE. The wave with $E_{1/2}$~ 0.53 V that occurs for acetonitrile solutions of both complexes is due to a reduction of Cu(II) to Cu(I). Since conductivity data have shown that both complexes are non-electrolytes in acetonitrile, $[CuCl_2 \cdot L1]_2$ and $[CuCl_2 \cdot L3]_2$ may undergo two one-electron reductions at the same potential ($E_1^f = E_2^f$) according to the consequence:

$$Cu^{II}\text{-}Cu^{II} \overset{E_1^f}{\rightleftharpoons} Cu^{II}\text{-}Cu^{I} \overset{E_2^f}{\rightleftharpoons} Cu^{I}\text{-}Cu^{I}$$

The cathodic and anodic separations for both complexes were 80 mV or more even at slow scan rates and increased with increasing scan rate, indicating that they are not truly reversible systems. It should be noted that 42 mV is the value of ΔEp predicted for reversible sequential transfer of two electrons in which the two potentials are identical (34). Furthermore, for a reversible process the cathodic and anodic waves should be symmetrical and have equal heights. The unsymmetrical cathodic and anodic waves and deviation of i_c/i_a ratio from unity provide strong evidence for the irreversibility of the electron transfer processes for $[CuCl_2 \cdot L1]_2$ and $[CuCl_2 \cdot L3]_2$.

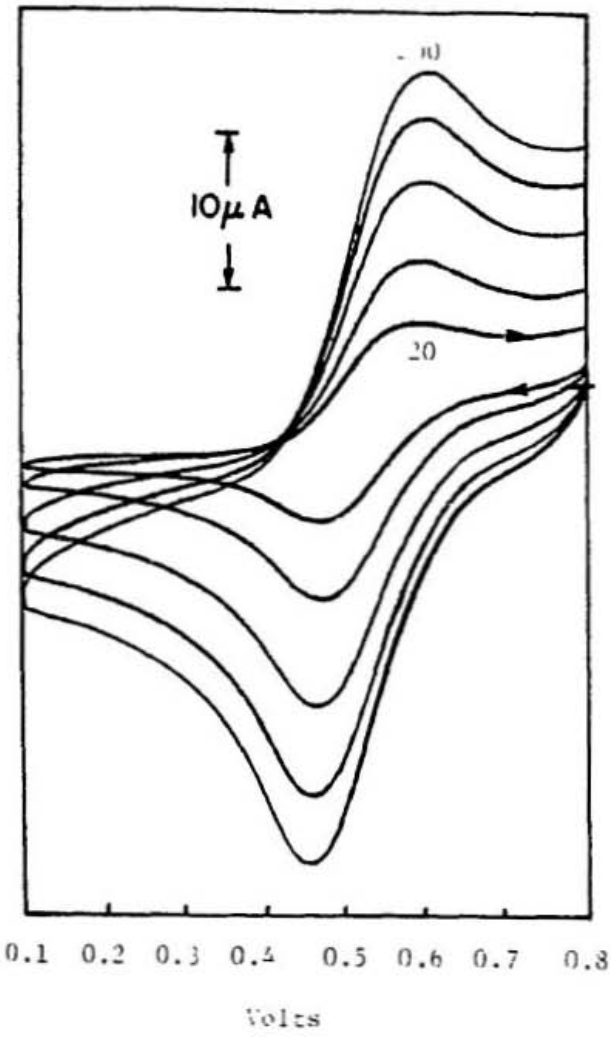

Figure 3-9. Cyclic voltammograms of $[CuCl_2 \cdot L1]_2$ in acetonitrile ($\sim 10^{-3}$ M, 0.1 M TEAP, glassy carbon working electrode, platinum wire counter electrode, SCE reference electrode) at scan rates: 20, 50, 100,150 and 200 mV/s.

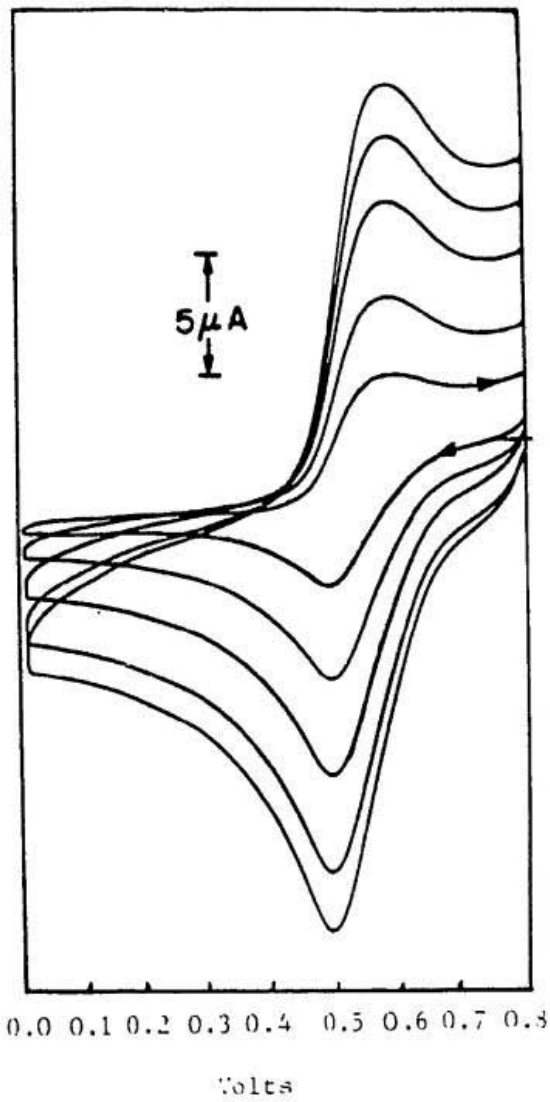

Figure 3-10. Cyclic voltammograms of $[CuCl_2 \cdot L3]_2$ in acetonitrile ($\sim 10^{-3}$ M, 0.1 M TEAP, glassy carbon working electrode, platinum wire counter electrode, SCE reference electrode) at scan rates: 20, 50, 100, 150 and 200 mV/s.

Table 3-6: Electrochemical properties of Cu(II) and Cu(I) complexes of thiophenophane ligands and 2,5-bis(2-hydroxyethylthiomethyl)thiophene.

Complex	Solvent	$E_{1/2}$ (mV)	ΔEp (mV)	K_{con}
$[CuCl_2 \cdot L1]_2$	$MeNO_2$	520	100	--
	MeCN	550	140	--
	DMSO	360	140	--
$[Cu(L1)_2]ClO_4$	DMF	150	170	--
$[(CuCl_2)_2 \cdot L2]$	$MeNO_2$	560	120	--
	MeCN	55, 535	70, 90	1.32×10^8
	DMSO	310	220	--
$[CuCl_2 \cdot L3]_2$	MeCN	530	90	--
	DMSO	310	180	--
$[(CuCl_2)_2 \cdot L7]$	$MeNO_2$	560	120	--
	MeCN	50, 535	60, 110	1.61×10^8
	DMSO	300	200	--
$[(CuCl_2)_2 \cdot L8]$	$MeNO_2$	550	120	--
	MeCN	50, 525	60, 110	1.09×10^8
	DMSO	290	220	--
$[CuCl_2 \cdot L9]_n$	$MeNO_2$	560	100	--
	MeCN	520	120	--
	DMSO	295	210	--

The coulometric experiments were carried out at a constant potential of +0.2 V, which is more negative than copper(II) reduction by about 0.3 V. For both complexes, transfers of two electrons per molecule (n = 1.8 ± 0.2) are observed. The large deviation from 2 may be caused by spontaneous reduction of the complex in acetonitrile. Green solutions of $[CuCl_2 \cdot L1]_2$ and $[CuCl_2 \cdot L3]_2$ on constant potential electrolysis (CPE) at +0.2 V turned colorless and lacked absorbance in the range of 950 to 450 nm, thereby indicating the absence of any copper(II) species.

It has been suggested that in order to observe two electron transfer in a single step, a prerequisite would be to have two adjacent and presumably strongly magnetically coupled copper(II) centers as in the case of binuclear copper(II) triketonate complexes (35). In the case under investigation, however, the two copper(II) centers in both complexes are weakly coupled and undergo single step two-electron transfers. Therefore, the actual electron-transfer behavior of a binuclear copper(II) complex does not necessarily depend on the extent of antiferromagnetic intramolecular coupling between the two copper(II) centers, and there must be some other perhaps subtle factors involved.

The electrochemical behavior of molecules containing two or more chemically equivalent and reversible redox sites have been the subject of theoretical and experimental studies (36-40). In the case of a molecule with two redox active sites, reduction potentials and the conproportionation constant, K_{con}, are related in the following way:

$$Cu^{II}\text{-}Cu^{II} \overset{E_1^f}{\rightleftharpoons} Cu^{II}\text{-}Cu^{I} \overset{E_2^f}{\rightleftharpoons} Cu^{I}\text{-}Cu^{I}$$

$$Cu^{II}\text{-}Cu^{II} + Cu^{I}\text{-}Cu^{I} \overset{K_{con}}{\rightleftharpoons} 2Cu^{II}\text{-}Cu^{I}$$

$$\log K_{con} = (E_1^f - E_2^f)/0.059$$

On the basis of the values of the conproportionation constant, it is natural to divide the two site systems into three categories (40, 41).

(1).K_{con}=4. This is the totally non-interacting case, in which the oxidation state of one site is not affected by oxidation state changes of the other. Although the two sites have the same microscopic redox potential, E_1^f and E_2^f are not equal but are separated by 35.6 mV due to statistical effects (39, 42).

(2).K_{con}<4. Since E_1^f-E_2^f<35.6 mV, it would imply that the second electron is easier to add than the first one and therefore the mixed-valence species Cu^{II}-Cu^{I} will be unstable with respect to disproportionation. In this situation, addition of the first electron is often followed by some geometrical and chemical changes such as rotation about a bond (39), bond-breaking (43, 44), protonation or solvation (47). Through one such process the second site becomes more prone to reduction.

(3).K_{con}>4. In this case, the second electron is more difficult to add than the first (E_1^f-E_2^f>35.6) and the mixed-valence species, Cu^{II}-Cu^{I} is stable. This is the most common case and has been observed in a number of binuclear copper(II) complexes (46-50).

The fact that $[CuCl_2 \cdot L1]_2$ and $[CuCl_2 \cdot L3]_2$ are reduced through two one-electron reductions at the same potential suggests that the mixed-valence species, Cu^{II}-Cu^{I}, is not stable and will be reduced to a Cu^{I}-Cu^{I} species as soon as it is produced. Since the two-electron transfer process is probably accompanied by a stereochemical change from tetragonal copper(II) geometry to distorted tetrahedral copper(I) geometry, the slow kinetics, as demonstrated by irreversibility in cyclic voltammograms (Figures 3-9 and 3-10), could be explained in terms of ECEC or EEC mechanisms (with C indicating the chemical complication following the charge

transfer E) rather than a simple EE mechanism. In the former cases, the activation barrier to electron transfer is increased by the chemical complication, thereby slowing down the rate of heterogeneous charge transfer and causing a marked deviation from pure reversible character of the charge transfer.

It should be noted that the electron transfer process in acetonitrile is more reversible for $[CuCl_2 \cdot L3]_2$ than for $[CuCl_2 \cdot L1]_2$. This may be attributed to the smaller activation energy barrier to electron transfer for the L3 complex than for the L1 complex. Since both processes presumably lead to essentially similar tetrahedral Cu(I) geometries, as demonstrated for a variety of thioether ligands, the energy barrier to this state is apparently lower starting from a distorted square planar copper(II) state in $[CuCl_2 \cdot L3]_2$ than from a distorted octahedral one in $[CuCl_2 \cdot L1]_2$. Thus, electron transfer is slower for octahedral species than for the square pyramidal species where an open axial site is involved. Similar conclusions have been drawn by Zubieta and coworkers (51).

Solvent plays an important role in the electrochemical behavior of these complexes. For both complexes, a strong σ-donor solvent DMSO gives lower reversibility (larger ΔEp) and reduced $E_{1/2}$ as shown in Figures 3-11 and 3-12. This suggests that the copper(II) state is stabilized by solvent ligation to the copper(II) centers. The degree to which stabilization occurs is determined by the extent of the saturation of the coordination sphere and by the donating ability of the solvent. The solvent induced changes in $E_{1/2}$ and ΔEp parallel changes in the d-d band shifts and ligand field strength of the solvent. Working electrode and supporting electrolyte also affect the electrochemical behavior of these complexes.

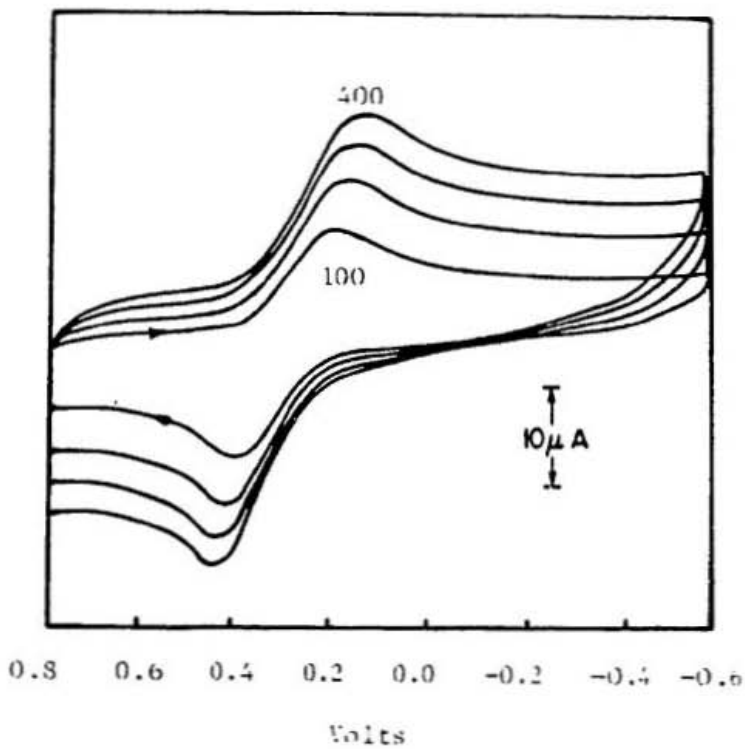

Figure 3-11. Cyclic voltammograms of $[CuCl_2 \cdot L1]_2$ in DMSO ($\sim 10^{-3}$ M, 0.1 M TEAP, glassy carbon working electrode, platinum wire counter electrode, SCE reference electrode) at scan rates: 100, 200, 300 and 400 mV/s.

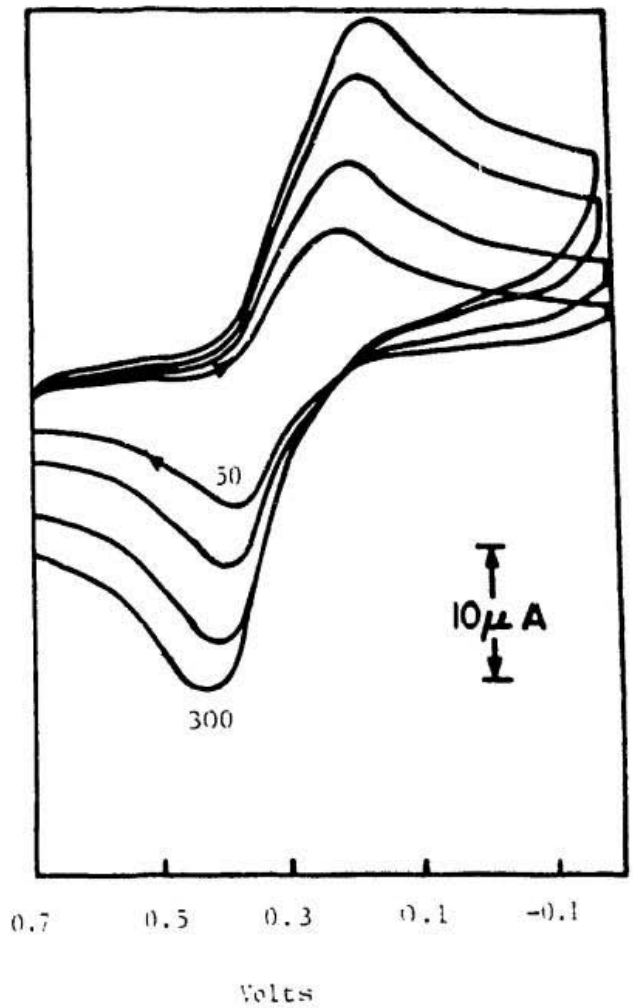

Figure 3-12. Cyclic voltammograms of $[CuCl_2 \cdot L3]_2$ in DMSO ($\sim 10^{-3}$ M, 0.1 M TEAP, glassy carbon working electrode, platinum wire counter electrode, SCE reference electrode) at scan rates: 50, 100, 200 and 300 mV/s.

3.3.3. Complexes $[(CuCl_2)_2 \cdot L]$ (L=L2, L7 and L8)

Complexes $[(CuCl_2)_2 \cdot L]$ (L=L2, L7 and L8) were prepared from the reaction of $CuCl_2 \cdot 2H_2O$ and the appropriate ligand in THF. Crystals obtained for these three complexes were not suitable for X-ray studies and are only sparingly soluble in common organic solvents. This suggests that they may have polymeric structures. They are soluble in DMF and DMSO, but they can not be recovered unchanged from these solvents, which indicates that they may decompose due to the strong σ-donor character of both solvents.

The ir spectra (Table 3-4) of $[(CuCl_2)_2 \cdot L]$ (L=L2, L7 and L8) resemble those of $[CuCl_2 \cdot L]_2$ (L=L1 and L3). Therefore, they may have very similar chlorine-bridged structures. The electronic spectra of $[(CuCl_2)_2 \cdot L2]$ both in the solid state and in solution are analogous to those of $[CuCl_2 \cdot L]$ (L=L1 and L3). The lowest energy bands in the region 650 to 900 nm are basically due to d-d transitions while the higher energy bands at about 450 and 350 nm are assigned to $\sigma(S) \rightarrow d_{x^2-y^2}$ and $\sigma(Cl) \rightarrow d_{x^2-y^2}$ charge transfer transitions, respectively. Due to the low solubility of $[(CuCl_2)_2 \cdot L7]$ and $[(CuCl_2)_2 \cdot L8]$, characterization by electronic spectroscopy in nitromethane is impossible. The mull spectra of $[(CuCl_2)_2 \cdot L7]$ and $[(CuCl_2)_2 \cdot L8]$ are similar to that of $[(CuCl_2)_2 \cdot L2]$. In DMF and DMSO, the maxima of the d-d envelope shifts to longer wavelength presumably due to the solvent effect as in cases of $[CuCl_2 \cdot L]_2$ (L=L1 and L3). In both solvents, replacement of one or more chlorine ligands is possible as is suggested by conductivity measurements in DMSO (Table 3-4), in which complexes $[(CuCl_2)_2 \cdot L]$ (L=L2, L7 and L8) were shown to be 1:4 electrolytes.

Magnetic moments (Table 3-5) were obtained at room temperature (298K). The values of μ_{eff} are 1.73, 2.10 and 1.71 BM for $[(CuCl_2)_2 \cdot L]$ (L=L2, L7 and L8), respec-

tively. Esr spectra of polycrystalline samples of $[(CuCl_2)_2 \cdot L]$ (L=L2 and L8) are similar to those of $[CuCl_2 \cdot L]_2$ (L=L1 and L3) and show simple axial spectra ($g_{||} > g_{|}$) with no resolvable metal hyperfine coupling. These observations suggest that $d_{x^2-y^2}$ is the singly occupied orbital of Cu(II) and the coordination geometry of each copper in these complexes is either square pyramidal or octahedral. However, in the absence of X-ray data any further structural discussion is largely speculation.

Cyclic voltammograms of $[(CuCl_2)_2 \cdot L]$ (L=L2, L7 and L8) are very similar, one example of which is shown in Figure 3-13. In acetonitrile, two redox waves were detected at 0.535 and 0.055 V vs. SCE. Since no X-ray data are available, two structures must be considered for this complex on the basis of synthetic and spectroscopic evidence. These are: a symmetrical dimer species or a dinuclear species in which the two copper centers are coordinated differently and are independent of each other. Either of these may be the repeated unit in a polymer or the complex may be monomeric. Since no redox reactivity has been detected for the free ligand (L2) in the range -1.5 V and +1.0 V vs. SCE, the very low half potential for the second electron transfer suggests that the two copper centers are not independent and therefore, the dicopper(II) complex is reduced from Cu^{II}-Cu^{II} to Cu^{I}-Cu^{I} in two distinct one-electron charge transfers at 0.535 and 0.055 V vs. SCE. Furthermore, the large separation in $E_{1/2}$ values for the two redox processes reveals the high stability of the mixed-valence species with respect to conproportionation. The value of K_{con} for $[(CuCl_2)_2 \cdot L2]$ is 1.30×10^8. Similar results were obtained for $[(CuCl_2)_2 \cdot L]$ (L=L7 and L8 in the same solvent and values of K_{con} are 1.61×10^8 and 1.09×10^8 for both complexes, respectively.

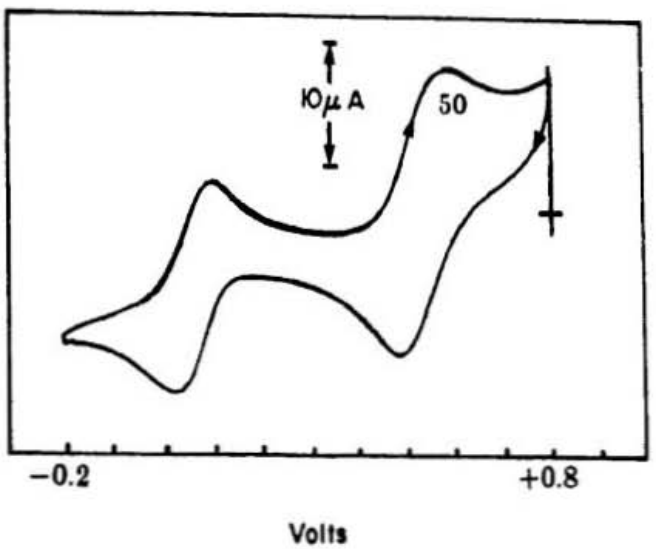

Figure 3-13. Cyclic voltammogram of $[(CuCl_2)_2 \cdot L2]$ in acetonitrile (saturated solution, 0.1 M TEAP, glassy carbon working electrode, platinum wire counter electrode, SCE reference electrode) at a scan rate of 50 mV/s.

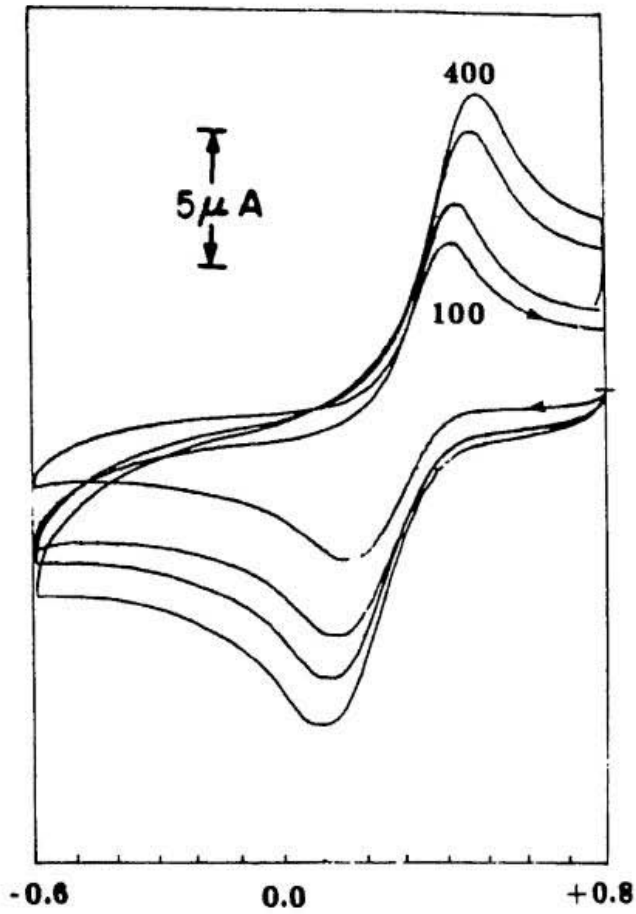

Figure 3-14. Cyclic voltammograms of $[(CuCl_2)_2 \cdot L2]$ in DMSO ($\sim 10^{-3}$ M, 0.1 M TEAP, glassy carbon working electrode, platinum wire counter electrode, SCE reference electrode) at scan rates: 100, 200, 300 and 400 mV/s.

Substitution of acetonitrile by DMSO causes remarkable changes in the cyclic voltammograms (Figure 3-14). The two redox waves at 0.535 and 0.055 V vs. SCE vanish and the complex $[(CuCl_2)_2 \cdot L2]$ is reduced at a single potential (0.295 V vs SCE). The similarity of the half potentials (Table 3-6) in DMSO for all five complexes discussed so far is consistent with their similar electronic spectral properties in that solvent (Table 3-3). It is possible that a DMSO solvated copper(II) is produced by ligand dissociation in all five cases.

3.3.4. $[Cu_2Cl_3(L5)_2]_n$

As discussed before, L1 coordinates to Cu(II) as a tridentate ligand and to Cu(I) as a bidentate one depending on the geometrical requirement of the metal center. In all cases, S3 is important for the formation of a five-membered chelate ring. It is interesting to study the complexing properties of L5, in which S3 is replaced by an oxygen donor atom.

Complex $[Cu_2Cl_3(L5)_2]_n$ was obtained as reddish brown crystals from the reaction of $CuCl_2 \cdot 2H_2O$ with L5 in THF. These crystals are insoluble in acetone and acetonitrile but are soluble in DMSO. The magnetic moment at room temperature is 1.39 BM, which suggests that the compound contains either both oxidation states (Cu(II) and Cu(I)) or a strongly antiferromagnetically coupled Cu(II) system. An X-ray structural study (Figure 3-15) shows that the former is true and the complex is a polymeric mixed-valence one. Characterization by methods other than X-ray diffraction is difficult because of the low solubility of the compound.

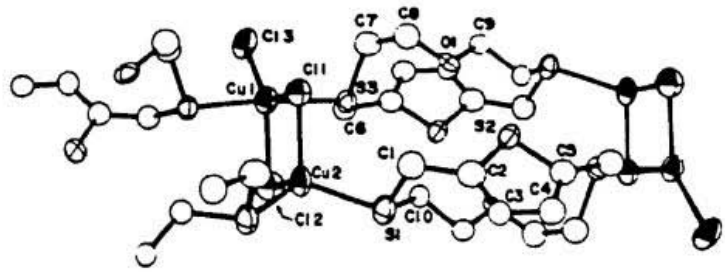

ORTEP drawing

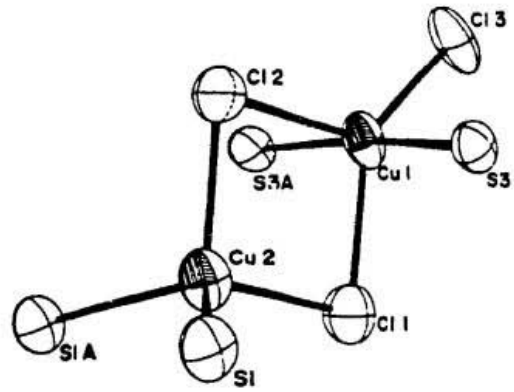

Cu(1)-Cl(1)	2.446(10)	Cl(1)-Cu(1)-Cl(2)	97.7(3)
Cu(1)-Cl(2)	2.412(9)	Cl(1)-Cu(1)-Cl(3)	136.7(4)
Cu(1)-Cl(3)	2.228(9)	Cl(1)-Cu(1)-S(3)	87.12(17)
Cu(1)-S(3)	2.334(5)	Cl(1)-Cu(2)-S(1)a	116.84(21)
Cu(1)-S(3)a	2.334(5)	Cl(2)-Cu(2)-S(1)	108.34(22)
Cu(2)-Cl(1)	2.352(9)	Cl(2)-Cu(2)-S(1)a	108.34(22)
Cu(2)-Cl(2)	2.420(9)	S(1)-Cu(2)-S(1)a	105.81(25)
Cu(2)-S(1)	2.308(6)	Cu(1)-Cl(1)-Cu(2)	81.4(3)
Cu(2)-S(1)a	2.308(6)	Cu(1)-Cl(2)-Cu(2)	80.7(3)

Figure 3-15. ORTEP drawing of polymeric $[Cu_2Cl_3 \cdot (L5)_2]_n$ and selected bond lengths (Å) and angles (degrees).

3.3.5. $[(CuX)_2 \cdot L]_n$ (X=Cl, L=L2, L3, L7 and L8; X=Br, L=L2 and L7)

Complexes $[(CuCl)_2 \cdot L]_n$ (L=L2, L3, L7 and L8) were prepared from the reaction of cuprous chloride in acetonitrile and the appropriate thiophenophane ligand in dichloromethane. Complexes $[(CuBr)_2 \cdot L]_n$ (L=L2 and L7) were prepared similarly using L2 or L7 and $CuBr \cdot S(CH_3)_2$ instead of cuprous chloride. All these compounds are air-stable both in solution and in the solid state, suggesting that the Cu(I) state is strongly stabilized by thiophenophane ligands. Since they all have very low solubility in many organic solvents, characterization by conventional spectroscopic methods is impossible. The polymeric structures of $[(CuCl)_2 \cdot L2]_n$ (Figure 3-16) and $[(CuBr)_2 \cdot L7]_n$ (Figure 3-17) have been confirmed by X-ray diffraction methods.

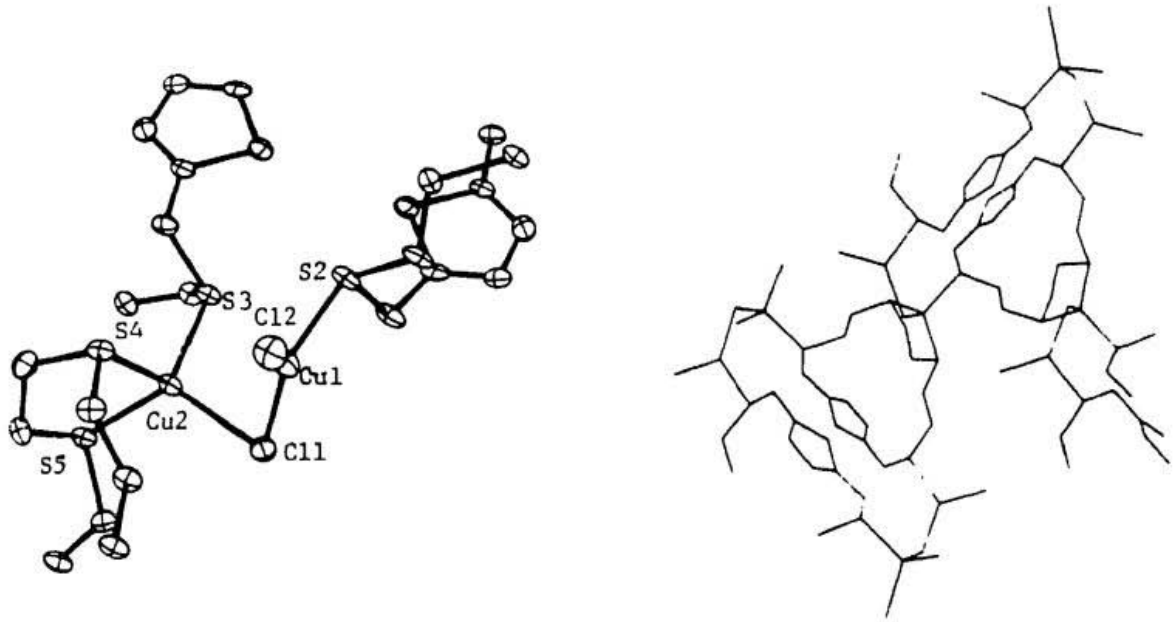

Cu(1)-Cl(1)	2.2762(24)	Cl(1)-Cu(1)-Cl(2)	129.93(10)
Cu(1)-Cl(2)	2.195(3)	Cl(1)-Cu(1)-S(2)	117.28(9)
Cu(1)-S(2)	2.2823(23)	Cl(2)-Cu(1)-S(2)	112.26(10)
Cu(2)-Cl(1)	2.3146(24)	Cl(1)-Cu(2)-S(3)	105.88(9)
Cu(2)-S(3)	2.3197(22)	Cl(1)-Cu(2)-S(4)	118.92(9)
Cu(2)-S(4)	2.3208(23)	Cl(1)-Cu(2)-S(5)	115.09(9)
Cu(2)-S(5)	2.3450(23)	S(3)-Cu(2)-S(4)	107.77(8)
		S(3)-Cu(2)-S(5)	116.12(8)
		S(4)-Cu(2)-S(5)	93.04(8)
		Cu(1)-Cl(1)-Cu(2)	80.28(8)

Figure 3-16. ORTEP (showing coordination spheres) and stick model (showing mode of polymerization) with some bond lengths (Å) and angles (degrees) for $[(CuCl)_2 \cdot L2]_n$.

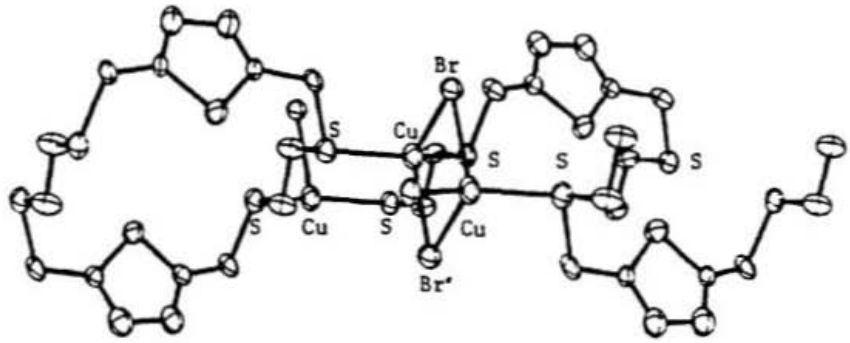

Cu-Br	2.579(3)	Cu-Br-Cu'	70.48(9)
Cu-Br'	2.483(3)	Br-Cu-Br'	109.52(11)
Cu-S	2.291(3)	Br-Cu-S	99.77(10)
Cu-S'	2.291(3)	Br-Cu-S'	105.21(11)
Cu-Cu	2.928(5)	Br'-Cu-S	99.77(10)
		Br'-Cu-S'	105.21(11)
		S-Cu-S'	135.51(18)

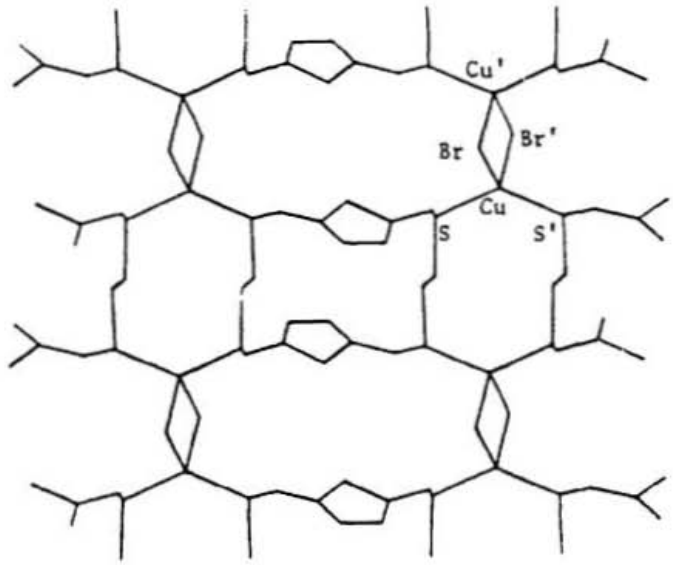

Figure 3-17. ORTEP (showing coordination spheres) and stick model (showing mode of polymerization) with some bond lengths (Å) and angles (degrees) for $[(CuBr)_2 \cdot L7]_n$.

3.3.6. $[CuCl_2 \cdot L9]_n$

During studies of the macrocyclic thiophenophane ligands it was found advantageous to examine the coordination chemistry of some related acyclic ligands. Here, synthesis and characterization of 2,5-bis(2-hydroxyethylthiomethyl)thiophene (L9) and its copper(II) complex $[CuCl_2 \cdot L9]_n$ are described.

3.3.6.1. Preparation

L9 was prepared from the reaction of 2,5-bis(chloromethyl)thiophene and 2-mercaptoethanol in basic medium. Reaction of L9 with copper(II) dichloride dihydrate in acetone produces greenish brown crystals suitable for X-ray study. These crystals are insoluble in acetone, acetonitrile and methanol suggesting that the compound is polymeric as confirmed by X-ray diffraction methods (Figure 3-18). The compound is soluble in DMF and DMSO, but it cannot be recovered unchanged from the solution, which indicates that it may decompose in DMF and DMSO due to the strong σ-donor character of both solvents.

3.3.6.2. Ir spectra

The ir spectrum of $[CuCl_2 \cdot L9]_n$ (nujol mull) exhibits strong bands at 295-305 cm^{-1} and 215-240 cm^{-1}, which are absent from the spectrum of the free ligand. As for $[CuCl_2 \cdot L1]_2$ and $[CuCl_2 \cdot L3]_2$ the higher energy bands near 300 cm^{-1} are tentatively assigned to terminal Cu-Cl stretching vibrations. In the spectrum of the free ligand, a strong absorption band has been observed at 3350 cm^{-1} due to a free OH stretching vibration. Upon coordination to a copper atom, this band is shifted by 190 cm^{-1}, appearing at about 3160 cm^{-1}. This suggests that the oxygen atom in the OH group is bonded to the metal, which is supported by X-ray structural data (Figure 3-18).

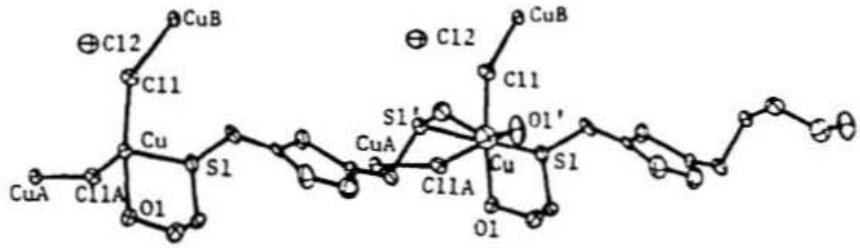

Cu-Cl(1)	2.261(3)	Cl(1)-Cu-Cl(1)A	96.05(9)
Cu-Cl(1)A	2.772(3)	Cl(1)-Cu-S(1)	91.02(10)
Cu-S(1)	2.338(3)	Cl(1)-Cu-O(1)	173.12(20)
Cu-S(1')	2.345(3)	Cl(1)-Cu-O(1')	94.33(21)
Cu-O(1)	2.045(6)	Cl(1)A-Cu-S(1)	83.85(9)
Cu-O(1')	2.380(7)	Cl(1)A-Cu-S(1')	91.27(9)
		Cl(1)A-Cu-O(1)	87.64(20)
		Cl(1)A-Cu-O(1')	167.22(20)
		S(1)-Cu-S(1')	174.38(20)
		S(1)-Cu-O(1)	83.59(19)
		S(1)-Cu-O(1')	103.41(18)
		S(1')-Cu-O(1)	99.05(19)
		S(1')-Cu-O(1')	81.90(18)
		O(1)-Cu-O(1')	82.8(3)
		Cu-Cl(1)-CuA	144.30(12)

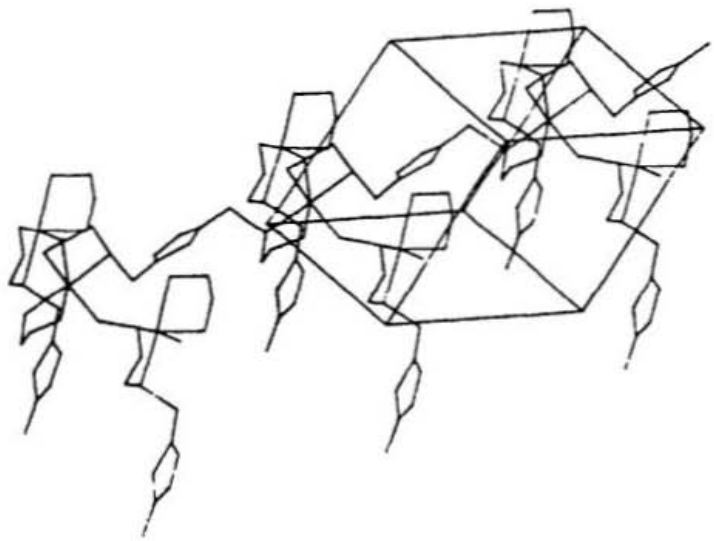

Figure 3-18. ORTEP (showing coordination spheres) and stick model (showing polymerization) with some bond lengths (Å) and angles (degrees) for $[CuCl_2 \cdot L9]_n$.

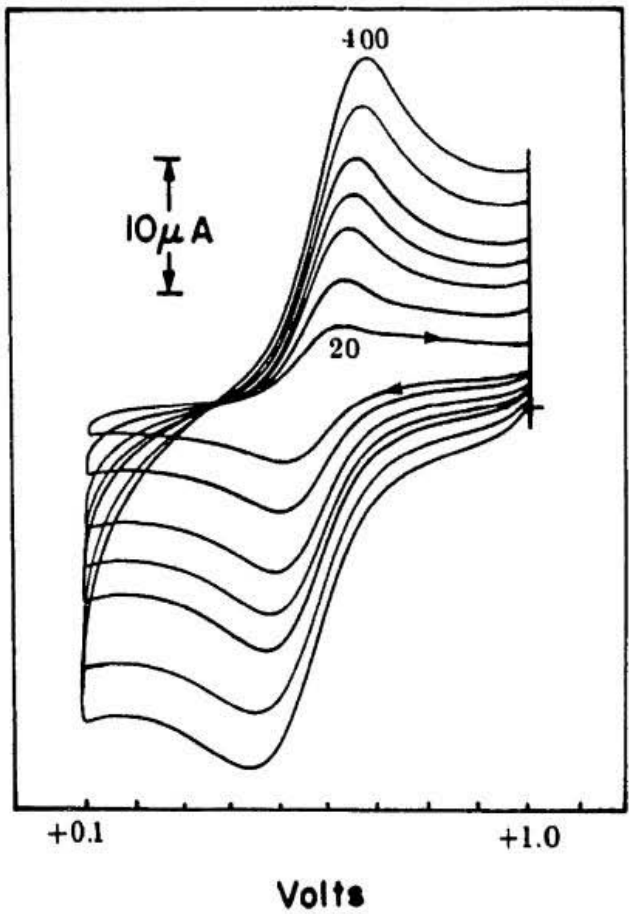

Figure 3-19. Cyclic voltammograms of $[CuCl_2 \cdot L9]_n$ in nitromethane (saturated solution, 0.1 M TEAP, glassy carbon working electrode, platinum wire counter electrode, SCE reference electrode) at scan rates: 20, 50, 100, 200, 300 and 400 mV/s.

3.3.6.3. Electronic Spectra and Conductivity

Due to the low solubility of $[CuCl_2 \cdot L9]_n$, characterization by electronic spectroscopy in acetonitrile and acetone is impossible. The mull spectrum, however, displays absorption bands at 650, 450 and 350 nm. The lowest energy band in the spectrum is basically a d-d transition while the higher energy bands at 450 and 350 nm are assigned to $\sigma(S) \rightarrow d_{x^2-y^2}$ and $\sigma(Cl) \rightarrow d_{x^2-y^2}$ charge transfer transitions, respectively. In DMF and DMSO, the maximum of the ligand field envelope shifts to longer wavelength. This shift is probably caused by the replacement of oxygen or chlorine donor atoms by solvent molecules. This interpretation has been supported by conductivity results that show $[CuCl_2 \cdot L9]_n$ to be a 1:2 electrolyte in DMSO (Figure 3-5).

3.3.6.4. Magnetic Properties

The room temperature magnetic moment of $[CuCl_2 \cdot L9]_n$ is 1.77 BM. This low value of μ_{eff} suggests that there may be antiferromagnetic interactions between adjacent copper(II) centers. This is in agreement with the three dimensional structure of the complex, in which copper centers are bridged by two chlorine atoms in one direction and SCH_2-thiophene-CH_2S moieties in the other two directions (Figure 3-18).

3.3.6.5. Electrochemistry

Cyclic voltammetry of $[CuCl_2 \cdot L9]_n$ (Figure 3-19) in nitromethane (saturated solution) shows a quasi-reversible redox process at 0.52 V vs. SCE with $\Delta Ep = 100$ mV at a scan rate of 50 mV/s. Since no redox activity has been detected for the free ligand in the range -1.0 V to +1.0 V vs. SCE, the reduction is assigned to an electron transfer process converting Cu(II) to Cu(I). The large ΔEp value and deviation of i_c/i_a ratio from unity are consistent with the quasi-reversible character of the process above. In comparison with acetonitrile solutions, the lower redox potential ($E_{1/2}$) and increased

irreversibility found in DMSO are probably caused by the strong solvent effect of DMSO. Similar results have been observed for other copper(II) complexes of thiophenophane ligands.

3.4. References

1. R.E. DeSimone and M.D. Glick. J. Am. Chem. Soc. *98*, 762 (1976).
2. R.E.W. Wolf, J.R. Hartman, J.M.E. Storey, B.M. Foxman and S.R. Cooper. J. Am. Chem. Soc. *109*, 4328(1987).
3. B. de Groot and S.J. Loeb. Inorg. Chem. *28*, 3573 (1989).
4. R.J. Angelici. Acc. Chem. Res. *21*, 387 (1988).
5. N.J. Hill. J. Chem. Soc., Faraday Trans. *72*, 631 (1976).
6. K.B. Yatsimirskii, V.V. Paulishchuk and P.E. Strizhak. Zh. Obshch. Khim. *59*, 359(1989).
7. V.V. Paulishchuk, K.B. Yatsimirskii, P.E. Strizhak and J. Labuda. Inorg. Chim. Acta, *164*, 65 (1989).
8. V.B. Pett, L.L. Diaddario, E.R. Dockal, P.W. Corfield, C. Ceccarelli, M.D. Glick, L.A. Ochrymowycz and D.B. Rorabacher. Inorg. Chem. *22*, 3611 (1983).
9. E.N. Baker and G.E. Norris, J. Chem. Soc. Dalton Trans. 877 (1977).
10. P.W. Corfield, C. Ceccarelli, M.D. Glick, I.W.Y. Moy, L.A. Ochrymowycz and D.B. Rorabacher. J. Am. Chem. Soc. *107*, 2399 (1985).
11. L.L. Diaddario, E.R. Dockal, M.D. Glick, L.A. Ochrymowycz and D.B. Rorabacher. Inorg. Chem. *24*, 356 (1985).

12. N.W. Alcock, N. Herron and P. More. J. Chem. Soc. Dalton Trans. 394 (1978).

13. J.E. Hueey. *Inorganic chemistry*. 3rd Ed. Harper and Row, New York. 1983. p. 258.

14. E.R. Dockal, T.E. Jones, W.F. Sokol, R.J. Engerer, D.B. Rorabacher and L.A. Ochrymowycz. J. Am Chem. Soc. *98*, 4322 (1976).

15. B. Cohen, C.C. Ou, R.A. Lalancette, W. Borowski, J.A. Potenza and H.J. Schugar. Inorg. Chem. *18*, 217 (1979).

16. F.A. Cotton and G. Wilkinson. *Advanced inorganic chemistry*. 4th Ed. Wiley, Toronto. 1981. p. 815.

17. J.D. Goodrich, P.N. Nickias and J.P. Selegue. Inorg. Chem. *26*, 3424 (1987).

18. S.M. Bucknor, M. Draganjac, T.B. Rauchfuss, C.J. Ruffing, W.C.F. Fultz and A.L. Rheingold. J. Am. Chem. Soc. *106*, 5379 (1984).

19. A.L. Spek, A.J.M. Duisenberg, G.C. van Stein, G. van Koten. Acta Crystallogr. *C41*, 347 (1985).

20. G.C. van Stein, G. van Koten, K. Vrieze, A.L. Spek. E.A. Klop and C. Brevard. Inorg. Chem. *24*, 1367 (1985).

21. J. Gazo, I.B. Bersuker, J. Garaj, M. Kabseova, J. Kohout, H. Langfelderova, M. Melnik, M. Serator and F. Velach. Coord. Chem. Rev. *19*, 253 (1976).

22. J.R. Ferraro. *Low frequency vibrations of inorganic and coordination Compounds*. Plenum, New York. 1971. p. 175.

23. V.M. Miskowski, J.A. Thich, R. Solomon and H.S. Schugar. J. Am. Chem. Soc. *98*, 8344 (1976).

24. A.I. Scott. *Interpretation of the ultraviolet spectra of natural products*. Pergamon

Press, Oxford. 1964. p. 135.

25. R.D. Feltham and R.G. Hayter. J. Chem. Soc. 4587 (1964).

26. L.K. Thompson, B.S. Ramaswamy and R.D. Dawe. Can. J. Chem. *56*, 1311 (1978).

27. H.M.J. Hendriks and J. Reedijk. Inorg. Chim. Acta *37*, L507 (1979).

28. A.W. Addison, H.M.J. Hendriks, J. Reedijk and L.K. Thompson. Inorg. Chem. *20*, 103 (1981).

29. A.W. Addison, P.J. Burke, K. Henrick, T.N. Rao and E. Sinn. Inorg. Chem. *22*, 3645 (1983).

30. A.W. Addison, T.N. Rao, J. Reedijk, J. van. Rijn and G.C. Verschoor. J. Chem. Soc. Dalton Trans. 1349 (1984).

31. J.V. Dagdigian, V. McKee and C.A. Reed. Inorg. Chem. *21*, 1332 (1982).

32. C.R. Lucas, S. Liu and L.K. Thompson. Inorg. Chem. *29*, 85 (1990).

33. B.E. Myers, L. Berger and S.A. Friedberg. J. Appl. Phys. *40*, 1149 (1969).

34. J. Heinze. Angew Chem. Int. Ed. Engl. *23*, 831 (1984).

35. D.E. Fenton and R.L. Lintvedt. J. Am. Chem. Soc. *100*, 6367 (1978).

36. D.S. Polcyn and I. Shain. Anal. Chem. *45*, 2043 (1973).

37. F. Ammar and J.M. Saveant. J. Electroanal. Chem., Interfacial Electrochem. *47*, 115 , 215 (1973).

38. M. Goto and K.B. Oldham. Anal. Chem. *45*, 2043 (1973).

39. J.B. Flanagan, S. Mangel, A.J. Bard and F.C. Anson. J. Am. Chem. Soc. *100*, 4248 (1978).

40. J. Phaphs and A.J. Bard. J. Electroanal. Chem. *68*, 313(1976).

41. A.J. Bard. Pure & Appl. Chem. *25*, 379 (1971).

42. W.H. Morrison, S. Krogsrud and D.N. Hendrickson. Inorg. Chem. *12*, 1998 (1973).

43. R.E. Dessy, P.M. Weissman and R.P. Pohl. J. Am. Chem. Soc. *88*, 5117 (1966).

44. R.E. Dessy, R. Kornmann, C. Smith and R. Haytor. J. Am. Chem. Soc. *90*, 2001 (1968).

45. T.N. Sorrell, M. R. Malachowski and D.L. Jameson. Inorg. Chem. *21*, 3250 (1982).

46. G.H. Patterson and R.H. Holm. Bioinorg. Chem. *4*, 257 (1975).

47. A.W. Addison. Inorg. Nucl. Chem. Lett. *12*, 257 (1976).

48. R.R. Gagné, C.A. Koval and T.J. Smith. J. Am. Chem. Soc. *99*, 8367 (1977).

49. R.R. Gagné, R.P. Kreh and J.A. Dodge. J. Am. Chem. Soc. *101*, 6917 (1979).

50. J.J. Crzybowski, P.H. Merreland, F.L. Urbach. Inorg. Chem. *17*, 3078 (1978).

51. K.D. Karlin and J. Zubieta. *Copper coordination chemistry: Biochemical and inorganic perspectives*. Adenine Press; Guilderland, New York. 1983. p. 97.

CHAPTER 4

SYNTHESIS AND CHARACTERIZATION OF PALLADIUM(II) AND PLATINUM(II) COMPLEXES OF OPEN-CHAIN AND MACROCYCLIC THIOETHER LIGANDS

Abstract:

Part I. Palladium(II) and Platinum(II) Complexes of Thioether Ligands

Complexes $[MX_2 \cdot L]$ (M=Pt, X=Cl; M=Pd, X=Cl, Br, I, SCN; L=L1, L10-L14) and $[M(L)_2]X_2$ (M=Pt, Pd; X=ClO_4^- or $CF_3SO_3^-$; L=L1, L10, L12 and L14) have been prepared for 2,5,8-trithia[9](2,5)thiophenophane (L1) and open-chain dithioethers, 1,2-bis(benzylthio)ethane (L10), 1,3-bis(benzylthio)propane (L11), 1,2-bis-(benzylthiomethyl)benzene (L12), 1,2-bis(2-hydroxyethylthiomethyl)benzene (L13) and 1,2-bis(p-chlorophenylthiomethyl)benzene (L14). The molecular structure of $[PdBr_2 \cdot L1]$ which contains a rare thiophene-sulfur-to-palladium bond, has been determined. The electronic, low frequency ir and ^{13}C nmr spectra are described. The $[Pd(L)_2]X_2$ (L=L1, L10-L12, L14; X=ClO_4^- or $CF_3SO_3^-$) complexes are 1:2 electrolytes. The variable temperature ^1H nmr spectra are discussed and it is concluded that the open-chain dithioether complexes undergo rapid conformational exchange at room temperature but are configurationally rigid. The configurational stability of these complexes is dependent on the nature of the trans ligands, X, with stabilities in the order of Cl>Br>I, and of the dithioether ligand itself. Variation of the backbone of the ligand gives the order CH_2CH_2 > $CH_2CH_2CH_2$ ~ ortho-$C_6H_4(CH_2)_2$ for configurational stability. In contrast, the macrocyclic thioether complexes undergo very limited conformational and no configurational exchange up to their decomposition temperatures. This is interpreted as strong evidence for non-dissociative inversion at coordinated sulfur being the mechanism for configurational exchange that is

observed in complexes of open-chain dithioether ligands. Chemical exchange of acidic ligand hydrogens and a metal-ligand dissociative equilibrium were also detected when X=SCN in $[PdX_2 \cdot L1]$.

Part II. π-Allylpalladium Complexes of Thioether Ligands

Preparation of π-allylpalladium complexes $[Pd(C_3H_5) \cdot L]X$ (L=L1, $X=CF_3SO_3^-$; L=L10, L12, L14, $X=PF_6^-$) and $[Pd_2(C_3H_5)_2 \cdot L](PF_6)_2$ (L=2,5,8,11-tetrathia[12](2,5)thiophenophane (L2), 2,5-dithia[6,6](2,5)thiophenophane (L7) and 2,6-dithia[7,7](2,5)thiophenophane (L8) are described. The molecular structure of $[Pd(C_3H_5) \cdot L1]^+$ reveals an asymmetric π-allyl group and a rare, unusually short apical Pd-S(thiophene) bond (2.786(4) Å). The $[Pd(C_3H_5) \cdot L]X$ ($X=PF_6^-$ or $CF_3SO_3^-$; L=L1, L10, L12 and L14) complexes are 1:1 electrolytes and $[Pd_2(C_3H_5)_2 \cdot L](PF_6)_2$ (L=L2, L7 and L8) are 1:2 electrolytes. The ^1H nmr spectra are discussed and it is concluded that dithioether complexes undergo rapid inversion at coordinated sulfurs while thiophenophane complexes undergo a 1,4-metallotropic shift on the heteroatoms of the macrocycle at room temperature and a dissociative inversion at thioether sulfurs at elevated temperatures. A solvent-assisted σ-π interconversion mechanism is proposed for the syn/anti interchange of the π-allyl group.

Part I. Palladium(II) and Platinum(II) Complexes of Thioether Ligands

4.1.1. Introduction

In the preceding chapter, copper(II) and copper(I) complexes of thiophenophane ligands were discussed and in this chapter a study of palladium(II) and platinum(II) complexes of open-chain and macrocyclic thioether ligands will be presented. The ^{1}H nmr spectra of these complexes are of particular interest and will be discussed in the light of X-ray crystal structures.

The ligands used in this part of this chapter are given in Scheme 4-1.

Scheme 4-1

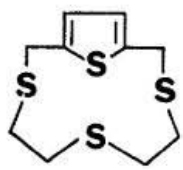

L1

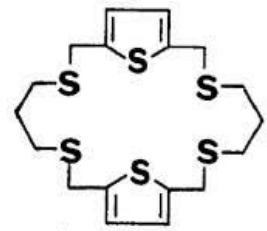

L8

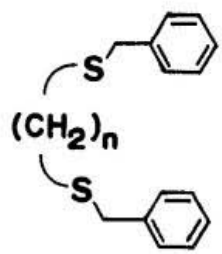

L 10 n=2
L 11 n=3

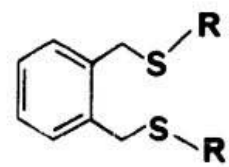

L 12 R = CH_2Ph
L 13 R = CH_2CH_2OH
L 14 R = p-C_6H_4Cl

4.1.2. Experimental

Reagents and instruments are the same as those described before. The nmr spectra were obtained using a General Electric 300-NB spectrometer and TMS as internal standard. Solvents for conductivity measurements were purified by standard purification procedures (1-2). Synthesis and characterization of thiophenophane ligands have been described in chapter 2. The open-chain dithioether ligands were prepared by the following general procedure.

4.1.2.1. Synthesis of Dithioether Ligands

Sodium metal (2.3 g, 0.1 mol) was dissolved in 300 ml of commercial absolute ethanol under a dry nitrogen atmosphere and 0.05 mol of dimercaptan was added cautiously. The solution was heated to reflux for about 10 minutes and 0.1 mol of alkyl halide in 150 ml of benzene was added dropwise. The mixture was refluxed for another hour after addition and volatiles were removed on a rotary evaporator. The residue was extracted with chloroform, washed with water and dried over anhydrous $MgSO_4$. Upon filtration, chloroform was removed under vacuum to give the crude product. Recrystallization of the crude product from ethanol or acetone gave white crystals of: (a) 1,2-bis(benzylthio)ethane (84%; m.p. 32-34°; mass spectrum, parent ion 274 $[C_{16}H_{18}S_2]^+$; nmr ($CDCl_3$, ppm from TMS int. std.), ^{1}H: 2.53 (s, 4H) CH_2CH_2, 3.52 (s, 4H) $PhCH_2$, 7.23 (m, 10H) C_6H_5); (b) 1,2-bis(benzylthiomethyl)benzene (86%; m.p. 56-57°; mass spectrum, parent ion 350 $[C_{22}H_{22}S_2]^+$; nmr ($CDCl_3$, TMS), ^{1}H: 3.68 (s,4H) $PhCH_2$, 3.76 (s, 4H) ortho-$C_6H_4(CH_2)_2$, 7.26 (s, 4H) C_6H_4, 7.38 (m, 10H) C_6H_5) and (c) 1,2-bis(p-chlorophenylthiomethyl)benzene (90%; m.p. 89-91°; mass spectrum, parent ion 390 $[C_{20}H_{20}Cl_2S_2]^+$; nmr ($CDCl_3$, TMS) ^{1}H: 4.16 (s, 4H) ortho-$C_6H_4(CH_2)_2$, 7.12 (s, 4H) C_6H_5, 7.17 (s, 8H) p-chloro-C_6H_4). Dithioether

ligands, 1,3-bis(benzylthio)propane and 1,2-bis(2-hydroxyethylthiomethyl)benzene, were isolated as viscous thick liquids at room temperature. No purification was carried out before further use.

4.1.2.2. Synthesis of Metal Complexes

4.1.2.2.1. [$PdCl_2$·L1]

Cis-dichlorobisbenzonitrilepalladium(II) (153 mg, 0.40 mmol) was dissolved in 15 ml of acetone and L1 (115 mg, 0.44 mmol) in 10 ml of dichloromethane was added with stirring. An orange precipitate formed which was filtered, washed with acetone, dichloromethane and diethyl ether and dried in air to yield 85% of product. Suitable crystals could be obtained for X-ray crystallography by the following procedure.

A solution of L1 in 15 ml of dichloromethane was added with care to the solution of cis-dichlorobisbenzonitrilepalladium(II) (15 ml) through a dropping pipette dipping into the bottom of a 100 ml beaker to form two layers of solvents. The beaker was left to stand without disturbance at room temperature. As the solvents diffused into each other, orange crystals were deposited. The crystals were filtered off, washed with acetone and diethyl ether and dried in air.

The corresponding [PdX_2·L1] (X=Br, I, SCN) complexes were prepared by treating a solution of cis-dichlorobisbenzonitrilepalladium(II) (153 mg, 0.40 mmol) in acetone (20 ml) with a solution of $AgCF_3SO_3$ (205 mg, 0.80 mmol) in 15 ml of the same solvent. The resulting precipitate was removed and discarded and to the filtrate, solutions of KX (0.80 mmol, X=Br, I, SCN) in 5 ml of H_2O and L1 (115 mg, 0.44 mmol) in 5 ml of dichloromethane were added in that order. The resulting solution was filtered quickly and the solvent allowed to evaporate slowly at room temperature until crystals appeared, which were separated, washed and dried in vacuum. Yields

range from 75% to 85%. Suitable crystals could be obtained for X-ray crystallography in a similar way to that for [$PdCl_2$·L1] using acetone and dichloromethane as solvents.

4.1.2.2.2. [$PtCl_2$·L1]

Potassium trichloro(ethylene)platinum(II) (74 mg, 0.20 mmol) was dissolved in 15 ml of acetone and the solution was filtered. L1 (65 mg, 0.25 mmol) in 5 ml of dichloromethane was added giving a pale yellow precipitate. The precipitate was filtered, washed with dichloromethane and dried in air to give 85 mg (79.6%) of [$PtCl_2$·L1].

4.1.2.2.3. [$PdCl_2$·L10]

Cis-dichlorobisbenzonitrilepalladium(II) (153 mg, 0.40 mmol) in 20 ml of acetone and L10 (110 mg, 0.4 mmol) in 10 ml of dichloromethane were mixed, yielding an orange colored solution. Upon standing at room temperature to evaporate solvent slowly, orange crystals formed, which were separated, washed with acetone and diethyl ether and dried in air to give 142 mg (79%) of product.

The same general procedure was employed to prepare other dithioether dichloride palladium(II) complexes. Dibromo- and diiodo-palladium(II) derivatives were prepared in a similar way in yields of 70% and 75%, respectively.

4.1.2.2.4. [$PtCl_2$·L10]

Potassium trichloro(ethylene)platinum(II) (74 mg, 0.30 mmol) was dissolved in 15 ml of acetone and the solution filtered. L10 (60 mg, 0.22 mmol) in 5 ml of dichloromethane was added and the resulting solution was kept standing at room temperature until evaporation of solvent gave yellow crystals of product, which were collected by filtration, washed with acetone and diethyl ether and dried in air to yield 86

mg (80%) of product.

A procedure similar to that above was followed to prepare other dithioether complexes of platinum(II) with yields ranging from 68% to 87%.

4.1.2.2.5. $[Pd(L)_2]X_2$ (L = L1, L10-L12 and L14; X = ClO_4^- or $CF_3SO_3^-$)

Cis-dichlorobisbenzonitrilepalladium(II) (153 mg, 0.40 mmol) was dissolved in 20 ml of acetone and silver perchlorate or triflate (0.80 mmol) in 5 ml of acetonitrile added. A precipitate formed immediately and after stirring at room temperature for about 15 minutes the mixture was filtered. To the filtrate the appropriate ligand (1.00 mmol) in dichloromethane (5 ml) was added carefully and a crystalline precipitate formed instantly or upon slow evaporation of the solvent. The crystals were collected by filtration, washed with diethyl ether and dried in air to give 50-75% yield of products.

The same method but with a longer reaction time was used to prepare the platinum(II) analog, $[Pt(L1)_2](CF_3SO_3)_2 \cdot CH_2Cl_2$, using $K[Pt(CH_2=CH_2)Cl_3]$ and $AgCF_3SO_3$.

4.1.3. Results and Discussion

4.1.3.1. Preparative

4.1.3.1.1. Dihalide Complexes

Macrocyclic and open-chain thioether ligands react with cis-dichlorobisbenzonitrilepalladium(II) in acetone or acetonitrile to give dichloro-complexes $[PdCl_2 \cdot L]$ in high yield. Complexes $[PdX_2 \cdot L]$ (X = Br, I, SCN) were prepared in a similar way, but chloride was first removed using $AgCF_3SO_3$ and the appropriate halide or pseudo-halide added as its potassium salt KX before addition of

the ligand solution. Crystals suitable for X-ray diffraction study were obtained by the solvent diffusion method using acetone and dichloromethane as the solvents.

Dichloroplatinum(II) complexes [$PtCl_2$·L] can be prepared from the reaction of potassium trichloro(ethylene)platinum(II) (Zeise's salt) and thioether ligands in acetone at room temperature, which is more convenient than a reported method (3) using K_2PtCl_4 as the starting material. The reaction gives the product directly and no platinum(II)-ethylene complex was isolated.

The isolated complexes are listed in Table 4-1. In general, complexes [MCl_2·L] are slightly soluble in halocarbons and rather more so in DMF and DMSO. All complexes but [PdX_2·L14] (X = Cl, Br) are non-electrolytes in nitromethane.

It is of interest to note that L14 has a strong tendency to form bis-ligand complexes [$Pd(L14)_2$]X_2 (X=Cl and Br) even though a 1:1 ratio of L14 to cis-dichlorobisbenzonitrilepalladium(II) was used. Reaction of L14 with potassium trichloro(ethylene)platinum(II) in acetone only produces [$PtCl_2$·L14]. This can be explained in terms of the lability of Pd-Cl and Pt-Cl bonds and the larger trans influence of L14 than other dithioether ligands. Because of the strong electron-withdrawing group, 4-chlorophenyl, the electron density of the Pd-S bond is shifted towards thioether sulfur through back-bonding and therefore the Pd-Cl bonds at the trans positions will be weakened. In this regard, as soon as the dichloride complex is formed, the two labile chloro-ligands will be replaced by a second L14 molecule to form a bis-ligand complex, [$Pd(L14)_2$]Cl_2. The Pt-Cl bonds are so strong relative to Pd-Cl that only the thermodynamically stable dichloride complex [$PtCl_2$·L14] was isolated even though L14 has a strong trans influence.

Table 4-1: Analytical and physical data for Pd(II) and Pt(II) complexes.

Complex	Color	C(%)*	H(%)	M(%)	X(%)	M.P. (°C)
$[PdCl_2 \cdot L1]$	orange	27.21(27.31)	3.20(3.21)	22.9(24.2)	16.29(16.13)	223-226d**
$[PdBr_2 \cdot L1]$	red	23.54(22.70)	2.76(2.67)	19.6(20.1)	31.71(32.23)	210-213d
$[Pd(SCN)_2 \cdot L1]$	red	29.71(29.70)	2.91(2.91)	22.5(21.9)	-	169-170d
$[PdI_2 \cdot L1]$	purple	19.43(19.27)	2.28(2.27)	15.5(17.1)	37.74(40.77)	237-240d
$[PtCl_2 \cdot L1]$	yellow	23.00(22.73)	2.75(2.67)	18.7(19.0)	-	235-240d
$[(PdCl_2)_2 \cdot L8]$	orange	27.81(27.44)	3.10(3.07)	-	-	220-230d
$[PdCl_2 \cdot L10]$	orange	42.77(42.52)	4.01(4.02)	22.6(23.6)	15.6(15.7)	184-185d
$[PdI_2 \cdot L10]$	purple	30.39(30.26)	2.87(2.86)	15.9(16.8)	-	179-180d
$[PtCl_2 \cdot L10]$	yellow	35.99(35.54)	3.56(3.34)	-	12.93(13.12)	180-186d
$[PdCl_2 \cdot L11]$	orange	43.83(43.82)	4.32(4.33)	23.3(22.9)	15.33(15.23)	214-217d
$[PdBr_2 \cdot L11]$	orange	38.22(37.97)	3.78(4.36)	-	-	216-219d
$[PtCl_2 \cdot L11]$	yellow	36.39(36.80)	3.56(3.64)	35.2(35.2)	12.96(12.79)	218-220d
$[PdCl_2 \cdot L12]$	orange	49.83(50.04)	4.20(4.20)	-	13.62(13.44)	203-205d
$[PdBr_2 \cdot L12]$	brown	42.71(42.82)	3.58(3.60)	16.7(17.3)	-	202-204d
$[PdI_2 \cdot L12]$	purple	36.58(37.15)	3.07(3.12)	-	-	166-168d
$[PtCl_2 \cdot L12]$	yellow	42.43(42.84)	3.63(3.60)	-	11.75(16.35)	210-213d
$[PdCl_2 \cdot L13]$	red	33.26(33.06)	4.20(4.16)	-	16.52(16.35)	203-204d
$[PdBr_2 \cdot L13] \cdot H_2O$	orange	26.99(26.54)	3.68(3.71)	18.1(19.6)	-	185-188d
$[PtCl_2 \cdot L13]$	yellow	27.80(27.47)	3.53(3.46)	-	13.66(13.58)	190-195d
$[Pd(L14)_2]Cl_2$	orange	50.18(50.04)	3.41(3.36)	9.94(11.1)	22.61(22.17)	177-178d
$[Pd(L14)_2]Br_2$	brown	45.99(45.78)	3.16(3.08)	10.5(10.2)	14.29(15.24)	176-177d
$[PtCl_2 \cdot L14]$	yellow	33.55(33.96)	2.34(2.44)	-	28.28(28.66)	196-198d

* Found (calculated).

** decomposition.

4.1.3.1.2. Bis-Ligand Complexes $[M(L)_2](ClO_4)_2$ or $[M(L)_2](CF_3SO_3)_2$

Halide ions can be removed from cis-$[Pd(PhCN)_2Cl_2]$ or $K[Pt(CH_2=CH_2)Cl_3]$ by reaction with silver perchlorate or triflate in acetonitrile to give the solvento-intermediates $[M(CH_3CN)_4]^{2+}$ (M=Pd and Pt), which were reacted with two equivalents of dithioether ligand to afford the bis-ligand complexes $[M(L)_2](ClO_4)_2$ or $[M(L)_2](CF_3SO_3)_2$. Most of the bis-ligand complexes (Table 4-2) are soluble in DMF and DMSO as well as in acetonitrile, sparingly soluble in nitromethane and methanol and insoluble in non-polar solvents. In some cases, dichloromethane is part of the solid state formula unit as has been confirmed by elemental analysis and ^1H nmr methods.

Table 4-2: Analytical and physical data for bis-ligand complexes.

Complex	Color	C(%)*	H(%)	M(%)	M.P. (°C)
$[Pt(L1)_2](CF_3SO_3)_2 \cdot CH_2Cl_2$	yellow	24.33(24.76)	2.62(2.70)	-	192-195d**
$[Pd(L1)_2](CF_3SO_3)_2$	orange	29.92(30.06)	3.37(3.43)	18.7(19.0)	192-195d
$[Pd(L1)_2](ClO_4)_2 \cdot CH_2Cl_2$	orange	27.34(27.54)	3.27(3.30)	11.7(11.6)	184-187d
$[Pd(L10)_2](ClO_4)_2$	orange	44.52(44.47)	4.27(4.25)	11.8(12.5)	214-217d
$[Pd(L11)_2](CF_3SO_3)_2$	yellow	44.02(43.99)	4.15(4.10)	-	228-230d
$[Pd(L12)_2(ClO_4)_2 \cdot (CH_2Cl_2)_{0.5}$	yellow	50.74(50.94)	4.83(4.33)	9.98(10.15)	186-188d
$[Pd(L12)_2](CF_3SO_3)_2$	yellow	49.65(49.95)	4.03(4.01)	9.05(9.63)	189-192d
$[Pd(L14)_2](ClO_4)_2 \cdot (CH_2Cl_2)_{0.5}$	yellow	43.35(42.97)	2.94(2.94)	8.42(9.63)	215-218d

* Found (calculated).

** decomposition.

4.1.3.2. Infrared Spectra

On the basis of C_{2v} symmetry, two ν_{M-X} (A_1, B_1) and two ν_{M-S} (A_1, B_1) infrared active vibrations are expected. The bands associated with M-S stretching appear as weak or moderately intense absorptions in the range of 320 ± 20 cm^{-1} (Table 4-3) with broad ill-defined maxima that are often masked by M-Cl stretching bands (3-4). The frequencies vary somewhat with L and X and in view of the extensive coupling between ν_{M-Cl} and ν_{M-S}, which are of the same symmetry, no attempts were made to assign these M-S vibrations. The bands due to M-X vibrations are generally more easily assigned and fall in the established range for cis-MX_2 groups (5-7). The variation in ν_{M-X} with changes in L and M is small and irregular. In comparison with the data for corresponding tertiary phosphines, arsines and amines (7-9), it is obvious that the trend in ν_{M-X} with trans donor atoms is P>As>S>N consistent with the established trans influence series. In the spectrum of [$Pd(SCN)_2$·L1], there is a single broad strong absorption at 2100 cm^{-1} assigned to CN stretching and three bands at 469 (w), 455 (m) and 422 (m) cm^{-1} due to SCN bending of S-bound thiocyanate (10). In the spectra of [MCl_2·L13] (M=Pd, Pt), a strong band at 3350 cm^{-1} indicates that hydroxyl oxygen is not bound to the metal center.

The mull infrared spectra of the bis-ligand complexes $[M(L)_2](ClO_4)_2$ exhibit perchlorate absorption bands at 1075 cm^{-1} (ν_3) and 617 cm^{-1} (ν_4), indicating uncoordinated perchlorate anions. The mull spectra of the corresponding triflate salts show no indication of coordinated triflate anions.

Table 4-3: Ir and electronic spectral data for Pd(II) and Pt(II) complexes.

Complex	ν (M-X)* cm^{-1}	λ_{max} in nm (ϵ) (solution)	λ_{max} in nm (mull)
$[PtCl_2 \cdot L1]$	318(vs),330(vs)	360(200)[a]	380,325
$[PdCl_2 \cdot L1]$	324(s),342(vs)	395(900),310(sh),260(14,000)[b]	400,325
$[PdBr_2 \cdot L1]$	225(s),238(s)	415(1,600),365(sh),260(13,000)[b]	380,325
$[PdI_2 \cdot L1]$	---	480(2,500),260(18,000)[b]	490,350
$[Pd(SCN)_2 \cdot L1]$	---	425(800),350(sh),300(16,000)[b]	480(sh),435,360
$[PtCl_2 \cdot L10]$	318(vs),329(vs)	360(300),315(2,000),250(30,000)[c]	
$[PdCl_2 \cdot L10]$	300(vs),324(vs)	390(2,000),360(sh),310(sh),255(24,000)[c]	405,330
$[PdI_2 \cdot L10]$	---	480(4,000),410(sh),280(30,000),255(sh)[c]	500,415,340
$[PtCl_2 \cdot L11]$	305(vs),325(vs)	365(500),315(5,000)[c]	370,320
$[PdCl_2 \cdot L11]$	300(vs),323(vs)	385(2,000),275(sh),255(30,000)[c]	415(sh),360,320
$[PdBr_2 \cdot L11] \cdot C_2H_5OH$	248(s)	375(600),280(sh),260(15,000)[c]	445,350
$[PtCl_2 \cdot L12]$	303(vs),321(vs)		390,325
$[PdCl_2 \cdot L12]$	312(vs),323(vs),349(s)	400(1,200),265(19,000)[b]	405,325
$[PdBr_2 \cdot L12]$	240(s),245(s)	545(100),415(2,000),280(22,000)[b]	410,355
$[PdI_2 \cdot L12]$	---	510(300),440(sh),350(sh),298(19,000)[c]	480,360
$[PtCl_2 \cdot L13]$	320(vs),345(s)	360(100)[d]	375,320
$[PdCl_2 \cdot L13]$	308(vs),340(sh)	400(1,000),360(800)[d]	400,325
$[PdBr_2 \cdot L13] \cdot H_2O$	218(vs),245(s)	406(1,300),355(1,200)[d]	410,325
$[PtCl_2 \cdot L14]$	310(vs),330(vs)	375(150)[a]	375(sh)
$[Pd(L14)_2]Cl_2$	300(w),332(s)	385(sh),225(12,000)[b]	400,360
$[Pd(L14)_2]Br_2$	236(s),245(s)	415(1,000),250(sh),225(--)[b]	470(sh),375

* Nujol mull

[a] N,N-Dimethylformamide; [b] 1,2-dichloroethane; [c] dichloromethane; [d] nitromethane.

4.1.3.3. Electronic Spectra

The electronic spectra of all complexes both in solution and in the solid state were characteristic of square planar d^8 systems (Tables 4-3 and 4-4) (11). In complexes $[MCl_2.L]$, the lower energy bands with moderate intensity can be assigned to a d-d transition. The intense absorption bands beyond 350 nm are predominantly S→M and X→M charge transfer transitions (3). A shift of d-d band maximum in the order of I < SCN < Br < Cl was seen and is expected from the spectrochemical effect. In comparison with tertiary phosphines and arsines (12, 13), dithioether ligands produce rather weak ligand fields. In solution spectra of the bis-ligand complexes $[Pd(L)_2](ClO_4)_2$ and $[Pd(L)_2](CF_3SO_3)_2$, the lowest energy absorption occurred between 425 nm and 340 nm, usually as a shoulder on the more intense S→M charge transfer bands.

4.1.3.4. Conductivities

Conductivities were measured at 25° in purified nitromethane (Table 4-4). Molar conductivities of complexes $[Pd(L)_2](ClO_4)_2$ and $[Pd(L)_2](CF_3SO_3)_2$ are similar to those of perchlorate salts of palladium(II) and platinum(II) complexes of the dithioethers $PhS(CH_2)_nSPh$ (n=2, 3) at a concentration of 5×10^{-4} (14, 15). Plots (Figure 4-1) of Λ_M versus $\sqrt{C}$ for most of the perchlorate and triflate salts in nitromethane are straight lines over the range from 1.0×10^{-3} to 1.0×10^{-4} M (Figure 4-1) and the Onsager slopes (Figure 4-2) are appropriate for 2:1 electrolytes. Some of the complexes gave curved plots as has been reported for the complexes of $PhS(CH_2)_nSPh$ (n=2 and 3) (3, 14, 15). Conductivity curves for complexes of L10 and L12 show a sharp increase in molar conductivity (Figure 4-1) with decreasing concentration such that at very low concentration the conductivities approach the values

characteristic of 1:3 or 1:4 electrolytes. At this time we have no logical explanation for this reproduciable phenomenon. Further study is required.

Table 4-4: Electronic spectral and conductivity data for bis-ligand complexes.

Complex	λ_{max} in nm (ϵ) (solutions)	λ_{max} in nm (mulls)	Λ_M[e](slope)
$[Pd(L1)_2](CF_3SO_3)_2$	400(sh),365(1,000),350(320)[a]	425,340	170(400)
$[Pd(L1)_2](ClO_4)_2 \cdot CH_2Cl_2$	360(2,000)[b]	420,375	175(460)
$[Pd(L10)_2](ClO_4)_2$	420(sh),365(4,000)[a]	475(sh),325	186(--)
$[Pd(L11)_2](CF_3SO_3)_2$	340(10,000)[c]	450(sh),350	163(545)
$[Pd(L12)_2](CF_3SO_3)_2$	365(1,000)[a]	415,355	206(--)
$[Pd(L12)_2](ClO_4)_2 \cdot (CH_2Cl_2)_{0.5}$	400(sh),265(9,000)[d]	425,365	---
$[Pd(L14)_2](ClO_4)_2 \cdot (CH_2Cl_2)_{0.5}$	360(700)[a]	415,345	---

[a] Nitromethane; [b] N,N-dimethylformamide; [c] dichloromethane; [d] dichloroethane;
[e] $ohm^{-1} \cdot cm^2 \cdot mol^{-1}$ in nitromethane at a concentration of 5×10^{-4} M (slope = $(\Lambda_O - \Lambda_M)/\sqrt{C}$).

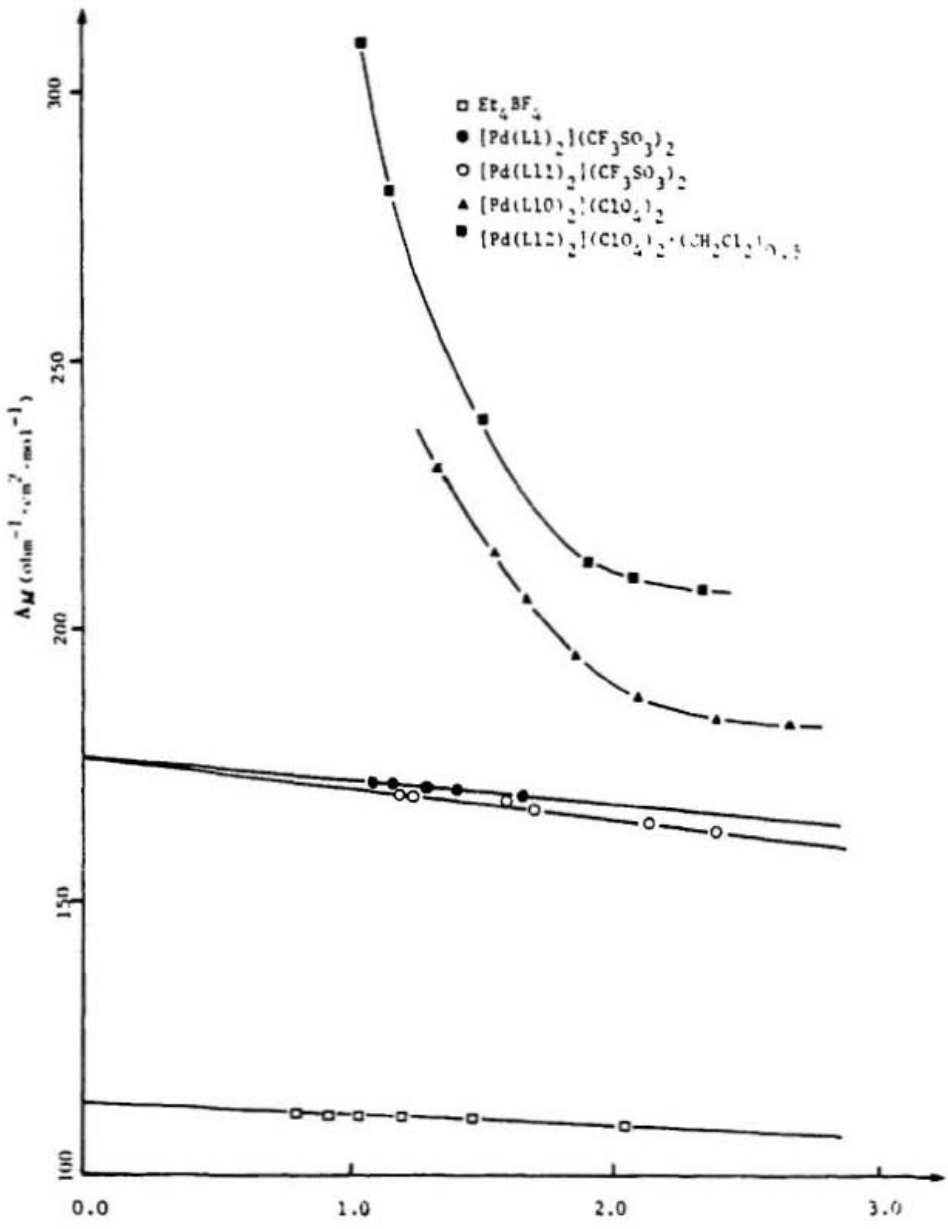

Figure 4-1. Plots of Λ_M vs. $\sqrt{C}$ for bis-ligand complexes.

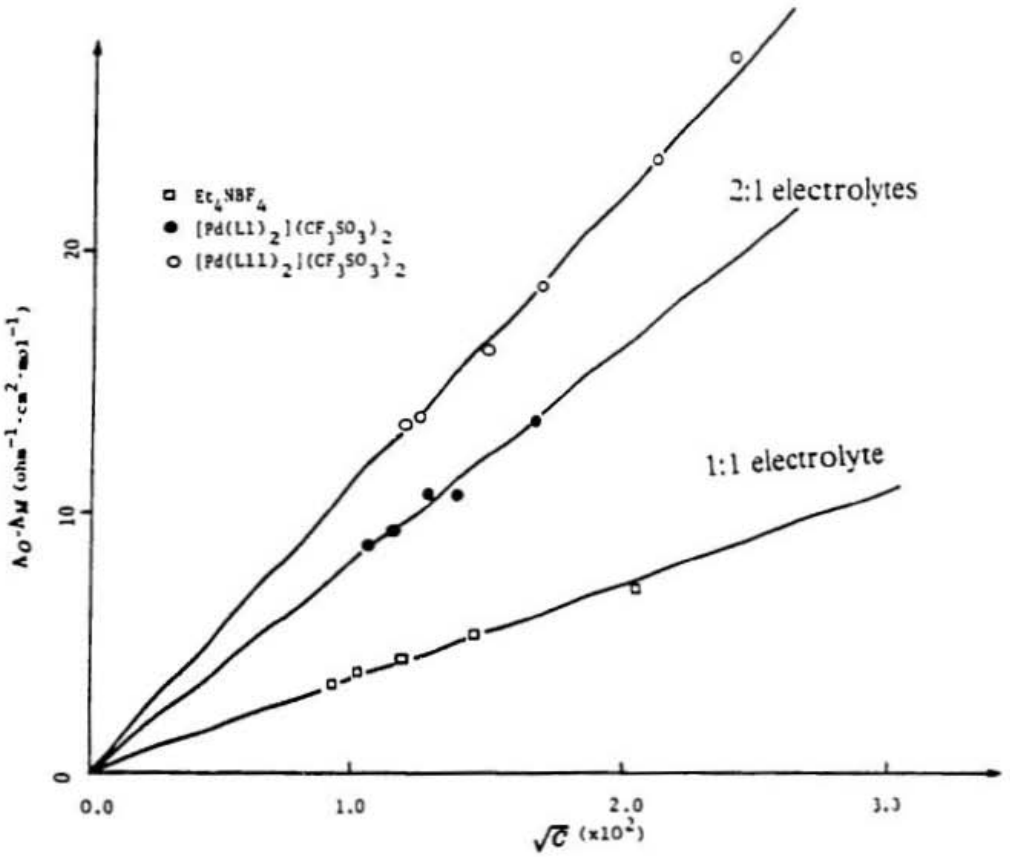

Figure 4-2. Onsager plots for bis-ligand complexes $[Pd(L)_2](CF_3SO_3)_2$ (L=L1 and L11).

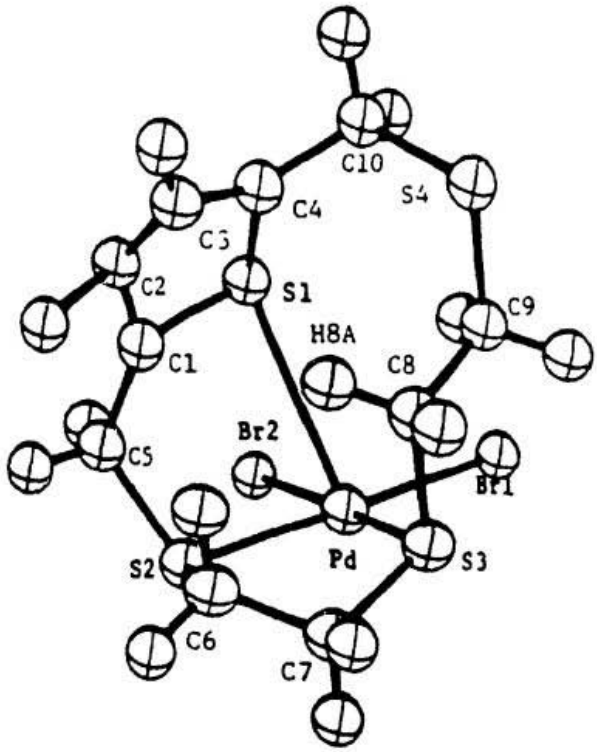

Pd-Br(1)	2.4171(19)	Br(1)-Pd-Br(2)	93.39(7)
Pd-Br(2)	2.4458(20)	Br(1)-Pd-S(1)	99.8 (3)
Pd-S (1)	3.1817(15)	Br(1)-Pd-S(2)	178.95(12)
Pd-S (2)	2.277 (3)	Br(1)-Pd-S(3)	89.14(10)
Pd-S (3)	2.282 (4)	Br(2)-Pd-S(1)	83.73(4)
		Br(2)-Pd-S(2)	87.34(11)
		Br(2)-Pd-S(3)	177.41(13)
		S (1)-Pd-S(2)	81.0 (3)
		S (1)-Pd-S(3)	95.3 (4)
		S (2)-Pd-S(3)	90.15(13)

Figure 4-3. ORTEP drawing of [$PdBr_2$·L1] and selected bond lengths (Å) and angles (degrees).

4.1.3.5. The Structure of [$PdBr_2$·L1]

As noted before, the shape of the cavity of L1 is roughly triangular with the S2-S4 distance (6.662 Å) representing the base and S1-S3 distance (4.579 Å) representing the height of the triangle. Apparently, L1 has no capacity to accommodate Pd coplanar with all four sulfur atoms because of the small cavity size and rigidity of the thiophene subunit and its two attached methylene groups. Since thiophene-sulfur is endocyclic, it is quite possible for L1 to coordinate Pd as a tridentate ligand as in $[CuCl_2 \cdot L1]_2$.

The ORTEP drawing of [$PdBr_2$·L1] and selected bond lengths and angles are shown in Figure 4-3. The unit cell contains four molecules of [$PdBr_2$·L1], each of which is asymmetrical. The Pd atom is bonded by a pair of thioether sulfurs and two bromine atoms with a cis-configuration. The Pd atom lies in the least squares plane formed by the Br_2S_2 donor set and has S(2)-Pd-S(3) and Br(1)-Pd-Br(2) angles of 90.15(13)° and 93.38(7)°, respectively. When S2 and S3 coordinate to Pd to form a five-membered chelate ring, the endodentate thiophene-sulfur interacts with the Pd atom at the axial position to complete a distorted square pyramidal geometry even though Pd(II) has a strong preference for square planar coordination. The Pd-S(thiophene) distance is 3.1817(15) Å, which is significantly shorter than the sum (3.40 Å) of the van der Waals' radii (16). The angles Pd-S(1)-C(1) and Pd-S(1)-C(4) are 133.3(3)° and 87.3(3)°, suggesting the bonding between the Pd atom and thiophene-sulfur is strained as in the case of $[CuCl_2 \cdot L1]_2$. The basal Pd-S distances are 2.277(3) and 2.282(4) Å with an average of 2.280 Å. The Pd-Br bond lengths are 2.4171(19) and 2.4458(20) Å with an average of 2.431 Å. These results can be compared with those found in [$PdBr_2$·[9]aneS3] (17), in which Pd-Br and Pd-S distances are 2.462(1) and 2.266(2) Å, respectively. Although the apical donor atoms are thiophene-sulfur in [$PdBr_2$·L1] and thioether-sulfur in [$PdBr_2$·[9]aneS3], the sums of Pd-Br and Pd-S bond

lengths remain constant (12.600 Å for [$PdBr_2$·L1] and 12.581 Å for [$PdBr_2$·[9]aneS3]). This is in agreement with the behavior of copper(II) complexes (18). Due to the low trans influence of Br relative to thioether sulfur, the equatorial Pd-S bonds in [$PdBr_2$·L1] are 0.037 Å shorter than those in $[Pd([9]aneS3)_2]^{2+}$ (15) and 0.049 Å shorter than those in $[Pd(L)]^{2+}$ (L=1,4,10,13-tetrathia-7,16-diazacyclooctadecane) (19), whereas the Pd-Br distance is 0.011 Å longer than that in $[PdBr_4]^{2-}$ (20).

It is interesting to note that H8A lies over the center of the thiophene ring. This hydrogen atom is therefore expected to exhibit a resonance signal that is strongly shielded.

4.1.3.6. Nmr Spectra

Metal complexes of thioether ligands have been the subject of many publications in the last decade and the pyramidal environment about a coordinated sulfur atom has been established conclu ·ly by X-ray methods (4). Rapid inversion at a coordinated sulfur atom is very common in both mono- and bidentate complexes of palladium(II) and platinum(II) and has been studied extensively by nmr techniques (21-25).

The ^1H nmr study (26) of [$PtCl_2$($MeSCH_2CH_2SMe$)] shows that at low temperatures two isomers exist, which interconvert at higher temperatures. The palladium complexes show very similar behaviour, but the coalescence of resonance signals occurs at much lower temperatures.

It has been suggested that the temperature dependence of the ^1H nmr spectra of coordinated dithioethers is primarily due to non-dissociative inversion at coordinated sulfur atoms (27). Therefore, this type of inversion mechanism should be sensitive to the nature of the trans ligands and to that of the dithioether ligand itself. In the present study, ^1H nmr spectra of benzyl-substituted dithioether ligands $PhCH_2S$-R-

SCH_2Ph (R=CH_2-CH_2, CH_2-CH_2-CH_2, and ortho-$C_6H_4(CH_2)_2$) have been examined to identify any effect of chelate backbone length or of sterically bulky benzyl groups on inversion at coordinated thioether sulfur atoms. Table 4-5 lists ^1H nmr parameters for palladium(II) and platinum(II) complexes of open chain dithioether ligands.

At room temperature in d_6-DMSO, the ^1H spectrum of [$PdCl_2$·L10] shows a typical phenyl multiplet at 7.40 ppm from internal tetramethylsilane, a pair of partially overlapped second-order AB quartets near 4.30 ppm due to benzylic methylenes and four distinct multiplets of equal intensity near 2.80 ppm due to CH_2CH_2 of the five-membered chelate ring. The integrated intensities of these three regions are in the ratio 10:4:4 as required. The occurrence of two sets of quartets near 4.30 ppm suggests that two isomers (Figure 4-4) are present in solution in the ratio 45%/55%. That which is present in the smaller amount has more deshielded benzylic methylenes and is probably the syn isomer (24). The fact that only two second-order AB quartets are seen may be attributed to conformational averaging of the axial and equatorial environments of the benzylic hydrogens in each isomer so that only one averaged benzyl group is detected per isomer.

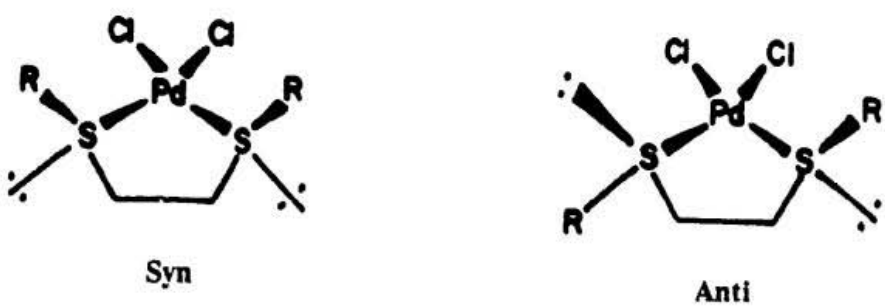

Figure 4-4. Syn and anti isomers of [$PdCl_2$·L10].

Table 4-5: ^1H nmr data for Pt(II) and Pd(II) complexes of open-chain dithioether ligands (chemical shifts in ppm vs. TMS).

Complex	Solvent	Aromatic Hydrogens	Benzylic Hydrogens	Methylene Hydrogens
$[PdCl_2 \cdot L10]$	d_6-DMSO	7.36(m,10H)	4.20(q,syn,$^2J_{HH}$ = 13.2Hz) 4.11(q,anti,$^2J_{HH}$ = 13.0Hz)	2.60(m,4H,AA'BB')
$[PdBr_2 \cdot L10]$	d_6-DMSO	2.39(m,10H)	4.38(q,syn,$^2J_{HH}$ = 13.2Hz) 4.15(q,anti,$^2J_{HH}$ = 13.4Hg)	2.80(m,4H,AA'BB')
	$CDCl_3$	7.40(m,10H)	4.53(q,syn,$^2J_{HH}$ = 13.6Hz) 4.20(q,anti,$^2J_{HH}$ = 13.6Hz)	2.80(m,4H,AA'BB')
$[PdI_2 \cdot L10]$	d_6-DMSO	2.34(m,10H)	4.40(s,4H)	2.70(m,4H)
	$CDCl_3$	2.41(m,10H)	4.38(s,4H)	2.50(s,4H)
$[Pd(L10)_2](ClO_4)_2$	d_6-DMSO	7.45(s,20H)	4.41(s,8H)	3.16(m,8H)
$[PtCl_2 \cdot L11]$	d_6-DMSO	7.38(m,10H)	4.24(s,4H)	2.42(m,4H),2.06(m,2H)
$[PdCl_2 \cdot L11]$	d_6-DMSO	7.40(m,10H)	4.26(s,4H)	2.50(m,4H),2.10(m,2H)
$[Pd(L11)_2](CF_3SO_3)_2$	d_6-DMSO	7.40(s,20H)	4.25(s,8H)	2.61(s,8H),2.52(s,4H)
$[PtCl_2 \cdot L12]$	d_6-DMSO	7.26(m,14H)	4.45(q,syn,$^2J_{HH}$ = 11.0Hz)* 3.80(q,anti,$^2J_{HH}$ = 13.5Hz)*	
$[PdCl_2 \cdot L12]$	d_6-DMSO	7.52(m,8H) 7.16(m,4H)	4.20(s,4H) 3.53(s,4H)	
$[Pd(L12)_2](ClO_4)_2 \cdot CH_2Cl_2$	d_6-DMSO	7.30(m,28H)	5.28(s,2H,CH_2Cl_2),4.19(s,4H) 4.11(s,4H),3.61(s,8H)	
$[PtCl_2 \cdot L14]$	d_6-DMSO	7.35(s,8H) 7.28(m,4H)	4.38(s,4H)	
$[Pd(L14)_2]Cl_2$	d_6-DMSO	7.36(s,8H) 7.28(m,4H)	4.37(s,4H)	
$[Pd(L14)_2](CF_3SO_3)_2$	d_6-DMSO	7.37(s,16H) 7.28(m,8H)	4.38(s,8H)	

* Free ligand signals were detected.

The ^1H nmr spectrum of [$PdCl_2$·L10] can be compared to that of [$PdCl_2$.BISE] (BISE = 1,2-bis(isopropylseleno)ethane) (25). The observation at room temperature of two sets of AA´BB´ multiplets, one with widely separated components (~0.45 ppm) and another with narrowly separated ones (~0.20 ppm), all of which are of similar intensity, is consistent with the presence of nearly equal amounts of two isomers, both of which are undergoing reversal of their ring conformations that is rapid on the nmr time scale. This is the same conclusion already reached by examination of the benzylic methylene portion of the spectrum.

At more elevated temperatures, two sets of second-order AB quartets and a pair of AA´BB´ resonance signals collapse to give a singlet at about 4.30 ppm and a singlet at around 2.90 ppm due to the benzylic methylenes and ethylene hydrogens on the chelate backbone, respectively. The coalescence point for [$PdCl_2$·L10] in d_6-DMSO is 353K, at which temperature the signal is at its broadest and splitting can not yet be observed. These observations are consistent with the onset of rapid interconversion of two isomers by either simultaneous or consecutive inversions at the two coordinated S-atoms (22, 25). The coalescence at 353K (Figure 4-5) for [$PdCl_2$.L10] may be compared to 400K for [$PdCl_2$(BISE)] (25) and 240K for [$Mo(CO)_4$BBTE] (BBTE = $BuSCH_2CH_2SBu$) (24). These are in accordance with the known trends in kinetic barriers to inversion as one changes either the identity of the inverting atom or the electropositive character of the metal to which the inverting atom is bound. In comparison with palladium(II) complexes of other dithioether ligands reported by Cross (27-28), [$PdCl_2$·L10] has a higher coalescence temperature, probably as a result of the greater steric effect of the two bulky benzyl groups. This is consistent with a non-dissociative mechanism of inversion at coordinated thioether S-atoms.

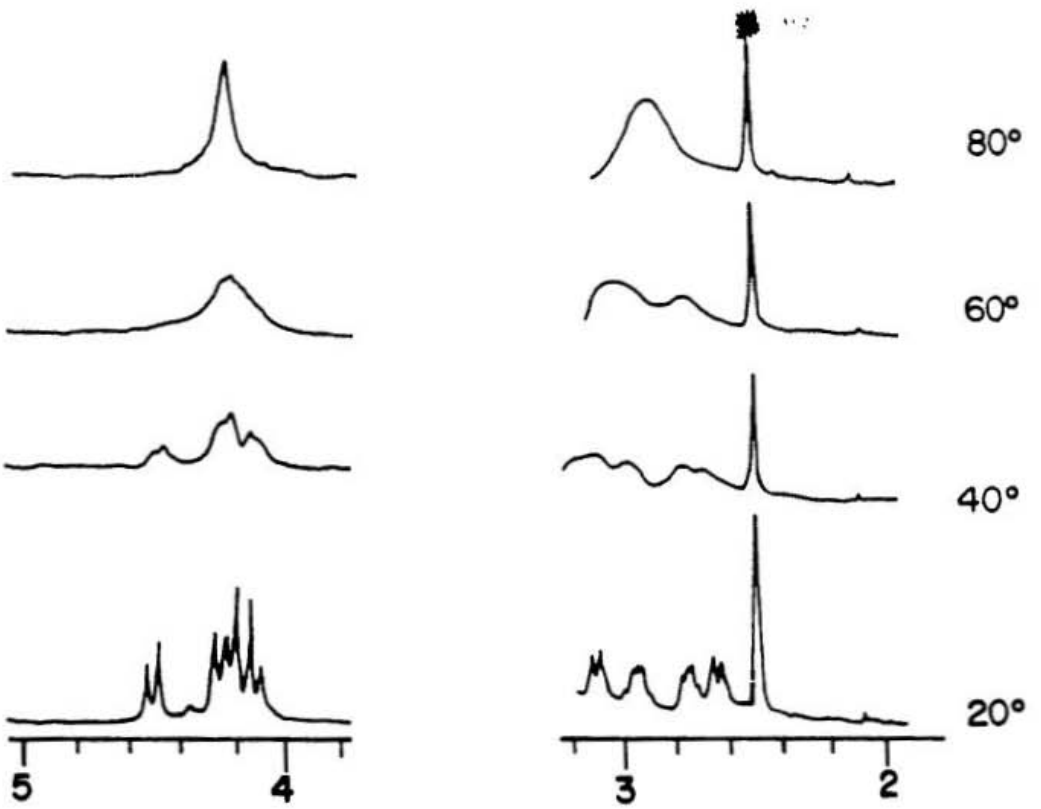

Figure 4-5. Variable temperature ^{1}H nmr spectra of [$PdCl_2$·L10] in d_6-DMSO.

The ^1H nmr spectrum of [$PtCl_2$·L10] in d_6-DMSO at room temperature is very similar to that of [$PdCl_2$·L10]. However, its coalescence temperature is much higher (>393K) than that of the Pd analog. Replacement of the ethylene bridge by propylene or ortho-$C_6H_4(CH_2)_2$ causes remarkable changes in the ^1H nmr spectra of the palladium(II) and platinum(II) complexes. Only a singlet appears in the benzylic methylene region due to rapid interconversion of the two isomers by inversion at coordinated thioether S-atoms. The trans halide ligands also affect the rates of inversion. The observation that diiodide complexes have much lower coalescence temperatures is in agreement with the established trans influence series (4, 24-25, 27).

Thus, we may conclude that at room temperature the Pd and Pt complexes of L10 are undergoing rapid exchange of the chelate ring conformations and of the axial and equatorial orientations of the lone pairs on the sulfurs. The complexes remain configurationally rigid, however, until the temperature is raised several tens of degrees when the inversions at coordinated sulfurs interconvert the syn and anti isomers. Changing the backbone of the chelate ring has a profound impact on the rate of this inversion at coordinated S-atoms. The fact that the Pd and Pt complexes of L11 and L12 have much lower coalescence temperatures than that of [$PdCl_2$·L10] demonstrates the greater stability of the five-membered chelate ring compared to that of six- or seven-membered chelate rings.

In palladium(II) and platinum(II) complexes of open-chain dithioether ligands, either simultaneous or consecutive inversion occurs at high temperatures as indicated by the coalescence of hydrogen resonance signals. In a metal complex of a macrocyclic thioether ligand, inversion of coordinated S-atoms is expected to be restricted due to the relative rigidity of the coordinated macrocycle, provided that a non-dissociative mechanism operates. To explore this further, variable temperature ^1H and ^1H-^1H

COSY nmr spectra of the complexes [MX_2·L1] (M=Pd, Pt; X=Cl, Br, I, SCN) have been examined.

Table 4-6: ^{1}H nmr data for complexes [MX_2·L1] and [Pd(L1)$_2$](CF_3SO_3)$_2$ in d_6-DMSO (chemical shifts in ppm vs. TMS).

[$PtCl_2$·L1][a]	[$PdCl_2$·L1]	[$PdBr_2$·L1]	[PdI_2·L1]	[Pd(SCN)$_2$·L1]	[Pd(L1)$_2$](CF_3SO_3)$_2$	Assignment
7.13(d)[b]	7.12(d)[b]	7.20(d)[b]	7.18(d)[b]	7.24(d)[b]	7.34(d)[b] 7.27(d)[b]	H3(H3´)
6.88(d)[b]	6.90(d)[b]	6.97(d)[b]	6.94(d)[b]	7.01(d)[b]	7.10(d)[b]	H2(H2´)
4.57(d)[b]	4.50(d)[c]	4.75(d)[c]	4.96(d)[c]		4.98(d)[d] 4.79(d)[d]	H5A(H5A´)
4.40(d)[c]	4.18(d)[c]	4.42(d)[c]	4.65(d)[c]	4.57(s)	4.87(d)[d] 4.71(d)[d]	H5B(H5B´)
4.13(d)[c]	4.08(d)[c]	4.15(d)[c]	4.4(d)[c]	4.16(d)[c]	4.22(d)[d] 4.20(d)[c]	H10A(H10A´)
4.04(d)[c]	3.96(d)[c]	4.02(d)[c]	3.98(d)[c]	4.06(d)[c]	4.12(d)[c] 4.11(d)[c]	H10B(H10B´)
3.04(m)	3.15(m)	3.20(m)	3.17(m)	3.39(m)	3.74(m)	H7B(H7B´)
.3.00(m)	3.08(m)	3.17(m)	3.15(m)	2.84(m)	3.30(m)	H8B(H8B´)
2.89(m)	3.07(m)	3.13(m)	3.02(m)	3.35(m)	3.69(m)	H7A(H7A´)
2.85(m)	2.74(m)	3.00(m)	2.96(m)	3.58(m)	3.54(m)	H6A(H6A´)
2.80(m)	2.78(m)	2.80(m)	2.90(m)	3.07(m)	3.08(m)	H9B(H9B´)
2.48(m)	2.45(m)	2.55(m)	2.53(m)	2.70(m)	2.82(m)	H6B(H6B´)
2.32(m)	2.29(m)	2.35(m)	2.29(m)	2.60(m)	2.80(m)	H9A(H9A´)
0.54(m)	0.61(m)	0.67(m)	0.64(m)	0.70(m)	0.78(m)	H8A(H8A´)

a ^{195}Pt satellites not detected; [b] $^3J_{HH}$ = 3.5 Hz; [c] $^3J_{HH}$ = 13.9 Hz; [d] $^3J_{HH}$ = 14.8 Hz.

The 300 MHz ^1H nmr spectra of the complexes [MX_2·L1] (M=Pd, Pt; X=Cl, Br, I, SCN) are similar (Table 4-6) and we shall therefore discuss in detail only that of [$PdBr_2$·L1] (Figure 4-6) for which we also nave X-ray structural data (Figure 4-3, p157). Subsequently, we will discuss the two differences between the spectra of [$PdBr_2$·L1] and [$Pd(SCN)_2$·L1], the latter being the only member of the series for which significant differences occur. Spectral assignments (Table 4-6) were carried out on the basis of ^1H-^1H COSY and the expectation that as usual (29), coordination to metal will deshield nearby hydrogens. In some cases, the two hydrogens on a single carbon atom were distinguished by their proximity to the doughnuts of electron density above and below the thiophene ring which shields one member of the pair more than the other or by the fact that ring hydrogens in pseudo-axial environments are usually more shielded than those in pseudo-equatorial ones (30).

In the free ligand, the two aromatic hydrogens, H2 and H3, are equivalent and the same is true for the hydrogens on C5 and C10. Upon coordination to a metal ion, however, H2 and H3 become non-equivalent as a result of the asymmetric way in which palladium is bound to the macrocycle and the resonance signal at about 7.00 ppm of the free ligand is split into two doublets near 7.20 and 7.00 ppm, respectively. The non-equivalence of these hydrogens indicates the absence of a 1,4-heteroatom fluxionality involving S2, S3 and S4, similar to that reported for the nitrogen donor complex $[Pd([9]aneN3)_2]^{2+}$ (31). This conclusion is supported by the ^{13}C spectrum (Table 4-7), which shows 9 signals assigned by ^{13}C-^1H COSY and Attached Proton Test to all but one of the ten carbons in the molecule. The missing signal is due to C7 and is expected to be obscured by the solvent signal. Were the molecule fluxional only five signals would be expected.

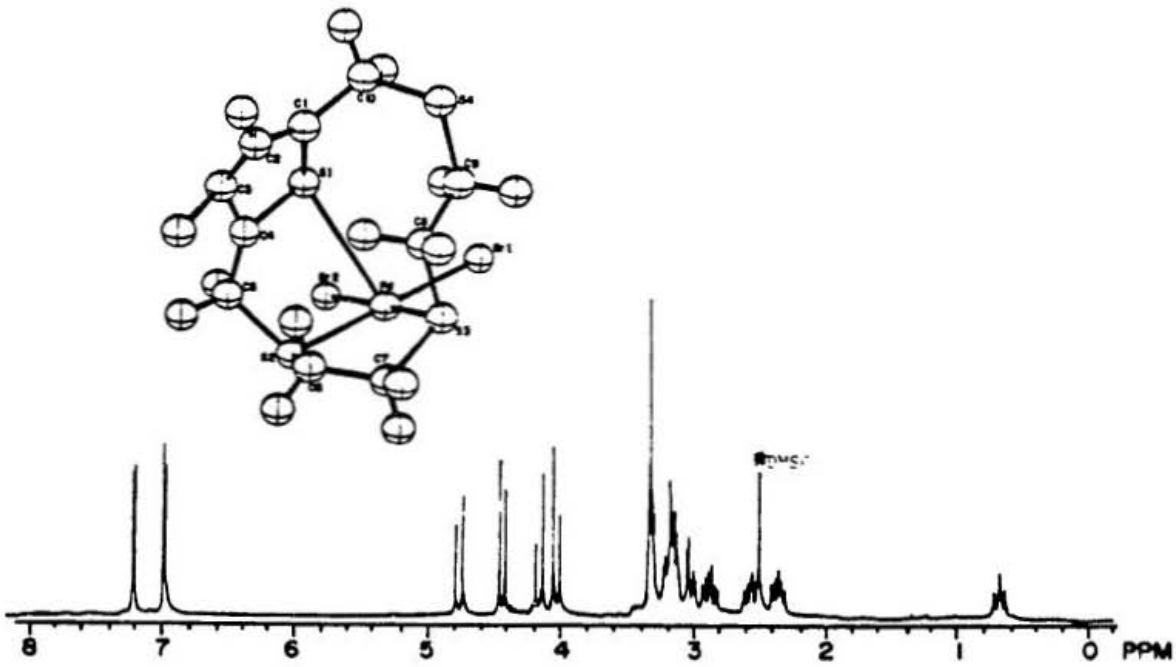

Figure 4-6. Room temperature ^{1}H nmr spectrum of [$PdBr_2$·L1] in d_6-DMSO.

Table 4-7: ^{13}C nmr data for complexes $[MX_2 \cdot L1]$ and $[Pd(L1)_2](CF_3SO_3)_2$ in d_6-DMSO (Chemical shift in ppm vs. TMS).

$[PtCl_2 \cdot L1]$	$[PdCl_2 \cdot L1]$	$[PdBr_2 \cdot L1]$	$[Pd(SCN)_2 \cdot L1]$	$[Pd(L1)_2](CF_3SO_3)_2$	Assignment
147.0	146.3	146.2	146.7	148.0,147.7	C4 (C4´)
136.3	134.7	134.8	135.1	136.2,135.4	C3 (C3´)
136.3	134.7	134.8	134.6	134.2,133.8	C1 (C1´)
125.4	124.8	124.8	125.5	126.3	C2 (C2´)
39.1	b	b	38.4	38.8	C7 (C7´)
38.2	37.9	38.3	37.6	36.8	C5 (C5´)
36.1	35.7	35.8	35.5	35.8	C8 (C8´)
35.4	34.8	35.4	35.4	35.4	C6 (C6´)
30.4	30.1	30.2	30.0	29.7,29.6	C10 (C10´)
27.9	27.6	28.3	27.5	27.5,27.2	C9 (C9´)
			117.8		SCN
			117.3		SCN
			122.0		SCN[c]

a: ^1H decoupled; b: obscured by solvent; c: due to Pd species produced by ligand dissociation, cf $[Pd(SCN)_4]^{2-}$ at 119.0 ppm ref. 29.

Near 4.50 ppm, there are two second-order AB quartets originating from the two pairs of hydrogens on C5 and C10. The more deshielded quartet is assigned to the pair of hydrogens on C5 and the other to the pair on C10. These assignments are based on the observation that the H5A-H5B quartet shifts significantly (~0.4 ppm) as X in [PdX_2·L1] is changed and only this quartet becomes a singlet when X=SCN (vide infra). Furthermore, the quartet assigned to H10A and H10B that lie in an environment more like the free ligand than H5A and H5B, is centered at 4.09 ppm which is closer than the other quartet to the 3.95 ppm shift for the same hydrogens in the free ligand (Table 2-2, p65).

The observation of a quartet for H10A and H10B is highly significant and is due to their non-equivalent environments that arise from the rigidity associated with the tridentate macrocycle. In fact, this rigidity causes non-equivalence of the members of every pair of CH_2-hydrogens in the molecule. Furthermore, this non-equivalence proves that inversions at S2 and S3 are not occurring since such inversions plus some rotations about C-C and C-S bonds would interchange the environments of the members of each pair of hydrogens bound to the same carbon throughout the molecule and result in a much less complex spectrum. For example, the quartets due to C5 and C10 methylenes would appear as singlets.

Thus, unlike [$PdCl_2$·L10], the two quartets near 4.50 ppm in the spectra of [PdX_2·L1] (X=Cl, Br and I) are not due to the presence of two isomers but rather to two different CH_2 groups in the same molecule. In fact, because S2 and S3 are part of a macrocyclic ring in which a third sulfur (S3) is also bound to the metal, the only configuration possible for the chelate ring corresponds to the syn isomer of [$PdCl_2$·L10]. The similarity of the assignments of the syn isomer spectrum of [$PdCl_2$·L10] and that of [$PdCl_2$·L1] may be noted. The remainder of the spectrum of

[$PdCl_2$·L1] involves separate signals for the 8 hydrogens comprising the two CH_2CH_2 units. One of these hydrogens is in a unique environment that is evidently much more shielded than the others since its signal is at comparatively high field (0.67 ppm). This is designated as H8A and is the hydrogen on C8 that lies over the center of the thiophene ring (Figure 4-3) and is therefore subjected to the shielding effect of the induced ring current in the aromatic π-system. Because of the rigidity of the molecule, the configurations available to the chelate ring, PdS2CH_2CH_2S3, are strictly limited. For example, the envelope conformation which requires both sulfur lone-pairs to be simultaneously axial or simultaneously equatorial is not possible. It is this envelope conformation that is usually the transition state between half-chair conformations and in its absence a pseudo-librational route between the two half-chair conformations is likely to be of significantly lower kinetic barrier and therefore to be undetectable by nmr methods (32). In either half-chair conformation, the CH_2CH_2 unit will be an ABCD spin system and the two such systems are unrelated by any symmetry element. Therefore, two ABCD spectra would be expected if conformational exchange is slow or one averaged ABCD spectrum if it is rapid. In view of the predicted low barrier to conformational exchange and our earlier observation of rapid conformational exchange in [$PdCl_2$·L10], we would anticipate just one ABCD pattern at room temperature as is observed (Figure 4-6). This interpretation is supported by the absence of change in these signals up to at least 120° by which temperature any barrier to this conformational exchange must surely have been overcome.

The other CH_2CH_2 unit is also an ABCD system. As a result of steric crowding, due at least in part to the Pd-S1 bond, conformational possibilities in this region of the molecule are also strictly limited and the spectrum observed at room temperature is consistent with the rigid structure in Figure 4-3.

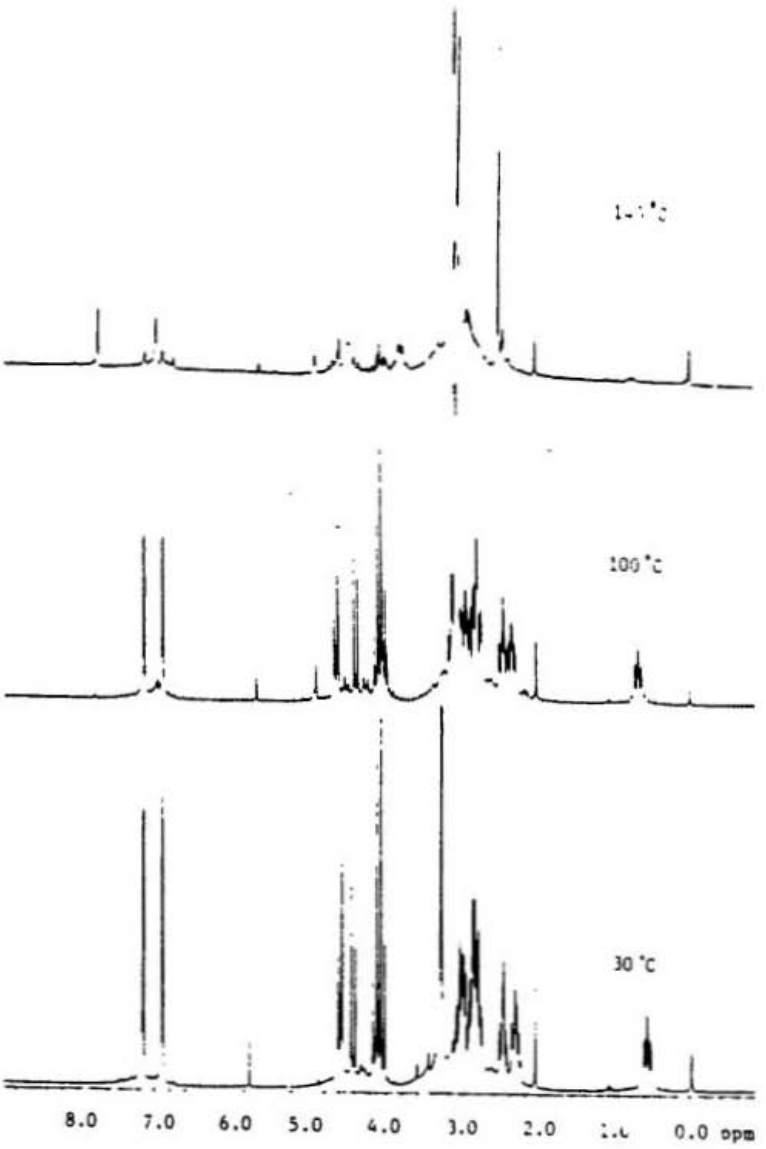

Figure 4-7. Variable temperature ^{1}H nmr spectra of [$PtCl_2$·L1] in d_6-DMSO.

The room temperature ^{1}H nmr spectrum (Figure 4-7) of [$PtCl_2$·L1] is almost the same as those of its palladium analog except for some ^{195}Pt satellite peaks in the methylene region. Due to the complexity of the spectrum, it is, however, difficult to determine the coupling constant $^{3}J_{Pt\text{-}H}$. At temperatures above 100°C, the samples in d_6-DMSO start to decompose and the resonance signals of the hydrogens of coordinated L1 begin to collapse. When the temperature has been raised to 140°C, the complex has been decomposed completely as is indicated by coalescence of signals of all hydrogens in the molecule. Reducing the temperature does not recover the original spectrum. The complex [$PdCl_2$·L1], however, remains stable at 120°C. This suggests that S-dealkylation reactions may take place in the platinum(II) complex when it is heated to >100°C. Such reactions are very common in Pt(II)-thioether complexes (4, 33) and apparently occur with greater ease for Pt(II) than for Pd(II) complexes.

The variable temperature ^{1}H nmr spectra of complexes [PdX_2·L1] (X=Br, I) are very similar to those of [$PdCl_2$·L1]. As the solution is warmed , the two pairs of peaks that comprise the H5A-H5B quartet at ~4.50 ppm move away from each other with, however, no change in coupling. The total movement is 0.02 ppm for the more shielded pair and 0.06 ppm for the lower field pair. There is no other change in the entire spectrum except that [PdI_2·L1] starts to decompose at temperatures above 100°C. This suggests that halide ligands at trans positions may affect the S-dealkylation reaction in Pd(II)-thioether complexes.

The curious behavior of the H5A-H5B quartet with temperature is observed to a greater or lesser extent for all members of the [MX_2·L1] series. It is in fact a neighbour anisotropic effect made possible by the rigid orientation of H5A and H5B with respect the the atom X (Figure 4-8). As the temperature is raised, thermal enhancement of the bending vibration of H5A-C5-H5B occurs. In this vibrational mode,

movement of one of the hydrogens is at a nearly constant radius from X whereas the other's motion is along a radius from X. Therefore, the extent of deshielding by this neighbour anisotropic contribution of X will vary with temperature for the nearer, more deshielded hydrogen but will remain more or less constant for the more distant or less deshielded hydrogen.

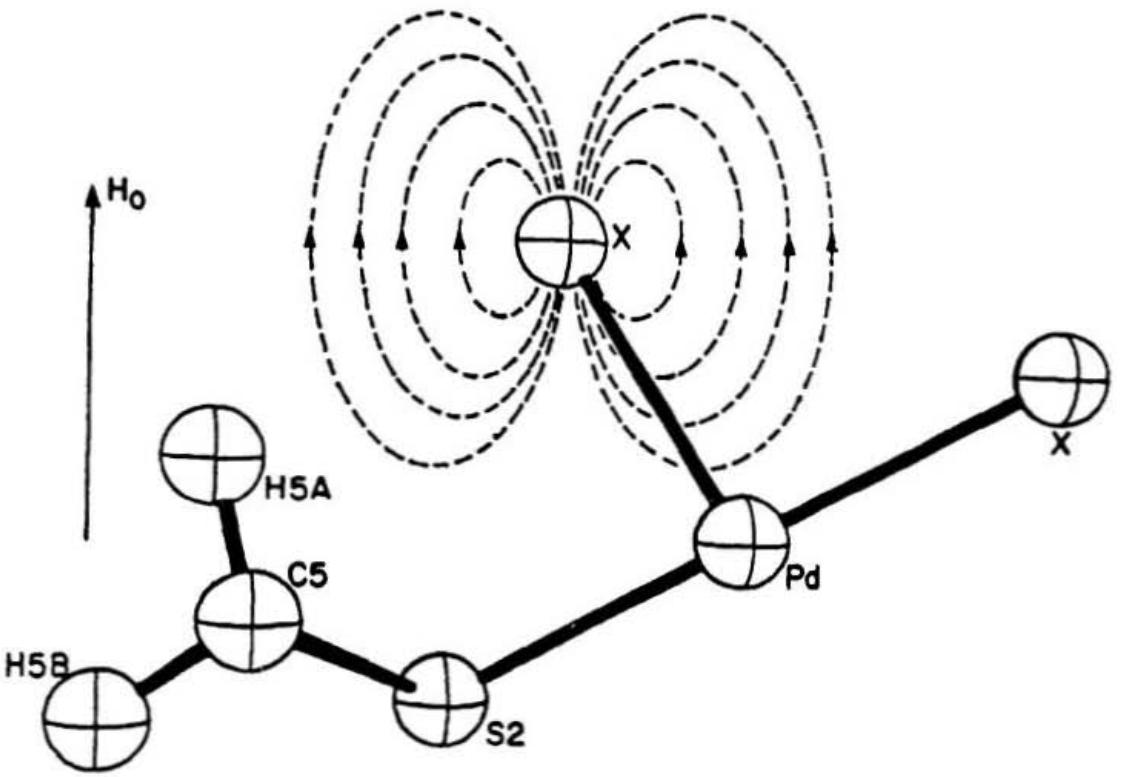

Figure 4-8. Neighbour effects at H5A and H5B from X in [PdX_2·L1].

There is a second manifestation of this neighbour effect made possible by stereochemical rigidity. The quartet due to H5A and H5B moves to lower field as X changes from Cl to Br to I but the shift is in the wrong direction for an electronegativity effect. It can however be attributed to the deshielding neighbour effect in which larger, more polarizable I will experience induced circulation of its electrons more readily than Cl. The induced field which is deshielding at H5A and H5B will therefore be larger for I than for Cl. This explanation is supported by the fact that the chemical shift difference between H5A and H5B is essentially the same for all X (ie. both hydrogens are affected proportionally the same as X is varied) and J_{gem} is the same in all cases.

The spectrum of $[Pd(SCN)_2 \cdot L1]$ shows two major differences from those of all other complexes in this series. The first difference is that free ligand is present and its signals grow in intensity as the temperature is raised. This indicates that formation of $[Pd(SCN)_2 \cdot L1]$ is an equilibrium process and that the formation is exothermic. The second striking difference is that the H5A-H5B signal is a singlet. The only way this can occur while maintaining all other hydrogens distinctive is by dissociative interchange of H5A and H5B. It is known (32) that M-SCN systems are usually bent (~110°) and that the N atom is appreciably basic (34). The pKa's (35) of DMSO (35.1), $PhCH_3$ (44.0) and $PhCH_2SPh$ (30.8) suggest that H5A and H5B should be significantly acidic and may therefore interchange by a process involving intermediate residence on the basic nitrogen of thiocyanate either in the same or a different molecule. This has been confirmed by a recent report (36) that complexes $[M([9]aneS3)_2]^{3+}$ (M=Co, Rh and Ir) undergo deprotonation and ring opening in the presence of bases such as Et_3N. Why the thiocyanate complex should dissociate its ligands when none of the other complexes in this series show any sign of dissociation until they reach their decomposition temperatures is not obvious. It may be that S-

bonded SCN is a better π-acceptor than halide and its presence weakens the trans M-S bond.

For [$PdCl_2$·L10], coalescence of the room temperature spectrum to two broad singlets occurs at 80°C (Figure 4-5) and for [PdI_2.L10] an even lower coalescence temperature has been detected because barriers to inversion at sulfur are usually higher for chloride than for analogous bromides and iodides (20). For [MX_2·L1] (M=Pt, Pd; X=Cl, Br, I, SCN), no coalescence has been observed until the temperature is raised so high that the complex decomposes. Clearly, the rigidity of [MX_2·L1] (M=Pt, Pd; X=Cl, Br, I, SCN) is such that non-dissociative inversions at S2 and S3 are prevented. These results strongly support the non-dissociative mechanism proposed for inversion at coordinated S-atoms in mono- and bidentate thioether complexes.

The ^1H nmr spectrum (Figure 4-9) of [$Pd(L1)_2$]($CF_3SO_3)_2$ in d_6-DMSO is much more complicated than that of [$PdBr_2$·L1] in the same solvent. There are two doublets at 7.34 and 7.27 ppm and a pair of overlapped doublets at 7.10 ppm. The integrated intensities in this region are in the ratio 1:1:2. Similarly, four sets of AB quartets were observed at 4.95, 4.78, 4.12 and 4.10 ppm originating from hydrogens on C5, C5′, C10 and C10′, respectively (Figure 4-10), of the two coordinated macrocycles. These observations indicate that in solution there are two configurational isomers (Figure 4-10) present in almost equal amounts as evidenced by the integrated intensities in these regions. Furthermore, the high field signal at 0.78 ppm is seen again as in the spectra of complexes [MX_2·L1] (M=Pt, Pd; X=Cl, Br, I, SCN). This suggests that the coordinated macrocycles remain as rigid as those in the dihalide and di-pseudohalide complexes.

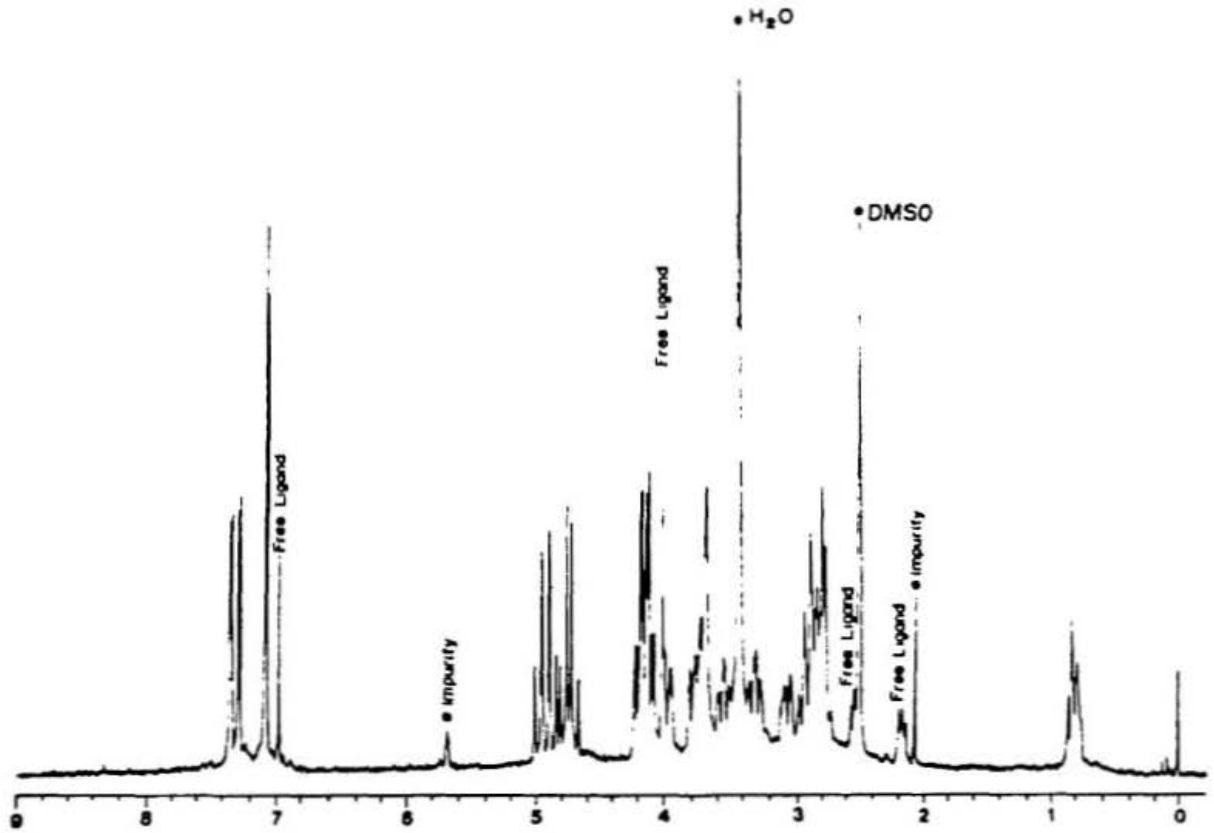

Figure 4-9. Room temperature ^{1}H nmr spectrum of $[Pd(L1)_2](CF_3SO_3)_2$ in d_6-DMSO.

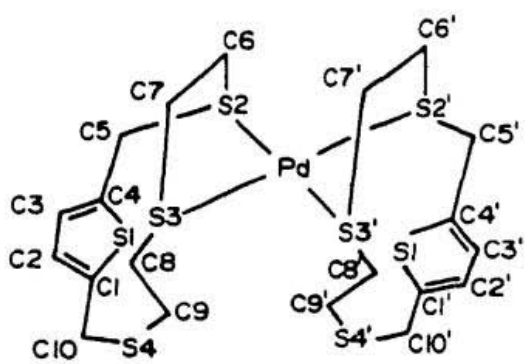

A

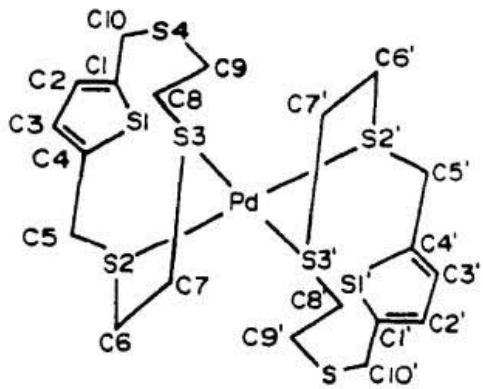

B

Figure 4-10. Two main configurational isomers of $[Pd(L1)_2]^{2+}$.

On the basis of these results, it is clear that inversion at coordinated S-atoms in macrocyclic ligand complexes like [MX_2·L1] (M=Pd, Pt; X=Cl, Br, I, SCN) is sufficiently hindered that there is no coalescence of resonance signals until the complex decomposes at extreme temperatures. The configurational stability of these complexes, unlike their open-chain analogs, is not sensitive to the nature of the halide ligands in the trans position; but the stability of the complex with respect to decomposition is sensitive to these trans ligands. The behaviour of these complexes in solution is of interest for a variety of reasons not the least of which involves their use or that of related substances as chemotherapeutic agents.

4.1.4. References

1. F.W. Parrett and M.S. Sun. J. Chem. Educ. *54*, 448 (1977).
2. J.F. Coetzee and T.H. Chang. Pure & Appl. Chem. *58*, 1541 (1986).
3. F.R. Hartley , S.G. Murray, W. Levason, H.E. Souter and C.A. McAuliffe. Inorg. Chim. Acta *21*, 265 (1979).
4. S.G. Murray and F.R. Hartley. Chem. Rev. *81*, 365 (1981).
5. J.R. Durig, R. Layton, D.W. Sink and B.R. Mitchell. Spectrochim. Acta *21*, 1367 (1965).
6. G.E. Coates and C. Parkin. J. Chem. Soc. 421 (1963).
7. D.M. Adams, J. Chatt, J. Gerratt and A.D. Westland. J. Chem. Soc. 734 (1964).
8. W. Levason and C.A. McAuliffe. J. Chem. Soc., Dalton Trans. 2238 (1974).
9. K.P. Beaumont, C.A. McAuliffe and M.J. Cleare. Chem. Biol.-Interact. *14*, 179

(1976).

10. K. Nakamoto. *Infrared and raman spectra of inorganic and coordination compounds*. 4th Ed. Wiley, Toronto. 1986. p. 283.

11. A.B.P. Lever. *Inorganic electronic spectroscopy*. 2nd Ed. Elsevier, New York. 1984. p. 341, 544.

12. W. Levason and C.A. McAuliffe. Inorg. Chem. *13*, 2765 (1974); Ibid Inorg. Chim. Acta *16*, 167 (1976).

13. W. Levason, C.A. McAuliffe and S.G. Murray. J. Organomet. Chem. *110*, C25 (1976).

14. A.D. Westland and J. Plúscec. Can. J. Chem. *46*, 2097 (1968).

15. W.J. Geary. Coord. Chem. Rev. *7*, 81 (1971).

16. A. Bondi. J. Phys. Chem. *68*, 441 (1964).

17. K. Wieghardt, H.J. Küppers, E. Raabe and C. Krüger. Angew Chem. Int. Ed. Engl. *25*, 1101 (1986).

18. J. Gazo, I.B. Bersuker, J. Garaj, M. Kabseova, H. Langfelderova, M. Melnik, M. Serator and F. Velach. Coord. Chem. Rev. 19, 253 (1976).

19. G. Reid, A.J. Blake, T.I. Hyde and M. Schrüder. J. Chem. Soc., Chem. Commun. 1397 (1988).

20. D.S. Martin, J.L. Bonte, R.M. Rush and R.A. Jacobson. Acta Crystallogr. *Sect. B 31*, 2538 (1975).

21. E.W. Abel, P.D. Beer, I. Moss, K.G. Orrell, V. Šik, P.A. Bates and M.B. Hurthouse. J. Chem. Soc., Chem. Commun. 978 (1987).

22. E.W. Abel, S.K. Bharghava and K.G. Orrell. Prog. Inorg. Chem. *32*, 1 (1984).

23. R.J. Cross, D.S. Rycroft, D.W.A. Sharp and Torrens. J. Chem. Soc., Dalton Trans. 2434 (1980).

24. R.J. Cross, G. Hunter and R.C. Massey. J. Chem. Soc., Dalton Trans. 2015 (1976).

25. G. Hunter and R.C. Massey. J. Chem. Soc., Dalton Trans. 2007 (1976).

26. E.W. Abel, R.P. Bush, F.J. Hopton and C.R. Jenkins. J. Chem. Soc., Chem. Commun. 58 (1966).

27. R.J. Cross, I.G. Dalgleish, G.R. Smith and R. Wardle. J. Chem. Soc. Dalton Trans. 992 (1972).

28. R.J. Cross. T. Green, R. Keat and I.F. Paterson. J. Chem. Soc., Dalton Trans. 1486 (1976).

29. E.W. Abel, K.G. Orrell, K.B. Qureshi and V. Šik. Polyhedron *7*, 1329 (1988).

30. F.A.L. Anet and R. Anet. In *Dynamic nuclear magnetic resonance spectroscopy*. Edited by L.M. Jackman and F.A. Cotton. Academic Press, New York. 1975. chap. 14.

31. G. Hunter, C.A. McAuley and T.W. Whitcombe. Inorg. Chem. *27*, 2634 (1988).

32. a: W.R. Scheidt, Y.J. Lee, D.K. Geiger, K. Taylor and K. Hatano. J. Am. Chem. Soc; *104*, 3367 (1982). b: T.N. Lockyer. Aust. J. Chem. *27*, 259 (1974).

34. J.A. Kargol, R.W. Crecely and J.L. Burmeister. Inorg. Chem. *18*, 2532 (1979).

35. E. Block. *Reactions of organosulfur compounds*. Academic Press, New York. 1978. p. 46.

36. A.J. Blake, AJ. Holder, T.I. Hyde, H.J. Küpers. M. Schröder, S. Stotzel and K. Wieghardt. J. Chem. Soc., Chem. Commun. 1600 (1989).

Part II. π-Allylpalladium Complexes of Thioether Ligands

4.2.1. Introduction

π-Allylpalladium compounds are important intermediates in palladium(II) catalyzed organic reactions (1-3). Cationic complexes $[Pd(C_3H_5)L_2]^+$ are known for L=PR_3, AsR_3; L_2=bipy, η^4-diene, etc., and the stereochemical non-rigidity of the allyl group in these complexes has been studied by nmr methods (4-11). However, very little information is available for those complexes, in which L_2 is a dithioether or macrocyclic polythioether ligand. Complexes of macrocyclic thioether ligands are also of interest for their potential application to regio-specific control of nucleophilic additions to π-allylpalladium systems (12-14).

4.2.1. Experimental

Reagents and instrumental techniques are as described before. Thioether ligands used in this part are shown in Scheme 4-2.

Scheme 4-2

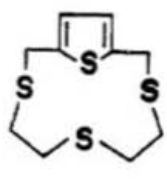

L1

L2

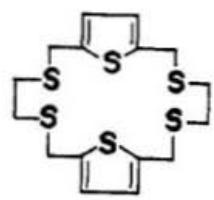

L7

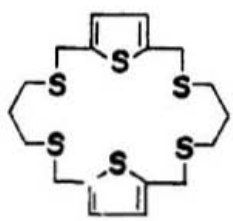

L8

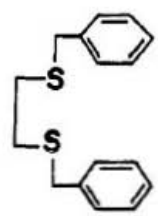

L10

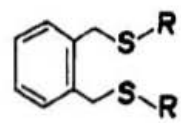

L12 R CH_2Ph

L14 R $p\text{-}C_6H_4Cl$

Synthesis of $[Pd(C_3H_5)\cdot L1]CF_3SO_3$

$[Pd(C_3H_5)Cl]_2$ (183 mg, 0.50 mmol) was dissolved in 15 ml of acetonitrile and $AgCF_3SO_3$ (257 mg, 1.00 mmol) in 5 ml of the same solvent was added. A precipitate formed instantly. The mixture was stirred for about 10 minutes and then filtered. To the filtrate, L1 (131 mg, 0.50 mmol) in 5 ml of dichloromethane was added. A small amount of precipitate was filtered and the filtrate was left standing to evaporate slowly until yellow crystals deposited. The crystals were collected by filtration, washed with acetone and diethylether and dried in air to give 375 mg (68%) of product.

The same procedure was employed to prepare π-allylpalladium complexes of other thioether ligands in yields ranging from 50% to 75%.

4.2.3. Results and Discussion

4.2.3.1. Preparative

Removal of chloride ligands was carried out by reaction of $[Pd(C_3H_5)Cl]_2$ with two equivalents of $AgCF_3SO_3$ or $AgPF_6$ in acetonitrile to give the solvento-intermediate $[Pd(C_3H_5)(CH_3CN)_2]^+$, which reacts with appropriate thioether ligands to afford complexes $[Pd(C_3H_5)\cdot L]^+$ (L=L1, L10, L12 and L14) and $[Pd_2(C_3H_5)_2\cdot L]^{2+}$ (L=L7, L8). All isolated compounds are air-stable, but some of them decompose in the presence of methanol or pyridine to give palladium metal and other organic products. In general, all complexes (in Table 4-8) are soluble in acetonitrile, DMF and DMSO except $[Pd_2(C_3H_5)_2\cdot L7]$, which is insoluble in all solvents except DMSO in which it is only slightly soluble.

Table 4-8: Analytical and physical properties of π-allylpalladium complexes.

Complex	C(%)	H(%)	Pd(%)	M.P.(°C)	Λ_M[a](slope)
$[Pd(L1)(C_3H_5)]CF_3SO_3$	29.92(30.06)	3.37(3.43)	18.7(19.0)	180-185d	88.5(260)
$[Pd_2(L2)(C_3H_5)_2](PF_6)_2$	24.23(23.81)	3.15(3.11)	19.1(18.1)	188-191d	205.0(---)
$[Pd_2(L7)(C_3H_5)_2](PF_6)_2$	27.10(26.68)	3.05(3.06)	16.4(21.5)	195-198d	---
$[Pd_2(L8)(C_3H_5)_2](PF_6)_2$	28.60(28.31)	3.38(3.37)	16.5(20.9)	195-200d	164.0(370)
$[Pd(L10)(C_3H_5)]PF_6$	40.53(40.27)	4.01(4.09)	---	132-133d	94.5(---)
$[Pd(L12)(C_3H_5)]PF_6$	46.79(46.68)	4.18(4.23)	13.4(16.6)	204-206d	83.5(173)
$[Pd(L14)(C_3H_5)]PF_6$	40.38(40.37)	3.02(3.10)	---	202-205d	88.5(280)

[a] $ohm^{-1}\cdot cm^2\cdot mol^{-1}$, in nitromethane at a concentration of 5×10^{-4} M (slope = $(\Lambda_O - \Lambda_M)/\sqrt{C}$).

4.2.3.2. Conductivities

Conductivities were measured in nitromethane at 25°C and are given in Table 4-8. Plots of Λ_M vs. $\sqrt{C}$ give straight lines over the range of 10^{-3} to 10^{-4} M for all π-allylpalladium complexes (Figure 4-11). Both molar conductivity and Onsager slope (Figure 4-12) values demonstrate that complexes of open-chain dithioether ligands and L1 give 1:1 electrolytes while those of larger macrocyclic thioether ligands give 1:2 electrolytes. No deviation has been observed in the plots of Λ_M vs. $\sqrt{C}$. It seems that ion-pair association is not significant over the concentration range examined. The larger the positive charge on a complex cation, the easier ion-pair formation might be expected to be. Thus it is not surprising that ion-pair association was observed only in some bis-ligand complexes as discussed previously.

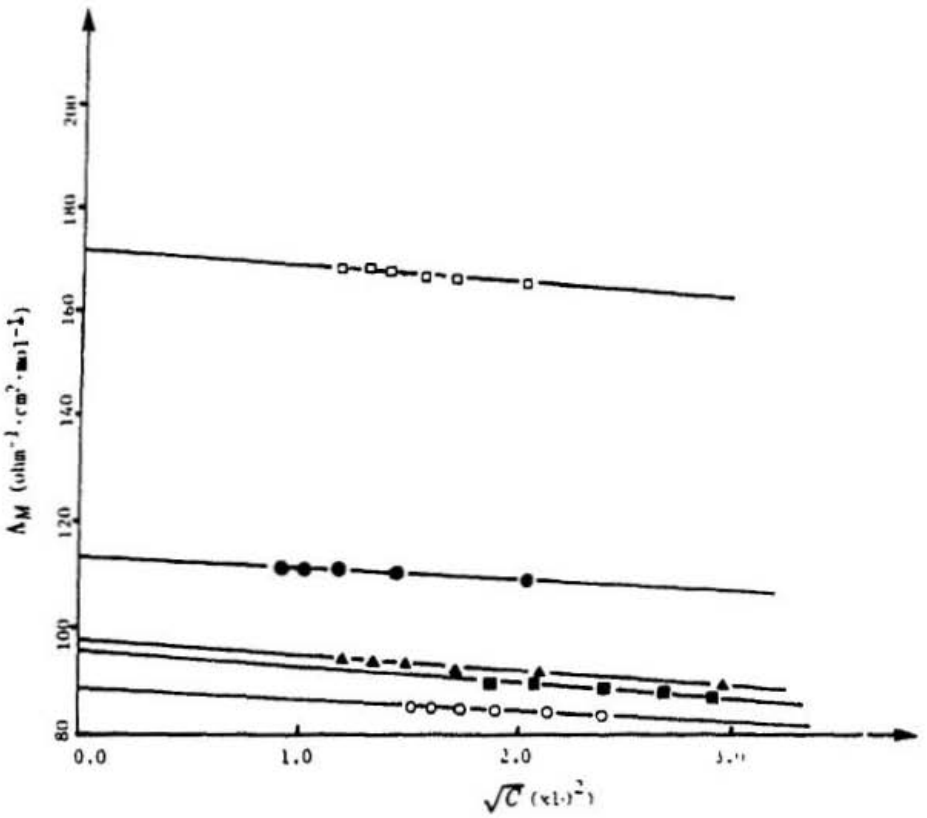

Figure 4-11. Plots of Λ_M vs. $\sqrt{C}$ for π-allylpalladium complexes.

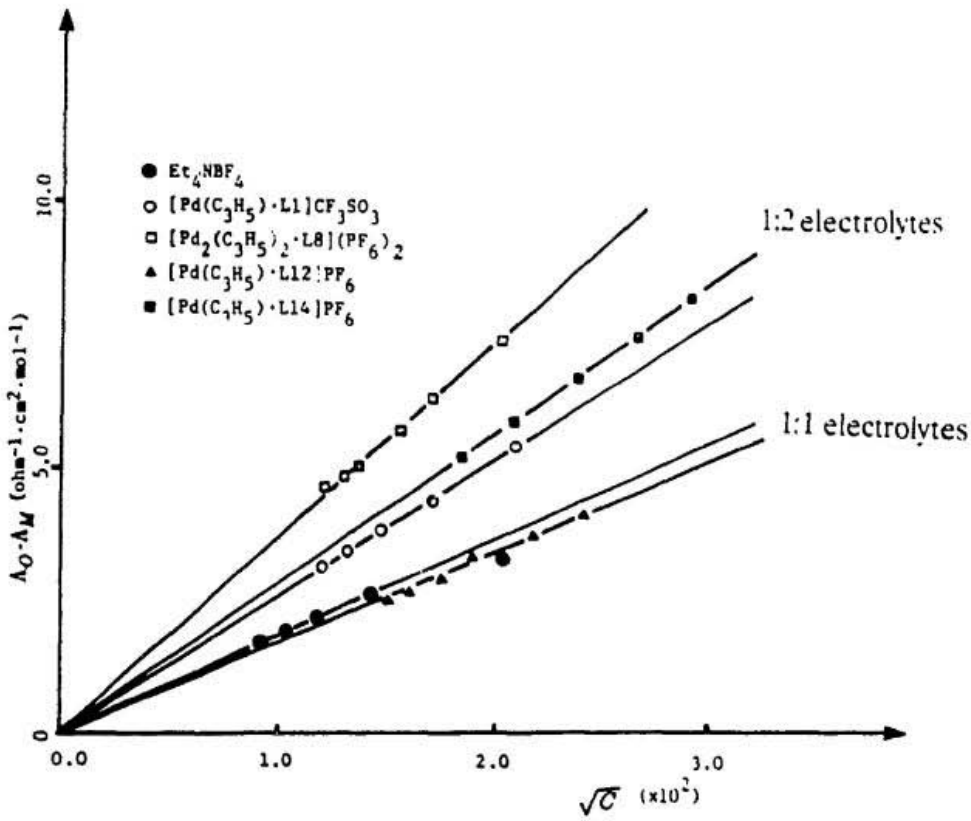

Figure 4-12. Onsager plots for π-allylpalladium complexes.

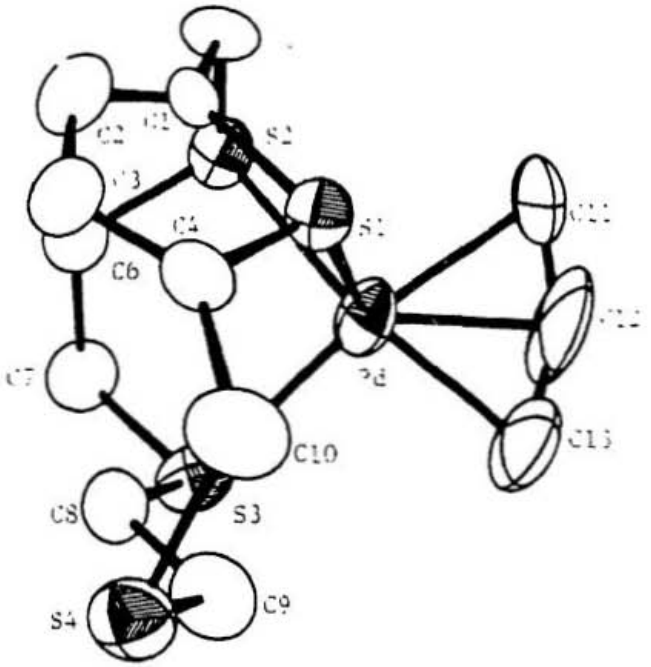

Pd-S(1)	2.786(4)	S(1)-Pd-S(2)	86.0(2)
Pd-S(2)	2.297(4)	S(1)-Pd-S(3)	96.1(1)
Pd-S(3)	2.343(4)	S(2)-Pd-S(3)	90.02(14)
Pd-C(11)	2.147(18)	S(1)-Pd-C(11)	87.6(2)
Pd-C(12)	1.995(22)	S(1)-Pd-C(12)	98.6(2)
Pd-C(13)	2.079(18)	S(1)-Pd-C(13)	96.8(2)
		S(2)-Pd-C(11)	99.1(7)
		S(2)-Pd-C(13)	167.8(7)
		S(3)-Pd-C(11)	169.4(6)
		S(3)-Pd-C(13)	100.4(7)
		C(11)-Pd-C(12)	34.1(12)
		C(11)-Pd-C(13)	69.2(9)
		C(12)-Pd-C(13)	36.1(12)

Figure 4-13. ORTEP drawing of $[Pd(C_3H_5)\cdot L1]^+$ and selected bond lengths (Å) and angles (degrees).

4.2.3.3. The Structure of $[Pd(C_3H_5)\cdot L1]CF_3SO_3$

The ORTEP drawing of $[Pd(C_3H_5)\cdot L1]^+$ and selected bond lengths and angles are shown in Figure 4-13. The unit cell contains four $[Pd(C_3H_5)\cdot L1]^+$ complex cations, each of which is asymmetric. The conformation of the coordinated ligand in solid state $[Pd(C_3H_5)\cdot L1]CF_3SO_3$ is the same as that in $[Cu(L1)_2]^+$ (Figure 3-1), $[CuCl_2\cdot L1]_2$ (Figure 3-3) and $[PdBr_2\cdot L1]$ (Figure 4-3). The macrocycle is bonded to the metal center as a tridentate ligand with two thioether sulfurs, S2 and S3, occupying the two equatorial sites and thiophene-sulfur (S1) interacting with the Pd atom at an apical position. The π-allyl group occupies the remaining two equatorial positions to complete a square pyramidal geometry. The Pd atom lies ~0.06 Å above the plane defined by a pair of thioether sulfurs, S2 and S3, and two terminal carbon atoms, C11 and C13, of the π-allyl group with an S(2)-Pd-S(3) angle of 90.02(14)°, which is almost the same as that (90.15(13)°) found in $[PdBr_2\cdot L1]$.

Apical bonds in five- or six-coordinated palladium(II) complexes tend to be longer than their equatorial counterparts. For example, the axial and average equatorial Pd-S bond lengths in five-coordinate $[PdBr_2\cdot$[9]aneS3] (15) are 3.125(4) and 2.266 Å while the average axial and equatorial Pd-S bond lengths in six-coordinate $[Pd([9]aneS3)_2]^{2+}$ (15) are 2.98 and 2.319 Å. In comparison, the apical (thiophene) and average basal Pd-S distances in $[Pd(C_3H_5)\cdot L1]^+$ are 2.786(4) and 2.322 Å. Due to the large trans influence of a π-allyl group, which is a better π-acceptor than Br, the Pd-S bond distances are 0.042 Å longer than those found in $[PdBr_2\cdot L1]$ (average basal Pd-S=2.280 Å). As a result, the thiophene-sulfur is brought closer to the metal center. This may account for the unusually short apical Pd-S(thiophene) bond. In fact, the present example provides the shortest known apical Pd-S bond in a five- or six-

coordinate palladium(II)-thioether complex even though thiophene does not usually form strong bonds through its sulfur atom to transition metals.

The π-allyl group is asymmetrically bonded to the Pd atom with Pd-C11, Pd-C12 and Pd-C13 distances being 2.148(16), 2.008(21) and 2.063(19) Å, respectively. This is probably caused by steric crowding from hydrogens on the macrocycle and two terminal hydrogens on C11. The asymmetry of the π-allyl group is significant in its potential application to the regiochemistry of nucleophilic additions to the asymmetric π-allyl group. In comparison with complexes $[Pd(C_3H_5)\cdot L_2]^+$ (L_2=phosphines) (1, 4, 16), the short Pd-C bond lengths in $[Pd(C_3H_5)\cdot L1]^+$ are consistent with the smaller trans influence of thioether-sulfurs compared to corresponding phosphine donors.

4.2.3.4. Nmr Study

The intramolecular motions of coordinated species leading to simplified nmr spectra, particularly of allylic ligands have been extensively studied (4-10, 17-20). In the present study, we have examined the variable temperature ^1H nmr spectra of π-allylpalladium complexes of open-chain and macrocyclic thioether ligands in order to characterize any motions of the π-allyl groups and the macrocyclic ligands. ^1H nmr spectral data are in Table 4-9. The assignments of the spectra were made on the basis of ^1H-^1H COSY spectroscopy, Attached Proton Tests and the following two principles: (i), the central proton of an allyl group interacts with the anti proton to exhibit a greater coupling constant than with a syn proton (5) and (ii), the anti protons are generally at higher field than the syn protons (5).

Table 4-9: ^1H nmr data for π-allylpalladium complexes (chemical shifts in ppm vs. TMS).

Complex	Solvent	π-allyl group	Thioether Ligand
$[Pd(C_3H_5)\cdot L1]CF_3SO_3$	CD_3NO_2	5.98(m,1H),4.93(d,$^3J_{HH}$ = 7.2Hz,2H)	7.04(s,2H),4.23(s,4H),3.06(m,2H)
		3.73(d,$^3J_{HH}$ = 12.95Hz)	2.83(m2H),2.58(m,2H),2.05(m,2H)
	CD_3CN	5.89(m,1H),4.83(d,$^3J_{HH}$ = 7.2Hz,2H)	6.97(s,2H),4.18(s,4H),2.95(m,2H)
		3.63(d,$^3J_{HH}$ = 13.0Hz,2H)	2.65(m,2H),2.45(m,2H),2.28(m,2H)
	d_6-DMSO	6.06(m,1H),4.84(d,$^3J_{HH}$ = 6.9Hz,2H)	7.01(s,2H),4.31(q,$^2J_{HH}$ = 14.0Hz,4H)
		3.72(d,$^3J_{HH}$ = 12.8Hz,2H)	3.00(m,2H),2.60(m,4H),2.03(m,2H)
$[Pd_2(C_3H_5)_2\cdot L2](PF_6)_2$	CD_3CN	5.77(m,2H),4.84(d,$^3J_{HH}$ = 5.5Hz,4H)	6.94(s,2H),4.35(s,4H)
		3.50(d,$^3J_{HH}$ = 13.0Hz,4H)	2.94(m,8H),2.56(s,4H)
	d_6-DMSO	5.84(m,2H),4.98(d,$^3J_{HH}$ = 6.7Hz,4H)	7.00(s,2H),4.62(s,4H)
		3.57(d,$^3J_{HH}$ = 12.7Hz,4H)	2.92(m,8H),2.60(s,4H)
$[Pd_2(C_3H_5)_2\cdot L8](PF_6)_2$	CD_3CN	5.72(m,2H),4.42(s,4H)	6.92(s,4H),4.28(s,8H)
		3.32(s,4H)	2.75(t,$^3J_{HH}$ = 4.7Hz,8H),1.98(m,4H)
$[Pd(C_3H_5)\cdot L10]PF_6$	CD_3CN	5.48(m,1H),4.15(d,$^3J_{HH}$ = 7.0Hz,2H)	7.40(m,10H)
		3.08(d,$^3J_{HH}$ = 13.1Hz,2H)	3.99(s,4H),3.00(s,4H)
$[Pd(C_3H_5)\cdot L12]PF_6$	CD_3NO_2	5.49(m,1H),4.44(d,$^3J_{HH}$ = 7.1Hz,2H)	7.52(m,10H),7.38(m,4H)
		3.10(d,$^3J_{HH}$ = 12.9Hz,2H)	4.24(s,4H),4.20(s,4H)
	CD_3CN	5.39(m,1H),3.93(d,$^3J_{HH}$ = 7.1Hz,2H)	7.46(m,10H),7.35(m,4H)
		3.01(d,$^3J_{HH}$ = 12.9Hz,2H)	4.12(s,4H),4.10(s,4H)
	d_6-DMSO	5.46(m,1H),3.95(d,$^3J_{HH}$ = 6.4Hz,2H)	7.47(m,10H),7.35(m,4H)
		3.11(d,$^3J_{HH}$ = 12.7Hz,2H)	4.30(s,4H),4.22(s,4H)
$[Pd(C_3H_5)\cdot L14]PF_6$	CD_3NO_2	5.81(m,1H),4.20(d,$^3J_{HH}$ = 7.1Hz,2H)	7.60(m,8H),7.10(m,4H)
		3.38(d,$^3J_{HH}$ = 13.0Hz,2H)	4.18(s,4H)
	CD_3CN	5.70(m,1H),4.18(d,$^3J_{HH}$ = 7.1Hz,2H)	7.42(m,8H),7.10(m,4H)
	d_6-DMSO	3.23(d,$^3J_{HH}$ = 13.0Hz,2H)	4.43(s,4H)
		6.00(m,1H),4.45(broad singlet,2H)	7.50(m,8H),7.18(m,4H)
		3.65(broad singlet,2H)	4.55(s,4H)

In general, the spectra of π-allylpalladium complexes are of an AM_2X_2 type at room temperature, which is typical of a fixed symmetrically bonded π-allyl group. The general features of the new complexes with thioether ligands are in agreement with those previously reported (21). In view of their different dynamic behaviour, the ^1H nmr spectra of π-allylpalladium complexes of open-chain and macrocyclic thioether ligands will be discussed separately.

4.2.3.4.1. π-Allylpalladium Complexes of Open-Chain Dithioether Ligands

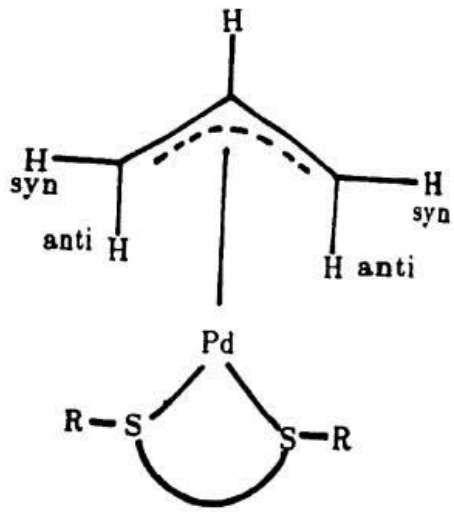

Figure 4-14. Structure of π-allylpalladium complexes of dithioether ligands.

The ^1H nmr spectra of symmetrically bonded static π-allylpalladium complexes have been interpreted in terms of AM_2X_2 or more precisely AMM´XX´ spin systems (22). "Dynamic" complexes, on the other hand, show AX_4 splitting patterns and several proposals have been made regarding the nature of the fluxional process

responsible for the exchange of syn and anti protons (4-10, 17-20). In order to avoid any confusion with the exchange of syn and anti isomers of the dithioether complexes, it should be noted that the following discussion about syn/anti exchange concerns the dynamic interconversion of syn and anti protons on the two terminal carbon atoms of the π-allyl group (Figure 4-14).

The ^1H nmr spectra of π-allylpalladium complexes of three open-chain dithioethers in CD_3NO_2 show multiplets (9 lines) at ~5.50 ppm due to the central allylic hydrogens and two doublets near 4.20 and 3.10 ppm, originating from the syn and anti hydrogens. Their intensity ratio is 1:2:2. This suggests a static symmetrically π-bonded allyl group in these complexes. Unlike that of $[PdCl_2 \cdot L10]$, the ^1H nmr spectrum of $[Pd(C_3H_5) \cdot L10]PF_6$ in CD_3NO_2 shows a singlet at about 4.00 ppm due to the benzylic hydrogens and a singlet at 3.00 ppm due to hydrogens in the CH_2CH_2 backbone. Apparently, both conformational changes and inversion at coordinated S-atoms have occurred as evidenced by the coalescence of two AB quartets due to the benzylic hydrogens in the syn and anti isomers of $[PdCl_2 \cdot L10]$. As a result, only an " averaged" L10 was observed. The rapid inversion at coordinated S-atoms is also responsible for the observation of only one π-allyl group. Were the inversion at sulfur slow enough, two different diastereotopic π-allyl groups would be expected due to the pyramidal environment about thioether sulfur. The marked difference between the spectra of $[PdCl_2 \cdot L10]$ and $[Pd(C_3H_5) \cdot L10]PF_6$ can be explained in terms of the much larger trans influence of a π-allyl ligand compared to chloro-ligands since the π-allyl group is a better π-acceptor than chloride. Similar explanations can be applied to the complexes $[Pd(C_3H_5) \cdot L]$ (L=L12, L14).

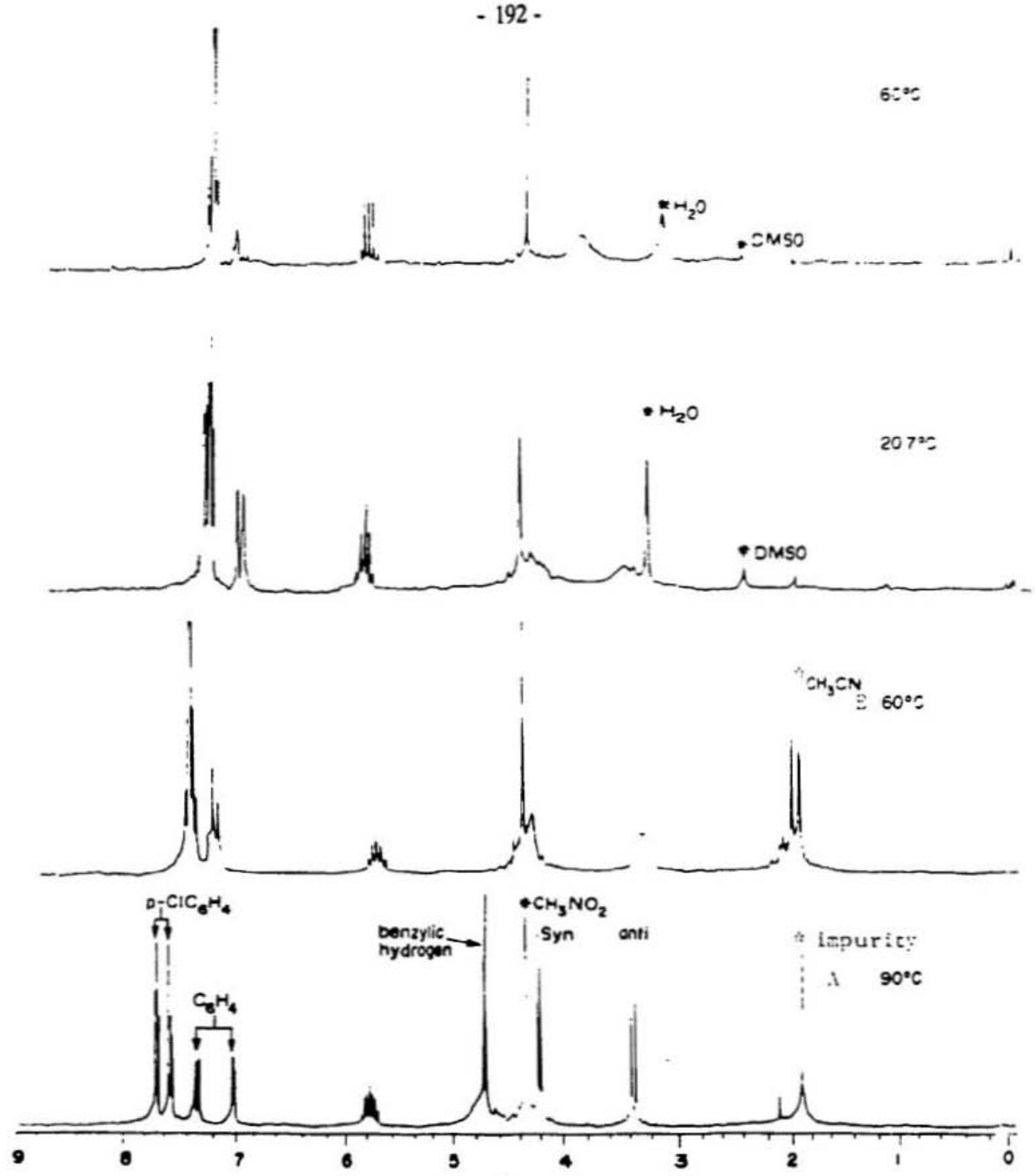

Figure 4-15. Variable temperature ^{1}H nmr spectra of [Pd(C_3H_5)·L14] in (A) CD_3NO_2 (90°C); (B) CD_3CN (60°C); (c) d_6-DMSO (22.7°C) and (D) d_6-DMSO (60°C).

It is of particular interest that the ^1H nmr spectra of the three open-chain dithioether π-allylpalladium complexes, one example of which is shown in Figure 4-15, are invariant with temperature in CD_3NO_2 to about 90°C. This observation establishes that in the absence of base or coordinating solvent the π-allyl group does not undergo any motion leading to interconversion of syn and anti hydrogens on the nmr time scale in the temperature interval studied. Therefore, the internal rotation mechanism, which involves rotation of the terminal CH_2 group about the carbon-carbon bond (19), is excluded for these π-allylpalladium complexes.

It should be noted that ^1H nmr spectra of dithioether complexes were strongly solvent dependent. In CD_3NO_2, all three complexes show no temperature dependence even at 95°C (Figure 4-15 (A)). In CD_3CN, however, they start to undergo syn/anti exchanges at temperatures above 60°C (Figure 4-15 (B)). When the strong σ-donor solvent d_6-DMSO is used, $[Pd(C_3H_5)\cdot L14]PF_6$ begins to undergo syn/anti exchange processes even at room temperature (Figure 4-15 (C)) while $[Pd(C_3H_5)\cdot L12]PF_6$ starts to undergo the same processes at temperatures over 30°C. Upon warming, the multiplet (9 lines) at about 5.60 ppm originating from the central allylic proton collapses to a quintet while two doublets at about 4.50 and 3.40 ppm originating from anti and syn protons, respectively, begin to broaden and then to coliapse to a broad singlet at about 3.90 ppm (Figure 4-15 (D)). This is expected to be eventually an AX_4 doublet at extreme temperatures if the complex does not decompose. In addition, no concentration dependence of the rate of syn/anti exchange was detected in CD_3CN or d_6-DMSO. This is significant in that it rules out any explanation of the temperature-dependence involving intermolecular exchange of the allyl ligand as in some platinum(II) complexes (23-24).

Scheme 4-3

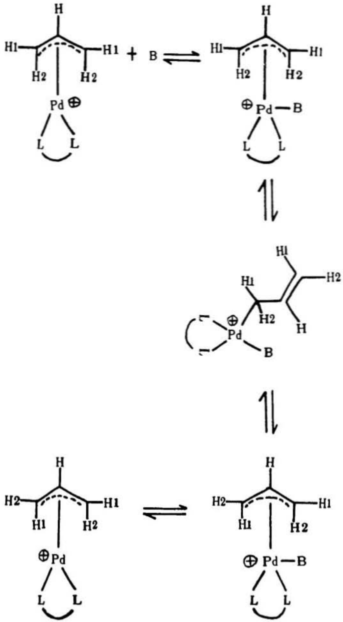
H
H1
H1
H2
H2
Pd ⊕
L
L
+ B
H
H1
H1
H2
H2
⊕ Pd — B
L
L
H1
H1
H2
H2
H
⊕
Pd
B
H
H2
H1
H1
H2
⊕Pd
L
L
H
H2
H1
H1
H2
⊕ Pd — B
L
L

Examination of variable temperature ^1H nmr spectra of dithioether complexes in different solvents indicates that (i) the chemical shift of the central allylic proton changes (~0.03 ppm) with temperature; (ii) the chemical shift of the terminal CH_2 resonance (a broad singlet has been observed) in the AX_4 spectrum is midway between the chemical shifts of the two doublets in the AM_2X_2 spectrum; and (iii) the chemical shifts of the allylic protons change irregularly with changes in polarity of the solvent and the rate of the syn/anti exchange process increases with increasing donor ability of the solvent. It seems difficult to explain these observations by an internal rotation mechanism, a more plausible explanation is the solvent-assisted π-σ equilibrium mechanism, in which a five- or six-coordinated intermediate or transition state is formed by solvent coordination and the π-bonded allyl group becomes momentarily σ-bonded. Rotation may then occur about the metal-carbon single bond, followed by reformation of the π-bonded form. The whole process is shown in Scheme 4-3.

Further evidence for the mechanism above has been obtained from a variable temperature ^1H nmr study of $[Pd(C_3H_5)\cdot L]$ (L=L12 and L14) in the mixed solvent CD_3NO_2/C_5D_5N (4:1, v:v). Both complexes start to undergo syn/anti exchange at temperatures higher than 60° in the mixed solvent and the exchange rate depends on the concentration of C_5D_5N.

4.2.3.4.2. π-Allylpalladium Complexes of Thiophenophane Ligands

The ^1H nmr spectrum of $[Pd(C_3H_5)\cdot L1]CF_3SO_3$ is more complex than those of $[MX_2\cdot L1]$ (M=Pd, Pt; X=Cl, Br, I, SCN). Intramolecular motions include ligand pivot fluxions of the macrocycle, inversion at thioether sulfurs and syn/anti interconversion of the terminal hydrogens of the π-allyl group. These motions will be discussed separately. We shall discuss in detail only $[Pd(C_3H_5)\cdot L1]CF_3SO_3$, for which we

also have X-ray structural data (Figure 4-13).

4.2.3.4.2.1. The Fluxionality of the Macrocycle

The spectrum (Figure 4-16) of $[Pd(C_3H_5)\cdot L1]CF_3SO_3$ in CD_3NO_2 at 25°C shows a singlet at 7.04 ppm due to the aromatic hydrogens, H2 and H3, a broad singlet at 4.23 ppm due to the hydrogens on C5 and C10, and four multiplets at 3.06, 2.83, 2.58 and 2.05 originating from hydrogens in the two CH_2CH_2 units with the integrated intensities of these regions being in the ratio 2:4:2:2:2:2 as required. In comparison with the spectrum (Figure 4-7) of $[PdBr_2\cdot L1]$ in d_6-DMSO, in which two doublets at about 7.05 ppm and an AB quartet at about 4.35 ppm were observed, the presence of a singlet at 7.04 ppm and a broad singlet at 4.23 ppm in the spectrum of $[Pd(C_3H_5)\cdot L1]CF_3SO_3$ (Figure 4-16) in CD_3NO_3 establishes that the macrocycle is fluxional through a 1,4-metallotropic shift at S2, S3 and S4 when two halide or pseudo-halide ligands (Figure 4-3) are replaced by a π-allyl group. The fluxionality of the macrocycle is also confirmed by the observation that only five signals were detected in the ^{13}C nmr spectrum of $[Pd(C_3H_5)\cdot L1]CF_3SO_3$ in CD_3CN. Were the macrocycle rigid, ten signals would be expected as in the case of $[PdCl_2\cdot L1]$. The fact that four multiplets between 2.00 ppm and 3.00 ppm are seen whereas only two triplets were detected in this region of the spectrum of the free ligand in $CDCl_3$ suggests that although the fluxional process is taking place, inversion at all thioether-sulfurs is not.

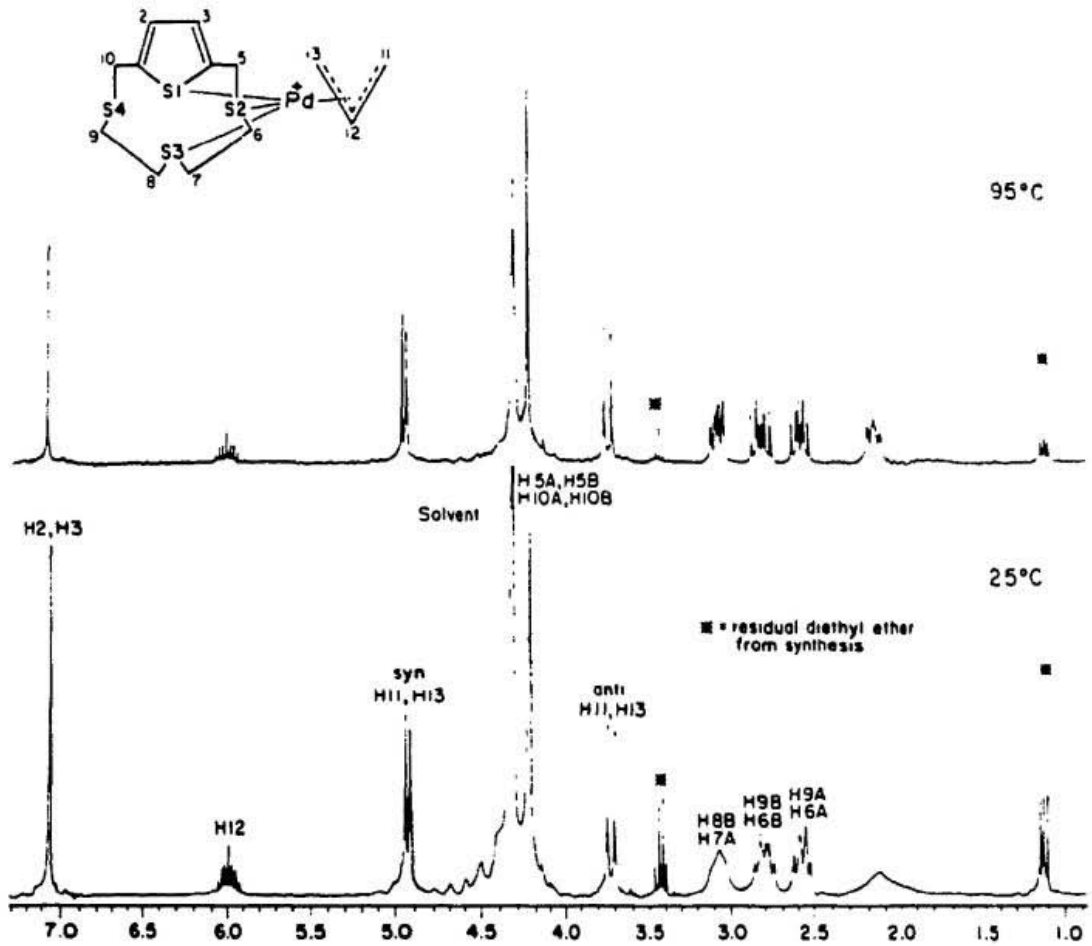

Figure 4-16. ^{1}H nmr spectra of $[Pd(C_3H_5)\cdot L1]CF_3SO_3$ in CD_3NO_2 at 25°C and 90°C.

As is shown in the solid state conformation (Figure 4-13), S4 in the coordinated macrocycle is exocyclic. When a 1,4-shift takes place, rotation at C-S and C-C bonds is required and the energy barrier to this process is low as demonstrated by the fluxionality of the macrocycle even at room temperature. It is this 1,4-shift that is responsible for the appearance of an nmr spectrum suggesting a static symmetrically bonded π-allyl group although it is shown to be asymmetric in the solid state of $[Pd(C_3H_5)\cdot L1]CF_3SO_3$. When the 1,4-shift occurs, the macrocycle is bonded to the Pd atom in such a way that S1 and S3 remain bound to the metal while the two outer ones (S2 and S4) take turns. As a result, H2 and H3 in the "averaged" macrocycle become equivalent and the same is true for the two methylene groups adjacent to the thiophene ring and for the two CH_2CH_2 units, from which only one ABCD splitting pattern originates. This is confirmed also by the coalescence of the upfield signal at -0.65 ppm due to H8A with the signal at 3.60 ppm due to H7B to give a multiplet at 2.27 ppm.

In complexes $[MX_2\cdot L1]$ (M=Pd, Pt; X=Cl, Br, I, SCN), the macrocycle is "locked" and intramolecular motions including inversion at coordinated S-atoms as well as rotations at M-S and C-S bonds are severely limited so that it remains rigid until decomposition occurs at high temperatures. When two halide or pseudo-halide ligands are replaced by a π-allyl group, remarkable changes occur and the macrocycle becomes fluxional. It seems that the fluxionality of the macrocycle is sensitive to the nature of ligands trans to the points of macrocycle attachment. This can be explained in terms of π-acidity of trans ligands. When ligands at trans positions are weak π-acceptors such as Cl, Br, I, SCN, the macrocycle is strongly bonded to the metal and there is no coalescence of resonance signals until the complex decomposes. When a strong π-acceptor such as a π-allyl group is at the trans positions, the M-S bonds have

been weakened and it is possible for the macrocycle to undergo a ligand pivot fluxion provided that the macrocycle has at least one uncoordinated thioether-sulfur atom, as in the case of $[PtMe_3 \cdot [14]aneS4]^+$ (25-26). The trans bond weakening effects of Br and π-allyl can be seen by comparing Pd-S bond lengths in $[PdBr_2 \cdot L1]$ (Figure 4-3) (the average equatorial Pd-S distance is 2.280 Å) and $[Pd(C_3H_5) \cdot L1]CF_3SO_3$ (Figure 4-13) (the average equatorial Pd-S distance is 2.322 Å). Thus, the fluxionality of a macrocycle is dependent on the strength of its M-S bonds and availability of uncoordinated donor atoms in the complex.

Similar ^1H nmr spectra have been obtained in CD_3CN except that the four multiplets in the region 2.00-3.00 ppm are better resolved in CD_3NO_2 than in CD_3CN. In d_6-DMSO (Figure 4-17, p202), however, changes occur and a solvent effect is observed again as in the case of open-chain dithioether π-allylpalladium complexes. The spectrum of $[Pd(C_3H_5) \cdot L1]CF_3SO_3$ in d_6-DMSO shows an AB quartet at about 4.35 ppm due to hydrogens on C5 and C10 and three multiplets at 3.00, 2.60 and 2.00 ppm due to hydrogens in the two CH_2CH_2 units with integrated intensities for these regions in the ratio 4:2:4:2. The presence of the AB quartet at about 4.35 ppm is significant and supports our previous conclusion that inversion at all sulfurs is not occurring and H5A and H5B or H10A and H10B remain non-equivalent when the 1,4-shift is taking place. The fact that only a broad singlet was observed in the spectrum of $[Pd(C_3H_5) \cdot L1]CF_3SO_3$ in CD_3NO_2 and CD_3CN suggests that the chemical environments around H5A and H5B or H10A and H10B are very similar. When the chemical shift difference of H5A and H5B or H10A and H10B is very small, it is likely that the spectrum would appear as a broad singlet in this region. This is supported by the observation that small peaks appear on both sides of the broad singlet at 4.35 ppm that are the outer pair of peaks of an AB quartet where $\Delta\delta$ is small enough that the

two center peaks have overlapped. The chemical shift of individual H's is well known (9) to shift with solvent even when no metal atoms are present.

4.2.3.4.2.2. Inversion at Thioether-Sulfurs

Upon warming the d_6-DMSO solution to 70°C, the AB quartet at 4.35 ppm starts to collapse and gives a singlet at the same position at 100°C whilst the three multiplets at 3.00, 2.60 and 2.00 ppm originating from the two CH_2CH_2 units begin to merge into two multiplets at about 2.60 and 2.10 ppm. This is an A_2B_2 type spectrum as shown in Figure 4-17. Since it is obvious that the 1,4-shift at S2, S3 and S4 does not interchange hydrogens on the same carbon atom, the only way for the A_2B_2 spectrum to arise is by a dissociative inversion route, in which S3 is replaced by a DMSO molecule and the macrocycle may become momentarily mono- or bidentate (S1 and S2). The inversion at S3, which involves rotation about C-S and C-C bonds, then takes place and is followed by reformation of the five-membered chelate ring. It is this inversion that interchanges pairs of hydrogens on each carbon atom. The fact that no free ligand signals were detected over the temperature range studied suggests that the macrocycle is not completely dissociated when inversion at S3 takes place. Further evidence has been obtained by the ^1H nmr study in the presence of the free ligand in CD_3NO_2 and d_6-DMSO. In CD_3NO_2, the intensities of the free ligand peaks do not change with temperature so that the ligand is not involved except as an impurity in the spectrum. In d_6-DMSO, however, the free ligand peaks change with the temperature and finally merge with those of coordinated ligand. This suggests that in this solvent the free ligand exchanges with the coordinated one, thereby interchanging pairs of hydrogens on each carbon atom.

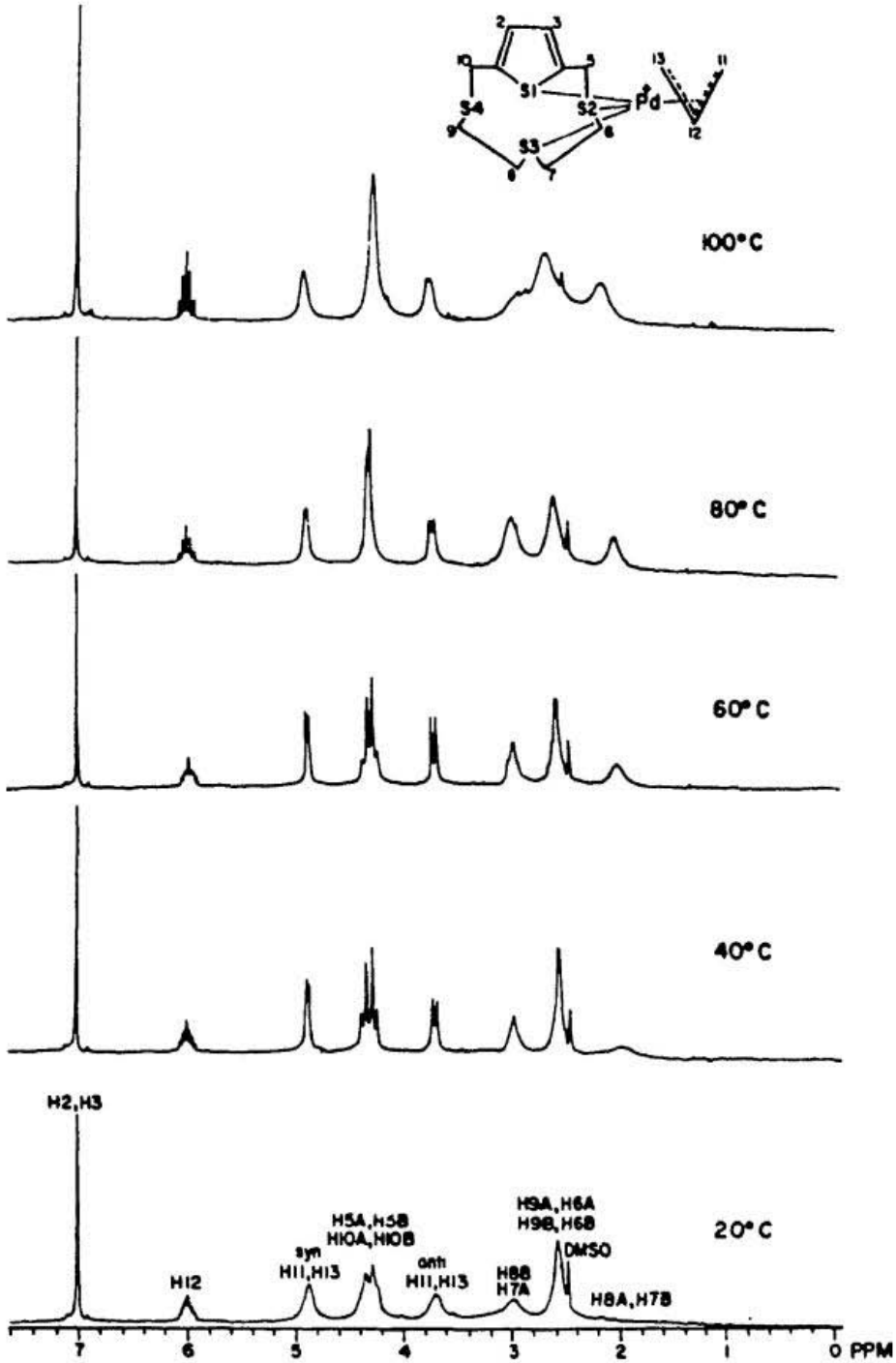

Figure 4-17. Variable temperature ^{1}H nmr spectra of $[Pd(C_3H_5)\cdot L1]CF_3SO_3$ in d_6-DMSO.

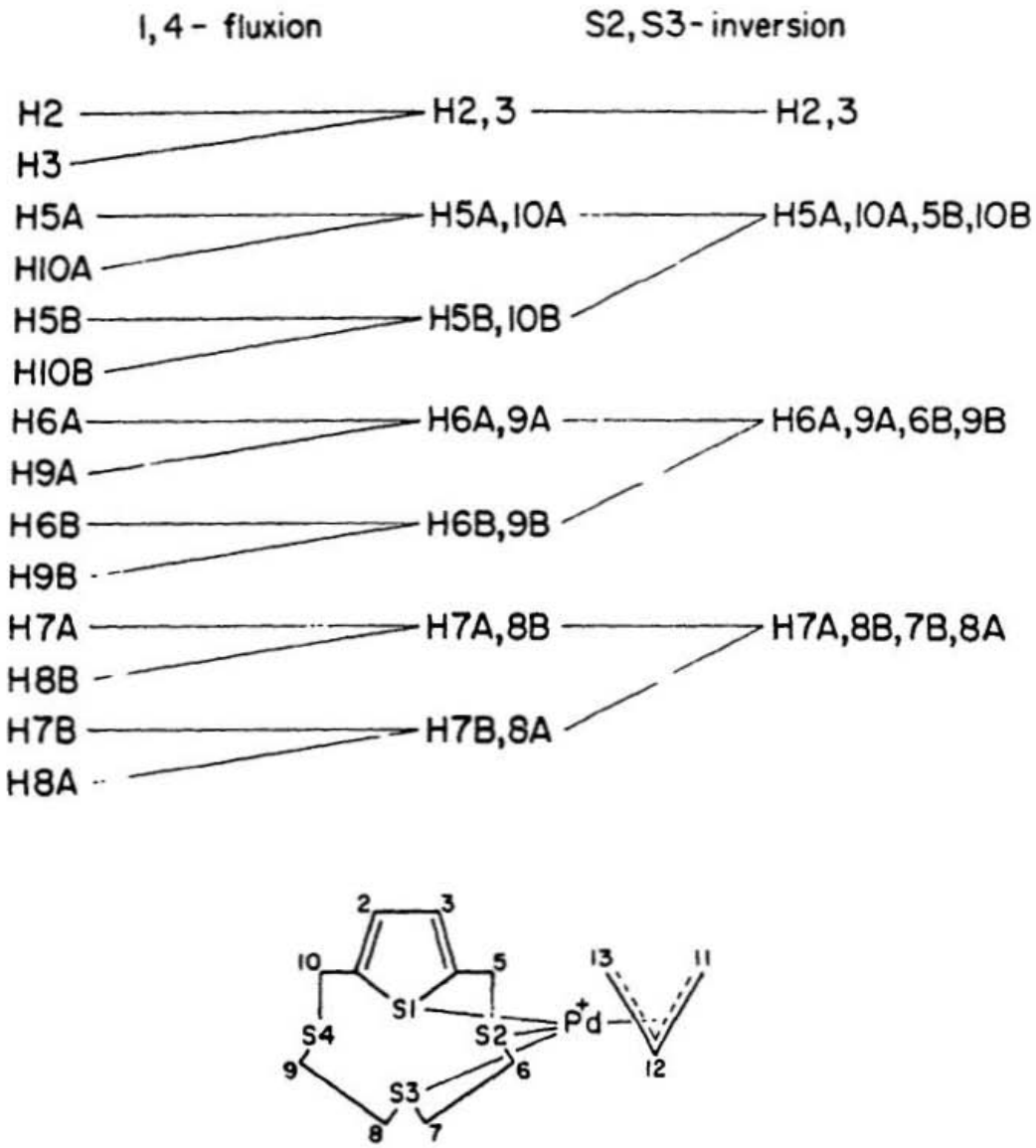

Figure 4-18. Intramolecular motions and interchange of hydrogen positions in the macrocycle.

Inspection of variable temperature ^1H nmr spectra of the coordinated macrocycle in $[Pd(C_3H_5)\cdot L1]CF_3SO_3$ in different solvents indicates that the donating ability of the solvent is important for inversion at thioether-sulfur(s). In a weak σ-donor solvent (CD_3NO_2), only a 1,4-shift due to the large trans influence of the π-allyl group is observed at temperatures from 25°C to 95°C with no indication of any inversion at S-atom(s). In a strong σ-donor solvent (d_6-DMSO), replacement of some thioether sulfur atoms is possible and inversion at S-atoms occurs at high temperatures in addition to the 1,4-shift. Therefore, the energy barrier for dissociative inversion at S-atoms is larger than that for the pivot fluxion of the macrocycle and the dissociative inversion at S-atoms is largely dependent on the σ-donating ability of the solvent employed.

4.2.3.4.2.3. Syn/Anti Interconversion of π-Allyl Group

In CD_3NO_2, the spectrum (Figure 4-16) shows a multiplet (9 lines) at 6.09 ppm due to the central allylic hydrogen and two doublets at 4.93 ppm ($^3J_{H\text{-}H}$=7.24 Hz) and 3.72 ppm ($^3J_{H\text{-}H}$=12.95 Hz) originating from the syn and anti hydrogens, respectively. These observations are consistent with a static symmetrically bonded π-allyl group. Although it has been shown to be somewhat asymmetric in the solid state, it appears symmetrical in the nmr spectrum because of the 1,4 fluxional behavior of the other ligand. Similar spectra of $[Pd(C_3H_5)\cdot L1]CF_3SO_3$ were obtained in CD_3CN and d_6-DMSO at room temperature.

Upon warming the solution of $[Pd(C_3H_5)\cdot L1]CF_3SO_3$ in d_6-DMSO to 80°, the multiplet (9 lines) at 6.06 ppm due to the central allylic hydrogen collapses to a quintet while two doublets at 4.93 and 3.72 ppm due to syn and anti hydrogens, respectively, begin to broaden and then to collapse to two broad singlets at the same positions at 100° (Figure 4-17). At higher temperatures, if the complex in solution remains stable

these two broad singlets are expected to merge to a doublet midway between the two doublets in the AM_2X_2 spectrum thereby giving an AX_4 spectrum as was found in the open-chain dithioether complexes. Thus, for σ-π interconversion of π-allyl group to occur, a higher coordination number must be achieved either by addition of a base such as pyridine or a strong σ-donor solvent. The enhancement of the rate of σ-π interconversion is probably caused by the the solvent molecule acting in a manner analogous to the entering group in a typical square planar substitution.

4.2.3.5. Electrochemistry

It has been shown that the coordinating properties of the ancillary ligands, L_2, in $[Pd(C_3H_5)\cdot L_2]^+$ (21) are very important in the stabilization of the metal-containing reduction products. When L_2= $2CH_3CN$ and 1,5-C_8H_{12}, the Pd(0)-L_2 systems are unstable and the electrochemically reduced products are Pd metal and the free ligand. When L_2= 2 $P(C_6H_{11})_3$, formation of $[Pd\{P(C_6H_{11})_3\}_2]$ may account for the much greater stabilizing effect of two $P(C_6H_{11})_3$ ligands than that of 1,5-C_8H_{12} and CH_3CN. It is of interest to examine the electrochemical behaviour of $[Pd(C_3H_5)\cdot L]^+$ (L=dithioether and macrocyclic thioether ligands) because of the potential similarity of thioether and phosphine ligands.

Table 4-10 lists the peak potentials obtained from cyclic voltammograms of these π-allylpalladium complexes. In all cases the reduction step is irreversible as evidenced by cyclic voltammograms, one example of which is shown in Figure 4-19. No oxidation peak could be observed even at scan rates higher than 100 mV/s. The formation of Pd metal (black powder) has been observed by recycling the voltammograms. These results suggest that the reduced species Pd(0)-L are not sufficiently stabilized by thioether ligands to permit isolation. In comparison with complexes $[Pd(C_3H_5)\cdot L_2]^+$

(L= CH_3CN and $P(C_6H_{11})_3$, the resistance to reduction (Table 4-10) follows the order: phosphine > thioether > CH_3CN, which is consistent with the order of π-acidity of the ligands.

Table 4-10: Electrochemical data for π-allylpalladium complexes.

Complex	Cathodic Peak (E_{cp},V)*
$[Pd(C_3H_5)\cdot L1]CF_3SO_3$	-1.62
$[Pd(C_3H_5)_2\cdot L2](PF_6)_2$	-1.38
$[Pd_2(C_3H_5)_2\cdot L8](PF_6)_2$	-1.36
$[Pd(C_3H_5)\cdot L10]PF_6$	-1.60
$[Pd(C_3H_5)\cdot L12]PF_6$	-1.59
$[Pd(C_3H_5)\cdot L14]PF_6$	-1.60
$[Pd(C_3H_5)(CH_3CN)_2]^+$	-1.02 (ref. 21)
$[Pd(C_3H_5)(P(C_6H_{11})_3)_2]PF_6$	-1.75 (ref. 21)

* In acetonitrile, room temperature, scan rate 50 mv/s, Glassy carbon working electrode, platinum wire counter electrode; saturated calomel reference electrode, TEAP supporting electrolyte (0.1 M).

The cyclic voltammograms of thioether π-allylpalladium complexes show a broad anodic peak at positive potentials. This may be caused by some labile organic products which are formed from the combination of allyl fragments and solvent molecules (21).

In all cases the cathodic reactions involve a one-electron transfer process as revealed by coulometric measurements of $[Pd(C_3H_5)\cdot L1]CF_3SO_3$ in CH_3CN ($n=0.95\pm0.10$). By analogy to $[Pd(C_3H_5)\cdot L_2]^+$ (L=CH_3CN and $P(C_6H_{11})_3$), the major organic reduction product should be diene from combination of two allyl fragments. Further studies of electrochemical and chemical reduction of these complexes are required and will be one of my future research interests.

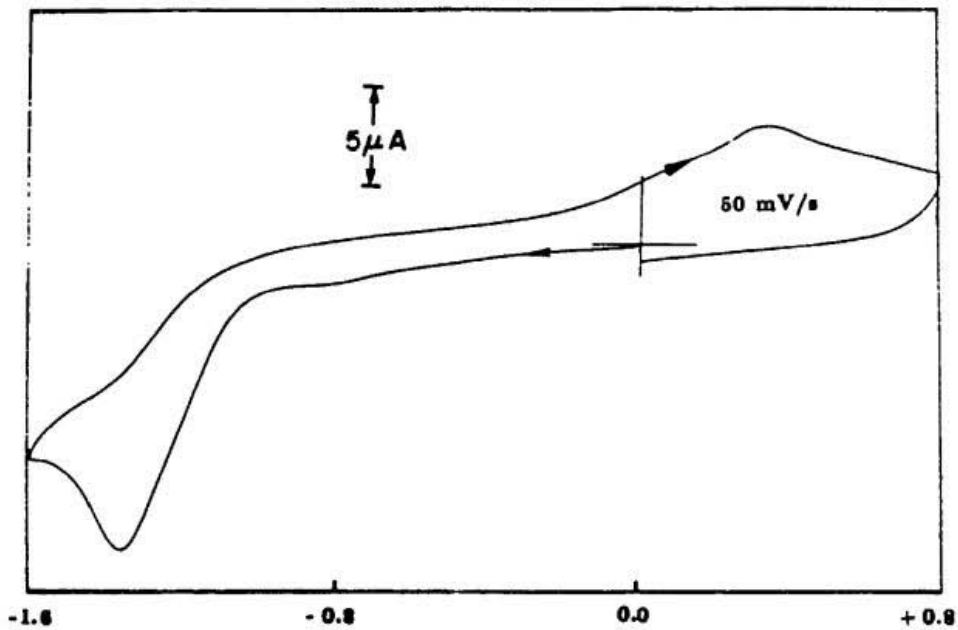

Figure 4-19. Cyclic voltammogram of $[Pd_2(C_3H_5)_2 \cdot L2](PF_6)_2$ in acetonitrile ($\sim 10^{-3}$ M, 0.1 M TEAP, glassy carbon working electrode, platinum wire counter electrode, SCE reference electrode) at a scan rate of 50 mV/s.

4.2.4. Conclusion

In the present study, π-allylpalladium complexes of open-chain and macrocyclic thioether ligands were prepared and studied by X-ray and ^1H nmr methods. The presence of an asymmetric π-allyl group indicates that it is possible to generate different chemical environments for the two terminal carbon atoms by introducing certain asymmetrically bonded ancillary ligands. This is of great importance in the regiospecific control of nucleophilic addition at terminal carbon atoms of a π-allyl group. The ^1H nmr measurements revealed a 1,4-metallotropic shift on the coordinated macrocyclic thioether ligand (L1). Although 1,3- and 1,5-shifts on sulfur atoms are well documented (28), 1,4-shifts are not. To our knowledge, only one example, $[PtMe_3 \cdot ([14]aneS4)]^+$, has been reported (25-26), which involves Pt(IV) not Pd(II) as in $[Pd(C_3H_5) \cdot L1]^+$. In the presence of base or strong σ-donor solvents, π-allylpalladium complexes undergo interconversion of syn and anti hydrogens of a π-allyl group through a solvent-assisted σ-π mechanism. Cyclic voltammetry of these complexes shows that in acetonitrile they undergo a totally irreversible one-electron reduction to give Pd metal and probably organic dienes from combination of two allyl fragments.

4.2.5. References

1. P.W. Jolly. Angew. Chem. Int. Ed. Engl. *24*, 283 (1985).

2. G. Wilkinson, F.G.A. Stone and E.W. Abel. *Comprehensive organometallic chemistry*. Pergamon, Oxford. 1982. Vol. 8, p. 799.

3. F.R. Hartley. *The chemistry of platinum and palladium*. Applied Science Publishers, London. 1973.

4. E. Cesarotti, M. Gassi and L. Prati. J. Chem. Soc., Dalton Trans. 161 (1989); Ibid. J. Organomet. Chem. 370, 407 (1989).

5. H.C. Clark, M.J. Hampden-Smith and H. Ruegger. Organometallics *7*, 2085 (1988).

6. P.M. Maitlis, P. Espinet and J.H. Russell. In *Comprehensive organometallic chemistry*. Edited by G. Wilkinson,
F.G.A. Stone and E.W. Abel. Pergamon, Oxford. 1982. Vol. 6, p. 385.

7. H.C. Clark and C.R. Jablonski. Inorg. Chem. *14*, 1518 (1975).

8. D.J. Mabbott, B.E. Mann and P.M. Maitlis. J. Chem. Soc., Dalton Trans. 294 (1977).

9. K. Vrieze. In *Dynamic nuclear magnetic resonance spectroscopy*. Edited by L.M. Jackman and F.A. Cotton. Academic Press, New York. 1975. p. 454.

10. D.L. Tibbetts and T.L. Brown. J. Am. Chem. Soc. *92*, 303 (1970).

11. S.R. Stephens and G.D. Shier. J. Organomet. Chem. *21*, 495 (1970).

12. L.S. Hegedus. Tetrahedron *40*, 2415 (1984).

13. B. Åkermark, S. Hanson, B. Krakenberger, K. Zetterberg and A. Vitagliano. Chem. Scr. *27*, 525 (1987).

14. B. Åkermark, S. Hanson, B. Krakenberger, B. Vitagliano and K. Zetterberg. Organometallics *3*, 679 (1984).

15. K. Wieghardt, H.J. Küppers, E. Raabe and C. Krüger. Angew. Chem. Int. Ed. Engl. *25*, 1101 (1986).

16. H.M. Buch, P. Binger, R. Benn, C. Krüger and A. Rufinska. Angew. Chem. In. Ed. Engl. *22*, 774 (1983).

17. K. Vrieze, P. Cossee, P. Pratt and C.W. Hilbers. J. Organomet. Chem. *11*, 353 (1968).

18. A. Davison and W.C. Rode. Inorg. Chem. *6* , 2124 (1967).

19. J.K. Becconsall, B.E. Job and S. O'Brien. J. Chem. Soc. A 423 (1967).

20. F.A. Cotton, J.W. Faller and Musco. Inorg. Chem. 6, 179 (1967).

21. G. Carturan, M. Biasiolo, S. Daniel, G.A. Mazzocchin and P. Ugo. Inorg. Chim. Acta *119*, 19 (1986).

22. B.E. Mann, R. Pietropaolo and B.L. Shaw. J. Chem. Soc., Dalton Trans. 2390 (1973).

23. G. Raper and W.S. McDonald. J. Chem. Soc., Dalton Trans. 265 (1972).

24. B.E. Mann, B.L. Shaw and G. Shaw. J. Chem. Soc. A 3536 (1971).

25. E.W. Abel, S.K. Bharghava, I. Moss, K.G. Orrell, V. Šik, P.A. Bates and M.B. Hursthouse. J. Chem. Soc., Chem. Commun. 978 (1987).

26. E.W. Abel, P.D. Beer, I. Moss, K.G. Orrell, V. Šik, P.A. Bates and M.B. Hursthouse. J. Organomet. Chem. *341*, 559 (1988).

27. E.W. Abel, S.K. Bharghava and K.G. Orrell. Prog. Inorg. Chem. *32*, 1 (1984).

CHAPTER 5

SYNTHESIS, CHARACTERIZATION AND PROPERTIES OF SILVER(I) COMPLEXES OF THIOPHENOPHANE LIGANDS

Abstract:

Silver(I) complexes $[Ag(L1)_2]X$ ($X=ClO_4^-$, BF_4^- and $CF_3SO_3^-$), $[Ag(L1)NO_3]$, $[Ag_2(L)_2]X$ (L=L2-L4; $X=ClO_4^-$, BF_4^- and $CF_3SO_3^-$), $[Ag{\cdot}L5]CF_3SO_3$ and $[Ag{\cdot}L]ClO_4$ have been prepared for thiophenophane ligands, 2,5,8-trithia[9](2,5)thiophenophane (L1), 2,5,8,11-tetrathia[12](2,5)thiophenophane (L2), 2,5,9,12-tetrathia[13](2,5)thiophenophane (L3), 2,6,10,14-tetrathia[15](2,5)thiophenophane (L4), 5-oxa-2,8-dithia[9](2,5)thiophenophane (L5) 2,5-dithia[6,6](2,5)thiophenophane (L7) and 2,6-dithia[7,7](2,5)thiophenophane (L8). The ir spectra of these complexes and fast atom bombardment mass spectra of $[Ag_2(L2)_2](ClO_4)_2$ are described. The effect of structure on the ligand's ability to form complexes is discussed. The X-ray structure of $[Ag_2(L2)_2](ClO_4)_2$ has been determined. The centrosymmetric dinuclear cation has a slightly distorted trigonal bipyramidal coordination geometry about each silver. The silver atoms are linked by one bridging thioether sulfur from each ligand while the remaining three sites on each silver are occupied by two terminal thioether sulfurs from one ligand molecule and one from the other ligand molecule. All these complexes are remarkably stable photochemically and chemically but under certain specific conditions react with loss of the ligand. This stability is discussed with respect to the structure of $[Ag_2(L2)_2]^{2+}$.

5.1. Introduction

It is well known (1) that silver(I) has a strong affinity for thioether ligands in agreement with the theory of hard and soft acids and bases. In general, silver(I) shows a preference for linear two-coordination (1) and, occasionally, tetrahedral four-coordination (1-4). However, recent studies (5-7) of silver(I) complexes of crown thioethers indicate that higher coordination numbers may be achieved with macrocyclic thioether ligands such as [9]aneS3 and [18]aneS6, which coordinate to Ag(I) in a distorted octahedral geometry. The octahedral geometry and hexathia coordination are suggested to contribute to the unusual electrochemical properties of these complexes (5).

In previous chapters, it has been shown that thiophenophane ligands when compared to simple crown thioethers, exhibit different conformations in the solid state and different complexing properties towards the transition metals platinum, palladium and copper. To extend the study of the coordination chemistry of these thiophenophane ligands, the synthesis and properties of several silver(I) complexes, and the X-ray structure of $[Ag_2(L2)_2]^{2+}$ are described. The structural study of $[Ag_2(L2)_2]^{2+}$, reveals a binuclear species, the geometry about each silver of which is slightly distorted trigonal bipyramidal. This stands in contrast to the structures of most silver complexes having coordination numbers of five or six (5, 8-10), which exhibit moderate or even severe distortions from idealized coordination geometry.

The ligands used in this chapter are given in Scheme 5-1.

Scheme 5-1

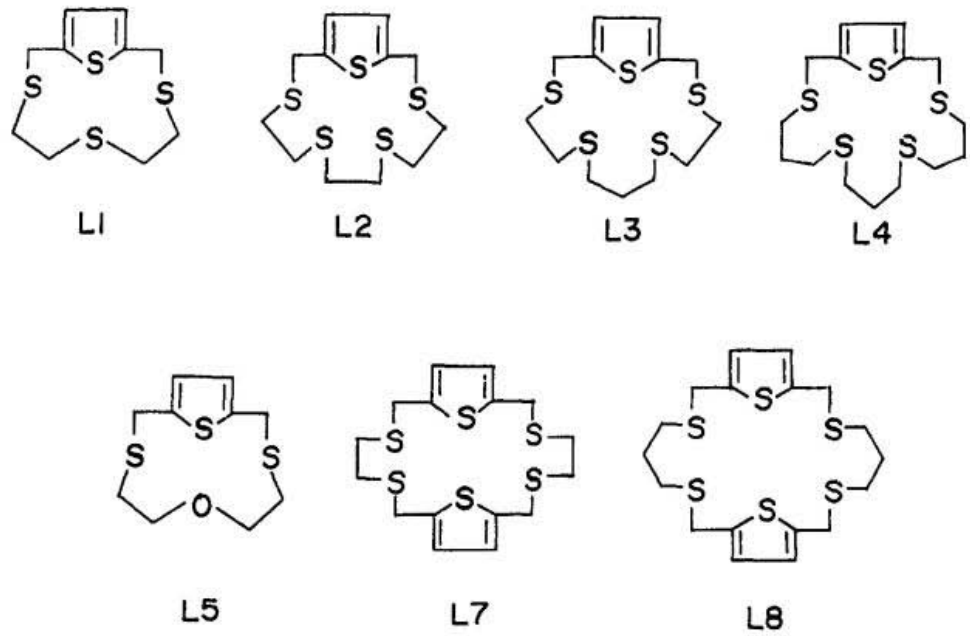

5.2. Experimental

Reagents and instruments are the same as those described in previous chapters. FAB mass spectra were obtained using a saddle-field FAB gun on a VG-7070HS mass spectrometer equipped with a VG2035 data system. The standard VG argon atom source was operated at 8 KeV and the silver salt was introduced as a mull in glycerol/para-toluensulfonic acid (approx. 3:1).

General Procedure for Preparation of Silver(I) Complexes

To a solution of $AgClO_4$ (52 mg, 0.025 mmol) in 10 ml of acetonitrile an equivalent of appropriate thiophenophane ligand in 5 ml of dichloromethane was added. The resulting solution was filtered immediately and the filtrate was left in a beaker to evaporate slowly giving eventually white crystals that were collected by filtration, washed with acetonitrile and dichloromethane and dried in air. Yields range

from 75% to 90%. Caution must be taken when handling perchlorate salts since those of thioether metal complexes are potentially explosive.

Procedures similar to that above were followed to prepare the corresponding tetrafluoroborate and triflate salts. Bis-ligand complexes $[Ag(L1)_2]X$ ($X=ClO_4^-$, BF_4^- and $CF_3SO_3^-$) were prepared in a similar way to that above using two equivalents of L1. Complex $[Ag(L1)NO_3]$ was obtained from the reaction of $AgNO_3$ with L1 even though a metal to ligand ratio of 1:2 was used.

5.3. Results and Discussion

5.3.1. Preparation

Reactions of thiophenophane ligands with Ag(I) were carried out in acetonitrile and dichloromethane. The isolated complexes with their analytical data and melting points are given in Table 5-1. In general, all complexes isolated are sparingly soluble in acetone and acetonitrile, but soluble in DMF and DMSO, from which no original complex could be isolated. Surprisingly, all silver(I) complexes of thiophenophane ligands are light-stable in contrast to silver halides (1), which are light-sensitive.

It is of interest to note that the reaction of AgX ($X=ClO_4^-$, BF_4^- and $CF_3SO_3^-$) with L1 gives bis-ligand complexes $[Ag(L1)_2]X$ ($X=ClO_4^-$, BF_4^- and $CF_3SO_3^-$) while that of $AgNO_3$ with L1 affords the complex $[Ag(L1)NO_3]$. The striking difference can be explained by the coordinating ability of the anion. In the presence of non-coordinating anions such as ClO_4^-, $CF_3SO_3^-$ and BF_4^-, two macrocycles coordinate to Ag(I) presumably in a similar way to those in $[Cu(L1)_2]^+$ (Figure 3-1) to give a tetrahedral geometry similar to that in $[Ag(L)_2]^+$ ($L=[HOOC(CH_2)_nSCH_2]_2$, n=1-3) (2, 10) which have two carboxylic acid moieties uncoordinated. In the presence of the coordinating anion NO_3^-, one of the L1's is replaced by bidentate NO_3^- to give

[Ag(L1)NO_3]. Other examples of bidentate NO_3^- are known (12-13). Therefore, the geometry of [Ag(L1)NO_3] is probably distorted tetrahedral with L1 and NO_3^- both acting as bidentate ligands.

5.3.2. Ir Spectra

Infrared spectra of perchlorate salts (nujol mull) show characteristic absorption bands of uncoordinated ClO_4^- at 1080 cm^{-1} and 619 cm^{-1}. The spectra of the corresponding tetrafluoroborate and triflate salts are similar to those of perchlorate salts except that bands at 1080 (vs) and 619 (vs) cm^{-1} have been replaced by bands at 1040 (s) and 521 (w) cm^{-1} due to uncoordinated BF_4^- and at 1250 (s, br), 1036 (sh), 1025 (m), 830 (m), 750 (m), 720 (m), 635 (s), 570 (m) and 515 (m) cm^{-1} due to $CF_3SO_3^-$. The ir spectrum of [Ag(L1)NO_3] is different. The splitting of the 1340 cm^{-1} free nitrate ion band and appearance of new bands (which are absent from the spectrum of the organic ligand) at 1420, 1320 and 1030 cm^{-1} suggest a coordinated NO_3^- (14).

Table 5-1: Analytical and physical properties of silver(I) complexes of thiophenophane ligands.

Complex	C(%)*	H(%)	M(%)	M.P. (°C)
$[Ag(L1)_2]ClO_4$	33.45(32.78)	3.91(3.86)	14.7(14.7)	160-163d**
$[Ag(L1)_2]BF_4$	33.48(33.35)	3.93(3.93)	---	155-160d
$[Ag(L1)_2]CF_3SO_3$	32.44(32.24)	3.59(3.61)	13.4(13.8)	174-176d
$[Ag(L1)]NO_3$	27.82(27.76)	3.25(3.27)	22.4(22.4)	167-170d
$[Ag_2(L2)_2](ClO_4)_2$	27.31(27.18)	3.42(3.42)	21.0(20.4)	175-178d
$[Ag_2(L2)_2](BF_4)_2$	27.88(27.79)	3.50(3.50)	21.3(20.8)	142-145d
$[Ag_2(L2)_2](CF_3SO_3)_2$	27.34(26.93)	3.21(3.13)	19.5(18.6)	177-182d
$[Ag_2(L3)_2](ClO_4)_2$	29.17(28.69)	3.80(3.71)	---	170-173d
$[Ag_2(L3)_2](CF_3SO_3)_2$	28.51(28.31)	3.41(3.40)	18.1(18.2)	172-175d
$[Ag_2(L4)_2](CF_3SO_3)_2$	30.99(30.90)	3.89(3.89)	17.4(17.3)	185-188d
$[Ag(L5)]CF_3SO_3$	26.59(26.23)	2.86(2.80)	20.8(21.4)	166-168d
$[Ag(L7)]ClO_4$	31.54(31.38)	3.39(3.29)	18.70(17.60)	176-180d
$[Ag(L8)]ClO_4$	34.13(33.76)	3.87(3.78)	---	150-153d

* Found (calculated)

** decomposition

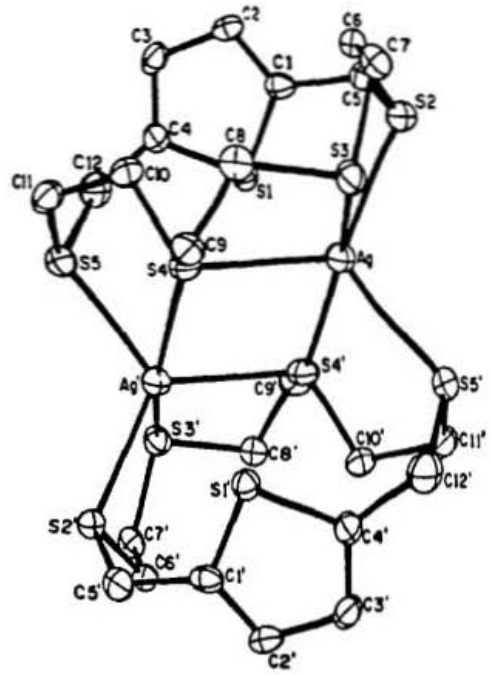

Ag-S(2)	2.567(2)	S(2)-Ag-S(3)	81.15(5)
Ag-S(3)	2.750(3)	S(2)-Ag-S(4)	121.69(5)
Ag-S(4)	2.600(2)	S(2)-Ag-S(4)'	115.79(6)
Ag-S(4)'	2.995(2)	S(2)-Ag-S(5)'	113.47(6)
Ag-S(5)'	2.564(2)	S(3)-Ag-S(4)	82.31(6)
		S(3)-Ag-S(4)'	162.94(5)
		S(3)-Ag-S(5)'	99.37(5)
		S(4)-Ag-S(4)'	86.55(5)
		S(4)-Ag-S(5)'	124.27(6)
		S(4)'-Ag-S(5)'	76.35(5)
		Ag-S(4)'-Ag'	93.45(5)

Figure 5-1. ORTEP drawing of $[Ag_2(L2)_2]^{2+}$ cation and selected bond lengths (Å) and angles (degrees). The primed and unprimed atoms are related by a symmetry center..

5.3.3. Description of the Structure of $[Ag_2(L2)_2]^{2+}$

As noted before, L2 has an open cavity in the macrocycle's center and the S-S distances of 5-7 Å across the cavity (Figure 2-2) seem to suggest that it is suitable to accept one or more metal atoms. In addition, the rigidity of the thiophene subunit and its two attached methylenes keeps S2 and S5 well separated (6.92 Å) and projecting away from the plane of the thiophene ring. These two sulfurs are thus placed appropriately to coordinate to two different metal atoms except that their lone pairs are directed towards opposite sides of the macrocycle in the solid state conformation. The solid state conformation of L2, also, involves the familiar exocyclic arrangement of lone pairs (15). In L2, this need not necessarily preclude complex formation since orientation of the lone pairs with respect to each other is such that a metal atom could perch above the cavity by bonding to only some of the sulfur atoms. Approach to L2's cavity in its solid state conformation is however largely blocked by H atoms of the methylene groups. Clearly, this molecule has considerable latent potential as a ligand but will only form complexes in which it is binucleating or polydentate if conformational change first occurs in its flexible thioether chain. In this respect L2 is similar to L1 and L3.

The ORTEP drawing of $[Ag_2(L2)_2]^{2+}$ is given in Figure 5-1. The unit cell contains two centrosymmetric molecules of $[Ag_2(L2)_2]^{2+}$. Inspection of the structure of $[Ag_2(L2)_2]^{2+}$ reveals that the dinucleating capability of the ligand has been utilized with S2 and S5 of the ligand coordinating in the equatorial positions of two separate silver atoms. Pairs of thioether sulfurs separated by two methylene groups are known (16) to have a tendency to form five-membered chelate rings with S-M-S bond angles close to 90°. Therefore, bearing in mind the total number of donors available the

remainder of the available sulfur sites are poised for formation of trigonal-bipyramidal coordination about each silver atom. Conformational rearrangement in the thioether chain has occurred from C5 to C9 inclusive so that the lone pairs on the thioether sulfurs are oriented into the cavity towards the silver atoms. The dipositive complex cation (Figure 5-1) which is centrosymmetric consists of two silver atoms 4.082(3) Å apart (compared to 2.88 Å in metallic silver) and each is surrounded by a slightly distorted trigonal bipyramidal array of thioether sulfurs from two molecules of ligand. Neither ligand's thiophene sulfur is bonded to silver. The Ag-S (thiophene) distances are 3.7069(8) Å to the nearer thiophene sulfur and 3.9384(7) Å to the more distant one which may be compared to 3.50 Å which is the sum of the van der Waals' radii (17). Sulfurs S2 and S5 which hang below their thiophene's plane, bond to equatorial sites of separate silver atoms and one sulfur in each ligand (S4) bridges the two metals assuming an axial position with respect to one and an equatorial with respect to the other. The remaining two sites of a particular silver (an axial and an equatorial) are filled by adjacent sulfurs (S2 and S3) of one ligand so that a five-membered chelate ring with an average S-Ag-S angle of 81.15(6)° is formed. The coordination sphere of each silver is distorted somewhat from idealized trigonal bipyramidal geometry. This is revealed most obviously by the S3-Ag-S4' angle between axial positions which is 162.94(5)° instead of 180°. As a result, one equatorial-to-axial angle (S2-Ag-S4') is also larger (115.79(6)°) than expected (90°). Each silver lies 0.62 Å out of the plane defined by three equatorial S-donors and is part of three five-membered chelate rings with angles of 81.15(6), 82.31(5) and 76.35(5)°. These represent half the axial-to-equatorial angles about each silver. The other half involves a further three inter-ligand S-Ag-S angles, one of which (S4-Ag-S4' = 86.55(5)°) is part of the Ag_2S_2 bridging system and two of which (S5'-Ag-S3 = 99.37(6); S2-Ag-S4' = 115.79(6)°) are not part of a

ring and so are relatively free to open as required to relieve any stereochemical strain.

The Ag-S lengths with an average of 2.695 Å and a range of 2.564-2.995 Å are comparable to those in other silver thioether complexes (5, 10). They show the usual slight (~11%) lengthening of average axial over average equatorial distances but the axial Ag-S4′ length is significantly longer (0.245 Å) than the other axial bond length (Ag-S3), presumably because S4′ is bridging whereas S3 is terminal and also because it reduces interaction of a hydrogen on C9 with S1′ of the other ligand. Upon coordination, L2 becomes so rigid that any further rotation of the C-C and C-S bonds has to overcome a very high energy barrier.

From models, it can be seen that silver(I) complexes of L3 and L4 may have similar dinuclear structures to that of $[Ag_2(L2)_2]^{2+}$. This is consistent with their similar chemical properties.

Characterizing the cation $[Ag_2(L2)_2]^{2+}$ by methods other than X-ray diffraction is difficult since most conventional spectroscopic techniques give no indication of its dinuclear nature. Fast atom bombardment mass spectroscopy has been applied to non-volatile thermally fragile organometallics (18) and we had hoped to apply it successfully to detect $[Ag_2(L2)_2]^{2+}$. The spectrum finally obtained, however, consisted of two peaks of equal intensity with m/e=429 and 431 corresponding to ions containing ^{107}Ag (51.8% rel. abundance) and ^{109}Ag (48.2% rel. abundance), respectively. The values of m/e and the relative peak intensities are consistent with $[Ag(L2)]^+$ from cleavage of the dinuclear cation into two monomer fragments. It is of interest to note that no spectrum was obtained when the matrix was glycerol and only when p-toluenesulfonic acid was added to the matrix was a spectrum of the complex silver cation detected. It seems reasonable to speculate therefore, that the role of the acid is

to add a proton to the anion of the silver salt thereby freeing the complex cation so that it may be accelerated from the source into the mass-analyzing sections of the spectrometer.

Although the dimer cleaves in the mass spectrometer it is surprisingly robust under normal conditions. For example, unlike polynitrogen ligand complexes (19-20) it does not disproportionate under any conditions. Both crystalline samples and solutions in benzonitrile of the perchlorate salt can be subjected to uv radiation from a 100 W Hanovia lamp for 24 hours with no sign of darkening. Stirred aqueous suspensions of the perchlorate salt containing thiosulfate, ammonia or concentrated hydrochloric acid show no reaction after several hours and even a heated solution in benzonitrile of the perchlorate salt and p-thiocresol shows only limited reaction after 24 hours. In contrast, solutions of the ion seem highly reactive in the presence of a base such as pyridine. For example, when pyridine is added to the unreactive solution of p-thiocresol and $[Ag_2(L2)_2](ClO_4)_2$, a yellow precipitate of $[AgSC_6H_4CH_3]_n$ is formed rapidly in 93% yield. This insoluble mercaptide was identified by elemental analysis and by its ir spectrum which is devoid of any bands attributable to L2 but contains bands typical of p-thiocresol.

It has been observed that coordinated thioethers generally stabilize low oxidation states (2). Exceptions (5) have been attributed to special geometric considerations or, in complexes having large coordination numbers, to high electron density on the metal which should make oxidation easy. Following this reasoning, we attempted unsuccessfully to oxidize the perchlorate salt by both chemical and electrochemical means. Oxidation by concentrated sulfuric acid leads to decomposition of the complex and formation of a precipitate of silver sulfate. No silver(II) species were detected in suspensions of the silver triflate in 70% $HClO_4$. Use of ceric ammonium nitrate in methanol

caused precipitation of a solid which appears to be the less soluble nitrate salt of $[Ag_2(L2)_2]^{2+}$ while electrochemical oxidation of an acetonitrile solution using a saturated calomel reference electrode gave a precipitate of silver chloride. This result stands in contrast to the inertness to chloride mentioned previously and may be a consequence of the special steric requirements of the ligand. For example, silver(II) with 9 d-electrons is usually found in square planar or distorted octahedral environments. Either of these geometries would be difficult to attain from the distorted trigonal bipyramidal structure of $[Ag_2(L2)_2]^{2+}$ due to the rigidity of the coordinated thiophenophane ligand. Thus, attempted oxidation could lead to destruction of the dinuclear complex and release of one or more silver(I) ions that would precipitate as AgCl. On the other hand, the silver atoms are wrapped by two hydrophobic ligand molecules and strongly bonded by thioether sulfurs. Therefore, it is very hard for other donors to approach the metal center and to replace the macrocycle. In this regard, it is not surprising that the dinuclear complex is extremely stable under normal chemical conditions. Furthermore, it appears that the special geometric requirements of L2 stabilize Ag(I). Thus, unlike cyclam (19-20), which promotes disproportionation to Ag(0) and Ag(II) or [9]aneS3 (5), which provides a coordination sphere compatible with both Ag(I) and Ag(II) leading to reversible oxidation at low electrochemical potential for its Ag(I) complex, the ligand L2 provides a coordination geometry particularly favorable to Ag(I) thereby stabilizing that oxidation state.

5.4. Conclusions

In conclusion, the π-acidity of thioether sulfur donors in thiophenophane ligands stabilizes Ag(I). In contrast to simple macrocyclic thioether ligands such as [9]aneS3 (5) and [18]aneS6 (6), the failure of thiophenophane L2 to stabilize Ag(II) is caused by

its special geometric requirements that stabilize Ag(I). The chemical and photochemical stability of this and other thiophenophane silver(I) complexes arises from the strong bonding of thioether donors to Ag(I) and from the high rigidity of the coordinated thiophenophane ligand(s).

5.5. References

1. F.A. Cotton and G. Wilkinson. *Advanced inorganic chemistry*. 4th Ed. Wiley, Toronto. 1980. p 970.
2. S.G. Murray and F.R. Hartley. Chem. Rev. *81*, 365 (1981).
3. R. Heber and E. Hoyer. J. Prakt. Chem. *318*, 19 (1976).
4. K. Aurivillius, A. Cassel and L. Faith. Chem. Scr. *5*, 9 (1974).
5. J. Clarkson, R. Yagbasan, P.J. Blower, S.C. Rawle and S.R. Cooper. J. Chem. Soc., Chem. Commun. 950 (1987).
6. A.J. Blake, R.O. Gould, A.J. Holder, T.I. Hyde and M. Schröder. Polyhedron. *8*, 513 (1989).
7. P.J. Blower, J.A. Clarkson, S.C. Rawle, J.R. Hartman, R.E. Wolf, R. Yagbasan, S.G. Bott and S.R. Cooper. Inorg. Chem. *28*, 4040 (1989).
8. S.M. Nelson, S.G. McFall, M.G.B. Drew and A.H.B. Othman. J. chem. Soc., Chem. Commun. 370 (1977).
9. S.M. Nelson, S.G. McFall, M.G.B. Drew, A.H.B. Othman and N.B. Mason. J. Chem. Soc., Chem. Commun. 167 (1977).
10. H.W. Roesky, H. Hofmann, P.G. Jones, W. Pinkert and G.M. Sheldrick. J. Chem. Soc., Dalton Trans. 1215 (1983).

11. A.C. Bellart. Z. Anorg. Allg. Chem. *412*, 155 (1975).

12. C.S.W. Harker and E.R.T. Tiekink. Acta Cryst. *C45*, 1815 (1989).

13. P.F. Barron, J.C. Dyason, P.C. Healy, L.M. Engelhardt, B.W. Skelton and A.H. White. J. Chem. Soc., Dalton Trans. 1965 (1986).

14. K. Burger. *Coordination chemistry: Experimental methods*. Edited by I.T. Milar and D.W. Allen. CRC Press, Ohio. 1973. p 90.

15. R.E. Wolf, J.R. Hartman, J.M.E. Storey, B.M. Foxman and S.R. Cooper. J. Am. Chem. Soc. *109*, 4328 (1987).

16. P.W.R. Corfield, C. Ceccarelli, M.D. Glick, I.W.Y. Moy, L.A. Ochrymowycz and D.B. Rorabacher. J. Am. Chem. Soc. *107*, 2399 (1985).

17. A.Bondi. J. Phys. Chem. *68*, 441 (1964).

18. B. Gregory, C.R. Jablonski and Y.P. Wang. J. Organomet. Chem. *269*, 74 (1984).

19. T. Ito, H. Ito and K. Toriumi. Chem. Lett. 1101 (1981).

20. K.B. Mertes. Inorg. Chem. *17*, 49 (1978).

APPENDIX. CRYSTAL DATA

Table 1: Crystal data for L1 ($C_{10}H_{14}S_4$)

Parameter	Value
Empirical formula	$C_{10}H_{14}S_4$
Formula weight	263.27
Crystal dimensions, mm	0.3 x 0.3 x 0.5
Space group	Monoclinic $P2_1/a$
a, Å	7.9347(2)[a]
b, Å	18.7479(3)
c, Å	8.8596(2)
β, deg	108.446(2)
Z (molecules/cell)	4
$F(000)$ electrons	608.28
Volume, Å^3	1254.50
d_{calc}, g/cm^3	1.394
Linear absolute coefficient, mm^{-1}	0.70
Radiation (MoKα_1), Å	λ = 0.70930
2Θ(max), deg	49
No. reflections measured	2182
No. of unique reflections	2174
No. unique reflections, $I_{net} > 3.0\sigma(I_{net})$	1337
Last least-square cycle calculated with	28 atoms
	184 parameters
	1337 reflections
R_f (sig. refl.)	0.048[b]
R_w (sig. refl.)	0.034[c]
Goodness of fit (last cycle)	2.407[d]
R_f (all refl.)	0.080[b]
R_w (all refl.)	0.036[c]
Maxinum shift/σ	0.002
Last D-map:	
deepest hole, e/Å^3	-0.260
highest peak, e/Å^3	0.310
Secondary extinction coefficient	0.581149
σ	0.051029

[a] Throughout this work, esd's are in parentheses and refer to the last digit printed.

[b] $R_f = \Sigma\,||F_o| - |F_c||/\Sigma\,|F_o|$.

[c] $R_w = [\Sigma w(|F_o| - |F_c|)^2/\Sigma(w|F_o|)^2]^{1/2}$ where $w = 1/\sigma^2 I$.

[d] Goodness of fit = $[\Sigma w(|F_o| - |F_c|)^2/(\text{number of reflections - number of parameters.})]^{1/2}$.

Table 2: Crystal data for L2 ($C_{12}H_{18}S_5$)

Parameter	Value
Empirical formula	$C_{12}H_{18}S_5$
Formula weight	322.40
Crystal dimensions, mm	0.12 x 0.17 x 0.31
Space group	Monoclinic $P2_1/n$
a, Å	10.8866(2)[a]
b, Å	9.4419(4)
c, Å	14.9608(2)
β, deg	97.132(1)
Z (molecules/cell)	4
$F(000)$ electrons	680.27
Volume, Å^3	1525.71
d_{calc}, g/cm^3	1.404
Linear absolute coefficient, mm^{-1}	6.73
Radiation (CuKα_1), Å	λ = 1.54056
2Θ(max), deg	139
No. reflections measured	2950
No. of unique reflections	2871
No. unique reflections, $I_{net} > 3.0\sigma(I_{net})$	2278
Last least-square cycle calculated with	35 atoms
	227 parameters
	2278 reflections
R_f (sig. refl.)	0.057[b]
R_w (sig. refl.)	0.045[c]
Goodness of fit (last cycle)	4.349[d]
R_f (all refl.)	0.069[b]
R_w (all refl.)	0.046[c]
Maxinum shift/σ	0.063
Last D-map:	
deepest hole, e/Å^3	-0.470
highest peak, e/Å^3	0.560
Secondary extinction coefficient	7.21

[a] Throughout this work, esd's are in parentheses and refer to the last digit printed.

[b] $R_f = \Sigma ||F_o| - |F_c|| / \Sigma |F_o|$.

[c] $R_w = [\Sigma w(|F_o| - |F_c|)^2 / \Sigma (w|F_o|)^2]^{1/2}$ where $w = 1/\sigma^2 I$.

[d] Goodness of fit = $[\Sigma w(|F_o| - |F_c|)^2 / (\text{number of reflections - number of parameters.})]^{1/2}$.

Table 3: Crystal data for L3 ($C_{12}H_{18}S_5$)

Parameter	Value
Empirical formula	$C_{13}H_{20}S_5$
Formula weight	336.60
Crystal dimensions, mm	0.13 x 0.30 x 0.35
Space group	Monoclinic $P2_1/a$
a, Å	14.658(1)[a]
b, Å	5.9800(3)
c, Å	19.772(2)
β, deg	111.00(1)
Z (molecules/cell)	4
$F(000)$ electrons	712.27
Volume, Å^3	1618.55
d_{calc}, g/cm^3	1.381
Linear absolute coefficient, mm^{-1}	6.36
Radiation (CuKα_1), Å	λ = 1.54056
2Θ(max), deg	151.9
No. reflections measured	3816
No. of unique reflections	3381
No. unique reflections, $I_{net} > 3.0\sigma(I_{net})$	2845
Last least-square cycle calculated with	38 atoms
	244 parameters
	2845 reflections
R_f (sig. refl.)	0.050[b]
R_w (sig. refl.)	0.046[c]
Goodness of fit (last cycle)	5.788[d]
R_f (all refl.)	0.057[b]
R_w (all refl.)	0.046[c]
Maxinum shift/σ	0.269
Last D-map:	
deepest hole, e/Å^3	-0.500
highest peak, e/Å^3	0.430
Secondary extinction coefficient	10.2(5)

[a] Throughout this work, esd's are in parentheses and refer to the last digit printed.

[b] $R_f = \Sigma \, | \, |F_o| - |F_c| \, | / \Sigma \, |F_o|$.

[c] $R_w = [\Sigma w(|F_o| - |F_c|)^2 / \Sigma (w|F_o|)^2]^{1/2}$ where $w = 1/\sigma^2 I$.

[d] Goodness of fit = $[\Sigma w(|F_o| - |F_c|)^2 / (\text{number of reflections - number of parameters.})]^{1/2}$.

Table 4: Crystal data for $[Cu(L1)_2]ClO_4$

Parameter	Value
Empirical formula	$C_{20}H_{28}ClCuO_4S_8$
Formula weight	687.44
Crystal dimensions, mm	0.20 x 0.20 x 0.30
Space group	Monoclinic $P2_1/c$
a, Å	9.4363(1)[a]
b, Å	18.2768(3)
c, Å	19.2157(3)
β, deg	96.520(2)
Z (molecules/cell)	4
$F(000)$ electrons	1059.89
Volume, Å^3	2777.95
d_{calc}, g/cm^3	1.644
Linear absolute coefficient, mm^{-1}	1.29
Radiation (MoKα_1), Å	λ = 0.70930
2Θ(max), deg	44.9
No. reflections measured	4151
No. of unique reflections	3589
No. unique reflections, $I_{net} > 2.5\sigma(I_{net})$	2539
Last least-square cycle calculated with	65 atoms
	411 parameters
	2539 reflections
R_f (sig. refl.)	0.056[b]
R_w (sig. refl.)	0.037[c]
Goodness of fit (last cycle)	2.977[d]
R_f (all refl.)	0.081[b]
R_w (all refl.)	0.039[c]
Maxinum shift/σ	0.394
Last D-map:	
deepest hole, e/Å^3	-0.990
highest peak, e/Å^3	0.970
Secondary extinction coefficient	0.581149
σ	0.051029

[a] Throughout this work, esd's are in parentheses and refer to the last digit printed.

[b] $R_f = \Sigma \, ||F_o| - |F_c|| / \Sigma \, |F_o|$.

[c] $R_w = [\Sigma w(|F_o| - |F_c|)^2 / \Sigma (w|F_o|)^2]^{1/2}$ where $w = 1/\sigma^2 I$.

[d] Goodness of fit = $[\Sigma w(|F_o| - |F_c|)^2 / (\text{number of reflections - number of parameters.})]^{1/2}$.

Table 5: Crystal data for $[CuCl_2 \cdot L1]_2$

Parameter	Value
Empirical formula	$C_{20}H_{28}Cl_4Cu_2S_8$
Formula weight	793.82
Crystal dimensions, mm	0.15 x 0.20 x 0.20
Space group	Orthorhombic *Pbca*
a, Å	15.383(6)[a]
b, Å	11.409(3)
c, Å	17.423(4)
Z (molecules/cell)	4
F(000) electrons	1607.82
Volume, $Å^3$	3057.82
d_{calc}, g/cm^3	1.724
Linear absolute coefficient, mm^{-1}	2.29
Radiation ($MoK\alpha_1$), Å	λ = 0.70930
2Θ(max), deg	50.0
No. reflections measured	5461
No. of unique reflections	2713
No. unique reflections, $I_{net} > 2.5\sigma(I_{net})$	1322
Last least-square cycle calculated with	31 atoms
	191 parameters
	1322 reflections
R_f (sig. refl.)	0.057[b]
R_w (sig. refl.)	0.036[c]
Goodness of fit (last cycle)	2.520[d]
R_f (all refl.)	0.147[b]
R_w (all refl.)	0.039[c]
Maxinum shift/σ	0.469
Last D-map:	
deepest hole, $e/Å^3$	-0.880
highest peak, $e/Å^3$	0.910
Secondary extinction coefficient	0.05(2)

[a] Throughout this work, esd's are in parentheses and refer to the last digit printed.

[b] $R_f = \Sigma \, ||F_o| - |F_c|| / \Sigma \, |F_o|$.

[c] $R_w = [\Sigma w(|F_o| - |F_c|)^2 / \Sigma (w|F_o|)^2]^{1/2}$ where $w = 1/\sigma^2 I$.

[d] Goodness of fit = $[\Sigma w(|F_o| - |F_c|)^2 / (\text{number of reflections - number of parameters.})]^{1/2}$.

Table 6: Crystal data for $[CuCl_2 \cdot L3]_2$

Parameter	Value
Empirical formula	$C_{26}H_{40}Cl_4Cu_2S_{10}$
Formula weight	942.11
Crystal dimensions, mm	0.14 x 0.12 x 0.02
Space group	Monoclinic A_2/a
a, Å	12.616(1)[a]
b, Å	10.0542(6)
c, Å	29.180(2)
β, deg	95.81(1)
Z (molecules/cell)	4
$F(000)$ electrons	1927.80
Volume, Å^3	3682.38
d_{calc}, g/cm^3	1.699
Linear absolute coefficient, mm^{-1}	2.02
Radiation (MoKα_1), Å	λ = 0.70930
2Θ(max), deg	45.0
No. reflections measured	2797
No. of unique reflections	2433
No. unique reflections, $I_{net} > 3.0\sigma(I_{net})$	1073
Last least-square cycle calculated with	41 atoms
	191 parameters
	1073 reflections
R_f (sig. refl.)	0.055[b]
R_w (sig. refl.)	0.038[c]
Goodness of fit (last cycle)	1.374[d]
R_f (all refl.)	0.145[b]
R_w (all refl.)	0.055[c]
Maxinum shift/σ	0.002
Last D-map:	
deepest hole, e/Å^3	-0.530
highest peak, e/Å^3	0.590
Secondary extinction coefficient	0.14(2)

[a] Throughout this work, esd's are in parentheses and refer to the last digit printed.

[b] $R_f = \Sigma \, ||F_o| - |F_c|| / \Sigma \, |F_o|$.

[c] $R_w = [\Sigma w(|F_o| - |F_c|)^2 / \Sigma (w|F_o|)^2]^{1/2}$ where $w = 1/\sigma^2 I$.

[d] Goodness of fit = $[\Sigma w(|F_o| - |F_c|)^2 / (\text{number of reflections - number of parameters.})]^{1/2}$.

Table 7: Crystal data for $[Cu_2Cl_3(L5)_2]_n$

Parameter	Value
Empirical formula	$C_{20}H_{28}Cl_3Cu_2O_2S_6$
Formula weight	726.01
Crystal dimensions, *mm*	0.05 x 0.08 x 0.15
Space group	Orthorhombic *Pbnm*
a, Å	10.4108(20)[a]
b, Å	14.5204(24)
c, Å	20.348(5)
Z (molecules/cell)	8
F(000) electrons	2951.63
Volume, $Å^3$	3075.99
d_{calc}, g/cm^3	1.585
Linear absolute coefficient, mm^{-1}	4.12
Radiation (MoKα_1), Å	λ = 0.70930
2Θ(max), deg	44.9
No. reflections measured	5031
No. of unique reflections	2053
No. unique reflections, $I_{net} > 2.5\sigma(I_{net})$	874
Last least-square cycle calculated with	38 atoms
	118 parameters
	874 reflections
R_f (sig. refl.)	0.065[b]
R_w (sig. refl.)	0.075[c]
Goodness of fit (last cycle)	0.285[d]
R_f (all refl.)	0.185[b]
R_w (all refl.)	0.184[c]
Maxinum shift/σ	0.273
Last D-map:	
deepest hole, $e/Å^3$	-0.650
highest peak, $e/Å^3$	0.650

[a] Throughout this work, esd's are in parentheses and refer to the last digit printed.

[b] $R_f = \Sigma \, ||F_o| - |F_c|| / \Sigma |F_o|$.

[c] $R_w = [\Sigma w(|F_o| - |F_c|)^2 / \Sigma (w|F_o|)^2]^{1/2}$ where $w = 1/\sigma^2 I$.

[d] Goodness of fit = $[\Sigma w(|F_o| - |F_c|)^2 / (\text{number of reflections - number of parameters.})]^{1/2}$.

Table 8: Crystal data for $[(CuCl)_2 \cdot L2]_n$

Parameter	Value
Empirical formula	$C_{12}H_{18}Cl_2Cu_2S_5$
Formula weight	520.39
Crystal dimensions, mm	0.15 x 0.35 x 0.35
Space group	Monoclinic $P2_1/a$
a, Å	7.9687(4)[a]
b, Å	19.2312(9)
c, Å	12.0060(6)
β, deg	97.185(4)
Z (molecules/cell)	4
$F(000)$ electrons	1047.85
Volume, Å^3	1825.44
d_{calc}, g/cm^3	1.894
Linear absolute coefficient, mm^{-1}	3.17
Radiation (MoKα_1), Å	λ = 0.70930
2Θ(max), deg	44.9
No. reflections measured	2391
No. of unique reflections	2388
No. unique reflections, $I_{net} > 2.5\sigma(I_{net})$	1975
Last least-square cycle calculated with	39 atoms
	262 parameters
	1975 reflections
R_f (sig. refl.)	0.042[b]
R_w (sig. refl.)	0.049[c]
Goodness of fit (last cycle)	0.873[d]
R_f (all refl.)	0.049[b]
R_w (all refl.)	0.055[c]
Maxinum shift/σ	0.016
Last D-map:	
deepest hole, e/Å^3	-0.590
highest peak, e/Å^3	1.190

[a] Throughout this work, esd's are in parentheses and refer to the last digit printed.

[b] $R_f = \Sigma \, ||F_o| - |F_c|| / \Sigma \, |F_o|$.

[c] $R_w = [\Sigma w(|F_o| - |F_c|)^2 / \Sigma (w|F_o|)^2]^{1/2}$ where $w = 1/\sigma^2 I$.

[d] Goodness of fit = $[\Sigma w(|F_o| - |F_c|)^2 / (\text{number of reflections - number of parameters.})]^{1/2}$.

Table 9: Crystal data for $[(CuBr)_2 \cdot L7]_n$

Parameter	Value
Empirical formula	$C_{16}H_{20}Br_2Cu_2S_6$
Formula weight	671.43
Crystal dimensions, mm	0.07 x 0.07 x 0.15
Space group	Orthorhombic *Pcma*
a, Å	8.1720(6)[a]
b, Å	10.7791(5)
c, Å	12.0929(5)
Z (molecules/cell)	2
F(000) electrons	659.89
Volume, $Å^3$	1135.61
d_{calc}, g/cm^3	1.964
Linear absolute coefficient, mm^{-1}	5.90
Radiation ($MoK\alpha_1$), Å	λ = 0.70930
2Θ(max), deg	44.9
No. reflections measured	1011
No. of unique reflections	799
No. unique reflections, $I_{net} > 2.5\sigma(I_{net})$	521
Last least-square cycle calculated with	8 atoms
	64 parameters
	521 reflections
R_f (sig. refl.)	0.045[b]
R_w (sig. refl.)	0.052[c]
Goodness of fit (last cycle)	0.293[d]
R_f (all refl.)	0.084[b]
R_w (all refl.)	0.090[c]
Maxinum shift/σ	0.013
Last D-map:	
deepest hole, $e/Å^3$	-0.710
highest peak, $e/Å^3$	0.740

[a] Throughout this work, esd's are in parentheses and refer to the last digit printed.

[b] $R_f = \Sigma \, ||F_o| - |F_c|| / \Sigma \, |F_o|$.

[c] $R_w = [\Sigma w(|F_o| - |F_c|)^2 / \Sigma(w|F_o|)^2]^{1/2}$ where $w = 1/\sigma^2 I$.

[d] Goodness of fit = $[\Sigma w(|F_o| - |F_c|)^2 / (\text{number of reflections - number of parameters.})]^{1/2}$.

Table 10: Crystal data for $[CuCl_2 \cdot L9]_n$

Parameter	Value
Empirical formula	$C_{10}H_{14}Cl_2CuO_2S_3$
Formula weight	396.85
Crystal dimensions, mm	0.10 x 0.10 x 0.30
Space group	Orthorhombic $P2_12_12_1$
a, Å	6.8096(4)[a]
b, Å	9.4542(5)
c, Å	22.899(2)
Z (molecules/cell)	4
$F(000)$ electrons	803.91
Volume, Å^3	1474.23
d_{calc}, g/cm^3	1.788
Linear absolute coefficient, mm^{-1}	2.25
Radiation (MoKα_1), Å	λ = 0.70930
2Θ(max), deg	45.0
No. reflections measured	2017
No. of unique reflections	1703
No. unique reflections, $I_{net} > 2.5\sigma(I_{net})$	1433
Last least-square cycle calculated with	32 atoms
	165 parameters
	926 reflections
R_f (sig. refl.)	0.031[b]
R_w (sig. refl.)	0.034[c]
Goodness of fit (last cycle)	0.228[d]
R_f (all refl.)	0.031[b]
R_w (all refl.)	0.034[c]
Maxinum shift/σ	0.055
Last D-map:	
deepest hole, e/Å^3	-0.370
highest peak, e/Å^3	0.430
Secondary extinction coefficient	0.054089
σ	0.027799

[a] Throughout this work, esd's are in parentheses and refer to the last digit printed.

[b] $R_f = \Sigma \, ||F_o| - |F_c|| / \Sigma \, |F_o|$.

[c] $R_w = [\Sigma w(|F_o| - |F_c|)^2 / \Sigma (w|F_o|)^2]^{1/2}$ where $w = 1/\sigma^2 I$.

[d] Goodness of fit = $[\Sigma w(|F_o| - |F_c|)^2 / (\text{number of reflections - number of parameters.})]^{1/2}$.

Table 11: Crystal data for [$PdBr_2$·L1]

Parameter	Value
Empirical formula	$C_{10}H_{14}Br_2PdS_4$
Formula weight	528.68
Crystal dimensions, mm	0.10 x 0.10 x 0.20
Space group	Monoclinic $P2_1/n$
a, Å	8.3569(3)[a]
b, Å	16.3254(15)
c, Å	11.1462(3)
β, deg	92.833(4)
Z (molecules/cell)	4
F(000) electrons	1031.91
Volume, Å^3	1518.81
d_{calc}, g/cm^3	2.312
Linear absolute coefficient, mm^{-1}	6.93
Radiation (MoKα_1), Å	λ = 0.70930
2Θ(max), deg	49.9
No. reflections measured	4158
No. of unique reflections	2652
No. unique reflections, $I_{net} > 2.5\sigma(I_{net})$	1446
Last least-square cycle calculated with	17 atoms
	105 parameters
	1446 reflections
R_f (sig. refl.)	0.060[b]
R_w (sig. refl.)	0.058[c]
Goodness of fit (last cycle)	1.780[d]
R_f (all refl.)	0.120[b]
R_w (all refl.)	0.066[c]
Maxinum shift/σ	1.026
Last D-map:	
deepest hole, e/Å^3	-1.330
highest peak, e/Å^3	1.350
Secondary extinction coefficient	0.69(7)

[a] Throughout this work, esd's are in parentheses and refer to the last digit printed.

[b] $R_f = \Sigma \, ||F_o| - |F_c|| / \Sigma \, |F_o|$.

[c] $R_w = [\Sigma w(|F_o| - |F_c|)^2 / \Sigma (w|F_o|)^2]^{1/2}$ where $w = 1/\sigma^2 I$.

[d] Goodness of fit = $[\Sigma w(|F_o| - |F_c|)^2 / (\text{number of reflections - number of parameters.})]^{1/2}$.

Table 12: Crystal data for $[Pd(\eta^3\text{-}C_3H_5)\cdot L1][CF_3SO_3]$

Parameter	Value
Empirical formula	$C_{14}H_{19}F_3O_3PdS_5$
Formula weight	559.02
Crystal dimensions, mm	0.20 x 0.20 x 0.20
Space group	Orthorhombic $P2_12_12_1$
a, Å	8.7067(4)[a]
b, Å	9.1259(3)
c, Å	22.5540(10)
Z (molecules/cell)	4
F(000) electrons	1119.94
Volume, Å^3	1792.06
d_{calc}, g/cm^3	2.072
Linear absolute coefficient, mm^{-1}	1.62
Radiation (MoKα_1), Å	λ = 0.70930
2Θ(max), deg	50.0
No. reflections measured	1960
No. of unique reflections	1815
No. unique reflections, $I_{net} > 2.5\sigma(I_{net})$	1341
Last least-square cycle calculated with	45 atoms
	236 parameters
	1341 reflections
R_f (sig. refl.)	0.048[b]
R_w (sig. refl.)	0.050[c]
Goodness of fit (last cycle)	0.502[d]
R_f (all refl.)	0.048[b]
R_w (all refl.)	0.050[c]
Maxinum shift/σ	3.363
Last D-map:	
deepest hole, e/Å^3	-0.890
highest peak, e/Å^3	0.490
Secondary extinction coefficient	-0.13(2)

[a] Throughout this work, esd's are in parentheses and refer to the last digit printed.

[b] $R_f = \Sigma\,||F_o| - |F_c||/\Sigma\,|F_o|$.

[c] $R_w = [\Sigma w(|F_o| - |F_c|)^2/\Sigma(w|F_o|)^2]^{1/2}$ where $w = 1/\sigma^2 I$.

[d] Goodness of fit = $[\Sigma w(|F_o| - |F_c|)^2/(\text{number of reflections - number of parameters.})]^{1/2}$.

Table 13: Crystal data for $[Ag_2(L2)_2][ClO_4)_2$

Parameter	Value
Empirical formula	$C_{24}H_{36}Ag_2Cl_2O_8S_{10}$
Formula weight	1059.42
Crystal dimensions, mm	0.20 x 0.40 x 0.40
Space group	Monoclinic $P2_1/n$
a, Å	9.7217(3)[a]
b, Å	19.8697(2)
c, Å	10.2654(4)
β, deg	100.592(2)
Z (molecules/cell)	2
$F(000)$ electrons	1063.94
Volume, Å^3	1858.93
d_{calc}, g/cm^3	1.893
Linear absolute coefficient, mm^{-1}	1.77
Radiation (MoKα_1), Å	λ = 0.70930
2Θ(max), deg	45.0
No. reflections measured	2570
No. of unique reflections	2433
No. unique reflections, $I_{net} > 2.5\sigma(I_{net})$	1940
Last least-square cycle calculated with	41 atoms
	281 parameters
	1940 reflections
R_f (sig. refl.)	0.036[b]
R_w (sig. refl.)	0.030[c]
Goodness of fit (last cycle)	3.657[d]
R_f (all refl.)	0.050[b]
R_w (all refl.)	0.030[c]
Maxinum shift/σ	0.110
Last D-map:	
deepest hole, e/Å^3	-0.580
highest peak, e/Å^3	0.540
Secondary extinction coefficient	0.44(3)

[a] Throughout this work, esd's are in parentheses and refer to the last digit printed.

[b] $R_f = \Sigma\,||F_o| - |F_c||/\Sigma\,|F_o|$.

[c] $R_w = [\Sigma w(|F_o| - |F_c|)^2/\Sigma(w|F_o|)^2]^{1/2}$ where $w = 1/\sigma^2 I$.

[d] Goodness of fit = $[\Sigma w(|F_o| - |F_c|)^2/(\text{number of reflections - number of parameters.})]^{1/2}$.